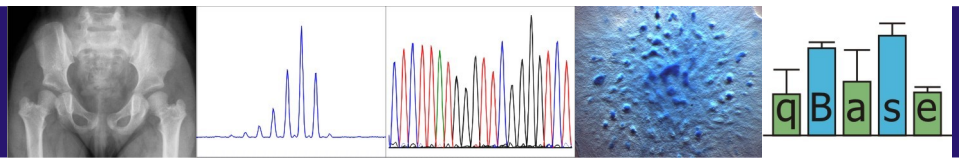

Identification and analysis of genes involved in skeletal dysplasias affecting growth and bone homeostasis

Center for Medical Genetics

Jan Hellemans

This thesis is dedicated to my family:
Petra, my wife
Lode and Lisa, my children
and my parents

Thesis submitted to fulfill the requirements for the degree of Doctor in Medical Sciences
November 2006

Promotor

Prof. Dr. Geert Mortier
Ghent University, Belgium

Co-promotor

Prof. Dr. Paul Coucke
Ghent University, Belgium

Members of the examination committee

Prof. Dr. Anne De Paepe
Ghent University, Belgium

Dr. Jo Vandesompele
Ghent University, Belgium

Prof. Dr. August Verbruggen
Ghent University, Belgium

Prof. Dr. Jean Kaufman
Ghent University, Belgium

Prof. Dr. Wim Van Hul
University of Antwerp, Belgium

Prof. Dr. Kristin Verschueren
Katholieke Universiteit Leuven, Belgium

Prof. Dr. Stephan Mundlos
Institut für Medizinische Genetik am Campus Charité Mitte, Germany
Max Planck Institute for Molecular Genetics, Germany

Prof. Dr. Valérie Cormier-Daire
Department of Genetics, Hôpital Necker Enfants Malades, France

The research described in this thesis was conducted in the Center for Medical Genetics, Ghent University Hospital, Ghent, Belgium.

From 01-04-2001 to 31-12-2002, Jan Hellemans was supported by the Fifth Framework of the specific research and technological development program "Quality of Life and Management of Living Resources" of the European Commission, Contract QLG1-CT-2001-02188

From 01-01-2003 to 31-12-2006, Jan Hellemans was an aspirant of the Institute for the Promotion of Innovation through Science and Technology in Flanders (IWT-Vlaanderen) with grants no. IWT-SB/21476 and IWT-SB/23476.

Acknowledgment – Dankwoord

A PhD thesis is not a one day nor a one mans work, but a project in which the help and support of many needs to be appreciated. My gratitude to these people has not always been apparent, but in this acknowledgment I would like to thank all those who have contributed directly or indirectly to the completion of this thesis.

I wish to express my sincere gratitude to my promoter Prof. Dr. Geert Mortier and co-promoter Prof. Dr. Paul Coucke.
Geert, in 2001 you introduced me to the fields of medical genetics and skeletal dysplasias. Although my education as a molecular biologist sometimes didn't seem to fit my job, I am grateful you gave me the opportunity to work on these fascinating research topics. I very much appreciate your qualities as a supportive promoter who guided me through this thesis without restricting personal initiatives. Also, without your help and understanding for my lack of medical knowledge, this thesis might not have been possible. Your enthusiastic appreciation of the progress in my research always made me feel good in my work.
Paul, it was a pleasure to work in your lab. Without the equipment, organization and atmosphere of this lab, research would have been much harder. I also appreciate the chance you gave me to help organize a sequencing and genotyping facility because tasks like this prevented me from becoming a blinkered specialist.
Geert and Paul, thank you for being kind (co-) promoters always open for a discussion or conversation, and not merely there for orders and complaints.
Prof. Dr. Anne De Paepe, the Center for Medical Genetics Ghent has become a highly regarded institute, in great part, because of you and I am grateful having been able to work in such a center.

I would also like to express my appreciation for all the people who have invested time in teaching me new methods and techniques.
Jo, thank you for teaching me how to perform correct real-time PCR quantification. Your qPCR expertise allowed us to swiftly complete our functional analyses and lies at the basis of a complete chapter of this thesis. Our long, and sometimes chaotic, discussions on the correct way to analyze qPCR data will long be remembered.
Prof. Dr. Stephan Mundlos, Petra Seemann and colleagues, working amongst you in a foreign lab was a nice and inspiring experience to me. Thank you for showing me a different kind of research and for the effort put into my training. Thanks for the good times.

Many thanks to all the colleagues from the Center of Medical Genetics. Chantal, Els, Ilse, Inge, Jozefien, Karen, Leen, Nilgul, Petra, Renée and Sofie, it was a real pleasure working with you. I really have appreciated the nice atmosphere in the lab and all the help you have provided, as well as your patience with me as a PhD student who often wanted to do things in another way. Chantal and Jozefien, thank you for all the help with *LEMD3* screenings. Renée, working with you to get the sequencing facility up and rolling was a pleasure.
Andy, Sofie and Sophie, it was nice sharing a bureau with you. Thank you for the good times, interesting discussions and, sometimes loud, conversations. Andy, when you joined us in the Center for Medical Genetics Ghent, you also freed me from isolation in my 'Nijntje' bureau in K5. Sofie and Sophie, thank you for all the help with vector construction and patient administration.
Piet and Joris, I remember the times without ICT professionals. Having your help allowed me to focus on my research in stead of solving PC problems. Thank you for that.
Veerle, it was a nice experience having you as a thesis student. I appreciate your work for the construction of an RNAi system which will be beneficial for future research.

A number of people from outside the Center for Medical Genetics Ghent have also contributed to the results presented in this thesis. I would like to thank all collaborating clinicians for providing us with the invaluable samples and clinical information, and all

patients for their willing participation, especially those having given us biopsy material.
I also appreciate the nice collaboration with the research groups of Prof. Dr. Kristin Verschueren and Prof. Dr. Wim Van Hul. They have provide us with beautiful data when faced with serious time pressure.
Mira, thank you for helping me out with the French translation of the summary of this thesis.

Een heleboel mensen in mijn werkomgeving hebben bijgedragen tot het volbrengen van mijn doctoraatsthesis. Zonder de steun van mijn familie zou dit werk echter nooit afgeraakt zijn, en misschien zelfs nooit gestart zijn. Liefste ouders, bedankt voor alle steun en de kansen die jullie mij gegeven hebben. Jullie interesse en aanmoedigingen hebben me gebracht tot waar ik nu sta.
Petra, liefste, al van tijdens mijn studies biotechnologie sta je naast mij. Bedankt voor de morele steun en de leuke tijden die we samen beleefd hebben. Lode en Lisa, jullie brachten niet enkel een hoop extra verantwoordelijkheden in mijn leven, maar vooral veel vreugde en het besef dat leven meer is dan werken alleen. Jullie vriendschap en gulle lach hebben me steeds veel plezier gedaan.

Table of Contents

List of abbreviations

A-P	anterior-posterior
ACFD	acrocapitofemoral dysplasia
AER	apical ectodermal ridge
ALK	anaplastic lymphoma kinase
ATF4	activating transcription factor 4
BAF	barrier to autointegration factor
BDA1	brachydactyly type A1
BMP	bone morphogenetic protein
BOS	Buschke-Ollendorff syndrome
bp	basepair
CCD	cleidocranial dysplasia
CED	Camurati-Engelmann disease
CIZ	Cas-interacting zinc finger protein
cM	centi Morgan
CLS	Coffin-Lowry syndrome
COL	collagen
Cq	quantification cycle
CSF	colony stimulating factor
Ct	threshold cycle
D-V	dorsal-ventral
DNA	deoxyribonucleic acid
E	amplification efficiency
FGF	fibroblast growth factor
FGFR	fibroblast growth factor receptor
GCL	germ cell less
GDF	growth and differentiation factor
gDNA	genomic DNA
GH	growth hormone
goi	gene of interest
HHIP	hedgehog interacting protein
IGF	insulin-like growth factor
IHH	indian hedgehog
IRC	inter-run calibrator
kDa	kilo Dalton
LEMD3	LEM (LAP2, emerin, MAN1) domain containing 3
LHRH	luteinizing hormone-releasing hormone
LMN	lamin
LOD	logarithm of odds
Mb	mega bases = 1.000.000 bases
MH2	MAD homology 2
MIM	mendelian inheritance in man
MM-C	micromass cultures
MOS	melorheostosis
MRI	magnetic resonance imaging
NOG	noggin
NRQ	normalized relative quantity
NTC	no template control
OPG	osteoprotegerin
OPOI	osteopoikilosis
OSX	osterix
PCR	polymerase chain reaction
Pr-D	proximal-distal
PTHLH	parathyroid hormone like hormone
PTHR	parathyroid hormone receptor
qPCR	real-time quantitative PCR
R-SMAD	receptor activated SMAD
RANK	receptor activator of nuclear factor kappa B
RANKL	receptor activator of nuclear factor kappa B ligand
RDML	Real-time PCR Data Markup Language
ref	reference gene
RFLP	restriction fragment length polymorphism
RHYNS	retinitis pigmentosa, hypopituitarism, nephronophthisis, and mild skeletal dysplasia
RNA	ribonucleic acid
RNAi	RNA interference
ROR	receptor tyrosine kinase-like orphan receptor
RQ	relative quantity
RRM	RNA recognition motif
RUNX	runt-related transcription factor
SANE	Smad antagonistic effector
SHH	sonic hedgehog
SMAD	MAD (mothers against decapentaplegic) homolog
SOX	SRY (sex determining region Y) box
TGF	transforming growth factor
TM	trans membrane
TNF	tumor necrosis factor
WNT9A	wingless-type MMTV integration site family, member 9A
XML	Extensible Markup Language
ZPA	zone of polarizing activity

Depending on the species, different gene nomenclature rules apply. The HUGO Gene Nomenclature Committee (HGNC, http://www.gene.ucl.ac.uk/nomenclature/) sets the rules for human genes. Human gene symbols are designated by upper-case Latin letters and it is recommended that they are italicized in print. Mouse gene symbols (http://www.informatics.jax.org/mgihome/nomen/), on the other hand, should begin with an uppercase letter, followed by all lowercase letters.

Chapter title pictures taken from:
De humani corporis fabrica
(On the fabric of the human body)
Andreas Vesalius 1543

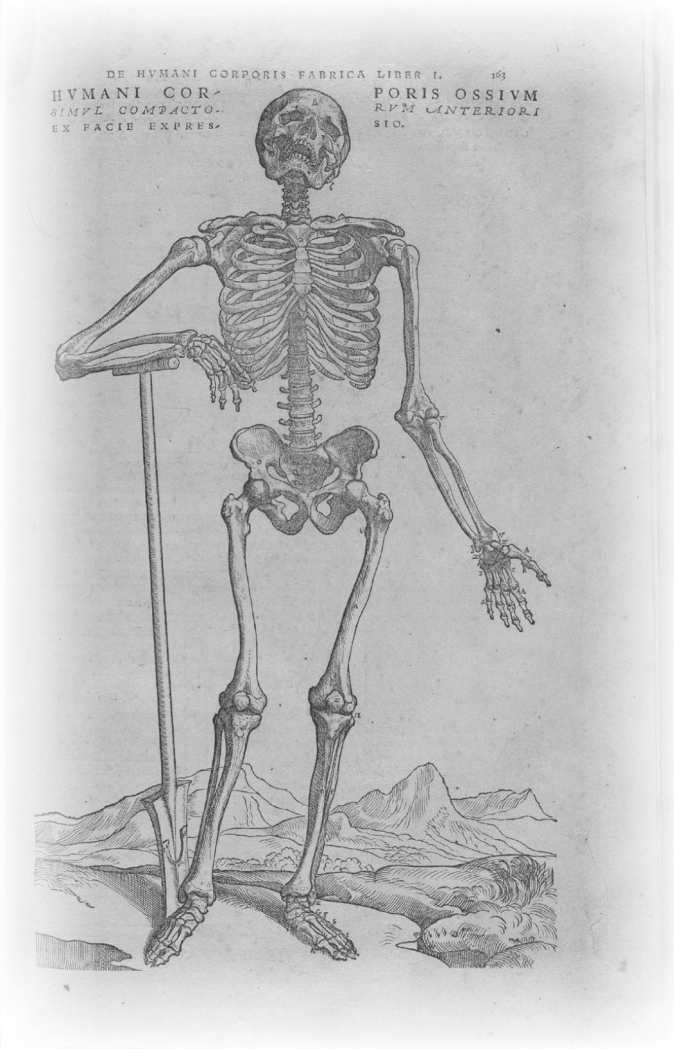

Chapter 1

Introduction

Outline

Genetic disorders of the skeleton comprise a large group of clinically diverse and genetically heterogeneous disorders. These disorders include both dysostoses, defined as malformations of individual bones or groups of bones, and osteochondrodysplasias, defined as developmental disorders of chondro-osseous tissue (*McKusick 1971*). They are usually monogenic and are characterized by defects in the formation, growth or homeostasis of the bone. The severity of this group of disorders ranges from asymptomatic, over mild growth retardation to neonatal lethality. Short stature is a very common feature. In its last published revision, the International Nosology and Classification of Constitutional Disorders of Bone lists a total of 294 osteochondrodysplasias and dysostoses (*Hall 2002*). Although they are individually rare, they are of clinical relevance because of their overall prevalence of 1 in 2000 (*Rasmussen 1996*).
The genetic defect of a growing list of disorders is being discovered. Causal mutations have now been identified in almost half of the disorders listed in the 2001 nosology (*Hall 2002*). These findings have both clinical and scientific implications. Identification of the causal genetic defect allows molecular confirmation of the diagnosis and helps in genetic counseling. From a scientific point of view, the identification of gene defects leading to skeletal dysplasias provides new insights into the genetic and molecular regulation of bone development, growth and homeostasis.
In this thesis, two (groups of) disorders were investigated: 1) acrocapitofemoral dysplasia (ACFD) (Chapter 2) and 2) osteopoikilosis and its related dysplasias Buschke-Ollendorff syndrome (BOS) and melorheostosis (Chapter 3).
Acrocapitofemoral dysplasia, abbreviated to ACFD, is a rare autosomal recessive dysplasia that only recently has been described. Radiographically, it is characterized by a premature epimetaphyseal fusion in the tubular bones of the hand and proximal femur, resulting in a short stature with brachydactyly (*Mortier 2003*).
Osteopoikilosis is a benign, autosomal dominant disorder that is usually detected incidentally. It is characterized by a symmetric but unequal distribution of multiple, small hyperostotic spots in different parts of the skeleton (*Stieda 1905, Benli 1992*). Osteopoikilosis can occur as an isolated anomaly or in association with other skin or bone manifestations. Osteopoikilosis often co-occurs with connective tissue nevi, and is then known as the Buschke-Ollendorff syndrome (BOS) (*Buschke 1928*). Melorheostosis is characterized by an asymmetric, flowing hyperostosis of the cortex of the tubular bones, that resembles wax dripping down the side of a candle (*Léri 1922, Green 1962*). It usually occurs as an isolated anomaly, but can co-occur with BOS in the same family (*Debeer 2003*).

The first objective of this thesis, the identification of the genetic defect underlying these disorders, was achieved by means of a classical genetic approach. This strategy is used to identify the gene by mapping it to a specific genomic locus and involves, for human genetics, the following steps:

1. Identification of a large family affected by the disorder of interest and establishment of a detailed phenotypical description of all family members.
2. Collection of genomic DNA from as much relatives as possible.
3. Genotyping of large numbers of informative markers spread all over the genome. In this thesis, Applied Biosystems Linkage Mapping set v2 consisting of 400 microsatellite markers was used to genotype patients and their relatives.
4. Analysis of genotypic data in order to detect linkage between the investigated phenotype (skeletal dysplasia) and a genetic marker with known location. For recessive phenotypes in inbred families an efficient homozygosity mapping can be performed. The basic idea in this approach is that all affected individuals have to be homozygous for a linked

marker. More generally, the genotypes are added to a pedigree and LOD-scores are calculated for every marker (*Lathrop 1984*). Markers with a LOD-score of at least 3 are considered to show significant linkage with the investigated phenotype.

5. Fine mapping of the candidate region. The boundaries of the linkage interval are determined by analyzing additional markers around the linked locus.
6. Identification of the causal mutation. Since complete sequencing of all genes in the candidate region is neither achievable nor an efficient strategy, a selection of genes is made based on their known function or involvement in related disorders (candidate gene approach). Mutation analysis is subsequently performed on this restricted set of candidate genes to pinpoint the causal mutation.

The second objective of this thesis, analysis of the identified genes, has two facets: a genetic and a functional. Genetic analysis is performed on a larger set of patients to verify whether the condition shows locus heterogeneity and to investigate what kind of mutations are responsible for the phenotype. Larger numbers of mutations also allow to investigate genotype-phenotype correlations. Functional analysis aims to investigate the normal function of the gene product or the effects of mutations on this function. This type of analysis often involves the determination of the expression levels of a selection of genes for which real-time quantitative PCR (qPCR) has become the method of choice.

Advancements in instruments and detection chemistry, and improved assay design guidelines have made the practical performance of qPCR measurements feasible for most users. However, accurate and straightforward processing of the raw data as well as the management of large data sets remain the major hurdles. The qBase framework was developed to improve these issues (Chapter 4). It consists of a set of guidelines and formulas for the correct conversion of raw Cq values into normalized and calibrated relative quantities, and is implemented in the qBase software. This freely available tool (http://medgen.ugent.be/qBase) is compatible with most qPCR data formats without imposing limits to the number or layout of data points, automates all calculations, and visualizes results in table and graph format. Together, the improved formulas and the automation of the numerous calculations solve some of the largest remaining problems in qPCR based expression analysis.

1 The human skeleton

The human skeleton (from the Greek σκελετοσ, dried up) is a complex organ consisting of 206 bones (126 appendicular, 74 axial, 6 ossicles). It has multiple embryonic origins and serves many key functions including mechanical support for movement, protection of vital organs, and acting as a blood and mineral reservoir. The skeleton consists of 2 tissues: bone and cartilage, and 3 cell lineages: those of osteoblasts, osteoclasts, and chondrocytes. Osteoblasts and osteoclasts cells are responsible for bone formation and bone resorption respectively, while chondrocytes make up the cartilage.

Only a small part of the bone is made up by cells, the remainder is filled with matrix which has both organic and inorganic components. Type I collagen is the most predominant peptide in bone and comprises 90-95% of the organic matrix. The collagen secreted by osteoblasts is typically deposited in parallel or concentric layers to produce mature (lamellar) bone. But when bone is rapidly formed, as in the fetus, the collagen is not deposited in a parallel array but in a basket-like weave and is called woven, immature, or primitive bone. The lamellar form confers more strength to the bone than the woven form. Osteocalcin is the most abundant non-collagenous protein of bone matrix. The main mineral component of bone is an imperfectly crystalline hydroxyapatite [$Ca_{10}(PO_4)_6(OH)_2$] which comprises about ¼ the volume and ½ the mass of normal adult bone. About 99% of the 1000g of calcium in an adult human resides in the skeleton in the form of hydroxyapatite. These calcium salts are responsible for the compressive strength of bone and provide the structural integrity of the skeleton. While bone is essentially brittle, it does have a degree of significant elasticity contributed by its organic components (Fig. 1).

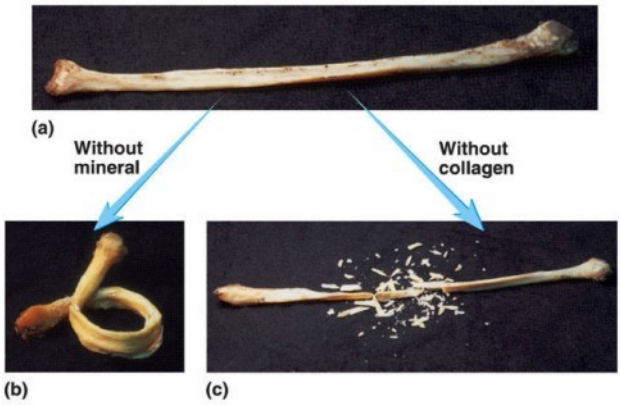

Figure 1: Contributions of mineral and collagen to bone strength (taken from Seeley, Anatomy and Physiology - McGraw-Hill)

Anatomically, four types of bones can be distinguished: long bones (e.g. tibia and femur), short bones (e.g. carpals and tarsals), flat bones (e.g. skull and ribs) and irregular bones (e.g. vertebrae) (*Shier, Hole's Human Anatomy & Physiology – McGraw-Hill*).

Long bones

Long bones are tubular in structure and have expanded ends. The central shaft of a long bone is called the diaphysis, and has a hollow middle, the medullar cavity, filled with bone marrow. Surrounding the medullar cavity is a thin layer of cancellous bone and an outer layer of compact cortical bone (Fig.2). The cancellous or spongy bone is trabecular and has an open, meshwork or honeycomb-like structure that helps reducing the weight of the bone. The spaces of the spongy bone are continuous with the medullary cavity and are filled with marrow. A thin layer of squamous epithelial cells, called endosteum, lines the cancellous bone. The ends of the bone are called the epiphyses and are mostly cancellous bone covered by a relatively thin layer of compact bone. Except for the articular cartilage, the bone is completely enclosed by a tough, vascular covering of fibrous tissue called the periosteum. In children, long bones are filled with red marrow, which is gradually replaced with yellow marrow as the child ages.

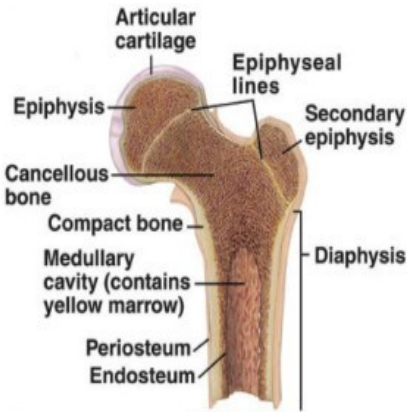

Figure 2: Structure of an adult long bone (taken from Seeley, Anatomy and Physiology - McGraw-Hill)

Short bones

Short bones have a similar structure to long bones, except that they have no medullar cavity. They have no shaft, as they do not increase dramatically in size during linear growth. They tend to be cuboidal in shape.

Flat bones

Flat bones consist of two layers of compact bone with a zone of cancellous bone in between them (Fig. 3).

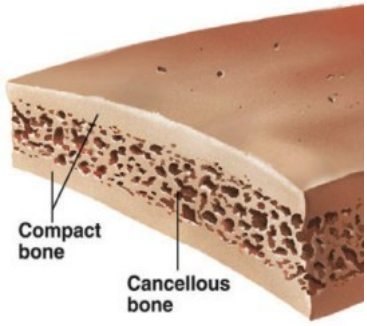

Figure 3: Structure of a flat bone (taken from Seeley, Anatomy and Physiology - McGraw-Hill)

Irregular bones

Bones which don't fit any of the previous forms are referred to as irregular. They have a variety of shapes and are usually connected to several other bones.

Despite the common misconception that the skeleton is made up of dead tissue, it does, in fact, contain cells, nerves, blood vessels and pain receptors. Bone is also not immutable but an ever-changing organ in which mass and shape are regulated by the remodeling activities of osteoblasts and osteoclasts.

The final state of the skeleton is determined by processes in different stages of development. Firstly, patterning determines the sites at which bone will be formed. Secondly, condensation of mesenchymal cells followed by their differentiation results in bone formation. Thirdly, growth affects the size of individual bones and, finally, homeostasis is responsible for the maintenance of the skeleton. Abnormalities in any of these steps can give rise to the many and varied forms of skeletal dysplasias or osteochondrodysplasias (*Kornak 2003*).

2 Patterning

The first step in skeletal formation is the determination of the position, number and shape of the elements that will develop into the bones that make up the skeleton. Many of the crucial genes that regulate growth and patterning of the limb in three dimensions are now well defined. This knowledge comes primarily from studies of limb development in chicken and mouse embryos. The developing limb has served as a model for studying the signal transduction pathways and cell biology that control pattern formation because the limbs are not necessary for embryonic survival, allowing them to be experimentally and molecularly manipulated (*Niswander 2003*).

In the human embryo, the appendicular skeleton develops from limb buds, first visible at around 4 weeks of gestation. By week 8, these buds have formed much of the mature limb structures (*O'Rahilly 1975*). The skeletal tissues in the limb are produced by cells derived from the lateral plate mesoderm. The patterning of the mesenchyme in the limb and the ultimate shaping of the limb bones are due to a series of interactions between the mesenchyme and the overlying epithelium. Vertebrate limbs display three axes of asymmetry referred to as proximal-distal (Pr-D; shoulder to digit tips), anterior-posterior (A-P; thumb to little finger), and dorsal-ventral (D-V; back of hand to palm). Patterning along these three axes of the embryonic limb is regulated by three key organizing centers (Fig. 4). Integration of three-dimensional patterning occurs as a result of the complex interplay

amongst these three signaling centers (*Niswander 2002*).

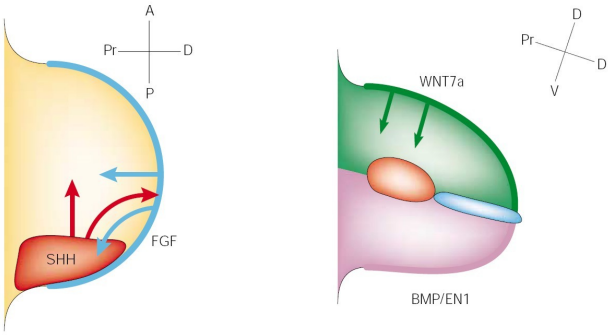

Figure 4: Molecular interactions that coordinate limb growth and patterning along the three limb axes. (Taken from Niswander 2003)

Proximal-distal

A strip of specialized epithelium at the distal tip of the limb bud, called the apical ectodermal ridge (AER, Fig. 4 light blue) is needed for Pr-D growth and for the realization of Pr-D patterning. Microsurgical removal of the AER from an early developing limb bud results in the loss of almost all limb structures, whereas its removal at progressively later stages results in progressively more distal loss, with proximal structures being unaffected. These findings are traditionally explained by the progress model (*Summerbell 1974*), but recent data now suggest an attractive alternative (*Dudley 2002*). Fibroblast growth factors (FGF) are essential to perform the functions of the AER: they induce or maintain the expression of many genes in the limb bud mesenchyme, control the initial size of the limb bud and influence cell survival and proliferation (*Sun 2002*).

Anterior-posterior

A population of cells in the posterior aspect of the limb mesenchyme, called the zone of polarizing activity (ZPA, Fig. 4 orange) controls A-P patterning. Grafting of ZPA cells to the anterior distal margin of a limb bud causes mirror-image duplications of skeletal elements (*Tickle 1981*). The finding that a similar digit duplication is obtained by anterior addition of sonic hedgehog (SHH), and other experiments in $Shh^{-/-}$ limbs, indicate that SHH is the key signal originating from the ZPA (*Riddle 1993*).

Dorsal-ventral

D-V patterning in the limb bud is regulated by the overlying ectoderm. When the limb ectoderm is rotated 180° relative to the mesenchyme, the mesenchymal structures (including the skeleton) become inverted such that they correspond to the polarity of the ectoderm (*MacCabe 1974*). Wnt7a expression in the dorsal limb ectoderm induces the production of the transcription factor Lmx1b which is responsible for the dorsal character of the mesenchyme. In the absence of Wnt7a, the dorsal pattern of the autopod is not established and the limbs appear bi-ventral. Bone morphogenetic protein (BMP) induced expression of engrailed1 (En1) in the ventral ectoderm restricts the expression of Wnt7a to the dorsal ectoderm. Consequently, loss of BMP signaling or En1 expression will result in bi-dorsal limbs (*Chen 1999*).

The mesenchymal cells of the growing limb bud differentiate to form the various tissues of the limb in a proximodistal sequence. The positional identity imposed by the three-dimensional coordinate system described above controls differentiation of these limb bud mesenchymal cells. The aggregation of mesenchymal cells to form prechondrogenic condensations triggers cellular differentiation and is arguably the most critical event in skeletal patterning.

Another crucial process for patterning is joint formation. It can occur either at the boundary between two adjacent condensations or within a single condensation. Two genes, growth differentiation factor 5 (GDF5) and noggin (NOG), which encodes a BMP antagonist, are required for normal joint formation. GDF5 is necessary for both cartilage development and the restriction of joint formation to the appropriate location (*Storm 1999*). Loss of Nog function causes complete failure of joint formation in the autopod, partly due to a failure to upregulate Gdf5 expression in the presumptive joint regions (*Brunet 1998*). In spite of the requirement of these factors in the formation of specific joints, GDF5 and NOG are not sufficient to induce joint formation. In contrast, WNT9A, which is expressed in joint forming regions prior to segmentation of the cartilage elements, was found to actively direct prechondrogenic cells into the joint forming pathway (*Hartmann 2001*).

Much of the patterning process is complete by the time that condensations have differentiated into cartilaginous templates

(see next section). However, the remaining steps in endochondral bone formation do influence final skeletal pattern.
The proteins described above (FGF, SHH, BMP-EN1) determine the major regulatory pathways in bone morphogenesis, but many genes regulating these signaling cascades or other pathways are are required for normal bone development. Mutations in these genes mainly cause dysostoses, disorders that affect specific embryologically defined skeletal elements while the rest of the skeleton remains unaffected. For example, many types of polydactyly are caused by defects in the hedgehog pathway. Mutations in GLI3, the downstream effector of SHH, give rise to postaxial polydactyly type I, preaxial polydactyly type IV, Greig cephalopolysyndactyly and Pallister-Hall syndrome (*Vortkamp 1991, Kang 1997*). Another example, with disturbed patterning involving the dorsoventral axis, is Nail-patella syndrome. This dysostosis is caused by haploinsufficiency of LMX1B (*Dreyer 1998*).

3 Differentiation into bone

The mesenchymal condensations, as defined by the patterning process described above, develop into bone either directly through intramembranous ossification or indirectly through endochondral ossification. In the human skeleton, only the membrane bones of the skull and part of the clavicle are completely formed by direct ossification of condensed mesenchyme (intramembranous ossification). For the large majority of bones, bone formation and linear growth proceed through an intermediate cartilaginous template or anlage in a process called endochondral ossification. In these bones intramembranous ossification is responsible for appositional growth which results in an increase in diameter.

Intramembranous ossification is initiated by the invasion of condensed mesenchyme with a dense network of blood vessels. Some of the connective tissue cells arrange around these vessels, enlarge and differentiate into bone forming cells. These cells, called osteoblasts, deposit bone matrix around themselves. As a result, spongy bone forms in all directions along blood vessels within the layers of primitive connective tissue (Shier, *Hole's Human Anatomy – McGraw-Hill*). The genes involved in osteoblast differentiation and activity play an important role in this process and will be discussed in the homeostasis section.

Endochondral ossification is the process by which long bones are formed from mesenchymal cells through an intermediate cartilaginous model. This multistage process starts with the formation of a mesenchymal condensation, the basic anlage, at the site where the future bone will be formed. Further differentiation of condensed mesenchymal cells into chondrocytes that produce hyaline cartilage instead of mesenchymal matrix, creates a cartilaginous model with shapes similar to the future bone. This model grows rapidly for a time and then begins to change extensively. Starting in the center, chondrocytes enlarge and differentiate to become hypertrophic chondrocytes, producing type X collagen. The matrix surrounding these cells will subsequently calcify, and the hypertrophic chondrocytes will undergo apoptosis. Concomitantly, a primary bone collar with associated periosteum and rudimentary vascular supply is formed at the presumptive diaphysis.
The newly formed spaces within the calcified cartilage are invaded by periosteal blood vessels and osteogenic cells, that soon differentiate into osteoblasts. The latter deposit a bony matrix on the calcified cartilage, resulting in the formation of the

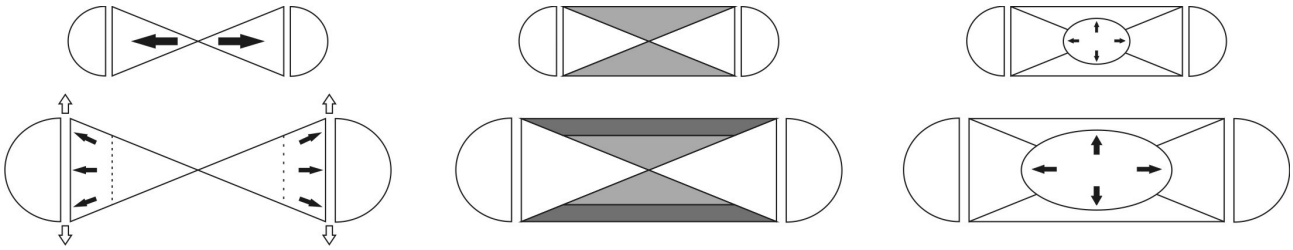

Figure 5. Schematic presentation of endochondral cones with left: growth of the cones, middle: filling in by membranous ossification, and right: creation of the marrow cavity (Adapted from Rockwood, Fractures in Children – Lippincott).

primary center of ossification. The first bone formed is a loose trabecular network connected to the adjacent periosteal shell of bone, which is the product of membranous ossification. Both processes of cartilage replacement by bone and bone collar formation subsequently spread towards the ends of the developing bone. Spreading of increased matrix formation, chondrocyte hypertrophy, cartilage calcification and replacement by bone results in the creation of endochondral cones. The apices of these cones juxtapose at the site of the original primary ossification center, whereas the bases are located towards the physeal region. Endochondral cones grow away from the apex, resulting in longitudinal growth, but also grow diametrically to increase the area of the cone base (Fig. 5, left). The surrounding bone collar expands by membranous ossification to fill in the gaps produced by the endochondral cones (Fig. 5, middle). Therefore, the periosteum is the primary contributor to latitudinal growth of the diaphysis and metaphysis of tubular bones. As the endochondral cones grow, bone tissue is resorbed from the center to create the marrow cavity (Fig. 5, right). Elaborate remodeling and tubulation in children's bones mask many of the steps described above. The concept of juxtaposed patterns of endochondral and membranous ossification is however apparent in most marine mammals who lack extensive remodeling (*Rockwood, Fractures in Children – Lippincott; Urist, Fundamental and Clinical Bone Physiology – Lippincott*).

At birth, the primary ossification center has expanded to replace the entire cartilaginous diaphysis with bone. The epiphyses of most long bones, with the exception of the distal femoral epiphysis, do however remain cartilaginous until after birth. At a time characteristic for each chondroepiphysis, a secondary center of ossification forms and gradually enlarges. As a result, the majority of the cartilaginous anlage will be replaced by bone, except for the physis, that closes around puberty, and the articular cartilage, that builds up the joint. Also postnatally, the membranous woven bone is remodeled to create a more rigid cortical bone (Fig. 5, middle: dark gray zone).

An overview of the complete process of endochondral ossification is depicted in Fig. 6.

A number of key regulatory elements in early bone formation have already been identified. SOX9 is an important transcription factor in the early steps of endochondral ossification. It is required for mesenchymal condensation and subsequent chondroblast differentiation, and controls the production of the major collagen of cartilage: type II collagen (*Lefebvre 1998, Bi 1999*). Inactivation of

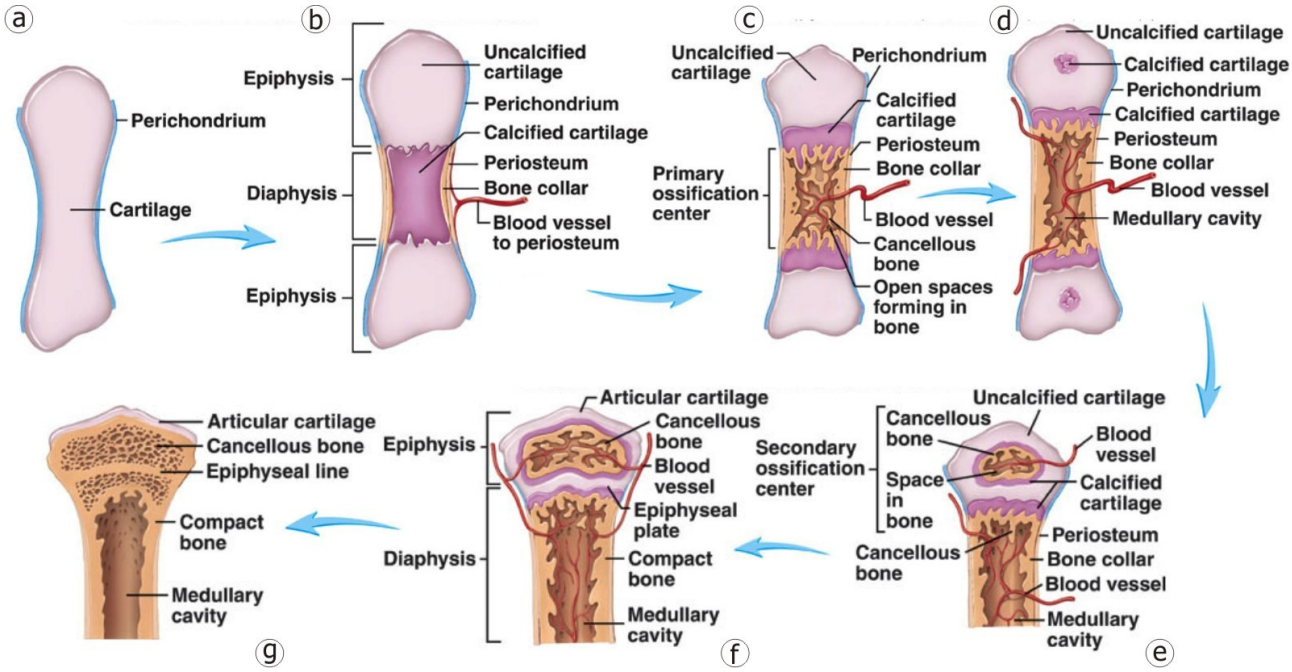

Figure 6. Overview of the process of endochondral ossification (Taken from Seeley, Anatomy and Physiology – McGraw-Hill)

Sox9 in mouse limb buds before mesenchymal condensation results in the complete absence of both cartilage and bone. The expression of Sox5 and Sox6, two other Sox genes involved in chondrogenesis, is no longer detected in these animals and expression of Runx2, a transcription factor required for osteoblast differentiation, is abolished. Sox9 is needed for the formation of mesenchymal condensations, whereas Sox5 and Sox6 are required for the differentiation of condensed cells into chondrocytes (*Akiyama 2002*). The TGFβ/BMP/GDF5 pathways also play an important role in the regulation of condensation and differentiation of condensed cells into chondrocytes (*Kornak 2003*).

The next step in endochondral ossification, osteoblast differentiation, is rather similar to the differentiation process in intramembranous ossification. The function of genes like *RUNX2* and *osterix* which regulate osteoblast differentiation are discussed in the homeostasis section.
Genetic defects that result in the disturbance of mesenchymal condensation and/or differentiation can be expected to have a patterning-like phenotype (loss or underdevelopment of certain bones) together with a growth defect. Such conditions have been termed "dysostoplasias", indicating that aspects of dysostosis occur together with those of dysplasias (Kornak 2003). Two examples are campomelic dysplasia and cleidocranial dysplasia, the former caused by haploinsufficiency of *SOX9* (sex determining region Y box 9) (*Foster 1994, Wagner 1994*), and the latter by mutations in *RUNX2* (runt-related transcription factor 2) (*Mundlos 1997*).

4 Growth

Postnatal growth of long bones involves two different processes. Endochondral ossification is responsible for integrated longitudinal and latitudinal growth at the epiphyseal plate, while intramembranous ossification results in appositional growth at the diaphysis (Fig. 7). The growth plate is a highly organized structure localized between the epiphysis (the secondary center of ossification) and the metaphysis (the distal end of the primary ossification center). It generates all of the longitudinal growth and remains active until the end of puberty when primary and secondary ossification centers fuse.
A developing bone thickens as compact bone is deposited on the outside, just beneath the periosteum. While this compact bone is formed on the surface, the bone tissue at the inside is eroded by osteoclasts. The resulting space becomes the medullary cavity (*Shier, Hole's Human Anatomy & Physiology – McGraw-Hill*).
During longitudinal growth, all the differentiation stages of initial endochondral bone formation are recapitulated. These stages are reflected by the different consecutive zones that make up the growth plate. From epiphysis to metaphysis the following zones can be distinguished: zone of resting cartilage, zone of proliferation, zone of hypertrophy, zone of calcification and finally bone formation (Fig. 8). The resting zone contains a pool of slowly proliferating chondrocytes that do not actively participate in growth, but act as the stem-like cells that replenish the pool of proliferative chondrocytes (*Abad 2002*). This layer anchors the epiphyseal disk to the bony tissue of the epiphysis. Cells leaving the resting zone start to multiply at a high rate and form columns of stacked, proliferating chondrocytes. The alignment of these columns, parallel to the axis of growth, is directed by a morphogen produced by the resting chondrocytes (*Abad 2002*). After a period of clonal expansion, chondrocytes stop dividing and terminally differentiate into hypertrophic chondrocytes. During the hypertrophic process, chondrocytes increase their height about 6 to 10-fold. Therefore

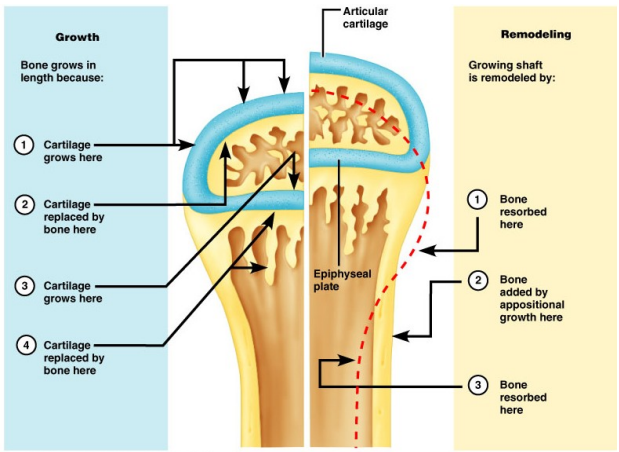

Figure 7. Longitudinal and latitudinal growth of long bones (Taken from Marieb, Human Anatomy & Physiology – Benjamin Cummings)

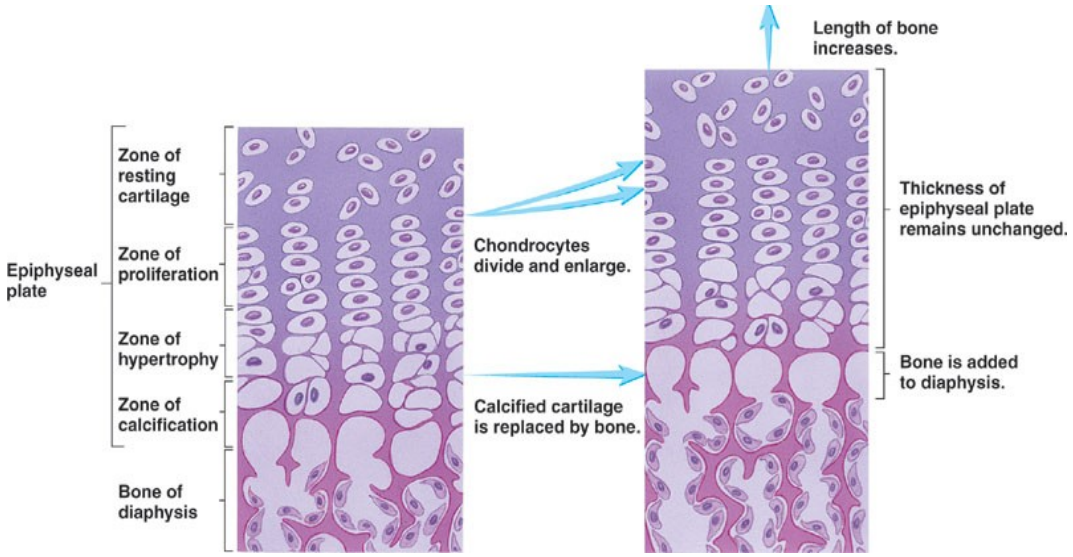

Figure 8. Epiphyseal plate: differentiation zones and growth process (Taken from Seeley, Anatomy and Physiology – McGraw-Hill)

hypertrophic differentiation, in concert with cellular proliferation and increased matrix volume, makes an important contribution to longitudinal growth (*Hunziker 1994*). Calcium salts accumulate in the intercellular matrix adjacent to the oldest cartilaginous cells, and as the matrix calcifies, the hypertrophic cells begin to die. This calcified cartilage is subsequently invaded by blood vessels and bone cells that change the cartilage into bone tissue, which then becomes part of the metaphysis.

GH	Proliferation of resting chondrocytes Stimulates local IGF-1 expression
IGF-1	Increses proliferation of resting and proliferative chondrocytes Increases hypertrophic cell size
Glucocorticoid	Inhibits chondrocyte proliferation Delays growth plate senescence Induces chondrocyte apoptosis
Thyroid hormone	Permissive for proliferation and differentiation
Estrogen	Inhibits proliferation in the proliferative zone Accelerates growth plate senescence
Androgen	Stimulates proliferation and matrix production Increases IGF-1 expression
Vitamin D	Permissive for normal differentiation and apoptosis of hypertrophic chondrocytes
Leptin	Stimulates proliferation and differentiation

Table 1: Effects of endocrine factors on growth plate chondrocytes

A very complex interplay of different signaling pathways (both endocrine and paracrine) regulates the rate of proliferation and the conversion of proliferating cells into hypertrophic chondrocytes. Most of these endocrine signals regulate growth plate function by acting locally on chondrocytes but also by modulating other endocrine signals in the network. Some of the local effects of hormones are mediated by changes in paracrine factors that control chondrocyte proliferation and differentiation (*Nilsson 2005*). An overview of the local effects of endocrine signals is shown in table 1.

Growth hormone (GH) and insulin-like growth factors (IGFs) are potent stimulators of longitudinal bone growth. GH excess, due to pituitary adenomas in childhood, results in gigantism. Conversely, GH deficiency or insensitivity due to GH-receptor mutations or defects in GH-signaling pathways markedly impairs postnatal growth and will result in proportionate short stature. The original somatedin hypothesis stipulates that the effect of GH on linear growth is mediated by the liver derived IGF-1. More recently, the dual effector hypothesis states that GH acts locally at the growth plate to recruit resting chondrocytes into a proliferative state, as well as to stimulate local IGF-1 production which then stimulates proliferation of chondrocytes in the proliferative zone (*Nilsson 2005*). The vast majority of other short-stature disorders, however, result in disproportionate dwarfism, presumably because they affect not only proliferation but

also differentiation of chondrocytes (*Kornak 2003*).
A number of growth factors, in conjunction with the macromolecules of the extracellular matrix, are essential for proper development and functioning of cartilage and bone. The major signaling pathways that control proliferation and differentiation of chondrocytes include the indian hedghog – parathyroid hormone related hormone (IHH-PTHLH) loop and signals from fibroblast growth factors (FGF) and bone morphogenetic proteins (BMP). The effects of these paracrine factors are more extensively described in Chapter 2: Overview. Briefly, IHH produced by prehypertrophic chondrocytes induces the expression of parathyroid hormone like hormone (PTHLH) which in turn suppresses the differentiation of columnar proliferating cells into hypertrophic chondrocytes (*Vortkamp 1996*). IHH also directly stimulates proliferation of chondrocytes in the growth plate (*Karp 2000*). Growth factors of the FGF and BMP families work next to IHH and have antagonistic effects on chondrocyte proliferation and differentiation. BMPs stimulate chondrocyte proliferation, induce IHH secretion and inhibit terminal chondrocyte differentiation whereas FGFs have the opposite effect (*Minina 2002*).
The importance of these pathways is exemplified by a number of skeletal dysplasias resulting from mutations in the genes encoding proteins of the IHH, FGF or BMP family.

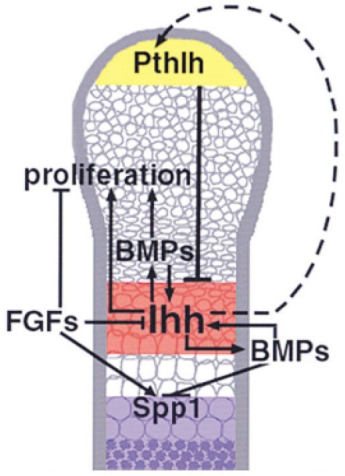

Figure 9: Interaction of FGFs and BMPs with the IHH-PTHLH loop (Taken from Minina 2002)

Homozygous and heterozygous missense mutations in *IHH* can result in acrocapitofemoral dysplasia (ACFD) or brachydactyly type A1 (BDA1), respectively (*Gao 2001, Paper 1: Hellemans 2003*). ACFD is a more generalized skeletal dysplasia whereas BDA1 is mainly characterized by brachydactyly.
Homozygous loss-of-function mutations and dominant activating mutations in the parathyroid hormone receptor (PTHR1) result in, respectively, Blomstrand chondrodysplasia and metaphyseal chondrodysplasia Jansen-type (*Jobert 1998, Schipani 1995*). The former is characterized by a short-limb-dwarfism with accelerated bone maturation whereas patients with the latter chondrodysplasia suffer from a severe growth retardation and bone deformations.

The importance of FGF signaling became apparent with the discovery of fibroblast growth factor receptor 3 (FGFR3) mutations in patients with achondroplasia, the most frequent form of dwarfism (*Shiang 1994*). Two allelic disorders exist: hypochondroplasia with less growth deficit and thanatophoric dysplasia which is characterized by severe disproportionate dwarfism and death in early infancy. All the *FGFR3* mutations involved in the three conditions have a receptor-activating effect, and a clear genotype-phenotype correlation has been described.

5 Homeostasis

Despite the common misconception that the skeleton is immutable, it is, in fact, an ever-changing organ in which mass and shape are regulated by the activities of osteoblasts and osteoclasts. Remodeling, the coordinated action of bone resorption by osteoclasts and bone formation by osteoblasts, is essential for the maintenance of the structural integrity of bone and for the regulation of the circulating Ca^{2+} concentration. If remodeling is out of balance, either a loss or an accumulation of bone occurs, resulting in osteoporotic or osteopetrotic phenotypes, respectively.

Bone formation by osteoblasts

Osteoblasts, responsible for bone formation, arise from cells in the condensing mesenchyme. Three forms of the osteoblast cell lineage are recognized: progenitor osteoblasts (pre-osteoblasts), mature osteoblasts and osteocytes. Pre-osteoblasts

have the capacity to divide, but have not yet acquired many of the protein-synthesizing characteristics of mature osteoblasts. As they mature, osteoblasts stop dividing and become highly metabolically active. They synthesize the collagenous constituents of the bone matrix and also regulate its mineralization.
During the process of bone formation, the osteoblast determines its own fate by calcifying itself into a lacuna. At the point of total encasement, the metabolic activity of the cell dramatically decreases as a result of the lack of nutrient diffusion. Approximately 15% of osteoblasts eventually survive as osteocytes.
Several factors, including RUNX2, ATF4, OSX and CIZ, have been found to be essential for the development, maturation and function of osteoblasts (Fig. 10).

RUNX2

In 1997, four independent papers in the same issue of Cell demonstrated the importance of Runx2 (runt related transcription factor 2) in osteoblast differentiation and development of calcified bone. Two groups created Runx2 knock-out mice that, when homozygous, died soon after birth due to respiratory insufficiency (*Otto 1997, Komori 1997*). The most striking feature of these mice was a total lack of bone, and retention of a partially calcified cartilaginous skeleton. Histochemical and gene expression analyses showed absence of osteoblastic cells. Heterozygous Runx2$^{+/-}$ mice were found to have a phenotype very similar to cleidocranial dysplasia (CCD). The identification of heterozygous inactivating *RUNX2* mutations in CCD patients is fully consistent with these findings (*Mundlos 1997*). Also, in a search for osteocalcin specific transcription factors, Runx2 was identified as a regulator of osteoblast differentiation (*Ducy 1997*). In vivo expression analysis of Runx2 suggests that this transcription factor may regulate expression of early markers for osteoblast differentiation, as well as expression of osteocalcin, a marker for differentiated osteoblasts. Runx2 overexpression induced the expression of type I collagen, osteopontin and osteocalcin in nonosteoblastic and pre-osteoblastic cells. Together these data

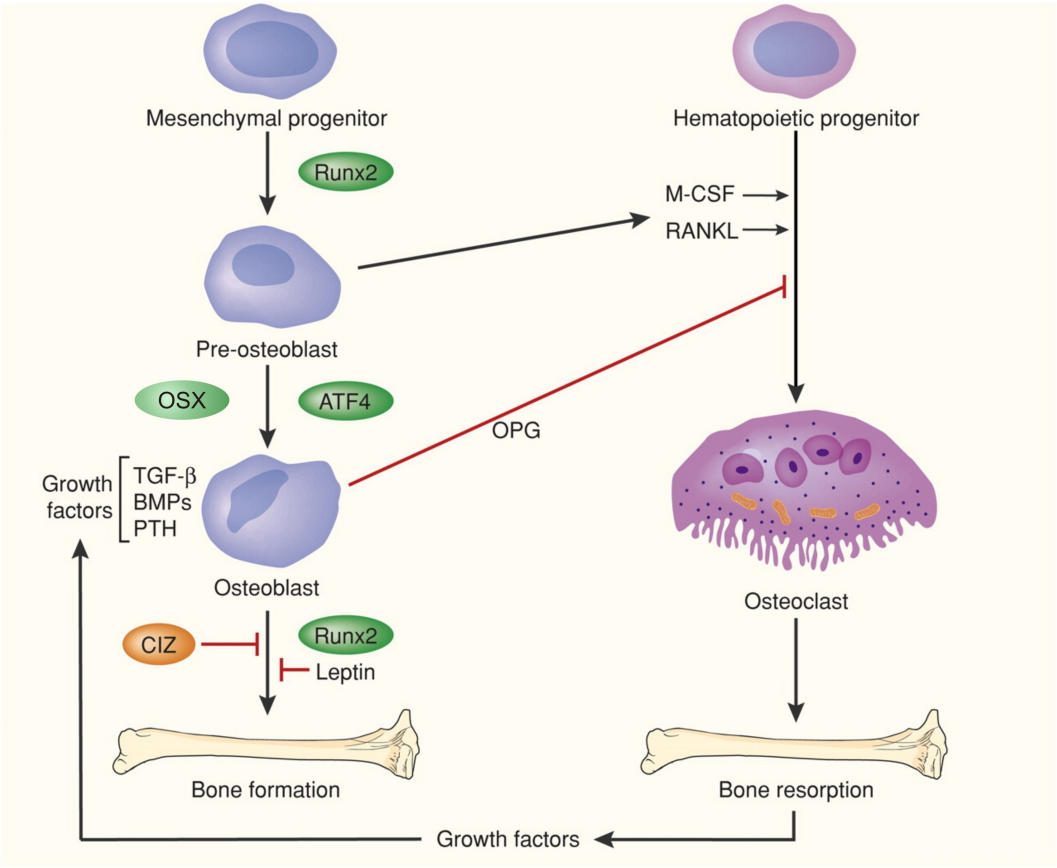

Figure 10: Signaling pathways regulating maturation and activity of osteoblasts and osteoclasts (Adapted from Krane 2005).

provide compelling evidence that Runx2 is indispensable for normal osteoblast differentiation.

OSX

Osterix (OSX) is another transcription factor that is essential for osteoblast differentiation (*Nakashima 2002*). Similarly to Runx2$^{-/-}$ mice, in the absence of Osx, no cortical bone and no bone trabeculae are formed. However, in contrast to Runx2$^{-/-}$ mice, absence of Osx does not deregulate chondrocyte differentiation. Nakashima et al. therefore concluded that Osterix acts downstream of Runx2 to regulate a later step in osteoblast differentiation. Runx2 was later shown to directly bind and transactivate the promoter of Osx (*Nishio 2006)*.

ATF4

ATF4 (activating transcription factor 4) is the target transcription factor of RSK2 (RPS6KA3 = ribosomal protein S6 kinase, 90kDa, polypeptide 3). Mice deficient for the Atf4 gene show a delayed bone formation during embryonic development and a low bone mass characterized by a severe reduction in bone volume and in the number and thickness of trabeculae. This phenotype is due to a failure to achieve terminal osteoblast differentiation, to defects in osteoblast function and to a posttranscriptional decrease in type I collagen synthesis. These findings identify Atf4 as a critical regulator of osteoblast differentiation and function (*Yang 2004*). Also, Rsk2 deficient mice have a delayed mineralization of the skull and a significant reduction in long bone length at one month of age. These abnormalities are similar to those reported in patients with Coffin-Lowry syndrome (CLS), a condition with mental retardation and skeletal abnormalities caused by *RSK2* mutations (*Trivier 1996*), confirming the importance of the RSK2-ATF4 pathway in bone development.

CIZ

The recent identification of CIZ (ZNF384 = zinc finger protein 384) as a suppressor of adult bone mass is an interesting finding in view of the impact of osteoporosis on our aging population (*Morinobu 2005*). In Ciz deficient mice, bone volume and the rate of bone formation are increased whereas bone resorption is not altered. The absence of major alterations in skeletal morphogenesis during embryonic stages suggests that CIZ action is more important in bone metabolism in adulthood than in embryonic life. CIZ was found to reduce osteoblast activity by inhibition of SMAD mediated BMP signaling.

Bone resorption by osteoclasts

Osteoclasts are the highly specialized bone lining cells responsible for bone resorption. Before 1980, the origin of multinucleated osteoclasts was controversial. Experiments with radiation chimeras did, however, provide strong evidence for the haematopoietic origin of osteoclasts (*Ash 1980*). They differentiate in a late phase from the monocyte/macrophage cell lineage. At endosteal bone surfaces, the precursors proliferate and fuse to form giant, multinucleated cells containing 4 to 20 nuclei. Osteoclasts are usually found in contact with a calcified bone surface and within a lacuna (Howship's lacunae or resorption pit). Osteoclast are motile cells. They resorb bone to form a lacuna and then move across the bone surface to resorb a separate area of bone. Periods of locomotion are not associated with resorption.

In order for resorption to occur, osteoclasts need to attach to the bone surface. The zone of contact with the bone (the sealing zone) is characterized by the presence of a ruffled border with dense patches on each side. The plasma membrane in the ruffled border area contains proteins that are also found in lysosomal membranes, and a specific type of electrogenic proton ATPase necessary for acidification of the extracellular compartment. Lysosomal enzymes are

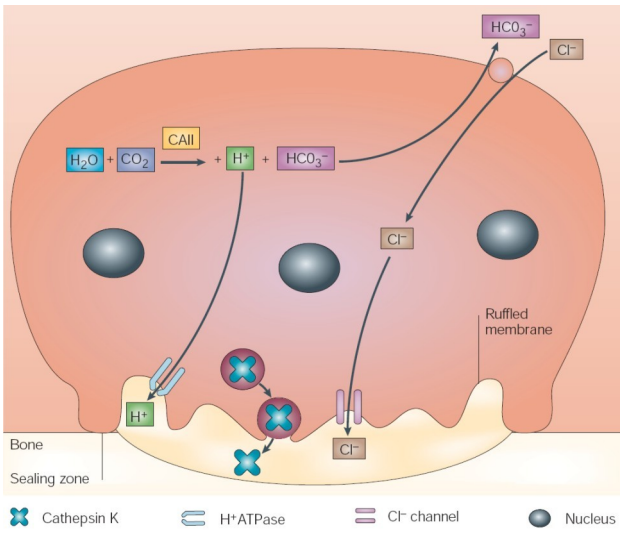

Figure 11: Resorption by osteoclast (Taken from Teitelbaum 2003).

actively synthesized by the osteoclast and secreted, via the ruffled border, into the extracellular bone-resorbing compartment where they reach a sufficiently high extracellular concentration because this compartment is sealed off (Fig. 11). The extracellular bone-resorbing compartment is therefore the functional equivalent of a secondary lysosome. The low pH in the sealing zone dissolves the hydroxyapatite crystals, thus exposing the matrix to lysosomal enzymes. These enzymes, now at optimal pH, subsequently degrade the matrix components. At the end of the resorbing phase, the osteoclasts undergo apoptosis (*Teitelbaum 2003*).

In vitro experiments revealed that a direct cell-to-cell contact with osteoblastic cells is required for the differentiation of osteoclast progenitors into multinucleated osteoclasts (*Takahashi 1988*). CSF1 and the RANK-RANKL-OPG system were found to be the essential osteoblast derived elements for the differentiation of haematopoietic progenitor cells into osteoclasts (Fig. 10).

CSF1

Macrophage colony stimulating factor (CSF1 = colony stimulating factor 1) is expressed by osteoblasts and their precursors as a soluble and membrane-bound protein. The finding that osteoclast deficiency in osteopetrotic (op/op) mice is due to an inability to produce functionally active Csf1 strongly indicates a critical role for this factor in osteoclast development (*Felix 1990a, Felix 1990b, Yoshida 1990*). CSF1 was shown to promote both proliferation and survival of osteoclast precursors.

RANK-RANKL-OPG

Osteoprotegerin (OPG or TNFRSF11B) is a soluble member of the tumor necrosis factor (TNF) receptor family secreted by the preosteoblastic/stromal cells. Studies of transgenic mice overexpressing osteoprotegerin (i.e. to protect bone) and animals injected with OPG have demonstrated that this protein inhibits osteoclastogenesis and suppresses bone resorption (*Simonet 1997, Yasuda 1998a*).
In 1998, the long sought ligand mediating the essential signal of osteoblastic cells to osteoclast progenitors for their differentiation into osteoclasts was identified: a soluble form of the membrane associated receptor activator of NF-κB ligand (RANKL or TNFSF11) was found to induce osteoclast formation from spleen cells in the absence of osteoblast/stromal cells (*Yasuda 1998b*). Addition of osteoprotegerin abolished this effect of RANKL indicating that OPG acts as a decoy receptor that binds directly to RANKL on osteoblasts/stromal cells. As such it interrupts RANKL-mediated signaling from osteoblasts/stromal cells to osteoclast progenitors, and inhibits osteoclastogenesis. In combination with CSF1, RANKL was found to be sufficient for osteoclast formation from monocytes or spleen cells (*Quinn 1998*).
The final piece of the puzzle of osteoclast formation fell into place with the the identification and characterization of the receptor for RANKL: RANK (TNFRSF11A). Rank knockout mice were found to develop a severe osteopetrosis due to the absence of osteoclasts (*Li 2000*). This confirms the requirement of RANK signaling to osteoclast precursors for the formation of mature osteoclasts. Thus, in conjunction with macrophage colony-stimulating factor, the RANK-RANKL-OPG system regulates osteoclast differentiation.

Coupling of bone formation and resorption

Under normal conditions, bone remodeling renews 5-10% of bone volume per year. In early life bone formation by osteoblasts predominates over bone resorption by osteoclasts. The highest velocities of bone mineral addition are achieved by the ages of 13 and 14.5 years for girls and boys, respectively. This gain in bone mass is mainly related to increasing bone volumes. About 90% of peak bone mass is acquired by age 18, with only minimal further bone acquisition until age 30 (*Heaney 2000*). Later in life, the rate of bone formation may not fully compensate for the bone lost by resorption, resulting in a net loss of bone tissue. When the process of bone remodeling becomes unbalanced then either osteopetrosis or osteoporosis may develop.
Bone formation and bone resorption do not occur along the bone surface at random, but in a coordinated fashion. In the adult skeleton, bone formation occurs only where bone resorption has previously taken place. Together, these processes constitute the turnover mechanism by which old bone is replaced by new bone. Osteoblasts and

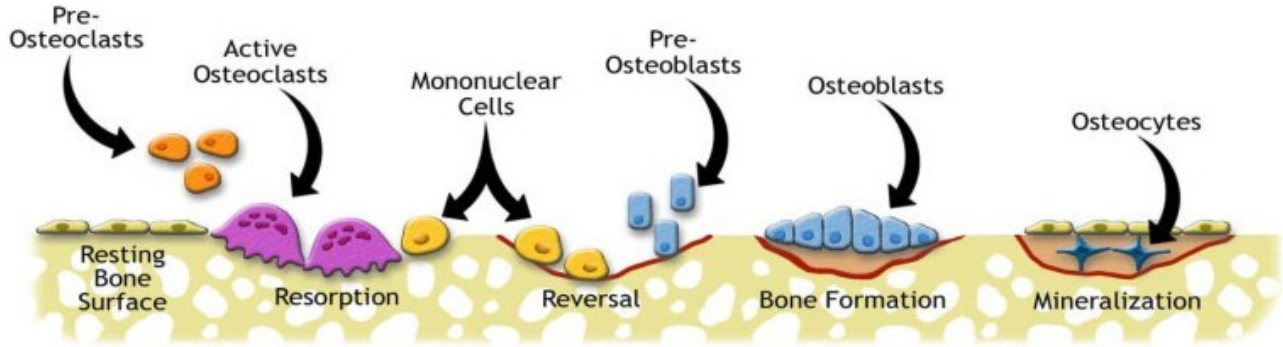

Figure 12: Bone remodeling process (Taken from http://www.umich.edu/news/Releases/2005/Feb05/bone.html)

osteoclasts, coupled together via paracrine cell signaling, are referred to as bone remodeling units. The complete remodeling cycle (Fig. 12) takes about 3 to 6 months to complete and consists of the following phases:

Quiescence phase:

Bone is at rest and no active remodeling is taking place.

Activation phase

The bone surface is activated by the retraction of bone lining cells and the digestion of the endosteal membrane by collagenase action. Once activated, the mineralized surface attracts the circulating osteoclast precursors supplied by nearby vessels.

Resorption phase

Multinucleated osteoclasts dissolve the mineral matrix and decompose the osteoid matrix.

Formation phase

Attracted by the growth factors released from the matrix, preosteoblasts migrate into the resorbed areas. Differentiated osteoblasts then synthesize the osteoid material which fills the resorbed areas.

Mineralization phase

Mineralization begins approximately 1 month after deposition of the osteoid (organic bone matrix), ending at about 90 days in the trabecular and at 130 days on the average in the cortical bone. The quiescent phase then begins again.

In general, bone remodeling is regulated and influenced by genetic constitution, systemic hormones, nutrition and mechanical factors (Fig. 13). A number of epidemiological, family and twin studies have revealed an important role for genetic factors in bone remodeling. Overall these studies suggest that 60-80% of variance in bone phenotypes (e.g. maximum bone density) at any age or group is genetically determined (*Eisman 1999*). On the other hand, environmental factors such as nutrition and physical loading (gravity and exercise) are known to be important as well. Physical activity is essential for the correct development of bone. In athletes, increased loading has been shown to be associated with increased bone mass, often located to the sites of loading. On the other hand, the absence of muscular activity, rest or weightlessness has an adverse effect on bone, by accelerating resorption. Nutrition can influence bone density in both ways: a minimum amount of calcium is needed for mineralization while toxic substances like alcohol or smoking constitute a risk factor for osteopenia.

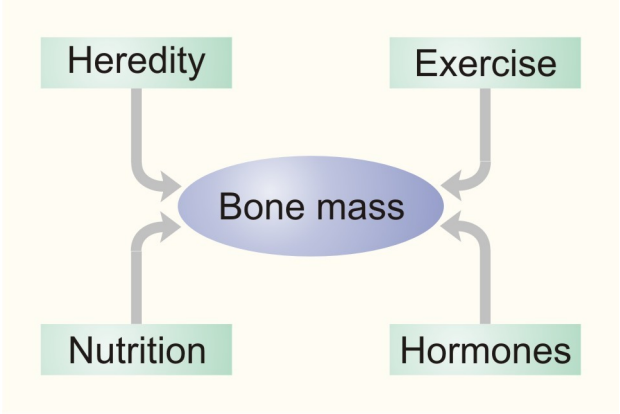

Figure 13: Regulation of bone mass

Bone remodeling is regulated by a number of hormones (thyroid and parathyroid hormone,

	Stimulate bone formation	Stimulate bone resorption	Inhibit bone resorption
Growth factors	BMP-2 BMP-4 BMP-6 BMP-7 IGF-I IGF-II TGF-β FGF PDGF	TNF EGF PDGF FGF M-CSF GM-CSF	
Cytokines		IL-1 IL-6 IL-8 IL-11 PGE2 PGE1 PGG2 PGI2 PGH2	IFN-γ IL-4

Table 2: Regulatory local factors in bone remodeling (Taken from Fernandez-Tresguerres-Hernandez-Gil 2006)

sex steroids, insulin, glucocorticoids and growth hormone) and local factors. An overview of the effect of these local acting growth factors and cytokines is shown in table 2. At the molecular level bone remodeling appears to be mainly controlled by the balance between RANKL (osteoclast inductive) and OPG (osteoclast inhibitive). Preosteoblasts express a high level of RANKL relative to osteoprotegerin which stimulates osteoclast differentiation and function, and allows resorption to start. More mature osteoblasts, by contrast, express high levels of osteoprotegerin relative to RANKL, which inhibits osteoclast differentiation and function (*Gori 2000*). This prevents further bone resorption and allows the mature osteoblasts to fill the resorption pits with fresh bone. It makes sense that the critical, initial step in bone remodeling, the development of osteoclasts, should be under the control of preosteoblastic/stromal cells. This ensures that the processes of bone resorption and formation will be tightly coupled, allowing for a wave of bone formation to follow each cycle of bone resorption. Further coupling between osteoblastogenesis and osteoclastogenesis is ensured by the fact that the osteoclast differentiation factor, RUNX2, is necessary for adequate expression of the osteoclast differentiation factor, RANKL, on the surface of preosteoblastic/stromal cells (*Gao 1998*).

Two of the growth factors listed in table 2, BMP and TGFβ, are of special importance in this thesis:

TGFβ

Strong evidence for a positive effect of TGFβ on bone formation in humans comes from the rare skeletal dysplasia, Camurati-Engelmann disease (CED). This autosomal dominant disorder is characterized by a progressive cortical thickening of the diaphyses of the long bones. Hyperostosis is bilateral and symmetrical, and usually starts during childhood. A total of 10 different mutations in the TGFB1 gene have been found in CED patients, all leading to increased TGFβ activity (*Janssens et al. 2006*). The identification of activating mutations in TGFB1 in patients with CED demonstrates that increased TGFβ signaling can lead to hyperostosis.

BMP

The positive effect of BMP signaling on bone formation was demonstrated in a number of transgene mice. Mice with a dominant-negative BMP receptor (BMPR-IB) mutation in osteoblasts suffer from impaired postnatal bone formation as the result of reduced BMP signaling. Bone mineral density, bone volume and bone formation rates in these mutant animals are severely reduced without changes in osteoblast and osteoclast numbers (*Zhao et al. 2002*). Also, transgenic mice overexpressing noggin, an extracellular BMP antagonist, have a reduced bone mineral density and decreased trabecular bone volume (*Devlin et al. 2003*).

The positive effect on bone formation of these growth factors was confirmed by our finding that loss of function mutations in *LEMD3*, encoding an inhibitor of SMAD mediated BMP and TGFβ signaling, result in the hyperostotic disorders osteopoikilosis, BOS and melorheostosis (*Paper 2: Hellemans 2004*).

1 Introduction

As indicated in the previous section, the final state of the skeleton is determined by the processes of patterning, endochondral and intramembranous ossification, growth and bone homeostasis. Abnormalities in any of these components can give rise to disorders of the heterogeneous group of skeletal dysplasias or osteochondrodysplasias. The phenotypic spectrum of these disorders ranges from asymptomatic over various degrees of short stature to death in the neonatal period. Secondary complications of skeletal deformity and manifestations in extraskeletal organs add to the burden of this group of disorders.

Skeletal dysplasias are individually rare, but collectively quite common. Because of the rarity of some of these conditions, they can be difficult to diagnose. The prevalence has been assessed by a number of investigators and ranges from 0.95 to 7.6 depending on the cited source (Table 3, *Rasmussen 1996*). Prevalence rates of about 1 in 10,000 have been found by three groups that only took lethal cases into account. Five papers report a prevalence between 2 and 5 per 10,000 newborns. This rate increases to about 7.6 when dysplasias noted at older ages are taken into account as well.

Population	Rate per 10,000	Reference
Lethal neonatal	0.95	*Rasmussen 1996*
Lethal neonatal	1.1	*Connor 1985*
Lethal	1.5	*Andersen 1989*
Not specified	1.6	*Källén 1993*
Newborn	2.1	*Rasmussen 1996*
Newborn	2.3	*Orioli 1986*
Newborn	2.4	*Camera 1982*
Newborn	3.2	*Stoll 1989*
Newborn	4.7	*Gustavson 1975*
All dysplasias	7.6	*Andersen 1989*

Table 3: Prevalence of osteochondrodysplasias (Adjusted from Rasmussen 1996)

2 Classification

At the end of the 19th century the term "achondroplasia" was introduced to distinguish patients with disproportionate short stature from persons with proportionate short stature (*Parrot 1886*). Subsequently, the diagnosis of achondroplasia was retained for those with short-limb dwarfism and the term Morquio syndrome for those with short-trunk dwarfism. Further heterogeneity within the group of skeletal dysplasias was recognized by the middle of last century. The description of many new chondrodysplasias required the development of a uniform and consistent nomenclature and classification system for these conditions. The 'International Working Group on Constitutional Diseases of Bone' formulated the first 'International Nomenclature of Constitutional Diseases of Bone' in 1970 in Paris. They classified genetic disorders of the skeleton in a few classes. *Dysostoses* were defined as 'malformations of individual bone, singly or in combination' whereas *osteochondrodysplasias* were described as 'abnormalities of cartilage and/or bone growth and development'. (*McKuscik 1971*) In his book 'Bone Dysplasias' Jürgen Spranger defined the constitutional errors of bone development as follows: *dysostoses* are malformations of single bones, alone or in combination, *disruptions* are secondary malformations of bones and *skeletal dysplasias* are developmental disorders of chondro-osseous tissue (*Spranger, Bone Dysplasia – Oxford University Press*).

Dysostoses

Dysostoses are manifestations of transient signaling defects in the first 6 weeks of fetal life resulting in abnormal organogenesis and defective bone formation. Because of the transient nature of the defective process, the malformations do not spread to involve previously normal bones and joints. Therefore, the dysostotic phenotype is static throughout life. Since dysostoses are finite disorders caused by a past, closed process,

there is no danger of malignant degeneration. The lesions may be asymmetrically distributed and, although they are malformations of individual bones, several bones may be affected in combination. Dwarfism is not a primary manifestation of dysostoses (unless bones of the vertical body axis are defective or missing) and the chondro-osseous histology is normal.

Disruptions

Toxic substances or infectious agents to which an embryo may be exposed act for limited periods of time, as do transiently expressed signaling genes. They may produce secondary malformations, but do, by definition, not result in dysplasias. Thalidomide and rubella embryopathy are prime examples of, respectively, a chemical and a viral insult resulting in skeletal disruptions.

Dysplasias

Defects of prenatally expressing genes that continue to be expressed in postnatal life lead to dysplasias. In contrast to dysostoses, however, most dysplasia genes are not expressed during organogenesis in a way that their defects would manifest. Mutations lead to postnatally ongoing errors of cell proliferation, differentiation and degeneration, and thus to defective skeletal growth and development. Malignant degeneration is possible but rare in skeletal dysplasias. Primary skeletal dysplasias result from mutated genes that are expressed in chondro-osseous tissue while secondary dysplasias are caused by abnormalities of extraosseus factors with secondary effects on the skeletal system (e.g. metabolic disorders). Since skeletal dysplasias are disorders of bone as tissue, mutations of dysplasia genes affect all anatomic sites in which a mutated gene is expressed. Homologous sites are affected and the resulting disorders are mostly symmetric. Eventual development of asymmetric lesions usually results from the influence of local mechanical factors or somatic mutations. In contrast to dysostoses, dwarfism is a common feature of skeletal dysplasias (*Spranger, Bone Dysplasia – Oxford University Press*).

Since its first description in 1970, the International Nomenclature of Constitutional Diseases of Bone has been officially revised and updated on 6 occasions: 1977, 1983, 1991, 1997, 2001 (*Hall 2002*) and 2005 (*Superti-Furga 2007*). The initial categorizations were purely descriptive and consisted of a mixture of the key clinical, radiographic, and histologic features of each condition. The recent advances in molecular biology and technology in conjunction with the progress of the human genome project have allowed the concept of groups of disorders to evolve, where conditions with similar genetic defects are put together.
The last published classification of constitutional disorders of bone is a hybrid that incorporates clinical (e.g. mesomelic dysplasia group), radiographic (e.g. metaphyseal dysplasia group), and molecular descriptors (e.g. type II collagenopathies group), as well as using various descriptive Greek terms to name conditions (e.g. atelosteogenesis omodysplasia group). The need for separate but parallel classifications, one based on clinical features and the other on molecular defects, was clearly identified at the 2001 meeting. Superti-Furga suggested a molecular and pathogenetic classification into 7 groups (*Superti-Furga 2001*):

1. defects in extracellular structural proteins
2. defects in metabolic pathways (including enzymes, ion channels, transporters)
3. defects in folding, processing and degradation of macromolecules
4. defects in hormones and signal transduction mechanisms
5. defects in oncogenes and tumor-suppressor genes
6. defects in RNA and DNA processing and metabolism

3 Diagnosis

The latest nosology and classification of genetic skeletal disorders (2006 revision) lists 372 distinct conditions, of which 215 are associated with one or more of 140 different genes (*Superti-Furga 2007*). The diversity together with the rarity of each individual disorder, makes a correct diagnosis often difficult for the clinician. The establishment of a correct diagnosis is however important for a number of reasons. It allows accurate genetic ounseling and is the cornerstone for proper clinical management.
The diagnosis usually requires a careful clinical examination of the patient and

thorough radiographic evaluation of the skeleton. Morphologic studies of the growth plate, cartilage and bone can be helpful in further narrowing the differential diagnosis, certainly in the lethal conditions where tissue specimens are easily available. Biochemical or molecular analysis can be used to confirm the diagnosis, provided that the causal gene is known (*Mortier 2001*).

A complete history, pedigree analysis and physical examination should be the first step in the diagnostic assessment of a patient suspected for having a skeletal dysplasia. Knowledge of birth length and postnatal growth curves are very important. The recognition of congenital malformations and other connective tissue abnormalities can be very helpful in the diagnostic work-up. The diagnosis of a skeletal dysplasia however still mainly relies on a careful radiographic evaluation of the skeleton. Because epiphyseal closure after puberty makes evaluation of the epiphyses and metaphyses difficult, if not impossible, a skeletal survey is preferably taken before puberty. Offiah and Hall have provided a schematic approach that can be followed when evaluating a skeletal survey (*Offiah 2003*). This scheme has been devised as an easy to remember mnemonic in which the A, B, C and D characteristics are to be investigated. They indicate respectively:

A – Anatomical localization

Some conditions are broadly named according to the anatomical sites involved. The anatomic localization of skeletal defects may occasionally be sufficient, but certainly gives a radiologist a good starting point and is usually required for the further classification of the condition.

B – Bones

The following is an aid memoir to the radiological analysis of bones (the five "S's"):

Structure

This applies to the general appearance of the bones, including abnormalities of bone density and the presence of tumorous lesions. The distribution of abnormalities is also important.

Shape

Alterations in shape may affect the whole bone or be restricted to part of a bone, such as the metaphyses or the epiphyses. Some shapes are very specific and can be used as a predictive marker.

Size

Abnormalities of size may be absolute or relative to the size of other bones. When considering size, it is also relevant to take the bone age into account.

Sum

Bones may be too many, too few, or fused.

Soft tissues

Abnormalities of soft tissues that should be looked for include wasting, excessive soft tissues, contractures and calcification. Soft tissue involvement may change not only the diagnosis, but also the patient's prognosis.

C – Complications

Although recognition of complications does not usually help in reaching a diagnosis, from the point of view of patient management it is important to exclude known complications of a condition once a diagnosis has been reached.

D – Dead/alive

The fact that a dysplasia is lethal can help to exclude or confirm a given diagnosis, or may affect the subtype of the condition.

Chapter 2

The IHH gene in acrocapitofemoral dysplasia

Paper 1

Hellemans et al. Am J Hum Genet. 2003

Hellemans J, Coucke PJ, Giedion A, De Paepe A, Kramer P, Beemer F, Mortier GR. Homozygous mutations in *IHH* cause acrocapitofemoral dysplasia, an autosomal recessive disorder with cone-shaped epiphyses in hands and hips. Am J Hum Genet. 2003 Apr;72(4):1040-6. Epub 2003 Mar 11.

Am. J. Hum. Genet. 72:1040–1046, 2003

Report

Homozygous Mutations in *IHH* Cause Acrocapitofemoral Dysplasia, an Autosomal Recessive Disorder with Cone-Shaped Epiphyses in Hands and Hips

Jan Hellemans,[1] Paul J. Coucke,[1] Andres Giedion,[2] Anne De Paepe,[1] Peter Kramer,[3] Frits Beemer,[4] and Geert R. Mortier[1]

[1]Department of Medical Genetics, Ghent University Hospital, Ghent, Belgium; [2]Department of Radiology, Children's Hospital Zürich, Zurich; and Departments of [3]Radiology and [4]Medical Genetics, Division of Biomedical Genetics, University Medical Center, Utrecht

Acrocapitofemoral dysplasia is a recently delineated autosomal recessive skeletal dysplasia, characterized clinically by short stature with short limbs and radiographically by cone-shaped epiphyses, mainly in hands and hips. Genomewide homozygosity mapping in two consanguineous families linked the locus to 2q35-q36 with a maximum two-point LOD score of 8.02 at marker D2S2248. Two recombination events defined the minimal critical region between markers D2S2248 and D2S2151 (3.74 cM). Using a candidate-gene approach, we identified two missense mutations in the amino-terminal signaling domain of the gene encoding Indian hedgehog (*IHH*). Both affected individuals of family 1 are homozygous for a 137C→T transition (P46L), and the three patients in family 2 are homozygous for a 569T→C transition (V190A). The two mutant amino acids are strongly conserved and predicted to be located outside the region where brachydactyly type A-1 mutations are clustered.

Recently, we delineated a new autosomal recessive skeletal dysplasia in two consanguineous families of Belgian and Dutch origin (Mortier et al. 2003). The clinical phenotype is characterized by short stature of variable degree with short limbs and brachydactyly, relatively large head, and narrow thorax with pectus deformities (fig. 1). Affected individuals do not exhibit associated congenital anomalies and are of normal intelligence. Radiographically, cone-shaped epiphyses (CSE) or a similar epiphyseal configuration are observed in the hands, the proximal part of the femur, and, to a variable degree, at the shoulders, knees, and ankles (fig. 2). These CSE appear early in childhood and disappear with the premature fusion of the growth plate before puberty, resulting in shortening of the involved skeletal components. This process leads, in the hips, to a characteristic egg-shaped femoral head attached to a very short femoral neck and, in the hands, to shortening of the tubular bones, especially the middle phalanges. Since all affected individuals show these striking and characteristic abnormalities in hands and hips, we named the disorder acrocapitofemoral dysplasia (ACFD).

To unravel the genetic basis of this skeletal dysplasia, we performed homozygosity mapping in both consanguineous families, using 400 genetic markers with an average spacing of 10 cM (ABI PRISM Linkage Mapping Set version 2) (Lander and Botstein 1987). Initially, the genomewide screening was performed on four affected individuals (VII-1, VII-4, IX-2, and IX-5) from both families (fig. 3). A fifth patient (IX-1), later identified, was subsequently used in the analysis. Appropriate informed consent was obtained from all human subjects involved in the study. Alleles were scored using the Genescan and Genemapper software (Applied Biosystems). After the initial screening, the region on 2q35-q36 was further investigated, because four affected individuals were homozygous by descent for two consecutive markers, D2S325 and D2S2382. Analysis with additional, closely spaced markers refined the candidate region to between D2S2382 and D2S163, a distance of about 5 cM (fig. 3). A recombination event between loci D2S2382 and D2S2248 in patient IX-2 (fig. 3*B*) defined the proximal boundary of the genetic interval. A recombination event between

Received November 21, 2002; accepted for publication January 13, 2003; electronically published March 11, 2003.

Address for correspondence and reprints: Dr. Geert R. Mortier, Department of Medical Genetics, Ghent University Hospital, De Pintelaan 185, B-9000, Ghent, Belgium. E-mail: geert.mortier@rug.ac.be

0002-9297/2003/7204-0027$15.00

loci D2S2151 and D2S163 in individual IX-4 (fig. 3*B*) defined the distal boundary of the candidate region. The MLINK program of the LINKAGE software package (Lathrop and Lalouel 1984) was used to calculate two-point LOD scores between the disease phenotype and each of the markers, assuming a recessive disease with an allele frequency of 0.001 and marker allele frequencies of 0.125. This resulted in a maximum LOD score of 8.02 at $\theta = 0$ for marker D2S2248 (table 1). A search on the human genome resources of the National Center for Biotechnology Information disclosed several candidate genes within the linked region on chromosome 2q35-q36: *IGFBP2* and *IGFBP5* (both encoding an insulin-like growth-factor–binding protein), *IHH* (encoding Indian hedgehog), and *STK36* (human homologue of the *Drosophila melanogaster* gene *fused*). We selected *IHH* as the strongest candidate because this gene is expressed in the growth plate (Kindblom et al. 2002), dominant mutations have been identified in brachydactyly type A1 (BDA1 [MIM 112500]) (Gao et al. 2001; McCready et al. 2002), and *Ihh*-null mice exhibit a short-limb dwarfism phenotype (St-Jacques et al. 1999).

Sequence analysis of Indian hedgehog (*IHH* [GenBank accession number Q14623]) in the affected individuals revealed two distinct nucleotide changes. In the two affected individuals in family 1, a homozygous 137C→T transition, predicted to result in a P46L substitution, was observed (fig. 4). In the three affected individuals in family 2, a homozygous 569T→C transition, predicted to result in a V190A substitution, was identified (fig. 4). Both substitutions are located in the amino-terminal domain of the Indian hedgehog protein, which is responsible for local and long-range signaling (Porter et al. 1995). Heterozygosity for the 137C→T and 569T→C mutation was observed in the unaffected parents in family 1 and 2, respectively. Both sequence changes were absent in 75 unrelated control subjects (150 chromosomes), confirming that they do not represent common polymorphisms. Finally, alignment of the protein sequence of homologues of Indian hedgehog in several species showed that both proline at position 46 and valine at position 190 are strongly conserved residues (fig. 5).

Indian hedgehog is one of the three mammalian homologues of the *D. melanogaster* segment polarity gene, *Hedgehog* (Jeong and McMahon 2002). The *Hedgehog* gene family encodes a group of secreted signaling molecules that are essential for growth and patterning of many different body parts of vertebrate and invertebrate embryos (Ingham and McMahon 2001). These molecules are processed after translation by internal cleavage to generate an amino-terminal fragment and a carboxy-terminal fragment with the subsequent addition of cholesterol at the C-terminus of the amino-terminal fragment. This amino-terminal fragment has all the known signaling activity, whereas the carboxy-terminal fragment is responsible for the autoproteolytic process (Lee et al. 1994; Porter et al. 1995).

The precise regulation of proliferation and hypertrophic differentiation of chondrocytes in the growth plate is critical for balancing longitudinal growth and ossification of bones (Erlebacher et al. 1995). Several lines of

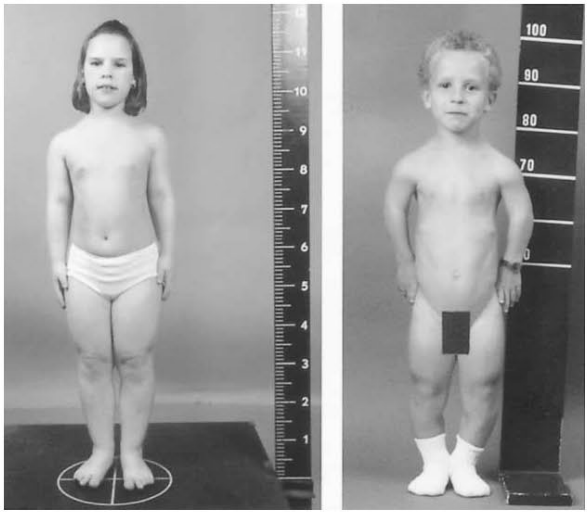

Figure 1 Clinical variability illustrated by two affected individuals. *Left panel,* Patient VII-4 at age 10.5 years. Note mild disproportionate short stature with brachydactyly. *Right panel,* Short-limb dwarfism with narrow thorax and genu varum in patient IX-2 at age 9 years.

Table 1

Two-Point LOD Scores for Linkage of the ACFD Locus to Chromosome 2q35-q36

		Combined LOD Score at $\theta =$					Family 1		Family 2		Families 1 and 2	
Marker	Position[a]	.00	.01	.05	.10	.30	Z_{max}	θ	Z_{max}	θ	Z_{max}	θ
D2S2382	213.49	−∞	7.01	6.81	5.96	2.03	3.24	0	3.89	.05	7.09	.02
D2S2248	214.71	8.02	7.80	6.92	5.789	1.66	1.90	0	6.12	0	8.02	0
D2S1371	215.25	6.32	6.11	5.28	4.26	.97	1.40	0	4.92	0	6.32	0
D2S2151	218.45	5.02	4.85	4.17	3.34	.74	.63	0	4.40	0	5.02	0
D2S163	218.45	−∞	10.85	10.62	9.72	4.98	2.02	0	8.89	.01	10.92	.02

[a] The position is given in centiMorgans according to the Marshfield map.

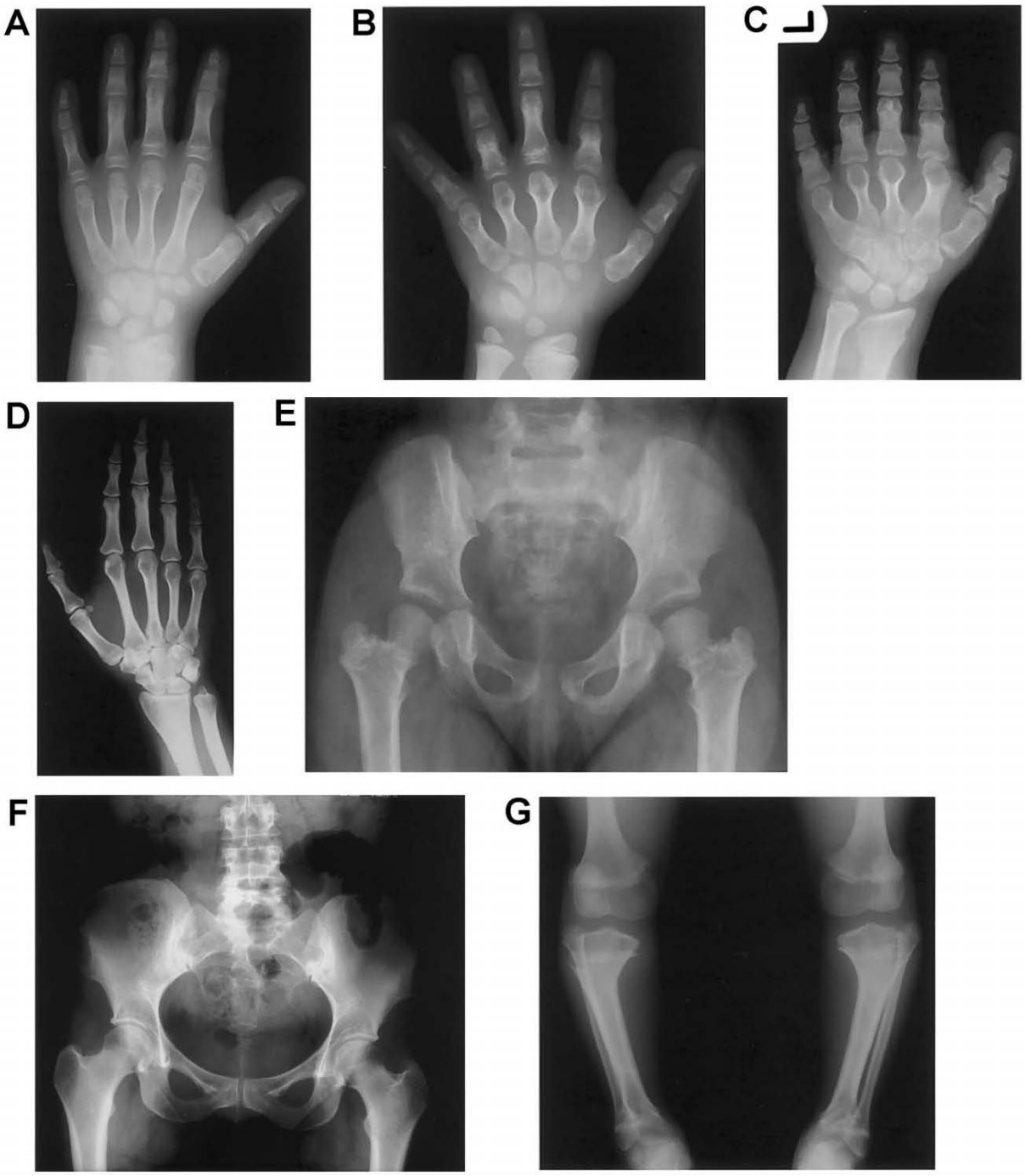

Figure 2 Most characteristic radiographic abnormalities in the affected individuals. *A–C,* Radiographs of the left hand. *A,* Cone-shaped epiphyses in the thumbs and the middle and distal phalanges of digits II–V of patient VII-4 at age 9.5 years. *B,* Shortening of the tubular bones more pronounced in patient IX-2 at age 11 years. Note the remnants of cone-shaped epiphyses and the fused "tear-drop" metacarpal epiphyses. *C,* Severe brachydactyly in patient IX-1 at age 14 years. Note complete epimetaphyseal fusion of metacarpals and phalanges. *D,* Radiograph of the right hand of parent VI-1, showing no obvious signs of BDA1. *E,* Radiograph of the pelvis in patient VII-4 at age 6 years, showing coxa vara with egg-shaped femoral head and very short femoral neck after epimetaphyseal fusion. *F,* Normal radiograph of the pelvis in parent VI-1, with no evidence of a premature fusion of the proximal femoral growth plate (normal femoral head and neck). *G,* Radiograph of the lower limbs in patient IX-2 at age 11 years. Varus deformity of the tibiae with proximal and distal premature epimetaphyseal fusion is most likely the result of cone-shaped epiphyses. Note the voluminous distal femoral epiphyses and the proximal overgrowth of the fibulae.

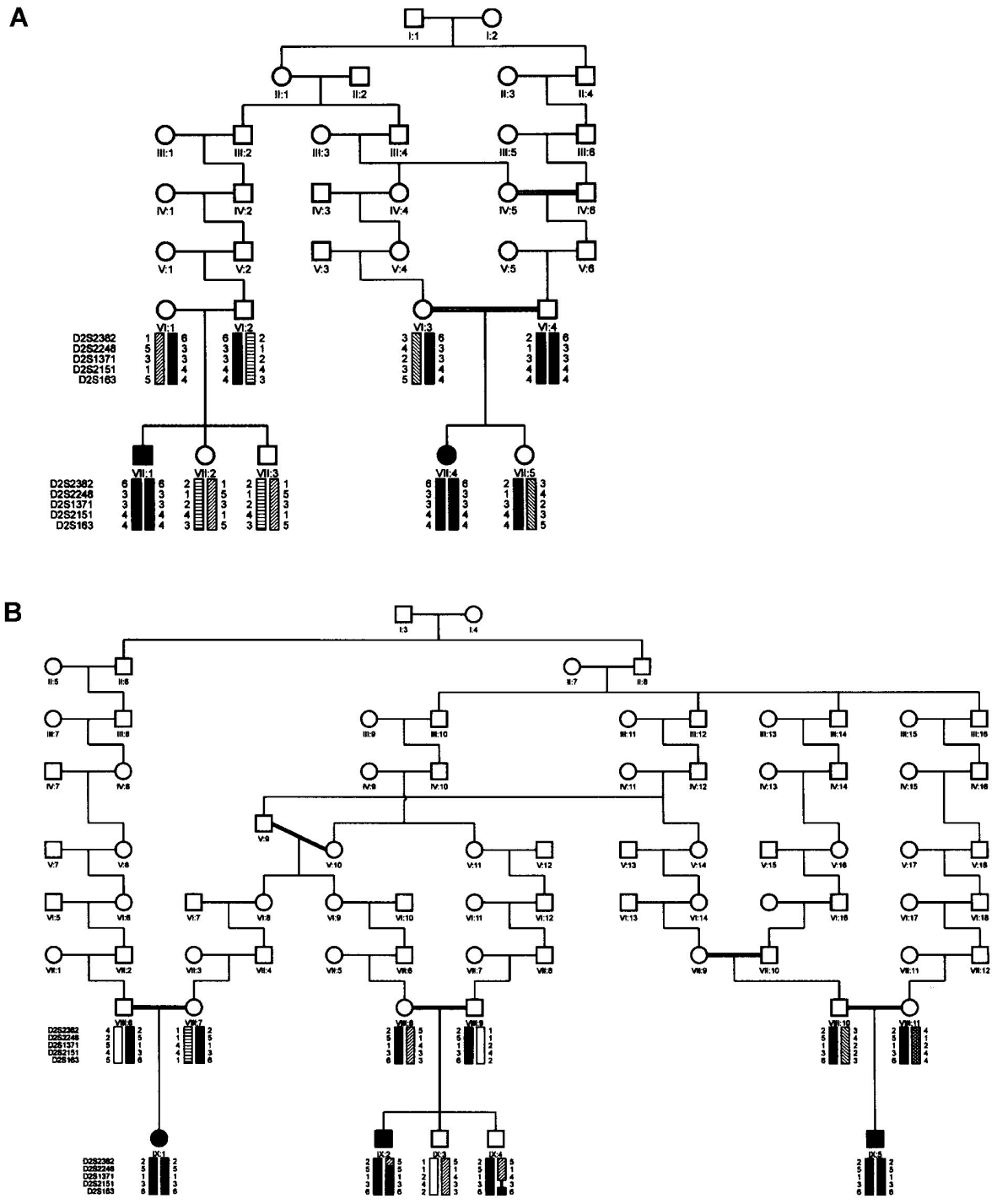

Figure 3 Pedigrees of (Belgian) family 1 (*A*) and (Dutch) family 2 (*B*). The genotypes of five markers within the linked region on chromosome 2 are shown. The haplotype cosegregating with the disorder is indicated with a black bar.

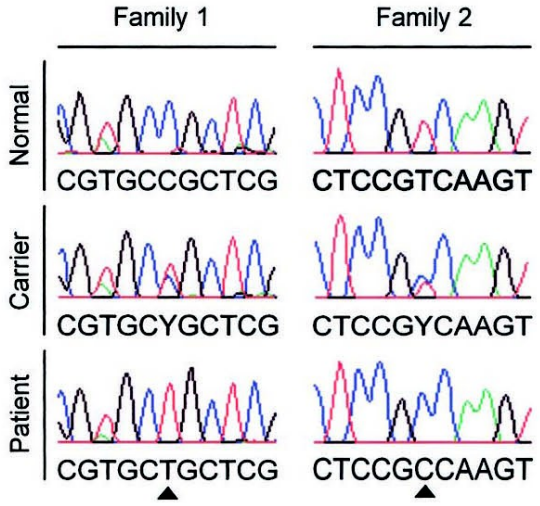

Figure 4 Sequence analysis of *IHH* in both families. The normal (*top*), heterozygous (*middle*), and homozygous mutant (*bottom*) sequences are shown. The 137C→T mutation is presented on the left, and the 569T→C mutation is shown on the right (*triangles*).

evidence indicate that Ihh signaling controls growth of bones by coordinating chondrocyte proliferation and differentiation (Vortkamp et al. 1996; Long et al. 2001). The regulation of differentiation is indirectly mediated through the production of parathyroid hormone–related peptide (PTHrP). By stimulating PTHrP production in the periarticular growth plate, Ihh delays the switch from proliferation to differentiation. In this way, Ihh determines the rate and site in the growth plate at which hypertrophic differentiation occurs (Karp et al. 2000). We postulate that the recessive mutations, identified in our patients with ACFD, cause an increased rate of chondrocyte differentiation by diminishing Indian hedgehog signaling in the growth plate. This increased rate of differentiation is radiographically reflected by the appearance of CSE and subsequent premature closure of the growth plate, with shortening of the bone as a consequence. The cone-shaped configuration of the epiphyses may indicate that this increased rate of differentiation is most pronounced or starts earlier at the center of the physis. There is no evidence for a concentration gradient of IHH and/or PTHrP within a certain zone of the growth plate that could explain an earlier fusion at the center. However, in normal conditions, the knee growth plates seem to close earlier in their central portion than in their peripheral portion (Sasaki et al. 2002). Of note are also the presence of CSE in other skeletal dysplasias affecting the balance between chondrocyte proliferation and differentiation in the growth plate (e.g., cartilage hair hypoplasia [MIM 250250]) and the appearance of CSE after infantile meningococcemia (Patriquin et al. 1981; Grogan et al. 1989; Giedion 1998).

Radiographic evaluation of the heterozygous parents of patients VII-1, VII-4 (family 1), and IX-2 (family 2) does not reveal obvious signs of BDA1 (fig. 2*D*). None of these parents show absent or rudimentary middle phalanges or middle phalanges fused with the distal phalanges. Mild shortening of middle phalanges II–IV (up to 2.5 SD below the mean) and severe shortening of the middle phalanx V (up to 5 SD below the mean) are observed only in the parents of patients VII-1 and VII-4. The parents of patient IX-2 show only relative shortening (>2 SD below the mean) of the metacarpals and proximal phalanges (data not shown). In addition, both parents of patients VII-1 and VII-4 (family 1) show normal radiographs of the pelvis (fig. 2*F*).

A similar situation, where heterozygotes of the recessive mutations do not exhibit the dominant phenotype, has been observed in brachydactyly type B (BDB [MIM 113000]) and Robinow syndrome (MIM 268310). Heterozygous mutations flanking the intracellular tyrosine

```
                                                                                *     *
HH Drome     CGPGRG-LG- -RHRARN-LY PLVLKQTIPN LSEYTNSASG PLEGVIRRDS PKFKDLVPNY NRDILFRDEE GTGADGLMSK RCKEKLNVLA
IHH Mouse    .....V.V.S R.RPP.K..V ..AY..FS.. VP.K.LG... RY..K.A.S. ER..E.T... .P..I.K... N....R..TQ ...DR..S..
IHH Brare    .......Y.. K.RTP.K..T ..AY..FS.. VA.K.LG... RY..KVTPS. ER..E.T... .P..I.K... N....RM.TQ ...D...S..
DHH Mouse    ......PV.. R.RYV.KQ.V ..LY..FV.S MP.R.LG... .A..RVT.G. ER.R...... .P..I.K... NS...R..TE ....RV.A..
DHH2 Xenla   ......PV.G R.RYM.R..V ..LY..FV.. VP.K.LG... KS..K...G. ER.IK..... .P..I.K... N....R..TE ...DRV.A..
TWHH Brare   .......Y.. K.RHPKK..T ..AY..F... VA.K.LG... KY..K.T.N. ER..E.I... .P..I.K... N.N..R..T. ...D...S..
AmphiHH      ....GR.F.. R.RHP.K..T ..F.Y..QM.A V..N.FG... LFN.R.T... ER.HT.KQ.F .T..I.K... K....RF.TQ ...D...A..

                  *
HH Drome     YSVMNEWPGI RLLVTESWDE DYHHGQESLH YEGRAVTIAT SDRDQSKYGM LARLAVEAGF DWVSYVSRRH IYCSVKSDSS ISSHVHG
IHH Mouse    I....Q...V K.R...G... .G..SE.... ......D.T. ....RN...L .......... ...Y.E.KA. VH.....EH. AAAKTG.
IHH Brare    I....L...V ..R...G... .GL.SE.... ......D.T. ....RN..R. .......... ...Y.E.KG. VH.....EH. VAAKTG.
DHH Mouse    IA...M...V ..R...G... .G..A.D... .....LD.T. ....RN...L .......... ...Y.E..N. .HV...A.N. LAVRAG.
DHH2 Xenla   I....M...L K.R...G... .G..AHD... .....LD.T. ....RN.... .......... ...Y.E.KA. .HV..NT.N. LGVRSG.
TWHH Brare   I....H...V K.R...G... .G..LE.... ......D.T. ....K..... .S........ ...Y.E.KA. .H....AEN. VAAKSG.
AmphiHH      I....Q.E.V K.R...G... .GF.TE.... ......D.T. ....RT.... .......... ...Y.E.KA. .H....AE.D TTATQG.
```

Figure 5 Cross-species alignment of the amino-terminal signaling domain of several Hedgehog homologues: HH Drome, IHH Mouse, IHH Brare, DHH Mouse, DHH2 Xenla, TWHH Brare, and AmphiHH (GenBank accession numbers Q02936, P97812, Q98862, Q61488, Q91611, Q90419, and CAA74169.1). Amino acids matching the HH Drome sequence are represented as dots. ACFD mutations are indicated with a gray bar and BDA1 mutations with an asterisk.

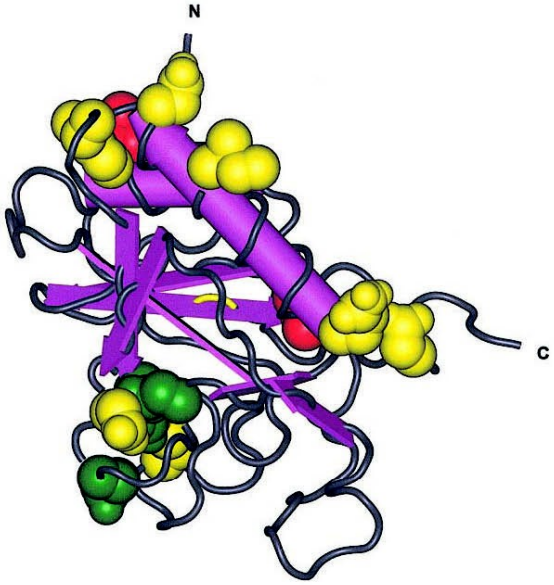

Figure 6 Tertiary structure of the amino-terminal signaling domain of mouse Shh with the indication of the corresponding location of the different missense mutations in human IHH and SHH (Human Gene Mutation Database). ACFD mutations (IHH) are represented in red, BDA1 mutations (IHH) in green, and HPE3 mutations (SHH) in yellow. The cluster in the middle (*bottom*) contains the four BDA1 mutations (E95K, D100E, D100N, and E131K) and two HPE3 mutations (D93V and H140P). The cluster at the carboxy-terminal end (*middle right*) contains one ACFD mutation (V190A) and two HPE3 mutations (Q105H and E193Q). The cluster at the amino-terminal end (*top*) contains one ACFD mutation (P46L) and four HPE3 mutations (I116F, N120K, W122G, and W122R).

kinase domain of *ROR2* cause BDB (Schwabe et al. 2000). Homozygous *ROR2* mutations scattered throughout the entire coding region cause Robinow syndrome. However, heterozygous carriers of Robinow syndrome do not seem to have BDB (Afzal et al. 2000; Schwabe et al. 2000; van Bokhoven et al. 2000). A possible explanation may be that Robinow mutations are loss-of-function mutations with no phenotypic consequences in carriers, whereas BDB mutations exert a dominant effect. In contrast to these observations, loss-of-function mutations of *GDF5* cause brachydactyly type C (BDC [MIM 113100]) in the heterozygous state and Grebe dysplasia (MIM 200700), an autosomal recessive acromesomelic dysplasia, in the homozygous state, with radiographic features of BDC in the heterozygous carriers of Grebe mutations (Costa et al. 1998; Everman et al. 2002; Faiyaz-Ul-Haque et al. 2002).

These studies together with our data indicate that the phenotypic outcome of mutations in genes involved in brachydactyly is not only dependent on the homozygous versus heterozygous state but also on the location and nature of the mutation. The mutations in *IHH*, causing either BDA1 or ACFD, are both missense mutations. However, their precise locations within the amino-terminal signaling domain differ. To compare the locations of different Hedgehog mutations, the crystal structure of the amino-terminal domain of mouse Shh (1VHH [Molecular Modeling DataBase accession number 3860]) can be used because of the high similarity between human IHH and mouse Shh (GenBank accession number Q62226) (Hall et al. 1995) (fig. 6). The mutations reported in BDA1 (fig. 6, *green*) are predicted to be clustered together on one side of the protein, whereas the ACFD (fig. 6, *red*) mutations seem to be located at the other side, in regions where mutations in *SHH* (GenBank accession number Q15465) have been reported to cause holoprosencephaly (HPE3 [MIM 142945]) (fig. 6, *yellow*). In addition, the P46L mutation is located in a region important for binding of the sonic hedgehog protein to its receptor Patched (Fuse et al. 1999). In conclusion, this study indicates that mutations in *IHH* can cause not only BDA1 but also a more severe skeletal dysplasia with short-limb dwarfism (ACFD). Additional in vitro and in vivo experiments are necessary to investigate the consequences of the different (BDA1 and ACFD) mutations on Indian hedgehog signaling in the growth plate.

Acknowledgments

We are indebted to the families for their interest and cooperation. Special thanks to M. L. Duyts for her excellent technical assistance in preparing the radiographic illustrations. We are grateful to Mike Briggs for critical review of the manuscript. This study is supported, in part, by the Fund for Scientific Research, Flanders, with a mandate "fundamental clinical research" to G.M., and by the Fifth Framework of the specific research and technological development program "Quality of Life and Management of Living Resources" of the European Commission (Contract QLG1-CT-2001-02188) to J.H., A.D.P., and G.M.

Electronic-Database Information

Accession numbers and URLs for data presented herein are as follows:

GenBank, http://ncbi.nlm.nih.gov/Genbank/ (for HH Drome [accession number Q02936], IHH Mouse [accession number P97812], IHH Brare [accession number Q98862], DHH Mouse [accession number Q61488], DHH2 Xenla [accession number Q91611], TWHH Brare [accession number Q90419], AmphiHH [accession number CAA74169.1], IHH Human [accession number Q14623], SHH Human [accession number Q15465], and SHH Mouse [accession number Q62226])

Human Gene Mutation Database, http://archive.uwcm.ac.uk/uwcm/mg/hgmd0.html

Marshfield Map, http://research.marshfieldclinic.org/genetics/Map_Markers/maps/IndexMapFrames.html

Molecular Modeling DataBase, http://ncbi.nlm.nih.gov/Structure/ (for 1VHH [accession number 3860])

Online Mendelian Inheritance in Man (OMIM), http://www.ncbi.nlm.nih.gov/Omim/ (for BDA1, BDB, BDC, Robinow syndrome, Grebe dysplasia, and HPE3)

References

Afzal AR, Rajab A, Fenske CD, Oldridge M, Elanko N, Ternes-Pereira E, Tuysuz B, Murday VA, Patton MA, Wilkie AO, Jeffery S (2000) Recessive Robinow syndrome, allelic to dominant brachydactyly type B, is caused by mutation of ROR2. Nat Genet 25:419–422

Costa T, Ramsby G, Cassia F, Peters KR, Soares J, Correa J, Quelce-Salgado A, Tsipouras P (1998) Grebe syndrome: clinical and radiographic findings in affected individuals and heterozygous carriers. Am J Med Genet 75:523–529

Erlebacher A, Filvaroff EH, Gitelman SE, Derynck R (1995) Toward a molecular understanding of skeletal development. Cell 80:371–378

Everman, DB, Bartels CF, Yang Y, Yanamandra N, Goodman FR, Mendoza-Londono JR, Savarirayan R, White SM, Graham JM Jr, Gale RP, Svarch E, Newman WG, Kleckers AR, Francomano CA, Govindaiah V, Singh L, Morrison S, Thomas JT, Warman ML (2002) The mutational spectrum of brachydactyly type C. Am J Med Genet 112:291–296

Faiyaz-Ul-Haque M, Ahmad W, Wahab A, Haque S, Azim AC, Zaidi SH, Teebi AS, Ahmad M, Cohn DH, Siddique T, Tsui LC (2002) Frameshift mutation in the cartilage-derived morphogenetic protein 1 (CDMP1) gene and severe acromesomelic chondrodysplasia resembling Grebe-type chondrodysplasia. Am J Med Genet 111:31–37

Fuse N, Maiti T, Wang B, Porter JA, Hall TM, Leahy DJ, Beachy PA (1999) Sonic hedgehog protein signals not as a hydrolytic enzyme but as an apparent ligand for patched. Proc Natl Acad Sci USA 96:10992–10999

Gao B, Guo J, She C, Shu A, Yang M, Tan Z, Yang X, Guo S, Feng G, He L (2001) Mutations in IHH, encoding Indian hedgehog, cause brachydactyly type A-1. Nat Genet 28:386–388

Giedion A (1998) Phalangeal cone-shaped epiphyses of the hand: their natural history, diagnostic sensitivity, and specificity in cartilage hair hypoplasia and the trichorhinophalangeal syndromes I and II. Pediatr Radiol 28:751–758

Grogan DP, Love SM, Ogden JA, Millar EA, Johnson LO (1989) Chondro-osseous growth abnormalities after meningococcemia: a clinical and histopathological study. J Bone Joint Surg Am 71:920–928

Hall TM, Porter JA, Beachy PA, Leahy DJ (1995) A potential catalytic site revealed by the 1.7-A crystal structure of the amino-terminal signalling domain of Sonic hedgehog. Nature 378:212–216

Ingham PW, McMahon AP (2001) Hedgehog signaling in animal development: paradigms and principles. Genes Dev 15: 3059–3087

Jeong J, McMahon AP (2002) Cholesterol modification of hedgehog family proteins. J Clin Invest 110:591–596

Karp SJ, Schipani E, St-Jacques B, Hunzelman J, Kronenberg H, McMahon APBR (2000) Indian hedgehog coordinates endochondral bone growth and morphogenesis via parathyroid hormone related-protein-dependent and -independent pathways. Development 127:543–548

Kindblom JM, Nilsson O, Hurme T, Ohlsson C, Savendahl L (2002) Expression and localization of Indian hedgehog (Ihh) and parathyroid hormone related protein (PTHrP) in the human growth plate during pubertal development. J Endocrinol 174:R1–R6

Lander ES, Botstein D (1987) Homozygosity mapping: a way to map human recessive traits with the DNA of inbred children. Science 236:1567–1570

Lathrop GM, Lalouel JM (1984) Easy calculations of LOD scores and genetic risks on small computers. Am J Hum Genet 36:460–465

Lee JJ, Ekker SC, von Kessler DP, Porter JA, Sun BI, Beachy PA (1994) Autoproteolysis in hedgehog protein biogenesis. Science 266:1528–1537

Long F, Zhang XM, Karp S, Yang Y, McMahon AP (2001) Genetic manipulation of hedgehog signaling in the endochondral skeleton reveals a direct role in the regulation of chondrocyte proliferation. Development 128:5099–5108

McCready ME, Sweeney E, Fryer AE, Donnai D, Baig A, Racacho L, Warman ML, Hunter AG, Bulman DE (2002) A novel mutation in the IHH gene causes brachydactyly type A1: a 95-year-old mystery resolved. Hum Genet 111:368–375

Mortier GR, Kramer PPG, Giedion A, Beemer FA (2003) Acrocapitofemoral dysplasia: an autosomal recessive skeletal dysplasia with cone-shaped epiphyses in hands and hips. J Med Genet 40:201–207

Patriquin HB, Trias A, Jecquier S, Marton D (1981) Late sequelae of infantile meningococcemia in growing bones of children. Radiology 141:77–82

Porter JA, von Kessler DP, Ekker SC, Young KE, Lee JJ, Moses K, Beachy PA (1995) The product of hedgehog autoproteolytic cleavage active in local and long-range signalling. Nature 374:363–366

Sasaki T, Ishibashi Y, Okamura Y, Toh S, Sasaki T (2002) MRI evaluation of growth plate closure rate and pattern in the normal knee joint. J Knee Surg 15:72–76

Schwabe GC, Tinschert S, Buschow C, Meinecke P, Wolff G, Gillessen-Kaesbach G, Oldridge M, Wilkie AOM, Kömec R, Mundlos S (2000) Distinct mutations in the receptor tyrosine kinase gene *ROR2* cause brachydactyly type B. Am J Hum Genet 67:822–831

St-Jacques B, Hammerschmidt M, McMahon AP (1999) Indian hedgehog signaling regulates proliferation and differentiation of chondrocytes and is essential for bone formation. Genes Dev 13:2072–2086

van Bokhoven H, Celli J, Kayserili H, van Beusekom E, Balci S, Brussel W, Skovby F, Kerr B, Percin EF, Akarsu N, Brunner HG (2000) Mutation of the gene encoding the ROR2 tyrosine kinase causes autosomal recessive Robinow syndrome. Nat Genet 25:423–426

Vortkamp A, Lee K, Lanske B, Segre GV, Kronenberg HM, Tabin CJBR (1996) Regulation of rate of cartilage differentiation by Indian hedgehog and PTH-related protein. Science 273:613–622

Paper 2

Hellemans and Mortier. Book chapter in Inborn Errors of Development

Role of IHH in skeletal development and dysplasias. Chapter for the second edition of CJ Epstein, RP Erickson, A Wynshaw-Boris (eds.) *Inborn Errors of Development.* Oxford University Press, New York. (submitted)

Brachydactyly type A1 (BDA1) and acrocapitofemoral dysplasia (ACFD) are two rare skeletal dysplasias with brachydactyly as a common characteristic. Whereas hand abnormalities are the only defects in BDA1 patients, individuals with ACFD have a disproportionate short stature resulting from premature epimetaphyseal fusion. Homozygous and heterozygous missense mutations in the signaling domain of indian hedgehog (IHH) are responsible for ACFD and BDA1, respectively. The heterozygous carriers of an ACFD mutation do, however, not show any sign of brachydactyly. IHH is a secreted signaling molecule essential for the regulation of endochondral ossification. It controls chondrocyte proliferation and differentiation, and determines the site of bone collar formation. It is not yet known how the different IHH missense mutations affect endochondral ossification to result in ACFD or BDA1.

Indian hedgehog (IHH) and the growth plate

The first steps in skeletal morphogenesis involve the induction of undifferentiated mesenchyme and its differentiation into condensed mesenchyme. In the human skeleton, only the membrane bones of the skull and part of the clavicle are formed by direct ossification of condensed mesenchyme (intramembranous ossification). For the large majority of bones, bone formation and growth proceeds through an intermediate cartilaginous template or anlage in a process called endochondral ossification (*Seeley, Anatomy and Physiology – McGraw-Hill*). These cartilaginous models are formed by further differentiation of condensed mesenchymal cells into chondrocytes that produce hyaline cartilage instead of mesenchymal matrix. In the center of these cartilaginous templates, chondrocytes will form columns of proliferating cells and subsequently enlarge to become hypertrophic chondrocytes, producing type X collagen. In parallel with the cellular differentiation, the extracellular cartilage matrix will be altered through the actions of carbonic anhydrase and alkaline phosphatase. Finally, the hypertrophic chondrocytes disintegrate and die with simultaneous calcification of the modified matrix. The newly formed spaces with calcified cartilage are invaded by periosteal blood vessels and osteogenic cells, which soon differentiate into osteoblasts (*Ballock 2003*). The latter deposit a bony matrix on the calcified cartilage, resulting in the formation of the primary center of ossification. This ossification center is formed within the central portion of the cartilage template and will expand both proximally and distally toward the ends (epiphyses) of the developing bone. Also, secondary ossification centers start appearing in the epiphyseal regions. As these ossifications centers enlarge, they replace almost all the cartilage by bone except, firstly, for a layer of specialized hyaline cartilage at the joint surfaces (articular cartilage) and, secondly, a thicker zone between the diaphysis and the epiphysis, representing the growth plate (*Seeley, Anatomy and Physiology – McGraw-Hill*).

The growth plate is a specialized and highly organized zone of hyaline cartilage responsible for linear skeletal growth. It is a very dynamic tissue with a high cellular turn-over. It forms a transition region between cartilage and bone and is divided into different zones, reflecting the several stages of chondrocyte differentiation (Fig. 22-1). In each zone a different pattern of gene expression is observed (*Provot 2005*). The reserve zone, containing resting chondrocytes, is located farthest from the center of the growing bone where it merges into the epiphyseal cartilage. In the proliferative zone, clusters or columns of proliferating flattened chondrocytes are found. These columns are oriented parallel to the axis of growth and separated from each other by septa of interterritorial matrix. The hypertrophic zone can be divided into areas of prehypertrophic, hypertrophic and terminally differentiated chondrocytes. Mineralization of the cartilage matrix (provisional calcification) starts in the hypertrophic zone. About every 24 hours, the

hypertrophic zone shows complete cellular turn-over. At the lower end of the growth plate, near the zone of primary spongiosa, the terminal hypertrophic chondrocytes and the surrounding matrix become invaded by metaphyseal blood vessels. This invasion results in degradation and degeneration of the matrix and apoptosis of the terminally differentiated chondrocytes. The remaining cartilaginous cores will serve as templates for the deposition of bone matrix (osteoid) by osteoblasts. This process of endochondral ossification goes on until the closure of the growth plate at the end of puberty which will result in a stop of linear growth of the involved bone.

A well-controlled balance between chondrocyte proliferation and differentiation is important for proper functioning of the growth plate (*van der Eerden 2003, Kronenberg 2003*). Several genes are playing an important role in regulating and maintaining this balance. One of them is the gene coding for the Indian hedgehog (IHH) protein. IHH is one of the three mammalian homologues of the *D. melanogaster* segment polarity gene, Hedgehog. The Hedgehog gene family encodes a group of secreted signaling molecules that are essential for growth and patterning of many different body parts of vertebrate and invertebrate embryos. As a common feature, these proteins are processed by internal cleavage to generate an amino-terminal fragment (HH-N) with all the known signaling activity, and a C-terminal fragment (HH-C) that is responsible for the autoproteolytic cleavage. The addition of cholesterol and palmitate to the HH-N fragment affects the spatial distribution and signaling activity of hedgehog proteins (*Porter et al. 1996; Chamoun et al. 2001*). Processing of and signaling by these hedgehog proteins have been reviewed comprehensively by Michael Cohen (*Cohen 2003*).

In the growth plate, IHH is mainly secreted by the prehypertrophic chondrocytes (*Vortkamp et al. 1996; Minina et al. 2002*). A series of experiments have revealed an important regulatory role of IHH in the process of endochondral ossification. Several lines of evidence indicate that IHH regulates chondrocyte proliferation, chondrocyte hypertrophic differentiation and bone formation.

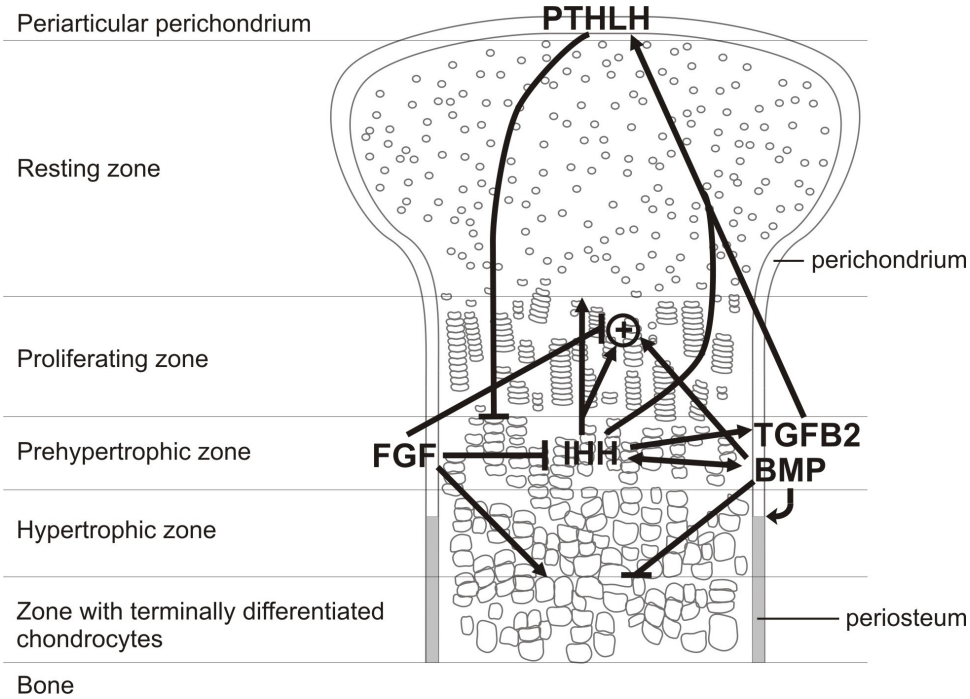

Fig. 22-1 Schematic representation of the growth plate with indication of the different zones. The effects of IHH, BMP and FGF signaling are shown by pointing arrows in case of stimulation and by blocking arrows in case of inhibition. Arrows directed to the horizontal lines (separating the different zones) indicate the effect on the transition from one zone to the other. The division rate of the chondrocytes in the proliferative zone is shown by the + sign.

Pioneering work by Vortkamp et al. demonstrated that IHH induces the expression of PTHLH (previously known as PTHrP) in the periarticular perichondrium and that this hormone inhibits the differentiation from columnar proliferating into prehypertrophic chondrocytes (*Lanske et al. 1996; Vortkamp et al. 1996*). In this way, IHH and PTHLH function in a feedback loop that regulates the rate of chondrocyte differentiation in the growth plate (Fig. 22-1). When chondrocytes become prehypertrophic they express IHH that upregulates the expression of PTHLH. PTHLH diffuses to the proliferative zone where it limits differentiation of additional proliferating cells into prehypertrophic chondrocytes. As prehypertrophic chondrocytes continue to differentiate they cease to express IHH, resulting in decreased PTHLH production and a consequent increase in chondrocyte differentiation (*Vortkamp et al. 1996*). In this way a constant pool of prehypertrophic chondrocytes is maintained in the growth plate.

It has, however, not been resolved how the IHH signal is propagated from the prehypertrophic chondrocytes to the periarticular region to upregulate the expression of PTHLH. Both IHH dependent secondary signals and direct long range IHH signaling have been proposed to activate PTHLH expression. Alvarez et al. provided evidence for TGFβ2 mediated effects of hedgehog on PTHLH expression and hypertrophic differentiation. They found that IHH stimulates TGFβ2 and TGFβ3 expression in the perichondrium and that the perichondrium is required to mediate the effects of hedgehog on hypertrophic differentiation. This effect was found to be dependent on TGFβ signaling in the perichondrium, and more specifically on the production of TGFβ2 (*Alvarez et al. 2002*). On the other hand, several experiments have also indicated that IHH can act as a long range morphogen, directly activating the expression of PTHLH. Although hydrophobic modification by cholesterol and palmitate suggested tethering of hedgehog to the plasma membrane, hedgehog was found to form freely diffusible multimers capable of mediating long-range signaling (*Zeng et al. 2001*). Experiments with Ext1 gene trap mice indicated that the signaling range of hedgehogs is regulated by heparin sulphate and suggested that IHH directly activates PTHLH expression to regulate chondrocyte proliferation (*Koziel et al. 2004*).

In addition to the effects of IHH via the aforementioned feedback loop, IHH regulates endochondral ossification in PTHLH independent ways as well. As a direct effect, IHH stimulates chondrocyte proliferation (*St-Jacques et al. 1999; Karp et al. 2000*) and induces the differentiation from periarticular chondrocytes into flat, columnar proliferating chondrocytes (*Kobayashi et al. 2005*). It also interacts with a number of additional signaling molecules and growth factors to create a complex regulatory network (Fig. 22-1). BMPs and FGFs were found to have antagonistic effects on bone development (*Minina et al. 2002*). BMPs stimulate chondrocyte proliferation, induce IHH secretion and inhibit terminal chondrocyte differentiation whereas FGFs reduce chondrocyte proliferation, inhibit IHH secretion and stimulate terminal chondrocyte differentiation.

Finally, IHH is also important in determining the site of bone collar formation in the adjacent perichondrium. Thus, by regulating chondrocyte proliferation and differentiation as well as bone formation, IHH couples chondrogenesis to osteogenesis in endochondral bone development (*Chung et al. 2001*).

Acrocapitofemoral dysplasia and brachydactyly type A1

Acrocapitofemoral dysplasia (ACFD, MIM #607778) and brachydactyly type A1 (BDA1, MIM #112500) are two distinct skeletal dysplasias that share brachydactyly as a common feature. BDA1 was first identified by Farabee in 1903, and has the distinction of being the first condition in man to be interpreted as a mendelian dominant trait (*Farabee 1903*). ACFD, on the other hand, was described exactly hundred years later (*Mortier et al. 2003*). The Nosology and Classification of Genetic Skeletal Disorders (2006 revision) classifies ACFD and BDA1 in groups 14 (acromelic dysplasias) and 34 (brachydactylies), respectively (*Superti-Furga 2007*).Acrocapitofemoral dysplasia is an autosomal recessive skeletal dysplasia characterized clinically by short stature with short limbs and radiographically by cone-shaped epiphyses, mainly in hands and hips. The condition was for the first time

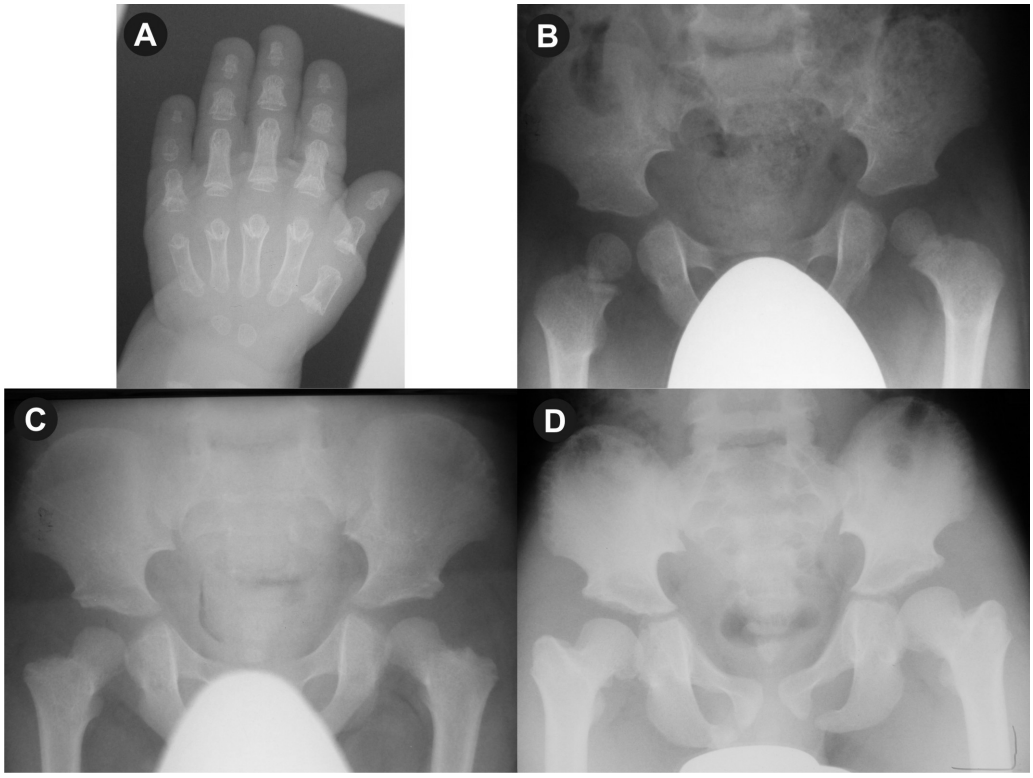

Fig. 22-2 Anteroposterior radiographs of hands and hips in acrocapitofemoral dysplasia. (A) Image of the left hand at the age of 3y5m showing cone shaped epiphyses in all phalanges and metacarpals except for the proximal phalanx of digits III and IV. (B) Image of the hips at the age of 22 months. The proximal femoral epiphysis starts to develop a small, thorn-like, outgrowth pointing to the centre of the femoral neck, resembling a tear drop (most visible on the right side). (C) Image of the hips at the age of 3y8m showing premature epimetaphyseal fusion of the proximal femoral growth plate. (D) Image of the hips at the age of 9y3m showing the abnormally shaped femoral head and hypoplastic femoral neck.

delineated in two consanguineous families of Belgian and Dutch origin (*Mortier et al. 2003*). The phenotype in these families showed some resemblance to the condition reported in a 12 year-old-boy by Hoeffel et al. (*Hoeffel et al. 1987*). The short stature in ACFD is usually of postnatal onset and of variable degree. Only 5 affected individuals have been reported so far with heights ranging from 2.3 to 8.6 standard deviations below the mean (*Paper 1: Hellemans et al. 2003; Mortier et al. 2003*). Shortening of the limbs is most pronounced in the acromelic segments (brachydactyly). Affected subjects do not exhibit associated congenital anomalies and are of normal intelligence. The head circumference is usually above the mean and severe cases show genu vara. Narrow thorax with a pectus deformity can be observed. The diagnosis relies on the recognition of the typical radiographic abnormalities in the hands and hips that usually disappear in late childhood. In the hands, cone-shaped epiphyses become apparent at an early age (around 2 years of age) and are mainly observed in the middle phalanges, the distal phalanges and all tubular bones of the thumb (Fig. 22-2 A). They can also be present in the proximal phalanges and metacarpals. The process of coning is followed by a complete epimetaphyseal fusion, the moment at which the cone-shaped epiphysis disappears and the growth plate closes. The onset of this closure depends on the bone involved but is usually observed before the age of 10 years in case of the distal and middle phalanges.

In the hips a similar process takes place. Around the age of 2 years the proximal femoral epiphysis starts to develop a small, thorn-like outgrowth pointing to the centre of the femoral neck, resembling a tear drop and to some extent reminiscent of a cone-shaped epiphysis (Fig. 22-2 B). This is followed by a premature epimetaphyseal fusion of the proximal femoral growth plate resulting in an

Fig. 22-3 Radiograph of both hands in an individual with brachydactyly type A1 caused by the p.Arg128Glu IHH mutation. Note the short middle phalanges of digits II to V and short metacarpal of digit I.

abnormal (egg-shaped) femoral head attached to a very short femoral neck (Fig. 22-2 C and D). Cone-shaped epiphyses can also be observed in the shoulders, knees and ankles but are less characteristic and not always present. Because the most distinguishing and constant radiographic anomalies were observed in the hands ("acra") and the hips (capital femoral epiphyses), this skeletal dysplasia was named acrocapitofemoral dysplasia.

The brachydactylies are a group of heritable skeletal disorders mainly affecting the tubular bones of the hands. They were initially classified in 5 different classes (A-E), with 3 subtypes (A1-A3) in the first class (*Bell 1951*). Brachydactyly type A1 (BDA1), also known as the Farabee-subtype brachydactyly, is mainly characterized by short middle phalanges of most digits and short proximal phalanx of the thumb (Fig. 22-3). In severe cases the middle phalanges may be absent and shortening of the metacarpals can also be present. BDA1 shows autosomal dominant inheritance. Affected individuals are usually shorter than their unaffected relatives (*Armour et al. 2000*). BDA1 is characterized by significant inter- and intra-familial phenotypic variability (*McCready et al. 2005*).

Mutations in Indian Hedgehog are the cause of acrocapitofemoral dysplasia and brachydactyly type A1

To unravel the genetic defect causing BDA1, a genome wide linkage study was performed in two large Chinese families. This allowed mapping of the disease gene to an 8.1 cM interval on chromosome 2q35-q36 (Yang et al. 2000). After having excluded the possibility of disease-causing mutations in the PAX3 gene, the investigators elected to sequence *IHH*, a second candidate gene residing in the linkage interval. They were successful in identifying different heterozygous *IHH* missense mutations: c.283G>A (p.Glu95Lys), c.300C>A (p.Asp100Glu) and c.391G>A (p.Glu131Lys) in three unrelated families (*Gao et al. 2001*). Subsequently, these mutations were also found in other unrelated patients with BDA1 confirming that heterozygous missense mutations in *IHH* can cause BDA1 (*McCready et al. 2002; Giordano et al. 2003; Kirkpatrick et al. 2003; McCready et al. 2005*). Interestingly, McCready et al showed that a founder mutation was responsible for the BDA1 phenotype in the original Farabee and Drinkwater families (*McCready et al. 2005*). The same c.298G>A mutation was also identified in an Italian kindred and in families from the USA and New Zealand (*Giordano et al. 2003; McCready et al. 2005*). These studies did also reveal evidence for locus heterogeneity in BDA1. This was confirmed by the identification of a balanced translocation between chromosome 5

Disease	Mutation	Reference
ACFD	c.137C>T; p.Pro46Leu	*Hellemans et al. 2003*
BDA1	c.283G>A; p.Glu95Lys	*Gao et al. 2001*
BDA1	c.284A>G; p.Glu95Gly	*Kirkpatrick et al. 2003*
BDA1	c.298G>A; p.Asp100Asn	*McCready et al. 2002; Giordano et al. 2003; McCready et al. 2005*
BDA1	c.300C>A; p.Asp100Glu	*Gao et al. 2001*
BDA1	c.383G>A; p.Arg128Glu	Unpublished results
BDA1	c.391G>A; p.Glu131Lys	*Gao et al. 2001*
ACFD	c.569T>C; p.Val190Ala	*Hellemans et al. 2003*

Table 1 Overview of IHH mutations in BDA1 and ACFD

(5q11.2) and chromosome 17 (17q23) in a girl with the Klippel-Feil anomaly and BDA1 (*Fukushima et al. 1995*) and a subsequent linkage study showing strong evidence for a second BDA1 locus on chromosome 5. The identified linkage interval on 5p13.2-p13.3 was however not located in the neighborhood of the 5q11.2 breakpoint (*Armour et al. 2000*). Finally, exclusion of linkage to both *IHH* and the locus on chromosome 5 in another family with BDA1 suggests the existence of even a third BDA1 locus (*Kirkpatrick et al. 2003*).
The genetic basis of ACFD was unraveled after a genome wide homozygosity mapping study in the two large consanguineous families in whom the disorder was initially delineated (*Paper 1: Hellemans et al. 2003*). Linkage analysis revealed a 5 cM candidate region on chromosome 2q35-q36 with a high LOD-score of 8.02 and without evidence for a common haplotype between both families. Sequence analysis of the most appealing candidate gene IHH in the linkage interval resulted in the identification of a disease-causing mutation in both families. The two affected individuals in the Belgian family were homozygous for a c.137C>T (p.Pro47Leu) mutation whereas the three affected individuals in the Dutch family were homozygous for a c.569T>C (p.Val190Ala) mutation. Both missense mutations are located in the N-terminal signaling domain of IHH and substitute a strongly conserved amino acid residue (*Paper 1: Hellemans et al. 2003*). Since this observation, no additional ACFD patients have been reported to our knowledge.

Establishing the diagnosis

The diagnosis of both BDA1 and ACFD mainly relies on a clinical examination and radiographic evaluation, and can be confirmed by mutation analysis of the IHH gene. Patients with BDA1 mainly show brachydactyly but can also be relatively short in comparison with their unaffected first degree relatives. Radiographic evaluation is necessary to confirm the diagnosis and to distinguish it from the other forms of brachydactyly (*Spranger et al. 2002*). Short middle phalanges can be seen in many conditions but the presence of other clinical findings help to distinguish them from BDA1.
The diagnosis of ACFD should be considered in every patient with disproportionate short stature and brachydactyly. The hands are usually short with typically broad and small finger nails. Other clinical signs that favor this diagnosis are a relatively large head, narrow thorax, lumbar lordosis and genu vara. Affected individuals do not have other congenital anomalies and are of normal intelligence. The diagnosis can be confirmed when radiographs reveal cone-shaped epiphyses in hands (mainly involving the middle and distal phalanges) in association with an early closure of the proximal femoral physis. The diagnosis can be difficult in an older child when the typical changes in hands and hips have disappeared after closure of the growth plate. Review of radiographs taken at an earlier age may be important in these instances. The differential diagnosis mainly include other bone dysplasias with cone-shaped epiphyses (*Mortier et al. 2003*). However the association of cone-shaped epiphyses in the hands with premature epimetaphyseal fusion of the proximal femoral physis is to our knowledge quite specific, if not pathognomonic, for this disorder. ACFD should also not be confused with hypochondroplasia. In both conditions brachydactyly and short femoral necks can be present. However, cone-shaped epiphyses are not observed in hypochondroplasia and in addition, normal shape of the femoral heads, interpedicular narrowing in the lumbar spine and short vertebral pedicles are important findings in hypochondroplasia that are not present in ACFD.

Treatment, management and counseling

BDA1 is a benign condition with good prognosis that usually does not require any specific treatment. The condition shows autosomal dominant inheritance. Affected individuals have a 50% chance of passing on the abnormal gene to their offspring. Prenatal diagnosis is not indicated.
ACFD is a more generalized skeletal dysplasia affecting linear growth and resulting in a disproportionate short stature. Since the condition has only been described in 5 patients, not much data are available on the final adult height. One patient (patient 4 in *Mortier et al. 2003*) has already reached adult age and measures 114 cm. The two Belgian patients are now both 15 years age old and measure respectively 137.2 cm (girl)

and 147 cm (boy). Both children have been treated with LHRH analogs with the aim to delay the onset of puberty (and in this way postpone the closure of the normal growth plates allowing maximal growth). The effect of this treatment on growth is currently under investigation. ACFD is an autosomal recessive disorder. The risk for an affected child when both parents are carrier of the mutated gene, is 25% for each pregnancy. Prenatal diagnosis is only possible after identification of the genetic defect.

Animal models

The effect of IHH on endochondral ossification has been examined in a number of animal models. In experiments conducted by Vortkamp et al. viral vectors were used to misexpress IHH during cartilage formation in chicken embryos. Using this model, IHH was shown to regulate the rate of hypertrophic differentiation of chondrocytes through a negative feedback loop involving PTHLH produced in the periarticular perichondrium (*Vortkamp et al. 1996*). The first mouse model, an Ihh null mouse ($Ihh^{-/-}$), was created in 1999 (*St-Jacques et al. 1999*). Almost half of the $Ihh^{-/-}$ embryos died between 10.5 and 12.5 days postcoitum. Most of the remaining $Ihh^{-/-}$ embryos developed to term but died at birth due to respiratory failure. At birth the mutant animals showed short-limb dwarfism. Both the axial and appendicular skeleton was affected with short ribs and short, somewhat misshapen limb bones. Not all joints were formed properly. There was failure of digit segmentation and also fusion of carpal bones. Endochondral ossification was clearly more affected than intramembranous ossification. Striking was also the absence of bone formation in the mutant mice. Studies on these mice supported the existence of an IHH feedback loop controlling chondrocyte differentiation, and also illustrated the requirement of IHH for normal chondrocyte proliferation and osteoblast development (*St-Jacques et al. 1999*). The short-limb dwarfism observed in the $Ihh^{-/-}$ mice was more severe than that of PTHLH mutants, suggesting that IHH also regulates growth independent of the PTHLH-related pathway (*Karaplis et al. 1994; St-Jacques et al. 1999*).
Various combinations of $Ihh^{-/-}$, $Pthlh^{-/-}$ and constitutively active Pthr1 mouse mutants have been created to investigate the interactions between IHH and PTHLH. These studies suggest that the molecular mechanisms that inhibit chondrocyte hypertrophic differentiation are different from those stimulating chondrocyte proliferation (*Karp et al. 2000*). IHH also seems to determine the site of bone collar formation (*Chung et al. 2001*). The experiments with Ihh knock-out mice were refined by creating conditional $Ihh^{-/-}$ mice that lack Ihh specifically in cartilage (Col2a1 expressing cells). The phenotype of these mice was similar to that reported for the conventional Ihh knock-out mice, but with lesser severity. Mutant animals contained no cortical or trabecular bone and had a disorganized growth plate (*Razzaque et al. 2005*).
Although a number of model organisms have been used to investigate the effect of IHH on endochondral ossification, animal models for BDA1 or ACFD have not yet been created.

From mutation to phenotype

For several genes that play a role in skeletal development, it has now been shown that heterozygous mutations cause some form of brachydactyly whereas homozygous or compound heterozygous mutations in the same gene cause a more generalized skeletal dysplasia affecting more than just the short tubular bones of the hands. Heterozygous mutations in *ROR2*, a cell surface receptor tyrosine kinase, cause brachydactyly type B whereas homozygous mutations in the same gene result in the recessive form of Robinow syndrome, a condition characterized by short stature with acromesomelic shortening of the limbs, dysmorphic face and vertebral segmentation defects (*Afzal et al. 2000; Schwabe et al. 2000; van Bokhoven et al. 2000*). A second example involves the GDF5 gene, coding for the growth/differentiation factor 5 that belongs to the TGF-beta superfamily of growth factors. Heterozygous mutations in GDF5 have been identified in patients with brachydactyly C or brachydactyly A2 (*Polinkovsky et al. 1997; Seemann et al. 2005*). Recessive mutations in *GDF5* can cause a more severe disorder such as the Hunter-Thompson and Grebe types of acromesomelic chondrodysplasia and Du Pan syndrome (*Thomas et al. 1996; Thomas et al. 1997; Faiyaz-Ul-Haque et al. 2002*). The same observation holds for *IHH*, where heterozygous mutations cause BDA1

and homozygous mutations ACFD. Interestingly, the heterozygous parents of the ACFD patients do not show signs of BDA1 (*Paper 1: Hellemans et al. 2003*). A similar situation where heterozygotes of the recessive mutations do not exhibit the dominant phenotype has been observed for the ROR2 gene (*Afzal et al. 2000*).
Both BDA1 and ACFD mutations are missense mutations that replace conserved amino acids in the amino-terminal signaling domain of the protein. They are located in domains where disease-causing mutations in other Hedgehog proteins have been identified. When plotted on a tertiary structure of the protein, both BDA1 and ACFD mutations seem to cluster on different sides of this part of the protein (*Paper 1: Hellemans et al. 2003*). These data suggest that the ACFD and BDA1 mutations must have a different effect on the normal function of the IHH protein. Experiments in mice have indicated that homozygous loss of Ihh results in embryonic or neonatal lethality with even absence of bone formation. The phenotype of these Ihh knock-out mice is far more severe than that seen in the human recessive counterpart, ACFD, suggesting that the ACFD mutations most likely do not result in a complete loss of function of the IHH protein.
It has been clearly demonstrated that IHH plays a key role during endochondral ossification in the growth plate. It stimulates chondrocyte proliferation and inhibits, through the action of PTHLH, the rate of chondrocyte differentiation. It is therefore not surprising that mutations in *IHH* can result in a growth plate disorder with shortening of the affected bones. The cone-shaped epiphyses observed in ACFD patients may represent the radiographic sign of a disturbed balance between chondrocyte proliferation and differentiation in the growth plate due to abnormal, probably reduced IHH signaling. To test this hypothesis, functional studies addressing the effect of the human *IHH* mutations on skeletal patterning, endochondral ossification and growth plate maintenance will be necessary.

References

Afzal AR, Rajab A, Fenske CD, Oldridge M, Elanko N, Ternes-Pereira E, Tuysuz B, Murday VA, Patton MA, Wilkie AO, Jeffery S (2000) Recessive Robinow syndrome, allelic to dominant brachydactyly type B, is caused by mutation of ROR2. Nat Genet 25:419-422.

Alvarez J, Sohn P, Zeng X, Doetschman T, Robbins DJ, Serra R (2002) TGFbeta2 mediates the effects of hedgehog on hypertrophic differentiation and PTHrP expression. Development 129:1913-1924.

Armour CM, Bulman DE, Hunter AG (2000) Clinical and radiological assessment of a family with mild brachydactyly type A1: the usefulness of metacarpophalangeal profiles. J Med Genet 37:292-296.

Ballock RT, O'Keefe RJ. 2003. The biology of the growth plate. J Bone Joint Surg Am 85-A(4):715-26.

Bell J (1951) On brachydactyly and symphalangism. In: Penrose L (ed) Treasury of human inheritance. Vol 5. Cambridge University Press, London

Chamoun Z, Mann RK, Nellen D, von Kessler DP, Bellotto M, Beachy PA, Basler K (2001) Skinny hedgehog, an acyltransferase required for palmitoylation and activity of the hedgehog signal. Science 293:2080-2084

Chung UI, Schipani E, McMahon AP, Kronenberg HMBR (2001) Indian hedgehog couples chondrogenesis to osteogenesis in endochondral bone development. J Clin Invest 107:295-304.

Cohen MM, Jr. (2003) The hedgehog signaling network. Am J Med Genet 123A:5-28

Faiyaz-Ul-Haque M, Ahmad W, Zaidi SH, Haque S, Teebi AS, Ahmad M, Cohn DH, Tsui LC (2002) Mutation in the cartilage-derived morphogenetic protein-1 (CDMP1) gene in a kindred affected with fibular hypoplasia and complex brachydactyly (DuPan syndrome). Clin Genet 61:454-458

Farabee W (1903) Hereditary and sexual influence in meristic variation. A study of digital malformations in man. PhD thesis. Harvard University

Fukushima Y, Ohashi H, Wakui K, Nishimoto H, Sato M, Aihara T (1995) De novo apparently balanced reciprocal translocation between 5q11.2 and 17q23 associated with Klippel-Feil anomaly and type A1 brachydactyly. Am J Med Genet 57:447-449

Gao B, Guo J, She C, Shu A, Yang M, Tan Z, Yang X, Guo S, Feng G, He L (2001) Mutations in IHH, encoding Indian hedgehog, cause brachydactyly type A- 1. Nat Genet 28:386-388.

Giordano N, Gennari L, Bruttini M, Mari F, Meloni I, Baldi C, Capoccia S, Geraci S, Merlotti D, Amendola A, Martini G, Nuti R, Gennari C, Renieri A (2003) Mild brachydactyly type A1 maps to chromosome 2q35-q36 and is caused by a novel IHH mutation in a three generation family. J Med Genet 40:132-135.

Hellemans J, Coucke PJ, Giedion A, Paepe AD, Kramer P, Beemer F, Mortier GR (2003) Homozygous Mutations in IHH Cause Acrocapitofemoral Dysplasia, an Autosomal Recessive Disorder with Cone-Shaped Epiphyses in Hands and Hips. Am J Hum Genet 72:1040-1046.

Hoeffel JC, Didier F, Chantereau D, Medoc JM, Muller JP (1987) Metaphyseal dyschondroplasia with cone-shaped epiphyses. Br J Radiol 60:707-710

Karaplis AC, Luz A, Glowacki J, Bronson RT, Tybulewicz VL, Kronenberg HM, Mulligan RC (1994) Lethal skeletal dysplasia from targeted disruption of the parathyroid hormone-related peptide gene. Genes Dev 8:277-289.

Karp SJ, Schipani E, St-Jacques B, Hunzelman J, Kronenberg H, McMahon APBR (2000) Indian hedgehog coordinates endochondral bone growth and morphogenesis via parathyroid hormone related-protein-dependent and -independent pathways. Development 127:543-548.

Kirkpatrick TJ, Au KS, Mastrobattista JM, McCready ME, Bulman DE, Northrup H (2003) Identification of a mutation in the Indian Hedgehog (IHH) gene causing brachydactyly type A1 and evidence for a third locus. J Med Genet 40:42-44.

Kobayashi T, Soegiarto DW, Yang Y, Lanske B, Schipani E, McMahon AP, Kronenberg HM (2005) Indian hedgehog stimulates periarticular chondrocyte differentiation to regulate growth plate length independently of PTHrP. J Clin Invest 115:1734-1742

Koziel L, Kunath M, Kelly OG, Vortkamp A (2004) Ext1-dependent heparan sulfate regulates the range of Ihh signaling during endochondral ossification. Dev Cell 6:801-813

Kronenberg HM. 2003 Developmental regulation of the growth plate. Nature. 423(6937):332-6.

Lanske B, Karaplis AC, Lee K, Luz A, Vortkamp A, Pirro A, Karperien M, Defize LH, Ho C, Mulligan RC, Abou-Samra AB, Juppner H, Segre GV, Kronenberg HMBR (1996) PTH/PTHrP receptor in early development and Indian hedgehog-regulated bone growth. Science 273:663-666.

McCready ME, Grimsey A, Styer T, Nikkel SM, Bulman DE (2005) A century later Farabee has his mutation. Hum Genet 117:285-287

McCready ME, Sweeney E, Fryer AE, Donnai D, Baig A, Racacho L, Warman ML, Hunter AG, Bulman DE (2002) A novel mutation in the IHH gene causes brachydactyly type A1: a 95- year-old mystery resolved. Hum Genet 111:368-375.

Minina E, Kreschel C, Naski MC, Ornitz DM, Vortkamp A (2002) Interaction of FGF, Ihh/Pthlh, and BMP signaling integrates chondrocyte proliferation and hypertrophic differentiation. Dev Cell 3:439-449.

Mortier GR, Kramer PP, Giedion A, Beemer FA (2003) Acrocapitofemoral dysplasia: an autosomal recessive skeletal dysplasia with cone shaped epiphyses in the hands and hips. J Med Genet 40:201-207.

Polinkovsky A, Robin NH, Thomas JT, Irons M, Lynn A, Goodman FR, Reardon W, Kant SG, Brunner HG, van der Burgt I, Chitayat D, McGaughran J, Donnai D, Luyten FP, Warman ML (1997) Mutations in CDMP1 cause autosomal dominant brachydactyly type C. Nat Genet 17:18-19

Porter JA, Ekker SC, Park WJ, von Kessler DP, Young KE, Chen CH, Ma Y, Woods AS, Cotter RJ, Koonin EV, Beachy PA (1996) Hedgehog patterning activity: role of a lipophilic modification mediated by the carboxy-terminal autoprocessing domain. Cell 86:21-34

Provot S, Schipani E. 2005. Molecular mechanisms of endochondral bone development. Biochem Biophys Res Commun 328(3):658-65.

Razzaque MS, Soegiarto DW, Chang D, Long F, Lanske B (2005) Conditional deletion of Indian hedgehog from collagen type 2alpha1-expressing cells results in abnormal endochondral bone formation. J Pathol 207:453-461

Schwabe GC, Tinschert S, Buschow C, Meinecke P, Wolff G, Gillessen-Kaesbach G, Oldridge M, Wilkie AO, Komec R, Mundlos S (2000) Distinct mutations in the receptor tyrosine kinase gene ROR2 cause brachydactyly type B. Am J Hum Genet 67:822-831

Seemann P, Schwappacher R, Kjaer KW, Krakow D, Lehmann K, Dawson K, Stricker S, Pohl J, Ploger F, Staub E, Nickel J, Sebald W, Knaus P, Mundlos S (2005) Activating and deactivating mutations in the receptor interaction site of GDF5 cause symphalangism or brachydactyly type A2. J Clin Invest 115:2373-2381

Spranger J, Brill P, Poznanski A (2002) Bone Dysplasia - An Atlas of Genetic Disorders of Skeletal Development. Oxford University Press

St-Jacques B, Hammerschmidt M, McMahon AP (1999) Indian hedgehog signaling regulates proliferation and differentiation of chondrocytes and is essential for bone formation. Genes Dev 13:2072-2086.

Superti-Furga A, Unger S. (2007) Nosology and classification of genetic skeletal disorders: 2006 revision. Am J Med Genet A. 143(1):1-18.

Thomas JT, Kilpatrick MW, Lin K, Erlacher L, Lembessis P, Costa T, Tsipouras P, Luyten FP (1997) Disruption of human limb morphogenesis by a dominant negative mutation in CDMP1. Nat Genet 17:58-64

Thomas JT, Lin K, Nandedkar M, Camargo M, Cervenka J, Luyten FP (1996) A human chondrodysplasia due to a mutation in a TGF-beta superfamily member. Nat Genet 12:315-317

van Bokhoven H, Celli J, Kayserili H, van Beusekom E, Balci S, Brussel W, Skovby F, Kerr B, Percin EF, Akarsu N, Brunner HG (2000) Mutation of the gene encoding the ROR2 tyrosine kinase causes autosomal recessive Robinow syndrome. Nat Genet 25:423-426

van der Eerden BC, Karperien M, Wit JM. 2003. Systemic and local regulation of the growth plate. Endocr Rev 24(6):782-801.

Vortkamp A, Lee K, Lanske B, Segre GV, Kronenberg HM, Tabin CJBR (1996) Regulation of rate of cartilage differentiation by Indian hedgehog and PTH-related protein. Science 273:613-622.

Yang X, She C, Guo J, Yu AC, Lu Y, Shi X, Feng G, He L (2000) A locus for brachydactyly type A-1 maps to chromosome 2q35-q36. Am J Hum Genet 66:892-903.

Zeng X, Goetz JA, Suber LM, Scott WJ, Jr., Schreiner CM, Robbins DJ (2001) A freely diffusible form of Sonic hedgehog mediates long-range signalling. Nature 411:716-720.

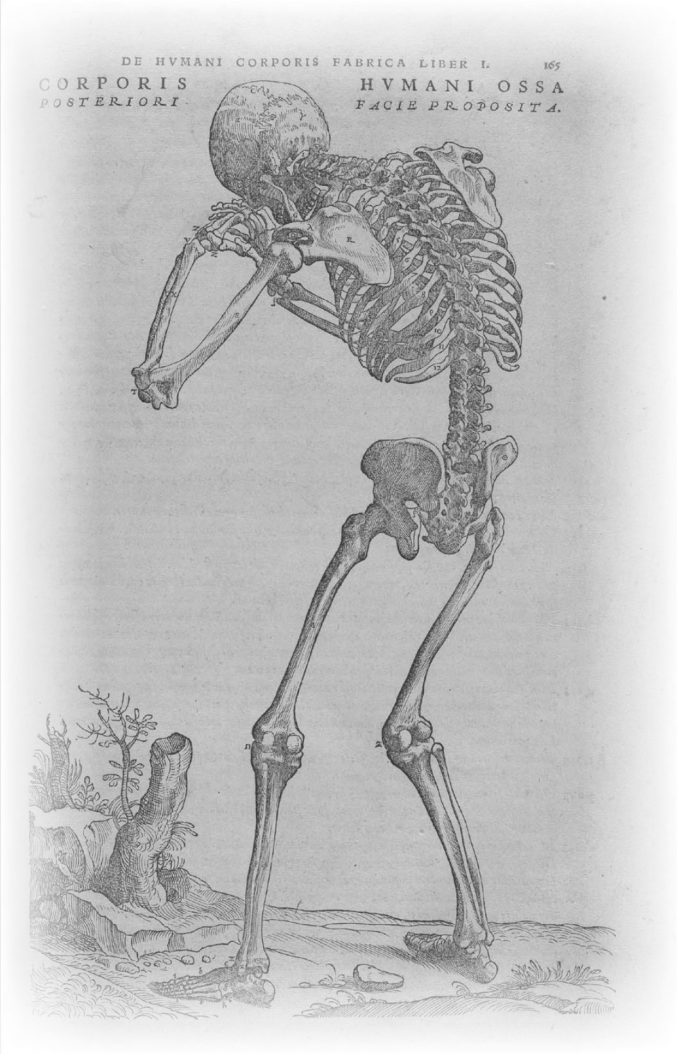

Chapter 3

The LEMD3 gene in osteopoikilosis, BOS and melorheostosis

Paper 3

Hellemans et al. Nat Genet 2004

Hellemans J, Preobrazhenska O, Willaert A, Debeer P, Verdonk PC, Costa T, Janssens K, Menten B, Van Roy N, Vermeulen SJ, Savarirayan R, Van Hul W, Vanhoenacker F, Huylebroeck D, De Paepe A, Naeyaert JM, Vandesompele J, Speleman F, Verschueren K, Coucke PJ, Mortier GR. Loss-of-function mutations in *LEMD3* result in osteopoikilosis, Buschke-Ollendorff syndrome and melorheostosis. Nat Genet. 2004 Nov;36(11):1213-8. Epub 2004 Oct 17.

nature genetics

Loss-of-function mutations in *LEMD3* result in osteopoikilosis, Buschke-Ollendorff syndrome and melorheostosis

Jan Hellemans[1], Olena Preobrazhenska[2], Andy Willaert[1], Philippe Debeer[3], Peter C M Verdonk[4], Teresa Costa[5], Katrien Janssens[6], Bjorn Menten[1], Nadine Van Roy[1], Stefan J T Vermeulen[1], Ravi Savarirayan[7], Wim Van Hul[6], Filip Vanhoenacker[8], Danny Huylebroeck[2], Anne De Paepe[1], Jean-Marie Naeyaert[9], Jo Vandesompele[1], Frank Speleman[1], Kristin Verschueren[2], Paul J Coucke[1] & Geert R Mortier[1]

Osteopoikilosis, Buschke-Ollendorff syndrome (BOS) and melorheostosis are disorders characterized by increased bone density[1]. The occurrence of one or more of these phenotypes in the same individual or family suggests that these entities might be allelic[2–4]. We collected data from three families in which affected individuals had osteopoikilosis with or without manifestations of BOS or melorheostosis. A genome-wide linkage analysis in these families, followed by the identification of a microdeletion in an unrelated individual with these diseases, allowed us to map the gene that is mutated in osteopoikilosis. All the affected individuals that we investigated were heterozygous with respect to a loss-of-function mutation in *LEMD3* (also called *MAN1*), which encodes an inner nuclear membrane protein. A somatic mutation in the second allele of *LEMD3* could not be identified in fibroblasts from affected skin of an individual with BOS and an individual with melorheostosis. XMAN1, the *Xenopus laevis* ortholog, antagonizes BMP signaling during embryogenesis[5]. In this study, LEMD3 interacted with BMP and activin-TGFβ receptor–activated Smads and antagonized both signaling pathways in human cells.

Osteopoikilosis (OMIM 166700) is an autosomal dominant skeletal dysplasia characterized by a symmetric but unequal distribution of multiple hyperostotic areas in different parts of the skeleton (**Fig. 1**)[6]. These lesions, usually detected incidentally, represent foci of old remodeled bone with lamellar structure, either connected to adjacent trabeculae of spongy bone or attached to the subchondral cortex[7]. Osteopoikilosis can occur either as an isolated anomaly or in association with other abnormalities of skin and bone. BOS (OMIM 166700), an autosomal dominant disorder, refers to the association of osteopoikilosis with disseminated connective-tissue nevi. Both elastic-type nevi (juvenile elastoma) and collagen-type nevi (dermatofibrosis lenticularis disseminata) have been described in BOS[8]. Skin or bony lesions can be absent in some family members, whereas other relatives may have both[9]. The co-occurrence of osteopoikilosis and melorheostosis in the same family has been reported in a few instances[2–4]. Melorheostosis (OMIM 155950) is characterized by a 'flowing' (rheos) hyperostosis of the cortex of tubular bones. These lesions are usually asymmetric: they may involve only one limb or correspond to a particular sclerotome. They are often accompanied by abnormalities of adjacent soft tissues, such as joint contractures, sclerodermatous skin lesions, muscle atrophy, hemangiomas and lymphoedema[10,11].

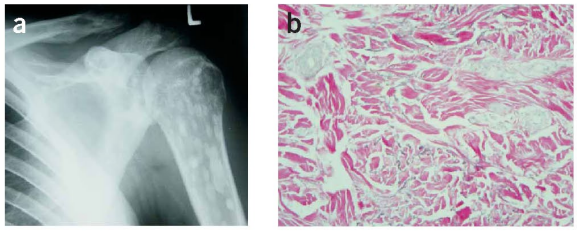

Figure 1 Osteopoikilosis lesions and elastic-type nevus in individual III-3 of family A. (**a**) Anteroposterior radiograph of the left shoulder showing multiple osteopoikilosis lesions, best visible in the left humerus. (**b**) Light micrograph of the elastic-type nevus stained with Van Gieson. Original magnification, ×100. Thick and coarse collagen bundles with numerous broad and irregular elastic fibers are present in the mid-dermis.

[1]Center for Medical Genetics, Ghent University Hospital, Ghent, Belgium. [2]Department of Developmental Biology, Flanders Interuniversity Institute for Biotechnology and Laboratory of Molecular Biology; and [3]Center for Human Genetics, University of Leuven, Leuven, Belgium. [4]Department of Orthopedic Surgery, Ghent University Hospital, Ghent, Belgium. [5]Medical Genetics Service, Sainte-Justine Hospital and University of Montréal, Montréal, Canada. [6]Department of Medical Genetics, University Hospital and University of Antwerp, Belgium. [7]Genetic Health Services Victoria, Murdoch Childrens Research Institute, and University of Melbourne, Australia.[8]Department of Radiology, University Hospital and University of Antwerp, Belgium. [9]Department of Dermatology, Ghent University Hospital, Ghent, Belgium. Correspondence should be addressed to G.R.M. (geert.mortier@ugent.be).

Published online 17 October 2004; doi:10.1038/ng1453

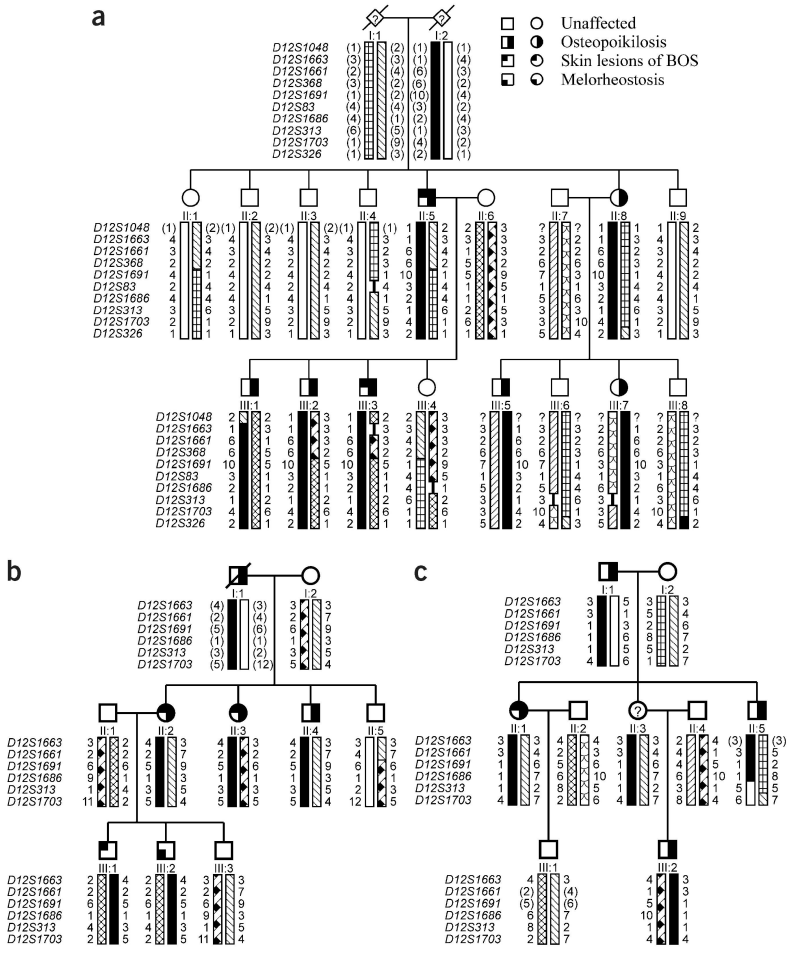

Figure 2 Pedigree structure and haplotypes of the three families with osteopoikilosis, family A (**a**), family B (**b**) and family C (**c**). Inferred alleles are shown in brackets. The haplotype cosegregating with the disorder is indicated with a black bar.

Affected individuals may be asymptomatic or may complain of chronic pain in the affected limb[12].

To unravel the genetic defect of osteopoikilosis, we started a genome-wide linkage analysis in family A (**Fig. 2a**). Screening of 400 markers with an average spacing of 10 cM resulted in a significant positive lod score (3.744) for two consecutive markers on chromosome 12q13: *D12S368* and *D12S83*. The results of the linkage analysis in the two other families, families B and C (**Fig. 2b**,**c**), were consistent with the linkage data obtained in family A. The centromeric boundary of the genetic interval was determined by a recombination event between *D12S1048* and *D12S1663* in individual III-1 (of family A). The telomeric boundary was defined by a recombination event between *D12S1686* and *D12S313* in individual II-5 (of family C), resulting in a candidate region of 23.55 cM on chromosome 12q12–12q14.3. We calculated a combined maximum two-point lod score of 6.691 at $\theta=0$ for markers *D12S1661* and *D12S1691* (**Supplementary Table 1** online).

The next step in the genetic analysis was the identification of individual G03-1858, who is affected with proportionate short stature, microcephaly, learning disabilities, ectopic kidneys and osteopoikilosis. We hypothesized that this individual might have a microdeletion, resulting in the loss of several contiguous genes, including the gene mutated in osteopoikilosis. We investigated this individual for loss of heterozygosity in the candidate region on 12q12–12q14.3 and found loss of heterozygosity for marker *D12S1686*, located in the telomeric part of the interval. The testing of additional markers confirmed the presence of a microdeletion with a centromeric boundary at marker *D12S329* (**Fig. 3**). The telomeric boundary of the microdeletion was defined at the single-nucleotide polymorphism tsc0527430 using the GeneChip Mapping 10K Array (results for whole genome in **Supplementary Fig. 1** online; results for chromosome 12 in **Fig. 4c**). We then tested more markers in the region of overlap between the microdeletion and the linkage interval in family C, which allowed us to narrow the linkage interval and define a 3.07-Mb critical region for association with osteopoikilosis between marker *D12S329* and μSAT12.10. This region contains 23 known genes (National Center for Biotechnology Information genome viewer; **Fig. 3**).

Two of these genes, *WIF1* (Wnt inhibitory factor 1) and *LEMD3* (LEM domain–containing 3), are good candidates for involvement in osteopoikilosis. *WIF1* is involved in Wnt signaling, and *LEMD3* functions in BMP signaling, two pathways important in bone development[13,14]. Mutation analysis of *WIF1* did not identify any abnormalities in the affected individuals. Sequencing of *LEMD3* identified loss-of-function mutations in all affected individuals of the three families and in three unrelated individuals with osteopoikilosis (**Table 1** and **Fig. 4e**). The splice-site mutation in individual G03-2881 caused skipping of exon 6, resulting in a frameshift and premature stop codon in exon 7 at position 2,021 (**Fig. 4d**). The deletion of one of the *LEMD3* alleles in individual G03-1858 was corroborated by fluorescence *in situ* hybridization (FISH) analysis with locus-specific probes (**Fig. 4b**). Re-evaluation of the karyotype (550-band level) was suggestive of, but not conclusive for, the presence of a deletion in the 12q14–15 region (**Fig. 4a**).

Some reports have suggested that the asymmetric distribution of skin lesions in BOS and the segmental involvement usually observed in melorheostosis result from a somatic mutation[4,15]. To investigate this possibility, we took skin biopsy samples from two affected individuals, one from an elastic-type nevus in individual III-3 (of family A) with BOS and a second from a hard sclerodermic-like lesion in individual III-2 (of family B) with melorheostosis. Sequence analysis of *LEMD3* on genomic DNA extracted from both skin lesions showed no evidence for an additional somatic mutation in *LEMD3* (or 'second hit'). Analysis of intragenic polymorphisms showed no loss of heterozygosity or allelic imbalance and therefore excluded the possible existence of a partial gene deletion as a somatic mutation. In cDNA from normal and affected skin of the individual

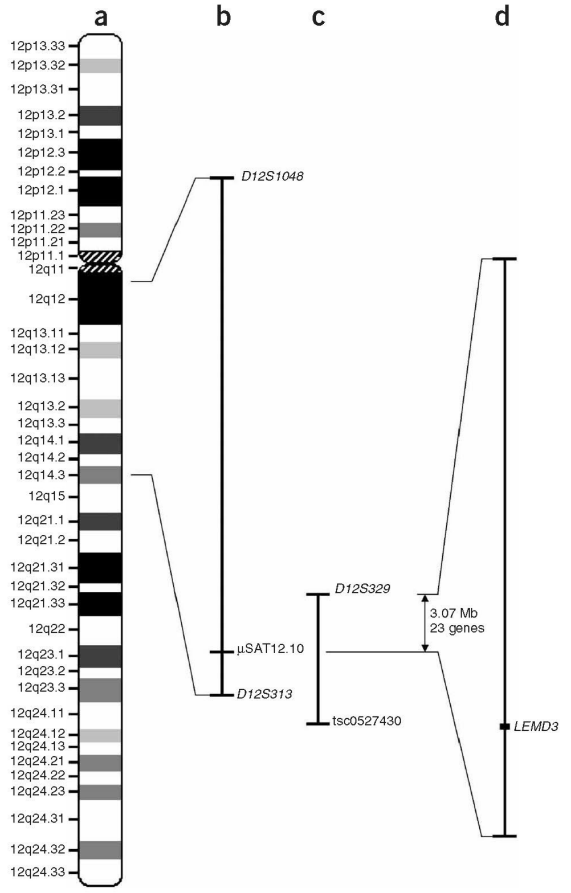

Figure 3 Ideogram of chromosome 12 showing the linkage interval, microdeletion and candidate region. (**a**) Ideogram of chromosome 12. (**b**) The 12q12–q14.3 linkage interval with indication of markers at the boundaries. (**c**) The microdeletion in individual G03-1858 in relation to the linkage interval. The region of interest is shown on the right (**d**), with *LEMD3* as the candidate gene.

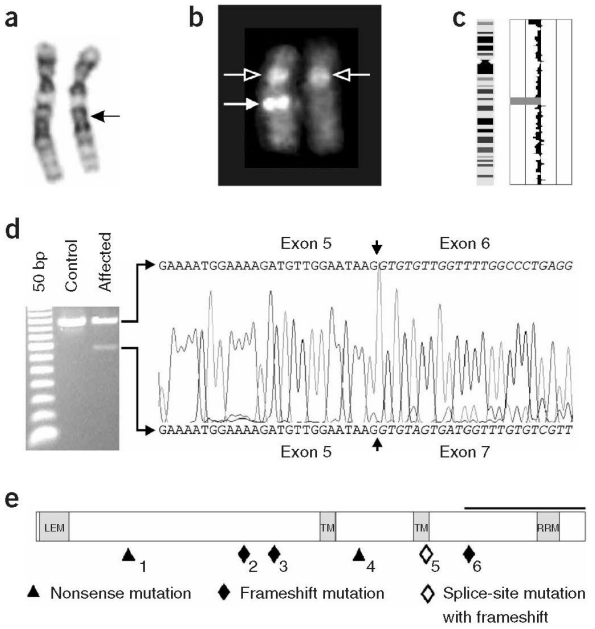

Figure 4 Overview of the cytogenetic and molecular defects found in affected individuals. (**a**) Partial karyotype from individual G03-1858 showing both chromosomes 12. The normal homolog is depicted on the left, and the homolog with the deletion (arrow) is shown on the right. (**b**) Metaphase FISH analysis with the BAC clone encompassing *LEMD3* (RP11-30506; filled arrow) and the centromeric 12 probe (open arrow), showing a microdeletion on the right homolog. (**c**) Results from the GeneChip Mapping 10K Array analysis for chromosome 12 of individual G03-1858. An ideogram of chromosome 12 is shown on the left; meta-analysis significance of the genetic copy-number variation of each SNP against the reference mean is shown on the right. The region with large negative values (bar to the left) indicates the presence of a microdeletion. (**d**) Effect of the *LEMD3* mutation in individual G03-2881. The electrophoretic analysis of an amplified cDNA fragment containing exons 4–8 shows the presence of a 146-bp shorter fragment as compared to the control. Partial nonsense-mediated decay is probably responsible for the weaker signal of this abnormal fragment. Sequence analysis shows skipping of exon 6 in the mutated allele (causing a frameshift with a premature stop codon in exon 7 at position 2,02; data not shown). (**e**) The positions of all *LEMD3* mutations identified in this study are shown below the structure of LEMD3 (see also **Table 1**). Functional domains are indicated in gray: the LEM-containing N-terminal domain, the two transmembrane (TM) domains and the C-terminal domain with the RNA-recognition motif (RRM) motif. The black horizontal bar indicates the Smad-interacting part and BMP-antagonizing portion (as shown in XMAN1; ref. 5) of the C-terminal domain.

with BOS, we found only the normal sequence, owing to nonsense-mediated decay of mRNA from the abnormal allele. Because bone specimens were not available, we could not investigate the possibility that a somatic mutation in osteoblasts could explain the spotty occurrence of bone lesions.

LEMD3 is an integral protein of the inner nuclear membrane[16]. It contains a nucleoplasmic N- and C-terminal domain and two transmembrane segments[16]. The N-terminal segment shares a conserved globular domain of ~40 amino acids with other inner nuclear membrane proteins, such as lamina-associated polypeptide 2 (LAP2) and emerin[16]. The *X. laevis* ortholog of LEMD3 (XMAN1) antagonizes BMP signaling. This antagonizing activity of XMAN1 resides in the C-terminal region that binds to Smad1, Smad5 and Smad8 (ref. 5).

To investigate whether LEMD3 interacts with BMP receptor–activated and TGFβ receptor–activated Smads, we carried out a yeast two-hybrid analysis using the C-terminal domain of LEMD3 as prey. This analysis identified interactions between the C-terminal domain of LEMD3 and the MH2 domains of Smad1 (BMP-specific) and Smad2 (TGFβ-specific), suggesting that LEMD3 is involved in both BMP and TGFβ signaling (**Fig. 5a**).

We further investigated the role of LEMD3 in both signaling pathways by overexpressing the protein in two different cell lines. In HEK293T cells, we measured the expression of several known target genes in basal conditions and after BMP4 stimulation by quantitative PCR (Q-PCR). Overexpression of LEMD3 reduced the capacity of BMP4 to upregulate Smad6, Smad7, Id2 and Id3 (**Fig. 5b**). In HepG2 cells, we measured the response of TGFβ using the activin-TGFβ–responsive 3TP-Lux reporter in basal conditions and in the presence of a constitutively active receptor ALK4, which activates Smad2 and Smad3. Overexpression of LEMD3 reduced the ALK4-induced

Table 1 ***LEMD3*** **mutations**

Number[a]	Affected family or individual	*LEMD3* mutation[b]
	G03-1858	Total gene deletion
1	G03-2882	457C→T
2	G03-1885	1033-1035delGGGinsC
3	Family C (G03-2457)	1185dupT
4	Family B (G02-1757)	1609C→T
5	G03-2881	1941+5delG
6	Family A (G02-1389)	2154dupA

[a]The numbers refer to the position of each mutation as shown in **Figure 4e**. [b]Numbering is according to cDNA sequence NM-014319.

activation of the 3TP-Lux reporter (**Fig. 5c**). These results indicate that LEMD3 can antagonize both BMP and TGFβ signaling in human cells.

Finally, we investigated the effect of the *LEMD3* mutations that we identified in affected individuals. We made three mutant LEMD3 constructs containing the 1185dupT, 1609C→T and 2154dupA mutations, respectively. We carried out a luciferase assay in HEK293T cells transfected with a TGFβ-responsive reporter and found that each mutant construct was unable to reduce TGFβ signaling, unlike the wild-type construct (**Fig. 5d**). The loss-of-function effect of these mutations most probably resulted from the absence of the Smad-interacting C-terminal domain in the truncated proteins, present on western blots. We therefore believe that the mutations found in this study are hypomorphic, either because of nonsense-mediated decay or because of the production of a truncated protein lacking the C-terminal domain. We measured by Q-PCR the expression of several target genes in skin fibroblasts from individual III-3 of family A with the 2154dupA mutation. This analysis confirmed that fibroblasts from this affected individual were haploinsufficient with respect to *LEMD3*. In addition, we found that expression of the gene *Id3* after TGFβ stimulation was significantly higher in these fibroblasts than in controls (**Fig. 5e**). This is the first evidence to our knowledge that haploinsufficiency of LEMD3 in human fibroblasts results in enhanced TGFβ signaling with upregulation of target genes downstream in the pathway. We observed no significant differences between fibroblasts from the elastic-type nevus and normal skin of the affected individual in all conditions tested.

In conclusion, we found that loss-of-function mutations in *LEMD3* can result in osteopoikilosis, BOS and melorheostosis. The failure to detect a somatic mutation in *LEMD3* in affected skin fibroblasts from an individual with BOS and one with melorheostosis may suggest that

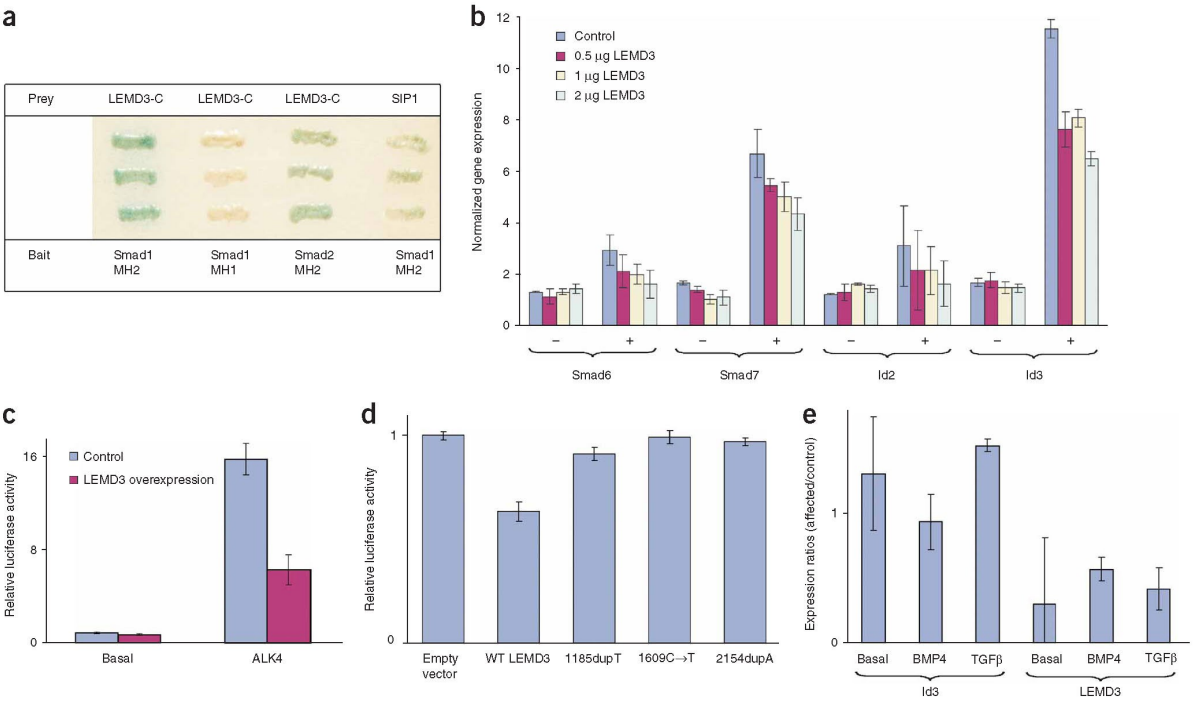

Figure 5 Analysis of normal and mutant LEMD3 in BMP and TGFβ signaling. (**a**) Yeast two-hybrid analysis shows that the C-terminal part of LEMD3 (LEMD3-C) specifically interacts with the MH2 domain of Smad1 and Smad2. SIP1–Smad1 interaction is included as a positive control. Interaction was assessed by activation of the gene *MEL1* encoding α-galactosidase, visualized by blue staining of the yeast. (**b**) Normalized gene expression for four known target genes in basal (–) and BMP4-stimulated (+) HEK293T cells. Overexpression of LEMD3 reduces the capacity of BMP4 to upregulate Smad6, Smad7, Id2 and Id3. (**c**) Relative luciferase activity from the 3TP-Lux reporter construct in HepG2 cells. Overexpression of LEMD3 reduces activation of the 3TP-Lux reporter gene in the presence of the constitutively active ALK4 receptor. (**d**) Relative luciferase activity from the $(CAGA)_{12}$ reporter construct cotransfected with plasmids expressing different LEMD3 mutants in HEK293T cells. Reduction of TGFβ signaling is not observed for the different mutant LEMD3 constructs. (**e**) Expression ratios between fibroblasts from an affected individual and control fibroblasts for *LEMD3* and *Id3* as measured by Q-PCR. The ratios for *Id3* in basal conditions and after BMP4 or TGFβ stimulation are shown on the left. Significantly ($P < 0.05$) higher expression of *Id3* was observed after TGFβ stimulation. The ratios for *LEMD3* are shown on the right and are indicative of haploinsufficiency in fibroblasts from the affected individual ($P < 0.05$).

other genetic factors contribute to the presence and distribution of skin and bone lesions in these disorders. In addition, we found evidence that LEMD3 can antagonize both the BMP and TGFβ signaling pathway. These results are in accordance with previous studies showing that genetic defects in both signaling pathways can result in hyperostotic bone disorders. Loss-of-function mutations in *SOST*, encoding the extracellular BMP antagonist sclerostin, lead to sclerosteosis[17,18] (OMIM 269500), whereas activating missense mutations in *TGFB1* can result in Camurati-Engelmann disease[19,20] (OMIM 131300). Finally, increased signaling in the TGFβ pathway has been observed in other fibrotic skin disorders, such as scleroderma, and may therefore explain the skin lesions in individuals with BOS and melorheostosis[21,22].

METHODS

Material from affected individuals. We obtained appropriate informed consent from all subjects involved in the study. Family A is a three-generation family of Belgian origin. All affected individuals had osteopoikilosis. Two affected individuals (II-5 and III-3) also had skin manifestations of BOS. In individual III-3, skin biopsy samples were taken from a connective-tissue nevus on the left thigh and from normal skin on the right thigh. Light microscopy showed more numerous elastin fibers in the middle and deep dermis on the affected side. These fibers had a slightly granular and thickened appearance (**Fig. 1b**). Ultrastructurally, the elastin fibers were much thicker and more numerous in the affected skin than in the normal skin. They had a well-developed amorphous matrix with delicate peripheral microfibrils. Results of light microscopy and electron microscopy analysis were consistent with the diagnosis of connective-tissue nevus of the elastic-tissue type. Fibroblasts from both biopsies were cultured for molecular analysis.

Family B is another three-generation family of Belgian origin, previously reported[2], illustrating the co-occurrence of osteopoikilosis and melorheostosis in one family. Family C is a three-generation British family with autosomal dominant osteopoikilosis and skin lesions reminiscent of BOS. Individual G03-1885 is an Australian with BOS. Individuals G03-2881 and G03-2882 have osteopoikilosis and are both of Belgian origin but are unrelated. Individual G03-1858 had a history of prenatal and postnatal growth retardation and learning disability that was diagnosed as Russell-Silver syndrome in early childhood. Investigations for hypertension in infancy revealed ectopic kidneys and aberrant renal arteries. Evaluation at the age of 16 years showed proportionate short stature with height of 131.5 cm (50th centile for a 9-y-old girl), weight of 31.8 kg (50th centile for a 10-y-old girl) and head circumference of 49 cm (50th centile for a 3-y-old girl). Physical examination revealed a subtly dysmorphic face with synophrys, mild hypertelorism, broad and high nasal bridge, micrognathia and maxillary overbite. In addition, a diffuse hyperpigmentation spot was noted on the left thigh. Osteopoikilosis lesions were found on skeletal survey.

Linkage analysis. We used all autosomal markers from the Applied Biosystems Linkage mapping set version 2 for a genome-wide linkage analysis. We used an improved protocol from the Centre National de Génotypage for pooling an average of four markers per PCR to carry out all reactions. Additional markers were taken from the Marshfield map or designed based on the simple-tandem-repeat finder in the University of California Santa Cruz genome browser. We carried out genotyping on an Applied Biosystems Prism 3100 Genetic Analyzer running Genemapper v2.0 software. We used the MLINK program of the LINKAGE software package[23] to calculate two-point lod scores between the disease phenotype and each of the markers, assuming a dominant mode of inheritance with a penetrance of 0.95 and a disease allele frequency of 0.0001. The frequency of most marker alleles was set to 1/8. For markers with more than eight alleles in the pedigrees, the allele frequency was set to $1/n$, where n is the number of alleles.

Cytogenetic and FISH analysis. We carried out karyotyping in accordance with standard procedures. We analyzed metaphases at the 550-band level. We carried out FISH analysis as described[24] using BAC clone RP11-30506 from the 12q14.3 region.

GeneChip Mapping 10K Array analysis. We analyzed DNA from individual G03-1858 using the GeneChip Mapping 10K Array (Affymetrix) as described[25]. We analyzed data with both the Affymetrix GCOS and GDAS software and the Affymetrix GeneChip Chromosome Copy Number Tool. We used copy number estimation (meta P value) to identify the microdeletion, the boundaries of which were defined by loss of heterozygosity. Results were visualized with arrayCGHbase (B. Menten *et al.*, unpublished data).

Sequence analysis. We amplified all exons by PCR using intronic primers and additional exonic primers for larger exons (primer sequences are available on request). We used a touchdown PCR program with an annealing temperature decreasing from 60 °C to 48 °C over 12 cycles, followed by 20 cycles with an annealing temperature of 48 °C. We sequenced PCR products using the BigDye v3.1 ET terminator cycle sequencing kit from Applied Biosystems. Sequencing reactions were loaded onto an Applied Biosystems Prism 3100 Genetic Analyzer and analyzed with Sequencing Analysis v3.7 and SeqScape v1.1 software (Applied Biosystems).

Yeast two-hybrid analysis. We cloned the C-terminal domain of human LEMD3, encoding amino acids 520–853, as a *Pvu*II-*Xho*I fragment into the *Sma*I and *Xho*I restriction sites of the prey vector pAct2 (Clontech). We cotransformed yeast strain AH109 with this vector or a positive control (SIP1) prey vector with different Smad bait vectors[26], using the Yeastmaker yeast transformation system 2 (Clontech). We assayed activation of the gene *MEL1* by interacting hybrid proteins in yeast on Trp-Leu drop-out medium containing the chromogenic substrate X-α-Gal (Clontech).

Luciferase assay. We carried out transfections of HepG2 cells in triplicate in 24-well plates using Fugene (Roche). Each well was transfected with a total amount of 500 ng of plasmid DNA, including 50 ng of 3TP-Lux reporter, 50 ng of RSV-promoter-based *lacZ* reporter and combinations of 50 ng of the constitutively active ALK4 receptor with 100 ng of LEMD3 or empty expression vector. We maintained a constant amount of DNA by adding pBluescript vector. Forty-eight hours after transfection, we assayed cell extracts for luciferase and β-galactosidase activities in accordance with the manufacturers' protocols (Promega and Clontech, respectively). We normalized the data by calculating the ratio of luciferase activity to β-galactosidase activity.

Q-PCR. We isolated RNA using RNeasy Mini Kit (Qiagen) and synthesized cDNA using SuperScript II Reverse Transcriptase Kit with random hexamer primers (Invitrogen) in a total volume of 20 μl. We used 5 μl of cDNA (1:10 dilution) in combination with the Q-PCR Core Kit for SYBR Green I (Eurogentec) and 250 nM gene-specific primers to carry out Q-PCR on a GeneAmp 5700 Sequence Detector (Applied Biosystems). The Q-PCR program consists of 40 cycles with 15 s at 95 °C and 1 min at 60 °C, followed by a dissociation run to determine melting curves. We carried out all reactions in duplicate and normalized them to the geometric mean of three stable reference genes (*GAPD*, *HPRT1* and *YWHAZ*)[27].

To investigate the effect of LEMD3 on Smad signaling, we seeded HEK293T cells in 9-cm dishes and transfected them with a total of 2 μg of *LEMD3* plasmid DNA (provided by H. Worman; Department of Medicine, College of Physicians and Surgeons, Columbia University, New York, New York, USA) using Fugene (Roche). Twenty-four hours after transfection, cells were serum-starved for 4 h and then stimulated with 5 ng ml^{-1} of human recombinant BMP4 (R&D Systems) for 1 h followed by RNA extraction.

In the screening for differentially expressed genes, we used fibroblasts from a control individual and from normal and affected skin of affected individual III-3 (of family A). We grew the cells in 13.5-cm dishes to 80% confluency and then serum-starved them for 2 h. We collected cells after 1 h of treatment with 1 ng ml^{-1} human recombinant TGFβ1 (R&D Systems) or with 5 ng ml^{-1} of BMP4. Expression levels for all genes were determined in four independent experiments. Differential gene expression was considered significant when the difference was at least 50% and the 95% confidence interval of the mean expression ratio did not include 1 (equivalent with $P < 0.05$).

We analyzed the following genes (their ID numbers in the RTPrimerDB database[28] are given in parentheses): *GAPD* (3), *HPRT1* (5), *YWHAZ* (9), *MMP2* (113), *CTGF* (596), *COL1A1* (1089), *COL3A1* (1090), *COL5A1* (1091), *FN1* (1092), *ELN* (1093), *ID1* (1094), *ID2* (1095), *ID3* (1096),

ID4 (1097), *LEMD3* (1098), *RUNX2* (1099), *SMAD6* (1100), *SMAD7* (1101) and *SERPINE1* (1102).

Analysis of mutant LEMD3 constructs. We modified the wild-type LEMD3 construct (provided by H. Worman; Department of Medicine, College of Physicians and Surgeons, Columbia University, New York, New York, USA) to contain the 1185dupT, 1609C→T or 2154dupA mutation using the QuickChange Site-Directed Mutagenesis kit (Stratagene) in accordance with the manufacturer's instructions. We plated HEK293T cells at a density of 4×10^5 cells per well in Dulbecco's modified Eagle medium plus (Invitrogen) and transferred them to Opti-MEM I (Invitrogen) after overnight adherence. We transiently transfected cells with 2 μg of each plasmid and 0.5 μg of the $(CAGA)_{12}$ TGFβ-responsive reporter construct[29] in duplicate using Lipofectamine (Invitrogen). We also transfected cells with 20 ng of pRL-TK (Promega) to correct for transfection efficiency. Cells were serum-starved for 7 h before stimulation with 7 ng ml^{-1} recombinant human TGFβ (R&D systems). We lysed cells 24 h after transfection. We quantified activities of firefly and *Renilla* luciferase using the Dual-Luciferase Reporter Assay System (Promega).

URLs. Improved linkage analysis protocols from the Centre National de Génotypage are available at http://www.cng.fr/. The arrayCGHbase visualization tool and RTPrimerDB database are available at http://medgen.ugent.be/arraycghbase/ and http://medgen.ugent.be/rtprimerdb/, respectively.

Note: Supplementary information is available on the Nature Genetics website.

ACKNOWLEDGMENTS

We thank the affected individuals and families for their interest and cooperation, M. Godfrey for critical review of the manuscript, P. Tylzanowski for suggestions and plasmid stocks and H. Worman for the expression vector encoding human LEMD3. This study was supported, in part, by the Fund for Scientific Research, Flanders, with a mandate fundamental clinical research to P.D. and G.R.M.; a research assistantship to P.C.M.V.; and research projects to F.S., S.J.T.V., W.V.H. and G.R.M. This study was also supported by an Interuniversity Attraction Pole grant to W.V.H. and by the Fifth Framework of the specific research and technological development program "Quality of Life and Management of Living Resources" of the European Commission to J.H., A.D.P. and G.R.M. J.H. is funded by, and J.V. is a postdoctoral researcher with, the Institute for the Promotion of Innovation by Science and Technology in Flanders. N.V.R. and K.J. are postdoctoral researchers of the Fund for Scientific Research, Flanders. The research at Flanders Interuniversity Institute for Biotechnology was supported by the Fund for Scientific Research, Flanders and the University of Leuven. O.P. is holder of a DWTC (Federal Services for Scientific, Technical and Cultural affairs) postdoctoral fellowship and is supported by the Interuniversity Attraction Pole Network. This text presents research results of the Belgian program of Interuniversity Poles of attraction initiated by the Belgian State, Prime Minister's Office, Science Policy Programming. The scientific responsibility is assumed by the authors.

COMPETING INTERESTS STATEMENT

The authors declare that they have no competing financial interests.

Received 22 July; accepted 17 September 2004
Published online at http://www.nature.com/naturegenetics/

1. Hall, C.M. International nosology and classification of constitutional disorders of bone (2001). *Am. J. Med. Genet.* **113**, 65–77 (2002).
2. Debeer, P., Pykels, E., Lammens, J., Devriendt, K. & Fryns, J.P. Melorheostosis in a family with autosomal dominant osteopoikilosis: Report of a third family. *Am. J. Med. Genet.* **119A**, 188–193 (2003).
3. Butkus, C.E., Michels, V.V., Lindor, N.M. & Cooney, W.P. 3rd Melorheostosis in a patient with familial osteopoikilosis. *Am. J. Med. Genet.* **72**, 43–46 (1997).
4. Nevin, N.C., Thomas, P.S., Davis, R.I. & Cowie, G.H. Melorheostosis in a family with autosomal dominant osteopoikilosis. *Am. J. Med. Genet.* **82**, 409–414 (1999).
5. Osada, S., Ohmori, S.Y. & Taira, M. XMAN1, an inner nuclear membrane protein, antagonizes BMP signaling by interacting with Smad1 in *Xenopus* embryos. *Development* **130**, 1783–1794 (2003).
6. Melnick, J.C. Osteopathia condensans disseminata (osteopoikilosis): study of a family of 4 generations. *Am. J. Roentgenol.* **82**, 229–238 (1959).
7. Lagier, R., Mbakop, A. & Bigler, A. Osteopoikilosis: a radiological and pathological study. *Skeletal Radiol.* **11**, 161–168 (1984).
8. Ehrig, T. & Cockerell, C.J. Buschke-Ollendorff syndrome: report of a case and interpretation of the clinical phenotype as a type 2 segmental manifestation of an autosomal dominant skin disease. *J. Am. Acad. Dermatol.* **49**, 1163–1166 (2003).
9. Berlin, R., Hedensio, B., Lilja, B. & Linder, L. Osteopoikilosis—a clinical and genetic study. *Acta. Med. Scand.* **181**, 305–314 (1967).
10. Campbell, C.J., Papademetriou, T. & Bonfiglio, M. Melorheostosis. A report of the clinical, roentgenographic, and pathological findings in fourteen cases. *J. Bone Joint Surg. Am.* **50**, 1281–1304 (1968).
11. Rozencwaig, R., Wilson, M.R. & McFarland, G.B. Jr. Melorheostosis. *Am. J. Orthop.* **26**, 83–89 (1997).
12. Freyschmidt, J. Melorheostosis: a review of 23 cases. *Eur. Radiol.* **11**, 474–479 (2001).
13. Gong, Y. *et al.* LDL receptor-related protein 5 (LRP5) affects bone accrual and eye development. *Cell* **107**, 513–523 (2001).
14. Canalis, E., Economides, A.N. & Gazzerro, E. Bone morphogenetic proteins, their antagonists, and the skeleton. *Endocr. Rev.* **24**, 218–235 (2003).
15. Happle, R. Melorheostosis may originate as a type 2 segmental manifestation of osteopoikilosis. *Am. J. Med. Genet.* **125A**, 221–223 (2004).
16. Lin, F. *et al.* MAN1, an inner nuclear membrane protein that shares the LEM domain with lamina-associated polypeptide 2 and emerin. *J. Biol. Chem.* **275**, 4840–4847 (2000).
17. Balemans, W. *et al.* Increased bone density in sclerosteosis is due to the deficiency of a novel secreted protein (SOST). *Hum. Mol. Genet.* **10**, 537–543 (2001).
18. Brunkow, M.E. *et al.* Bone dysplasia sclerosteosis results from loss of the *SOST* gene product, a novel cystine knot-containing protein. *Am. J. Hum. Genet.* **68**, 577–589 (2001).
19. Janssens, K. *et al.* Mutations in the gene encoding the latency-associated peptide of TGF-β 1 cause Camurati-Engelmann disease. *Nat. Genet.* **26**, 273–275 (2000).
20. Kinoshita, A. *et al.* Domain-specific mutations in TGF-β1 result in Camurati-Engelmann disease. *Nat. Genet.* **26**, 19–20 (2000).
21. Mori, Y., Chen, S.J. & Varga, J. Expression and regulation of intracellular SMAD signaling in scleroderma skin fibroblasts. *Arthritis Rheum.* **48**, 1964–1978 (2003).
22. Asano, Y., Ihn, H., Yamane, K., Kubo, M. & Tamaki, K. Impaired Smad7–Smurf-mediated negative regulation of TGF-β signaling in scleroderma fibroblasts. *J. Clin. Invest.* **113**, 253–264 (2004).
23. Lathrop, G.M. & Lalouel, J.M. Easy calculations of lod scores and genetic risks on small computers. *Am. J. Hum. Genet.* **36**, 460–465 (1984).
24. Van Roy, N. *et al.* 1;17 translocations and other chromosome 17 rearrangements in human primary neuroblastoma tumors and cell lines. *Genes Chromosomes Cancer* **10**, 103–114 (1994).
25. Matsuzaki, H. *et al.* Parallel genotyping of over 10,000 SNPs using a one-primer assay on a high-density oligonucleotide array. *Genome Res.* **14**, 414–425 (2004).
26. Verschueren, K. *et al.* SIP1, a novel zinc finger/homeodomain repressor, interacts with Smad proteins and binds to 5′-CACCT sequences in candidate target genes. *J. Biol. Chem.* **274**, 20489–20498 (1999).
27. Vandesompele, J. *et al.* Accurate normalization of real-time quantitative RT–PCR data by geometric averaging of multiple internal control genes. *Genome Biol.* **3** RESEARCH0034 (2002).
28. Pattyn, F., Speleman, F., De Paepe, A. & Vandesompele, J. RTPrimerDB: the real-time PCR primer and probe database. *Nucleic Acids Res.* **31**, 122–123 (2003).
29. Dennler, S. *et al.* Direct binding of Smad3 and Smad4 to critical TGF β-inducible elements in the promoter of human plasminogen activator inhibitor-type 1 gene. *EMBO J.* **17**, 3091–3100 (1998).

Paper 4

Hellemans et al. Hum Mutat 2006

Hellemans J, Debeer P, Wright M, Janecke A, Kjaer KW, Verdonk PC, Savarirayan R, Basel L, Moss C, Roth J, David A, De Paepe A, Coucke P, Mortier GR. Germline *LEMD3* mutations are rare in sporadic patients with isolated melorheostosis. Hum Mutat. 2006 Mar;27(3):290.

MUTATION IN BRIEF

Germline *LEMD3* Mutations Are Rare in Sporadic Patients With Isolated Melorheostosis

Jan Hellemans[1], Philippe Debeer[2], Michael Wright[3], Andreas Janecke[4], Klaus W Kjaer[5], Peter CM Verdonk[6], Ravi Savarirayan[7], Lina Basel[8], Celia Moss[9], Johannes Roth[10], Albert David[11], Anne De Paepe[1], Paul Coucke[1], and Geert R Mortier[1]

[1]Center for Medical Genetics and [6]Department of Orthopedic Surgery, Ghent University Hospital, Ghent, Belgium; [2]Center for Human Genetics, University of Leuven, Leuven, Belgium; [3]Institute of Human Genetics, International Centre for Life, Newcastle-upon-Tyne, United Kingdom; [4]Genetische Beratungs- und Untersuchungsstelle, Medizinische Universität Innsbruck, Innsbruck, Austria; [5]Wilhelm Johannsen Centre for Functional Genome Research, Dept. of Medical Genetics, Panum Institute, Copenhagen, Norway; [7]Genetic Health Services Victoria, Murdoch Childrens Research Institute, and University of Melbourne, Melbourne, Australia; [8]Department of Medical Genetics, Rabin Medical Center, Beilinson Campus, Petah Tikva, Israel; [9]West Midlands Regional Genetics Laboratory, Birmingham Women's Health Care NHS Trust, Birmingham, United Kingdom; [10]SPZ Rheumatologie, Charité Campus Virchow-Klinikum, Berlin, Germany; [11]Unite de Genetique Clinique, Centre Hospitalier Universitaire de Nantes, Nantes, France

*Correspondence to: Geert R Mortier, University Hospital Ghent 0K5, De Pintelaan 185, 9000 Gent, Belgium; Tel.: +32 9 240 49 70; E-mail: Geert.Mortier@ugent.be

Grant sponsor: Fund for Scientific Research, Flanders (FWO), Institute for the Promotion of Innovation by Science and Technology in Flanders (IWT), European Commission; Grant number: IWT-SB/23476, QLG1-CT-2001-02188.

Communicated by Iain McIntosh

To further explore the allelic heterogeneity within the group of LEMD3-related disorders, we have screened a larger series of patients including 5 probands with osteopoikilosis or Buschke-Ollendorff syndrome (BOS), 2 families with the co-occurrence of melorheostosis and BOS, and 12 unrelated patients with isolated melorheostosis. Seven novel *LEMD3* mutations were identified, all predicted to result in loss-of-function of the protein. We confirm that loss-of-function mutations in the LEMD3 gene can result in either osteopoikilosis or BOS. However, *LEMD3* germline mutations were only found in two melorheostosis patients belonging to a different BOS family and one sporadic patient with melorheostosis. The additional presence of osteopoikilosis lesions in these patients seemed to distinguish them from the group of sporadic melorheostosis patients where no germline *LEMD3* mutation was identified. Somatic mosaicism for a *LEMD3* mutation in the latter group was also not observed, and therefore we must conclude that the genetic defect in the majority of sporadic and isolated melorheostosis remains unknown. © 2006 Wiley-Liss, Inc.

KEY WORDS: LEMD3; osteopoikilosis; Buschke-Ollendorff syndrome; melorheostosis

Received 22 August 2005; accepted revised manuscript 10 November 2005.

DOI: 10.1002/humu.9403

INTRODUCTION

Osteopoikilosis (MIM# 166700), Buschke-Ollendorff syndrome (BOS) (MIM# 166700) and melorheostosis (MIM# 155950) are rare sclerosing bone dysplasias (Vanhoenacker, et al., 2000). Osteopoikilosis is a benign, usually asymptomatic condition characterized radiographically by multiple round foci of increased bone density. These lesions are usually located in the epimetaphyseal regions of the tubular bones and therefore do not affect the diaphyses (Benli, et al., 1992; Green, et al., 1962). Histological studies of these lesions show foci of numerous bone trabeculae of various thickness, arranged in a regular pattern, resembling the structure of spongy bone, and merging into the surrounding structures of normal spongiosa (Green, et al., 1962; Lagier, et al., 1984). BOS combines the characteristic bone lesions of osteopoikilosis with connective tissue nevi, either of the elastic type (juvenile elastoma) or the collagen type (dermatofibrosis lenticularis disseminata). The histopathology of these skin lesions varies from hyperplasia of collagen fibers with normal elastic tissue to hyperplasia of the elastic tissue with normal collagen, even within the same family (Schorr, et al., 1972). Osteopoikilosis and BOS show autosomal dominant inheritance whereas melorheostosis usually occurs sporadically. The co-occurrence of melorheostosis and osteopoikilosis in the same individual (Ghai and Sharma, 2003) or family (Butkus, et al., 1997; Debeer, et al., 2003; Nevin, et al., 1999) has, however, been reported.

Melorheostosis is characterized radiographically by bone sclerosis with a linear pattern mainly affecting the cortex of tubular bones. The lesions are usually asymmetric and monomelic but can involve multiple limbs on both sides of the body. The linear hyperostosis of the cortex can extend internally into the medullary canal or externally with periosteal involvement resulting in the characteristic waxy outline of the affected bone. In some patients with melorheostosis spotty lesions reminiscent of osteopoikilosis can be observed in the epiphyses of the long bones (Green, et al., 1962). Small bone deposits in the surrounding soft tissues have also been reported (Campbell, et al., 1968; Greenspan, 1991). Hyperostosis is often accompanied by hyperplasia and abnormalities of the adjacent connective tissues (e.g. scleroderma-like lesions or fibrosis) (Happle, 2004). Melorheostosis may be asymptomatic but often causes joint contractures, stiffness and chronic pain. Severe cases may even present with shortening of the affected bones. Histological examination reveals hyperostotic cortical bone formation with thickened trabeculae and fibrotic changes in the marrow spaces. The bone appears primitive and consists largely of primary haversian systems that are almost obliterated by the deposition of sclerotic, thickened and somewhat irregular lamellae (Greenspan and Azouz, 1999). Overproduction of extracellular matrix has been reported in affected bone and increased expression of the type I collagen genes has been described in skin lesions (Endo, et al., 2003).

We recently have identified *LEMD3* (MIM# 607844) mutations in patients with one or more of these three conditions (Hellemans, et al., 2004). The *LEMD3* gene codes for a protein of the inner nuclear membrane that inhibits both the BMP and TGFβ signaling pathways (Hellemans, et al., 2004; Lin, et al., 2005). This is the first evidence that inner nuclear membrane proteins can regulate intracellular signaling. Loss-of-function mutations were identified in 3 unrelated patients with osteopoikilosis or BOS and in 3 families where osteopoikilosis was associated with either BOS or melorheostosis. Analysis of fibroblasts from skin lesions in one BOS patient and in one melorheostosis patient did not reveal the presence of a somatic mutation in *LEMD3*. To further explore the allelic heterogeneity within this group of disorders, a larger series of patients was screened in this study.

MATERIALS AND METHODS

Informed consent was obtained for all patients included in the study. The 19 new patients were classified in three phenotypic groups based on their radiographic and clinical features, and family history (Table 1). Group A consisted of 5 osteopoikilosis patients with or without BOS skin lesions. Group B consisted of 2 melorheostosis patients who also had at least one first degree relative with osteopoikilosis or BOS. Group C comprised 12 unrelated sporadic patients with melorheostosis lesions.

Genomic DNA was extracted from blood lymphocytes using the Puregene DNA isolation kit (Gentra, Minneapolis, USA) or the QIAamp DNA blood mini kit (Qiagen, Hilden, Germany). Skin and bone biopsies were cut into small pieces and cultured in DMEM medium (Gibco-Invitrogen, Paisley, UK) with 10% fetal calf serum or Osteomed medium (Biochrom, Berlin, Germany) with an additional 10% fetal calf serum, respectively. When there was confluence of the fibroblasts or osteoblasts, gDNA was extracted with the Puregene DNA isolation kit (Gentra).

Mutation analysis of *LEMD3* was performed by PCR amplification of all exons using intronic primers and additional exonic primers for larger exons (primer sequences are available on request). A touchdown PCR

program was then used with an annealing temperature decreasing from 60°C to 48°C over 12 cycles, followed by 20 cycles with an annealing temperature of 48°C. PCR products were sequenced using the BigDye v3.1 ET terminator cycle sequencing kit from Applied Biosystems (Foster City, CA). Sequencing reactions were loaded on an Applied Biosystems Prism 3100 Genetic Analyzer and analyzed with Sequencing Analysis v3.7 and SeqScape v1.1 (Applied Biosystems). Nucleotide changes were numbered according to cDNA sequence NM-014319.3. Where normal results were obtained, microsatellite markers and polymorphisms within or near the LEMD3 gene (Table 2) were analyzed on an Applied Biosystems Prism 3100 Genetic Analyzer with GeneScan v3.7 to rule out loss of heterozygosity.

Table 1. Mutations identified in the LEMD3 gene in patients with osteopoikilosis, BOS, and/or melorheostosis

Group	Patient ID #	Phenotype	Nucleotide* and residue changes
A	04g3557	osteopoikilosis	c.1801G>T; p.Glu601X
	04g3867	BOS	c.1323C>A; p.Tyr441X
	04g3934	BOS	c.1873C>T; p.Arg625X
	D0501606	BOS	c.1914dupA; p.Leu638fs
	04g3820	osteopoikilosis	normal
B	D0503238	melorheostosis (BOS in other relatives)	c.830dupA; p.Lys277X
	D0500261	melorheostosis (BOS in other relatives)	[c.1963C>T;c.2488C>T]; p.Arg655X
C	D0402645	melorheostosis	c.1913T>A; p.Leu638X
	D0402644	melorheostosis	normal
	04g3961	melorheostosis	normal
	04g4301	melorheostosis	normal
	04g4289	melorheostosis	normal
	04g4319	melorheostosis	normal
	D0500232	melorheostosis	normal
	D0501013	melorheostosis	normal
	D0501602	melorheostosis	normal
	D0502108	melorheostosis	normal
	D0503242	melorheostosis	normal
	D0503152	melorheostosis	normal

*Numbering in accordance to cDNA sequence NM-014319.3, with +1 as the A of the ATG initiation codon.

Table 2. Markers used for loss of heterozygosity screening

Marker	Position	Heterozygosity
D12S329[1]	5' *LEMD3* (2.4Mb)	77%
D12S1649[1]	intron 1	64%
c.2024-30_2024-27delGATT[2]	intron 7	49%
c.2494-25_2494-22delTTTT[2]	intron 11	40%
D12S1686[1]	3' *LEMD3* (23kb)	80%

[1]Microsatellite markers and corresponding heterozygosity taken from the Marshfield database.

[2]New deletion polymorphisms found in this study with heterozygosity calculated from our data.

RESULTS

19 new patients with osteopoikilosis, Buschke-Ollendorff syndrome and/or melorheostosis were included in the study. In this panel of patients, 7 novel *LEMD3* mutations were identified (Table 1), all are predicted to result in a loss-of-function of the protein. The detection of only inactivating mutations was in accordance with our initial report (Hellemans, et al., 2004). A high mutation detection rate was observed for patients in groups A and B in contrast to group C. A *LEMD3* mutation was identified in only one sporadic patient (D0402645) with melorheostosis (group C).

The identification of nonsense or frameshift mutations in 4 out of 5 patients from group A confirms that loss-of-function mutations in *LEMD3* can result in osteopoikilosis and BOS. No missense mutations in the *LEMD3* gene were observed in this group of patients. No mutation was identified in only one patient (04g3820) with osteopoikilosis. Unfortunately the diagnosis in this patient was based on a radiographic report and could not be verified since radiographs were destroyed.

One family from group B has been reported before (Butkus, et al., 1997). The proband (D0500261) is an adult female patient with melorheostosis. Her left upper limb is mainly affected with shortening of the forearm and hand. She has radiological signs of melorheostosis in the upper limbs and widespread osteopoikilosis lesions in shoulders, hips and ankles. Her three sibs have both osteopoikilosis and BOS skin lesions (Fig 1). Radiographic evaluation of the parents did not reveal any abnormalities (Butkus, et al., 1997). In all affected individuals two nucleotide changes (c.1963C>T and c.2488C>T) in the LEMD3 gene were observed. The cosegregation of both mutations indicates that they are located in cis. The nonsense mutation (c.1963C>T, p.Arg655X) either results in nonsense mediated decay or the production of a truncated protein with loss-of-function. The missense mutation (c.2488C>T, p.Arg830Cys) is therefore unlikely to have any phenotypic effect. Both mutations are present in all three generations, but radiographic and clinical information was only available for the second generation.

The index patient (D0503238) of the second family in group B also has melorheostosis. His right upper limb is mainly affected with restricted movement in the shoulder and elbow. In addition, his right arm is shorter than the left and shows an extensive yellowish plaque-like skin lesion. Radiographs at a younger age showed osteopoikilosis lesions in the carpal bones and middle metacarpal of the right hand. In addition, mild cortical hyperostosis of the right radius was observed. This boy belongs to a larger family with BOS. Heterozygosity for a c.830dupA mutation was found in him and his affected mother (Table 1 and Fig. 1).

A nonsense mutation (c.1913T>A) was identified in only 1 patient (D0404645) from group C. The mutation was absent in both parents. This boy presented in infancy with flexion contractures of 2nd and 3rd fingers of the right hand. Radiographs showed mild cortical hyperostosis of second and third metacarpals and phalanges. Osteopoikilosis lesions were seen in the right elbow and shoulder. On follow-up the boy developed a scleroderma-like lesion on the right forearm. For the remaining 11 sporadic patients in group C with no detectable germline mutation, the possibility of somatic mosaicism for a *LEMD3* mutation was postulated. To further explore this hypothesis, biopsies were taken from affected skin and bone lesions in 2 patients with melorheostosis (04g3961 and D0501013). Analysis of gDNA extracted from these cell cultures provided no evidence of somatic mosaicism in these patients. No *LEMD3* mutation was found and allelic loss was excluded.

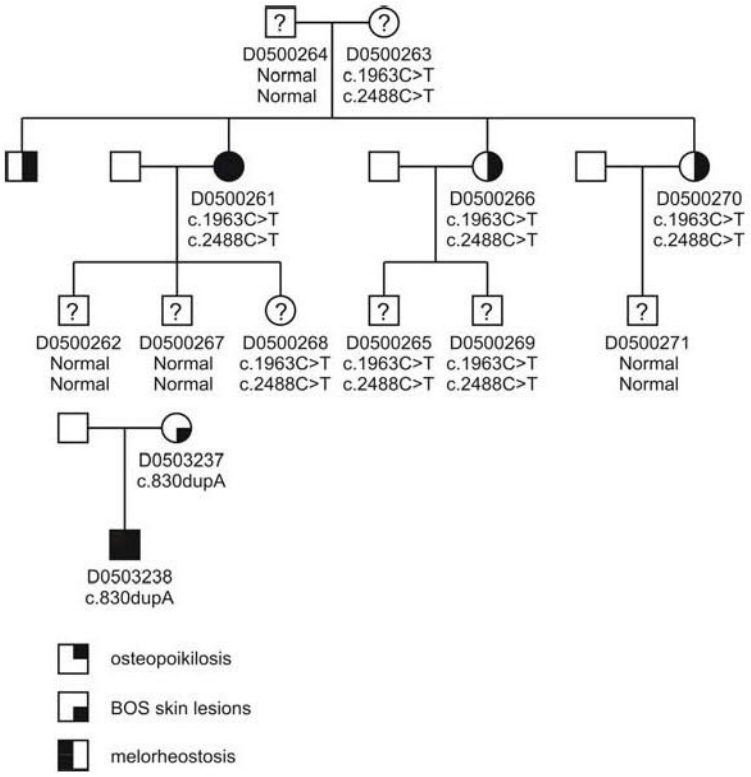

Figure 1. Pedigrees of the families in group B. The results of the *LEMD3* analysis are shown below the identification number of each individual. In the largest family (reported by Butkus et al.) clinical and radiographic information is only available for the second generation.

DISCUSSION

Using linkage analysis and microdeletion mapping we have recently identified loss-of-function *LEMD3* mutations in 6 unrelated osteopoikilosis patients with or without BOS skin lesion or melorheostosis (Hellemans, et al., 2004). To further explore the allelic heterogeneity within this group of disorders we screened a larger series of patients including a number of cases with isolated melorheostosis. In this panel of 19 patients, 7 novel *LEMD3* mutations were identified, all were predicted to result in loss-of-function of the LEMD3 protein. The identification of loss-of-function mutations in 4/5 patients with osteopoikilosis or BOS (group A), and in 2 families with the co-occurrence of BOS and melorheostosis (group B) are in agreement with our initial results (Hellemans, et al., 2004).

A *LEMD3* mutation could be identified in only 1/12 patients with isolated melorheostosis. In addition, no evidence of somatic mosaicism could be found when analyzing skin and bone lesions in two patients with melorheostosis. Since the biopsies may contain a mixture of both mutant and normal cells, the possibility of a somatic *LEMD3* mutation in these melorheostosis patients can not be totally excluded since the culturing procedures could, theoretically, have selected against mutant cells. Studies in patients with neurofibromatosis type I have shown that a somatic mutation is present in only a subset of cells and that optimized culturing conditions are necessary for the detection of the second hit in neurofibromas (Serra, et al., 2000). Also, the somatic mutation may reside outside the coding region and therefore be missed by our screening strategy. We did not analyze the promoter region or other regulatory sequences since these parts of the gene have not yet been fully characterized. Alternatively, the co-occurrence of osteopoikilosis and melorheostosis may just be a coincidence without implying that *LEMD3* is the disease-causing gene in the latter condition. Three families (Butkus, et al., 1997; Debeer, et al., 2003; Nevin, et al., 1999) and more than 20 cases (Ghai and Sharma, 2003) with this association however have been reported so far, making this assumption rather unlikely. It is possible that haploinsufficiency for LEMD3 is merely a predisposing factor for the development of melorheostosis lesions in families with osteopoikilosis or BOS

and another genetic defect, most likely at the somatic level and also involving the TGFβ/BMP pathway, is responsible for the majority of sporadic cases of isolated melorheostosis.

The observation that both melorheostosis patients from group B (D0503238; D0500261) and the one melorheostosis patient from group C with a *LEMD3* mutation (D0402645) had both melorheostosis and osteopoikilosis lesions on radiographs is intriguing. Osteopoikilosis lesions were not observed or reported in the other 11 mutation-negative melorheostosis patients from group C. However, not all of those patients had an extensive radiographic evaluation. We therefore conclude that further studies will be necessary to confirm that only melorheostosis patients with osteopoikilosis lesions have germline *LEMD3* mutations. The elucidation of the underlying genetic defect in the remaining and apparently larger population of sporadic melorheostosis patients should be the other major focus of future research in this group of sclerosing bone dysplasias.

ACKNOWLEDGMENTS

We thank the affected individuals and families for their interest and cooperation. This study was supported, in part, by the Fund for Scientific Research, Flanders, with a mandate fundamental clinical research to P.D. and G.R.M. and a research assistantship to P.C.M.V. J.H. is funded by the Institute for the Promotion of Innovation by Science and Technology in Flanders. This study was also supported by grants from the European Commission (grant QLG1-CT-2001-02188 to support the European Skeletal Dysplasia Network, www.esdn.org).

REFERENCES

Benli IT, Akalin S, Boysan E, Mumcu EF, Kis M, Turkoglu D. 1992. Epidemiological, clinical and radiological aspects of osteopoikilosis. J Bone Joint Surg Br 74(4):504-6.

Butkus CE, Michels VV, Lindor NM, Cooney WP, 3rd. 1997. Melorheostosis in a patient with familial osteopoikilosis. Am J Med Genet 72(1):43-6.

Campbell CJ, Papademetriou T, Bonfiglio M. 1968. Melorheostosis. A report of the clinical, roentgenographic, and pathological findings in fourteen cases. J Bone Joint Surg Am 50(7):1281-304.

Debeer P, Pykels E, Lammens J, Devriendt K, Fryns JP. 2003. Melorheostosis in a family with autosomal dominant osteopoikilosis: Report of a third family. Am J Med Genet 119A(2):188-93.

Endo H, Katsumi A, Kuroda K, Utani A, Moriya H, Shinkai H. 2003. Increased procollagen alpha1(I) mRNA expression by dermal fibroblasts in melorheostosis. Br J Dermatol 148(4):799-803.

Ghai S, Sharma R. 2003. Mixed sclerosing bone dysplasia--a case report with literature review. Clin Imaging 27(3):203-5.

Green AE, Jr., Ellswood WH, Collins JR. 1962. Melorheostosis and osteopoikilosis, with a review of the literature. Am J Roentgenol Radium Ther Nucl Med 87:1096-111.

Greenspan A. 1991. Sclerosing bone dysplasias--a target-site approach. Skeletal Radiol 20(8):561-83.

Greenspan A, Azouz EM. 1999. Bone dysplasia series. Melorheostosis: review and update. Can Assoc Radiol J 50(5):324-30.

Happle R. 2004. Melorheostosis may originate as a type 2 segmental manifestation of osteopoikilosis. Am J Med Genet 125A(3):221-3.

Hellemans J, Preobrazhenska O, Willaert A, Debeer P, Verdonk PC, Costa T, Janssens K, Menten B, Van Roy N, Vermeulen SJ, Savarirayan R, Van Hul W, Vanhoenacker F, Huylebroeck D, De Paepe A, Naeyaert JM, Vandesompele J, Speleman F, Verschueren K, Coucke PJ, Mortier GR. 2004. Loss-of-function mutations in LEMD3 result in osteopoikilosis, Buschke-Ollendorff syndrome and melorheostosis. Nat Genet 36(11):1213-8.

Lagier R, Mbakop A, Bigler A. 1984. Osteopoikilosis: a radiological and pathological study. Skeletal Radiol 11(3):161-8.

Lin F, Morrison JM, Wu W, Worman HJ. 2005. MAN1, an integral protein of the inner nuclear membrane, binds Smad2 and Smad3 and antagonizes transforming growth factor-beta signaling. Hum Mol Genet 14(3):437-45.

Nevin NC, Thomas PS, Davis RI, Cowie GH. 1999. Melorheostosis in a family with autosomal dominant osteopoikilosis. Am J Med Genet 82(5):409-14.

Schorr WF, Optiz JM, Reyes CN. 1972. The connective tissue nevus-osteopoikilosis syndrome. Arch Dermatol 106(2):208-14.

Serra E, Rosenbaum T, Winner U, Aledo R, Ars E, Estivill X, Lenard HG, Lazaro C. 2000. Schwann cells harbor the somatic NF1 mutation in neurofibromas: evidence of two different Schwann cell subpopulations. Hum Mol Genet 9(20):3055-64.

Vanhoenacker FM, De Beuckeleer LH, Van Hul W, Balemans W, Tan GJ, Hill SC, De Schepper AM. 2000. Sclerosing bone dysplasias: genetic and radioclinical features. Eur Radiol 10(9):1423-33.

Paper 5

Hellemans and Mortier. Book chapter in Inborn Errors of Development

Role of LEMD3 in skeletal development and dysplasias. Chapter for the second edition of CJ Epstein, RP Erickson, A Wynshaw-Boris (eds.) *Inborn Errors of Development.* Oxford University Press, New York. (submitted).

Osteopoikilosis, the Buschke-Ollendorff syndrome (BOS) and melorheostosis are rare sclerosing bone dysplasias that can co-occur within the same family. Osteopoikilosis and BOS are benign disorders with autosomal dominant inheritance, whereas melorheostosis is usually an isolated anomaly with symptoms like contractures, stiffness or chronic pain. These dysplasias can be caused by loss of function mutations in the LEMD3 gene which encodes a protein of the inner nuclear membrane. It interacts with receptor activated SMADs, leading to a suppression of SMAD mediated BMP and TGFβ signaling. Loss of suppression of these signaling pathways is suspected to be responsible for the sclerosis observed in these disorders.
This overview has been submitted as a chapter in Inborn Errors of Development, Chapter 39: LEMD3 in osteopoikilosis, the Buschke-Ollendorff syndrome and melorheostosis.

LEMD3: an inner nuclear membrane protein inhibiting the BMP and TGFβ signaling pathways

LEMD3 is an integral protein of the inner nuclear membrane and has a molecular mass of about 100 kDa. It is composed of a nucleoplasmic N-terminal domain, a first transmembrane segment, a luminal loop, a second transmembrane segment and a nucleoplasmic C-terminal domain (Fig. 39-1)(*Lin et al. 2000*). LEMD3 was previously known as MAN1. It was initially identified as a nuclear envelope protein recognized by autoantibodies from a patient (MAN refers to the initials of this patient) with an ill-defined collagen vascular disease (*Paulin-Levasseur et al. 1996*). To avoid confusion with the abbreviations of the different mannosidase enzymes, MAN1 was recently renamed as LEMD3 (LEM domain containing 3), herewith referring to the LEM domain in the N-terminal portion of the protein. The LEM domain is a conserved globular motif of approximately 40 amino acids found in several inner nuclear membrane and nucleoplasmic proteins. "LEM" refers to the three proteins in which the domain was initially characterized: LAP2, emerin and MAN1.

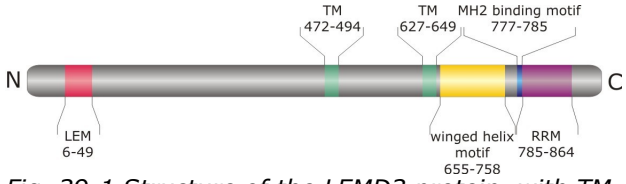

Fig. 39-1 Structure of the LEMD3 protein, with TM indicating the transmembrane domains

A subtractive proteomics study suggests that there are approximately 80 integral proteins of the inner nuclear membrane, many of which have been shown to bind to lamins, chromatin components or both. LEMD3 is no exception. Like all LEM-domain containing proteins tested, it binds directly to A- or B-type lamins and the barrier-to-autointegration factor (BAF) (*Gruenbaum et al. 2005*). Binding to lamin A and lamin B1 is mediated by the N-terminal domain of LEMD3 and is at least partially responsible for retainment of LEMD3 in the inner nuclear membrane (Fig. 39-2) (*Wu et al. 2002; Ostlund et al. 2006*). The importance of this interaction has been demonstrated for the *C. elegans* homologue of LEMD3, Ce-MAN1 that is undetectable at the nuclear envelope when lmn-1 expression is reduced (*Liu et al. 2003*). The N-terminal domain has been found to interact with emerin as well.
Structural analysis of the C-terminal region of LEMD3 revealed the presence of a winged helix motif, required for DNA binding and located outside the previously delineated RNA recognition motif (RRM) (*Caputo et al. 2006*). An MH2 binding domain, responsible for SMAD interaction, is located between both motifs (Fig. 39-1). This shows that the regions involved in DNA binding and SMAD interaction are essentially different, suggesting that LEMD3 binds simultaneously to R-SMADs and their targeted DNA sequences (*Caputo et al. 2006*). The C-terminal domain of LEMD3 binds to the transcriptional regulator germ cell-less (GCL)

and BAF, a protein that can form bridges between the LEM-domain proteins and the chromatin (*Mansharamani and Wilson 2005*) (Fig. 39-2).
In C. elegans, Ce-MAN1 and Ce-emerin have overlapping functions in chromosome segregation and cell division (*Liu et al. 2003*). In addition, the *Xenopus* ortholog XMAN1 has been shown to play a role in bone morphogenetic protein (BMP) signaling (*Osada et al. 2003; Raju et al. 2003*). In a functional screening for neuralizing factors, Osada et al. identified XMAN1 as a Smad-interacting protein regulating neural development by antagonizing BMP signaling. Using deletion mutant analysis, they showed that the BMP-antagonizing activities were located in the C-terminal portion of the protein and that this domain strongly associated with BMP responsive Smads (Smad1, Smad5 and Smad8), weakly with the transforming growth factor beta (TGFβ) responsive Smads (Smad2 and Smad3) but not with the common mediator Smad4 or the inhibitory Smads (Smad6 and Smad7) (*Osada et al. 2003*). Using a yeast-two hybrid screening for Smad1 interaction partners, Raju et al. identified SANE (Smad1 antagonistic effector) as a novel protein with significant sequence similarity to nuclear envelop proteins. SANE is identical to XMAN1 and shows 55% overall identity to human LEMD3, with greater similarity (up to 85%) in the C-terminal part. Except for the LEM domain, much of the N-terminal domain of LEMD3 diverges significantly from the

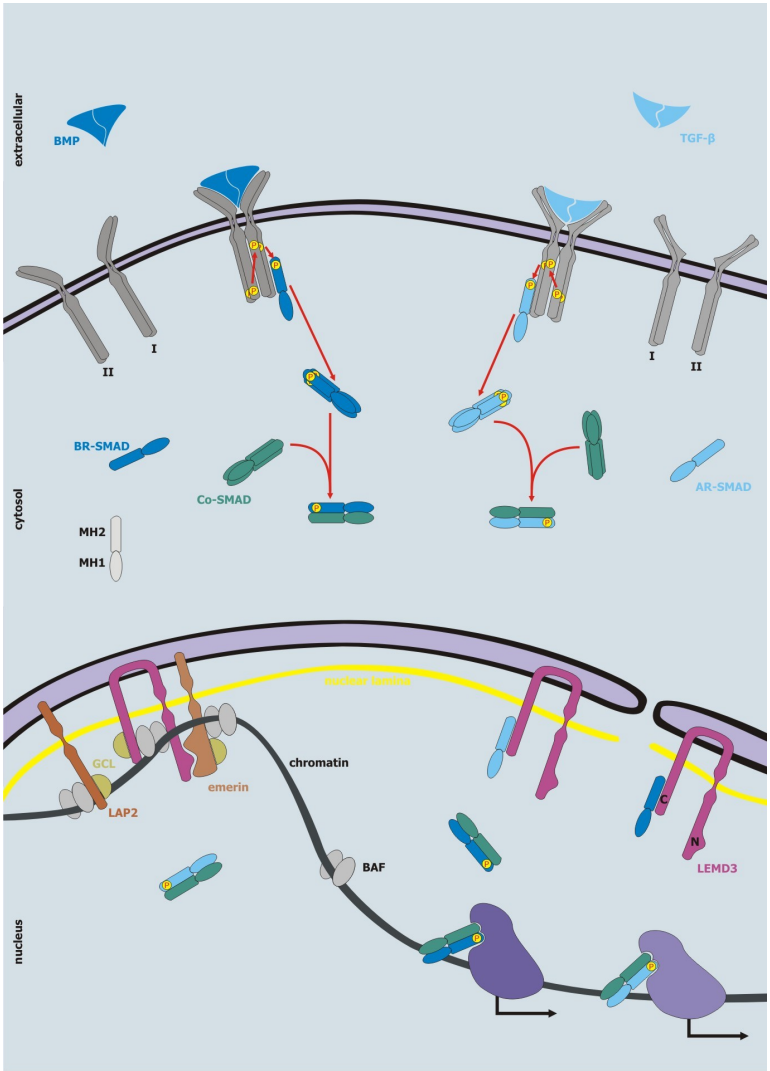

Fig. 39-2 Schematic presentation of SMAD mediated BMP and TGFβ signal transduction, and LEMD3 interaction partners in the nucleus. "P" indicates phosphorylation of receptors or R-SMADs. The arrows at the bottom of the picture represent transcription of BMP and TGFβ target genes.

corresponding region of SANE or XMAN1. Raju et al. showed that SANE co-immunoprecipitates with Smad1 and strongly interacts with the BMP-specific Smads but only weakly with TGFβ-specific Smads. In addition, the BMP-specific type I receptors (ALK3 and ALK6) strongly associated with SANE, but interaction with ALK2 and ALK4 was barely detectable. BMP type I receptor interaction was mediated through the N-terminal domain, while the C-terminal domain was required for Smad1 binding. SANE specifically reduced Smad-mediated BMP signaling but did not disrupt activin or TGFβ signaling. Inhibition appeared to be mediated by reducing BMP-induced Smad phosphorylation and nuclear translocation in a dose dependent manner (*Raju et al. 2003*). In contrast to its *Xenopus* ortholog, human LEMD3 interacts with all receptor activated SMAD proteins (R-SMADs) (Fig. 39-2). This interaction is mediated by the C-terminal domain of LEMD3 and the MH2 domain of the R-SMADs and is independent of the SMAD phosphorylation status. LEMD3 does not affect the expression or stability of R-SMADs, but reduces the amount of phosphorylated SMADs in the nucleus and blocks hetero-oligomerization of R-SMADs with SMAD4. Through its interaction with the R-SMADs, LEMD3 acts as a specific repressor of TGFβ, activin and BMP signaling (*Paper 2: Hellemans et al. 2004; Pan et al. 2005*). Decreasing LEMD3 expression results in an increase in transcriptional activation of TGFβ, activin or BMP responsive promotors. The expression level of LEMD3 appears to be important for cell survival since both overexpression and attempts to reduce LEMD3 expression with antisense constructs result in cell death (*Pan et al. 2005*).

Osteopoikilosis, the Buschke-Ollendorff syndrome and melorheostosis

Osteopoikilosis (MIM #166700), Buschke-Ollendorff syndrome (BOS, MIM #166700) and melorheostosis (MIM #155950) are rare sclerosing bone dysplasias that can co-occur within the same family. The Nosology and Classification of Genetic Skeletal Disorders (2006 revision) has classified these disorders in group 22 (increased density group, without modification of bone shape) (*Superti-Furga 2007*). Osteopoikilosis is a benign condition with autosomal dominant inheritance and an estimated prevalence of 1/20,000. The first patient found to have this disorder was described by the German surgeon Alfred Stieda in 1905 (*Stieda 1905*), but the term "osteopoikilie" (spotted bones) was not used until 1916 (*Ledoux-Rebard et al. 1916*). Osteopoikilosis is characterized radiographically by a symmetric but unequal distribution of multiple, small and round to oval hyperostotic lesions in different parts of the skeleton (Fig. 39-3A). The number can vary from a few to many lesions involving nearly all bones. This variable expression is not only observed between families but also within the same family. In a study of 4 families including 53 affected individuals, Benli et al. noted that the lesions are most common in the epimetaphyseal regions of the long tubular bones and that their number and bone density may increase with age (*Benli et al. 1992*). Lesions are usually not found in the diaphysis of the tubular bones.

Occurrence of sclerotic lesions (based on 53 patients in 4 families)	
Hand phalanges	100%
Carpals	97.4%
Metacarpals	92.3%
Foot phalanges	87.2%
Metatarsals	84.4%
Tarsals	84.6%
Pelvis	74.4%
Femur	74.4%
Radius	66.7%
Ulna	66.7%
Sacrum	58.9%
Humerus	28.2%
Tibia	20.5%
Fibula	12.8%
General characteristics	
Bilateral occurrence of lesions	94.8%
# foci per bone	1 - 1000
Size	1x1 mm – 12x16 mm
Shape	Linear, ellipsoid or bullet shaped
Lesions are most common in the metaphyses of the long tubular bones	
Number and radiodensity of lesions increased with age	

Table 1 Distribution of bone lesions in osteopoikilosis patients (adapted from Benli et al. 1992)

The size and number of lesions per bone ranged from 1x1 mm to 12x16 mm and from 1 to 1000, respectively. The hyperostotic lesions are most commonly found in the bones of hands and feet with the largest number usually detected in the pelvis (table 1). The axial skeleton (skull, ribs and vertebrae) is rarely affected.

The lesions usually become more apparent during childhood but osteopoikilosis has been observed in neonates and even in a 4-month-old fetus (*Green et al. 1962*). Affected individuals are by definition asymptomatic. The lesions do not affect the structure and function of the bone. There is no predisposition to fractures. Histopathologic studies show that the osteopoikilosis lesions are foci of numerous bone trabeculae that are slightly thicker than normal but still resemble the structure of spongy bone. They merge into the surrounding structures gradually, disappearing among those of normal spongiosa. The thicker trabeculae consist of lamellar bone with a parallel arrangement for the most part, but in a few instances they are arranged concentrically around blood vessels (*Schmorl 1931*).

Osteopoikilosis has been associated with various other anomalies, usually in single case reports, suggesting coincidental rather than causal relationships (*Green et al. 1962; Mindell et al. 1978; Weisz 1982; Ayling and Evans 1988; Gunal et al. 1993; Gunal and Kiter 2003*). However, there is at least one well-defined association, the Buschke-Ollendorff syndrome (BOS), that is characterized by osteopoikilosis and connective tissue nevi. In 1928 Buschke and

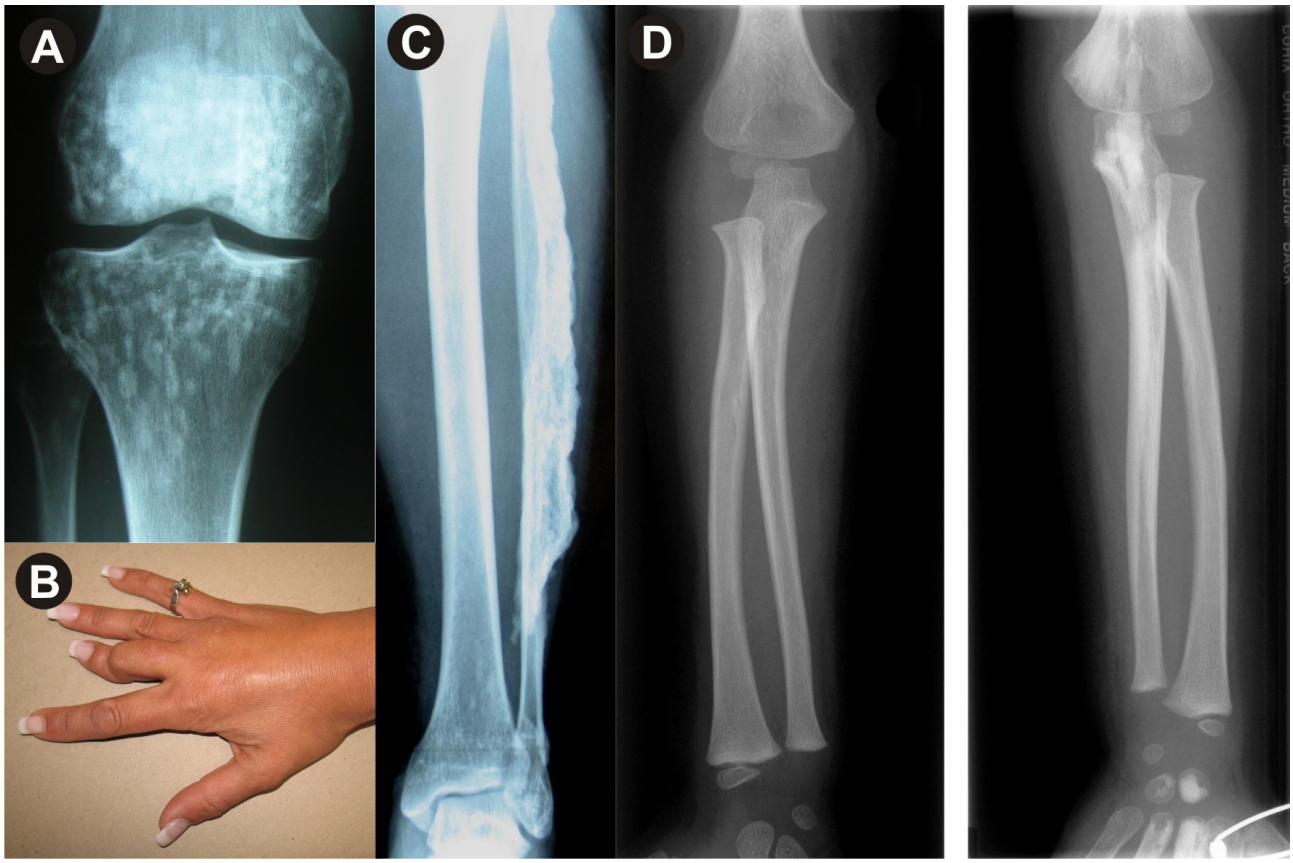

Fig. 39-3 (A) Anteroposterior radiograph of the knee showing multiple osteopoikilosis lesions in the distal portion of the femur and the proximal portion of the tibia. A few lesions are also present in the fibular head. (B) Joint contractures of the middle finger in a female patient with melorheostosis. (C) Anteroposterior radiograph of the left lower leg in a patient with melorheostosis (patient with p.Val759fs mutation listed in table 2). An extensive melorheostosis lesion, resembling dripping candle grease, is present along the diaphysis of the fibula. A few osteopoikilosis lesions are also visible in the distal portion of the tibia. (D) Radiograph of both forearms in a patient with melorheostosis. The affected left forearm is shown on the right side of the picture. The right forearm (shown on the left) is normal. The melorheostosis lesions in the left forearm start at the base of the third and fourth metacarpals (shown at bottom of figure), extend over the carpal bones towards the ulna and finally cross the elbow joint towards the distal portion of the humerus.

Ollendorff described dermatofibrosis lenticularis disseminata as the skin manifestation of osteopoikilosis (*Buschke and Ollendorff 1928*). The cutaneous lesions may be present at birth or appear later in childhood or even adulthood (*Morrison et al. 1977*). They are connective tissue nevi and appear as either numerous, widely disseminated, skin-colored to yellow small papules or more localized and asymmetrically distributed larger lesions known as yellow plaques. Histological studies of these skin lesions show variable degrees of connective tissue abnormalities affecting the collagen bundles and elastic fibers. The collagen bundles can be thickened or normal, the elastic fibers can be increased, broad and interlacing, diminished, fragmented or normal. This variability has been seen in patients within a family and even between different lesions in the same patient (*Schorr et al. 1972*). Calcification is not observed in the BOS skin lesions, distinguishing it from pseudoxanthoma elasticum.

In 1922, the French physicians, Léri and Joanny, described the first case of melorheostosis (*Léri and Joanny 1922*). They used the term "melorheostosis" for this sclerosing bone disorder because the cortical hyperostosis of affected bones resembles dripping candle grease ("melo" and "rhe(o)" are referring to Greek words for limb and flow respectively) (Fig. 39-3C). In contrast to osteopoikilosis, the hyperostotic lesions in melorheostosis usually affect the diaphysis (cortex) of the tubular bones. There is a tendency for monomelic distribution but also different, usually contiguous bones from the same sclerotome, can be affected. The lesions have a linear pattern and can cross joints when involving neighboring bones (Fig. 39-3D). The linear hyperostosis of the cortex can extend internally into the medullary canal or externally with periosteal involvement resulting in the characteristic wavy outline of the affected bone. In some patients with melorheostosis spotty lesions reminiscent of osteopoikilosis can be observed in the epiphyses of the affected long bones (*Green et al. 1962*). Small bone deposits in the surrounding soft tissues have also been reported (*Campbell et al. 1968; Greenspan 1991*). The hyperostosis is often accompanied by hyperplasia and abnormalities of the adjacent connective tissues (e.g. scleroderma-like lesions or fibrosis) (*Happle 2004*). Melorheostosis may be asymptomatic but often causes joint contractures (Fig. 39-3B), stiffness or chronic pain. Severe cases may even present with shortening of the affected bones. Histological examination reveals hyperostotic cortical bone formation with thickened trabeculae and fibrotic changes in the marrow spaces. The bone appears primitive and consists largely of primary haversian systems that are almost obliterated by the deposition of sclerotic, thickened and somewhat irregular lamellae (*Greenspan and Azouz 1999*).

Whereas osteopoikilosis and BOS are autosomal dominant conditions, melorheostosis is predominantly a sporadic disorder. However, individuals with melorheostosis have been observed in families with osteopoikilosis (*Butkus et al. 1997; Nevin et al. 1999; Debeer et al. 2003*). We are aware of at least one family with two affected cousins with melorheostosis. Also, sporadic patients with melorheostosis in association with osteopoikilosis and osteopathia striata have been described (*Ghai and Sharma 2003*).

Heterozygous *LEMD3* mutations can cause osteopoikilosis, the Buschke-Ollendorff syndrome and melorheostosis

Using a genome wide linkage analysis and subsequent candidate gene approach in three families with the variable co-occurrence of osteopoikilosis, BOS and melorheostosis, we were able to identify LEMD3 as the causal gene in this group of disorders (*Paper 2: Hellemans et al. 2004*). The LEMD3 gene is located on chromosome 12q14, contains 13 exons and has a size of 4,744 bp. It encodes a 911 amino acid protein, LEMD3.

All *LEMD3* mutations identified so far are predicted to result in a loss of function of the protein (*Paper 3: Hellemans et al. 2006*). The spectrum of *LEMD3* mutations includes complete gene deletions, nonsense mutations, frameshift mutations and splice site mutations that cause a frameshift with a premature stop codon as a consequence. The loss-of-function effect of these mutations results from either total deletion of the gene, nonsense mediated decay of the mutant transcripts or formation of a truncated protein that lacks the SMAD-interacting C-terminal domain (*Paper 2: Hellemans et al.*

2004). Since all mutations are predicted to result in haploinsufficiency for LEMD3, the germline mutation alone can not account for the phenotypic variability. Other factors such as modifying genes, environmental influences and perhaps (but yet unidentified) somatic defects at the other *LEMD3* allele or within the signaling pathways must influence the ultimate phenotype.

Table 2 summarizes the genotypic and phenotypic data in a series of 47 patients. The patients are classified in 4 groups depending on the phenotype and the familial occurrence of the disorder. Group A consists of three unrelated patients sharing osteopoikilosis, proportionate short stature and learning problems as common clinical features. In two of these patients a microdeletion of approximately 6 Mb in size and encompassing the LEMD3 gene on 12q14, was identified. The third patient reported by Jurenka et al. was not available for genetic testing. Group B contains sporadic and familial cases with osteopoikilosis and/or BOS skin lesions. A germline *LEMD3* mutation was identified in the majority of these patients (14/17). In one osteopoikilosis patient, for whom the diagnosis could not be

phenotype	nucleotide and residue changes	reference
Group A		
OPOI, MOS, short stature, MR	not tested	*Jurenka et al. 1995*
OPOI, short stature, MR, ectopic kidney	microdeletion	*Hellemans et al. 2004*
OPOI, short stature, MR	microdeletion	Unpublished
Group B		
BOS	c.2134dupT; p.Met712fs	*Hellemans et al. 2004*
BOS	c.1185dupT; p.Gly395fs	*Hellemans et al. 2004*
OPOI	c.1033_1035delGGGinsC; p.Gly345fs	*Hellemans et al. 2004*
OPOI	c.1921+5delG; exon skip - frameshift	*Hellemans et al. 2004*
OPOI	c.457C>T; p.Gln153X	*Hellemans et al. 2004*
OPOI	c.1801G>T; p.Glu601X	*Hellemans et al. 2006*
BOS	c.1323C>A; p.Tyr441X	*Hellemans et al. 2006*
BOS	c.1873C>T; p.Arg625X	*Hellemans et al. 2006*
BOS	c.1914dupA; p.Leu638fs	*Hellemans et al. 2006*
OPOI	c.2494-9A>G; splice site	*Hellemans et al. 2006*
BOS	c.1873C>T; p.Arg625X	*Hellemans et al. 2006*
BOS	c.2245C>T;p.Gln749X	*Hellemans et al. 2006*
BOS	c.1707_1708delTG; p.Pro569fs	Unpublished
OPOI	c.1813delA; p.Ile605fs	Unpublished
OPOI (1 patient)	normal	*Hellemans et al. 2006*
BOS (2 patients)*	normal	Unpublished
Group C		
MOS in BOS family	c.1609C>T; p.Arg537X	*Hellemans et al. 2004, Debeer et al. 2003*
MOS in BOS family	c.830dupA; p.Lys277X	*Hellemans et al. 2006*
MOS in BOS family	[c.1963C>T,c.2488C>T]; p.Arg655X	*Hellemans et al. 2006, Butkus et al. 1997*
MOS in BOS family	c.2275_2278delGTTA ; p.Val759fs	Unpublished
Group D		
MOS	c.1913T>A; p.Leu638X	*Hellemans et al. 2006*
MOS (22 patients)	normal	*Hellemans et al. 2006*

Table 2 Overview of LEMD3 mutations in 4 different patient groups (OPOI: osteopoikilosis, BOS: Buschke-Ollendorff syndrome, MOS: melorheostosis)

verified, and in 2 BOS patients, for whom the presence of bone lesions could not be demonstrated, no *LEMD3* mutation was found. Group C consists of 4 melorheostosis patients who belong to a family with other relatives affected with osteopoikilosis or BOS. Sporadic patients with melorheostosis are classified in group D. A germline *LEMD3* mutation was found in all 4 patients from group C but in only 1 patient from group D. In the latter patient, besides melorheostosis also remote osteopoikilosis lesions were visible on skeletal radiographs. The co-occurrence of osteopoikilosis and melorheostosis lesions in the same individual was also observed in patients from group C. On the other hand, osteopoikilosis lesions were not found in the 22 patients with normal *LEMD3* results from group D (but not all patients had an extensive radiographic evaluation). The presence of osteopoikilosis lesions seems therefore to be a good indicator for the existence of a germline *LEMD3* mutation.

The cause of the sporadic and isolated form of melorheostosis still remains unknown. The possibility of somatic mosaicism for a *LEMD3* mutation has been investigated in two patients from group D but no *LEMD3* mutations were found when analyzing affected skin and bone samples (*Paper 3: Hellemans et al. 2006*). In addition, a second somatic mutation in *LEMD3* as explanation for the localized character of the skin lesions in BOS patients, has not yet been identified (*Paper 2: Hellemans et al. 2004*).

The group of acromelic dysplasias contains 2 conditions which share the characteristic cone-shaped epiphyses with acrocapitofemoral dysplasia, and for which the causal genetic defect has not yet been discovered. Screening of the IHH gene in two patients with acrodysostosis and in one patient with Saldino-Mainzer dysplasia did, however, not reveal the presence of *IHH* mutations (unpublished data).

Establishing the diagnosis

Osteopoikilosis is a benign condition, usually found by chance when radiographs are taken for other purposes. The diagnosis of osteopoikilosis mainly relies on a careful radiographic evaluation. In our experience, the lesions are most commonly found in the shoulders, hands, pelvis, knees and feet. The lesions can be scarce at a young age and therefore be missed early on in life.

The diagnosis of BOS requires the presence of both osteopoikilosis lesions and connective tissue nevi, the latter preferentially confirmed at the histological level after skin biopsy. In families with BOS, affected individuals can either have both bone and skin lesions or just one of these manifestations.

The diagnosis of melorheostosis is usually based on clinical evaluation and the finding of the characteristic radiographic abnormalities. Plain radiographs are usually sufficient to confirm the diagnosis. Scintigraphy reveals increased tracer uptake in the affected bone and soft tissue areas. Computed tomography and magnetic resonance imaging (MRI) are usually not needed for diagnosis. The bone and soft tissue lesions have low signal activities on all MRI sequences (*Greenspan and Azouz 1999; Judkiewicz et al. 2001*).

Management and genetic counseling

Osteopoikilosis and BOS are benign conditions that do not require any treatment. Both conditions are inherited in an autosomal dominant manner. Affected individuals have a 50% risk of passing on the mutant allele to each offspring. Prenatal diagnosis is theoretically possible when the mutation has been identified but usually not indicated because of the benign nature of both disorders.

Melorheostosis is usually a sporadic condition with no increased risk for the offspring. However, individuals with a germline mutation in *LEMD3* have an increased risk to develop the disorder. Melorheostosis can be asymptomatic but often causes pain, joint contractures, deformity or even shortening of affected bones. The disease can be progressive with periodic exacerbations. There is currently no cure for the disorder. Surgery is possible to correct bone deformities and asymmetric bone growth. However, bone healing after osteotomy can be problematic in melorheostosis patients. Soft tissue releases in children have a high failure rate and are often complicated by abnormal scar formation. Contracture releases are more effective in adults and the outcome seems to improve with the use of rotation flaps. Prior to surgery, the

application of external fixators spanning the contracture area should be considered and this may even be the sole treatment. More details on these management issues can be found on the website of the Melorheostosis Association (www.melorheostosis.com – guidelines developed by Jeffrey C King, MD and James Dobyns, MD), a patient support group located in the USA. A second patient support group is based in the United Kingdom (www.melo.eu.com). Both organizations are important resources for both professionals and patients with melorheostosis.

Animal models

The function of LEMD3 orthologs has been examined in at least two animal models. In *Xenopus*, XMAN1 was found to neuralize the ectoderm and dorsalize the ventral mesoderm by antagonizing BMP signaling. Embryos injected with XMAN1 antisense morpholino oligos gastrulated normally but the development of the anterior structures was severely reduced and the eyes were absent or poorly formed (*Osada et al. 2003*). Knock-down experiments in *C. elegans* revealed that RNAi mediated removal of ~90% of Ce-Man1 was lethal to ~15% of embryos. However in the absence of Ce-emerin, ~90% reduction of Ce-Man1 was lethal to all embryos by the 100-cell stage (*Liu et al. 2003*). A Lemd3 knock-out mouse has been created (Baygenomics, California) but no data have yet been reported.

From mutation to phenotype

All data so far indicate that heterozygous inactivating germline mutations in *LEMD3* can cause osteopoikilosis and the Buschke-Ollendorff syndrome (*Paper 2: Hellemans et al. 2004; Paper 3: Hellemans et al. 2006*). The presence of a second, somatic *LEMD3* mutation as an explanation for the localized nature of the bone and skin lesions has not yet been shown. The situation for melorheostosis is more complex. Despite the evidence that haploinsufficiency for LEMD3 acts as a predisposing factor for the development of melorheostosis, the role of LEMD3 in the pathogenesis of isolated and sporadic melorheostosis is not yet fully understood. The overwhelming majority of patients with melorheostosis do not seem to harbor a germline mutation in *LEMD3*. Somatic mosaicism for a *LEMD3* mutation in these patients is a likely hypothesis but has not yet been shown when analyzing affected skin and/or bone tissues.

Osteopoikilosis, Buschke-Ollendorff syndrome and melorheostosis are characterized by bone lesions with increased bone density. This suggests that LEMD3 must play an important role in bone homeostasis. Several experiments have demonstrated the interaction of LEMD3 with BMP and TGFβ receptor activated SMADs (R-SMADs). This interaction leads to a decreased phosphorylation and nuclear localization of the R-SMADs, and ultimately in a reduced BMP and TGFβ signaling (*Paper 2: Hellemans et al. 2004; Pan et al. 2005*). Both pathways have been shown to be very important in bone homeostasis and the regulation of bone mineral density.

In-vitro and in-vivo experiments, analyzing the effect of TGFβ signaling on osteoblasts and osteoclasts, have revealed seemingly conflicting data suggesting both positive and negative effects on bone formation. For example, osteoblast proliferation, matrix deposition and collagen maturity are severely diminished in Tgfb1 knock-out mice, whereas mice with an increased Tgfb2 production show a dramatic, age-dependent loss of bone mass reminiscent of high-turnover osteoporosis (*Erlebacher and Derynck 1996; Geiser et al. 1998*). Strong evidence for a positive effect of TGFβ on bone formation in humans comes from the rare skeletal dysplasia, Camurati-Engelmann disease (CED). Camurati-Engelmann disease or progressive diaphyseal dysplasia is an autosomal dominant disorder characterized by a progressive cortical thickening of the diaphyses of the long bones. Hyperostosis is bilateral and symmetrical, and usually starts during childhood. A total of 10 different mutations in the TGFB1 gene have been found in CED patients, all leading to increased TGFβ activity (*Janssens et al. 2006*). The identification of activating mutations in *TGFB1* in patients with a CED demonstrates that increased TGFβ signaling can lead to hyperostosis.

Similarly, the effects of BMP signaling on bone formation have been studied. Reduction of BMP signaling, resulting from a dominant-negative BMP receptor (*BMPR-IB*) mutation in mice osteoblasts, impairs postnatal bone formation. Bone mineral density, bone volume and bone formation

rates in these mutant animals are severely reduced without changes in osteoblast and osteoclast numbers (*Zhao et al. 2002*). Transgenic mice overexpressing noggin, an extracellular BMP antagonist, have a reduced bone mineral density and decreased trabecular bone volume (*Devlin et al. 2003*). Both experiments demonstrate the positive effect of BMP signaling on bone formation.
In addition to its role in bone homeostasis, TGFβ signaling is also important for normal fibroblast activity. This may explain the skin involvement in BOS and melorheostosis. Patients with the latter disorder can show sclerodermatous skin lesions. Interestingly, increased TGFβ signaling has been observed in fibroblasts from patients with scleroderma, an autoimmune disorder characterized by progressive cutaneous and visceral fibrosis (*Mori et al. 2003; Asano et al. 2004*). A reduction in the expression of the inhibitory SMAD7 and upregulation of SMAD3 expression were found in the scleroderma skin lesions (*Dong et al. 2002*).
In conclusion, both BMP and TGFβ signaling seem to have a stimulatory effect on osteoblast and fibroblast function. Upregulation of BMP and TGFβ signaling as a consequence of LEMD3 haploinsufficiency may therefore explain both the skin and bone lesions in osteopoikilosis, BOS and melorheostosis patients.

References

Asano Y, Ihn H, Yamane K, Kubo M, Tamaki K (2004) Impaired Smad7-Smurf-mediated negative regulation of TGF-beta signaling in scleroderma fibroblasts. J Clin Invest 113:253-264

Ayling RM, Evans PE (1988) Giant cell tumor in a patient with osteopoikilosis. Acta Orthop Scand 59:74-76

Benli IT, Akalin S, Boysan E, Mumcu EF, Kis M, Turkoglu D (1992) Epidemiological, clinical and radiological aspects of osteopoikilosis. J Bone Joint Surg Br 74:504-506.

Buschke A, Ollendorff H (1928) Dermatofibrosis lenticularis disseminata und osteopathia condensans disseminata. Derm Wschr 86:257-262

Butkus CE, Michels VV, Lindor NM, Cooney WP, 3rd (1997) Melorheostosis in a patient with familial osteopoikilosis. Am J Med Genet 72:43-46.

Campbell CJ, Papademetriou T, Bonfiglio M (1968) Melorheostosis. A report of the clinical, roentgenographic, and pathological findings in fourteen cases. J Bone Joint Surg Am 50:1281-1304

Caputo S, Couprie J, Duband-Goulet I, Konde E, Lin F, Braud S, Gondry M, Gilquin B, Worman HJ, Zinn-Justin S (2006) The carboxyl-terminal nucleoplasmic region of MAN1 exhibits a DNA binding winged helix domain. J Biol Chem 281:18208-18215

Debeer P, Pykels E, Lammens J, Devriendt K, Fryns JP (2003) Melorheostosis in a family with autosomal dominant osteopoikilosis: Report of a third family. Am J Med Genet 119A:188-193

Devlin RD, Du Z, Pereira RC, Kimble RB, Economides AN, Jorgetti V, Canalis E (2003) Skeletal overexpression of noggin results in osteopenia and reduced bone formation. Endocrinology 144:1972-1978

Dong C, Zhu S, Wang T, Yoon W, Li Z, Alvarez RJ, ten Dijke P, White B, Wigley FM, Goldschmidt-Clermont PJ (2002) Deficient Smad7 expression: a putative molecular defect in scleroderma. Proc Natl Acad Sci U S A 99:3908-3913

Erlebacher A, Derynck R (1996) Increased expression of TGF-beta 2 in osteoblasts results in an osteoporosis-like phenotype. J Cell Biol 132:195-210

Geiser AG, Zeng QQ, Sato M, Helvering LM, Hirano T, Turner CH (1998) Decreased bone mass and bone elasticity in mice lacking the transforming growth factor-beta1 gene. Bone 23:87-93

Ghai S, Sharma R (2003) Mixed sclerosing bone dysplasia--a case report with literature review. Clin Imaging 27:203-205

Green AE, Jr., Ellswood WH, Collins JR (1962) Melorheostosis and osteopoikilosis, with a review of the literature. Am J Roentgenol Radium Ther Nucl Med 87:1096-1111

Greenspan A (1991) Sclerosing bone dysplasias--a target-site approach. Skeletal Radiol 20:561-583

Greenspan A, Azouz EM (1999) Bone dysplasia series. Melorheostosis: review

and update. Can Assoc Radiol J 50:324-330

Gruenbaum Y, Margalit A, Goldman RD, Shumaker DK, Wilson KL (2005) The nuclear lamina comes of age. Nat Rev Mol Cell Biol 6:21-31

Gunal I, Kiter E (2003) Disorders associated with osteopoikilosis: 5 different lesions in a family. Acta Orthop Scand 74:497-499

Gunal I, Seber S, Basaran N, Artan S, Gunal K, Gokturk E (1993) Dacryocystitis associated with osteopoikilosis. Clin Genet 44:211-213.

Happle R (2004) Melorheostosis may originate as a type 2 segmental manifestation of osteopoikilosis. Am J Med Genet 125A:221-223

Hellemans J, Debeer P, Wright M, Janecke A, Kjaer KW, Verdonk PC, Savarirayan R, Basel L, Moss C, Roth J, David A, De Paepe A, Coucke P, Mortier GR (2006) Germline LEMD3 mutations are rare in sporadic patients with isolated melorheostosis. Hum Mutat 27:290

Hellemans J, Preobrazhenska O, Willaert A, Debeer P, Verdonk PC, Costa T, Janssens K, Menten B, Van Roy N, Vermeulen SJ, Savarirayan R, Van Hul W, Vanhoenacker F, Huylebroeck D, De Paepe A, Naeyaert JM, Vandesompele J, Speleman F, Verschueren K, Coucke PJ, Mortier GR (2004) Loss-of-function mutations in LEMD3 result in osteopoikilosis, Buschke-Ollendorff syndrome and melorheostosis. Nat Genet 36:1213-1218

Janssens K, Vanhoenacker F, Bonduelle M, Verbruggen L, Van Maldergem L, Ralston S, Guanabens N, Migone N, Wientroub S, Divizia MT, Bergmann C, Bennett C, Simsek S, Melancon S, Cundy T, Van Hul W (2006) Camurati-Engelmann disease: review of the clinical, radiological, and molecular data of 24 families and implications for diagnosis and treatment. J Med Genet 43:1-11

Judkiewicz AM, Murphey MD, Resnik CS, Newberg AH, Temple HT, Smith WS (2001) Advanced imaging of melorheostosis with emphasis on MRI. Skeletal Radiol 30:447-453

Ledoux-Rebard R, Chabeneix, Dessane (1916) L'ostéopoicilie: forme nouvelle d'ostéite condensante généralisée sans symptomes cliniques. J Radiol Electrol 2:133-134

Léri A, Joanny J (1922) Une affection non décrite des os. Hyperostose "en coulée" sur toute la longueur d'un membre ou "mélorhéostose". Bull et Mém Soc Méd Hôp paris 46:1141-1145

Lin F, Blake DL, Callebaut I, Skerjanc IS, Holmer L, McBurney MW, Paulin-Levasseur M, Worman HJ (2000) MAN1, an inner nuclear membrane protein that shares the LEM domain with lamina-associated polypeptide 2 and emerin. J Biol Chem 275:4840-4847

Liu J, Lee KK, Segura-Totten M, Neufeld E, Wilson KL, Gruenbaum Y (2003) MAN1 and emerin have overlapping function(s) essential for chromosome segregation and cell division in Caenorhabditis elegans. Proc Natl Acad Sci U S A 100:4598-4603

Mansharamani M, Wilson KL (2005) Direct binding of nuclear membrane protein MAN1 to emerin in vitro and two modes of binding to barrier-to-autointegration factor. J Biol Chem 280:13863-13870

Mindell ER, Northup CS, Douglass HO, Jr. (1978) Osteosarcoma associated with osteopoikilosis. J Bone Joint Surg Am 60:406-408

Mori Y, Chen SJ, Varga J (2003) Expression and regulation of intracellular SMAD signaling in scleroderma skin fibroblasts. Arthritis Rheum 48:1964-1978

Morrison JG, Jones EW, MacDonald DM (1977) Juvenile elastoma and osteopoikilosis (the Buschke--Ollendorff syndrome). Br J Dermatol 97:417-422

Nevin NC, Thomas PS, Davis RI, Cowie GH (1999) Melorheostosis in a family with autosomal dominant osteopoikilosis. Am J Med Genet 82:409-414.

Osada S, Ohmori SY, Taira M (2003) XMAN1, an inner nuclear membrane protein, antagonizes BMP signaling by interacting with Smad1 in Xenopus embryos. Development 130:1783-1794

Ostlund C, Sullivan T, Stewart CL, Worman HJ (2006) Dependence of diffusional mobility of integral inner nuclear membrane proteins on A-type lamins. Biochemistry 45:1374-1382

Pan D, Estevez-Salmeron LD, Stroschein SL, Zhu X, He J, Zhou S, Luo K (2005) The integral inner nuclear membrane protein MAN1 physically interacts with the R-Smad proteins to repress signaling by the transforming growth factor-{beta} superfamily of cytokines. J Biol Chem 280:15992-16001

Paulin-Levasseur M, Blake DL, Julien M, Rouleau L (1996) The MAN antigens are non-lamin constituents of the nuclear lamina in vertebrate cells. Chromosoma 104:367-379

Raju GP, Dimova N, Klein PS, Huang HC (2003) SANE, a novel LEM domain protein, regulates bone morphogenetic protein signaling through interaction with Smad1. J Biol Chem 278:428-437

Schmorl G (1931) Anatomische Befunde bei einem Falle von Osteopoikilie. Fortschr a d Geb d Röntgenstrahlen 44:1-8

Schorr WF, Optiz JM, Reyes CN (1972) The connective tissue nevus-osteopoikilosis syndrome. Arch Dermatol 106:208-214

Stieda A (1905) Über umschriebene Knochenverdichtungen im Bereich der Substantia spongiosa in Roentgenbilde. Beitr Klin Chir 45:700-703

Superti-Furga A, Unger S. (2007) Nosology and classification of genetic skeletal disorders: 2006 revision. Am J Med Genet A. 143(1):1-18.

Weisz GM (1982) Lumbar spinal canal stenosis in osteopoikilosis. Clin Orthop Relat Res:89-92

Wu W, Lin F, Worman HJ (2002) Intracellular trafficking of MAN1, an integral protein of the nuclear envelope inner membrane. J Cell Sci 115:1361-1371

Zhao M, Harris SE, Horn D, Geng Z, Nishimura R, Mundy GR, Chen D (2002) Bone morphogenetic protein receptor signaling is necessary for normal murine postnatal bone formation. J Cell Biol 157:1049-1060

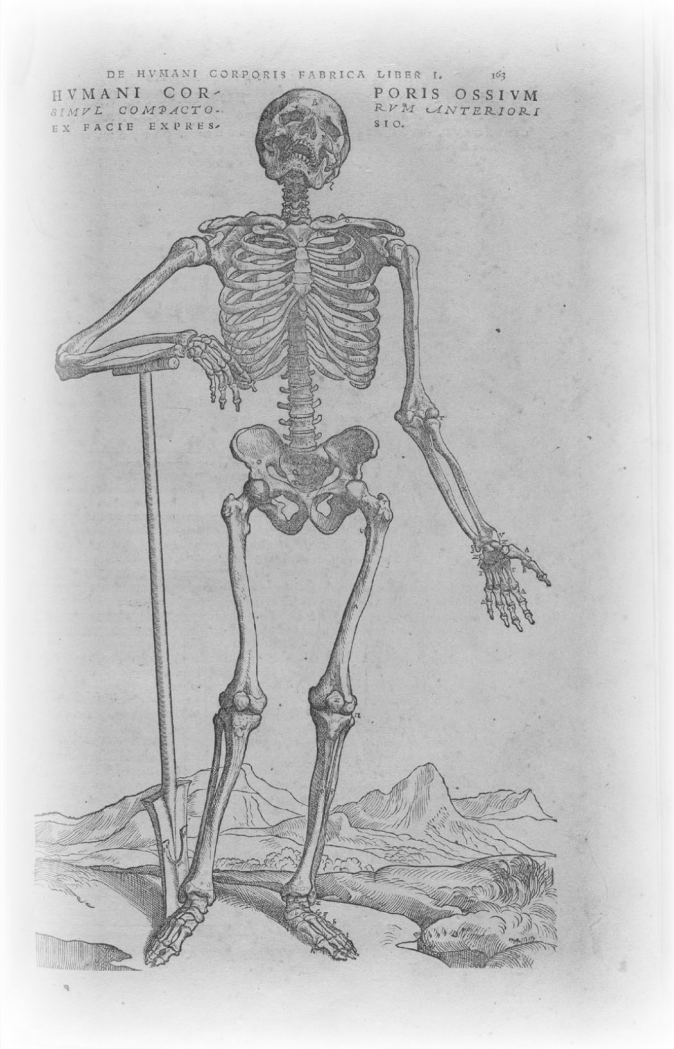

Chapter 4

qBase framework and software for qPCR data analysis

1 Introduction to qPCR

History

The polymerase chain reaction or PCR technique is the technology by which small amounts of template DNA can be specifically and exponentially amplified in an enzymatic reaction. For the invention of this technology, Karry B. Mullis received the Nobel Prize in Chemistry in 1993.

At the time of the first demonstration of the polymerase chain reaction in 1985, thermo-labile polymerase needed to be added to the reaction in each PCR cycle (*Saiki 1985*). The usage of thermo-stable polymerases was first reported in 1988, and unlocked the full potential of the PCR technology (*Saiki 1988*). Since amplification products of a PCR are analyzed after the completion of the reaction, classical PCR is called an endpoint detection technology. Endpoint detection is usually used for qualitative analysis but is not very well suited for quantitative measurements. It can at best be used semi-quantitatively. Real-time quantitative PCR (qPCR), on the other hand, does not use endpoint detection but measures the increase in DNA during the reaction (*Higuchi 1993*). The advantage of real time measurements is that they allow the determination of starting template copy number with high accuracy and sensitivity over a wide dynamic range. In addition they do not require any post PCR steps and can be analyzed without requiring gel electrophoresis. Therefore, qPCR is considered the method of choice for quantification of a limited number of target sequences for multiple samples in parallel.

Principles

In a normal PCR, template DNA is mixed with specific complementary oligonucleotides, free nucleotides and a thermostable polymerase in a suitable buffer. This mix is then placed in a thermocycler that cycles 25-40 times between 3 different temperatures: 94°C for the denaturation of the DNA, 45-65°C for the annealing of the oligonucleotides, and 72°C for the elongation of the oligonucleotides. In principle there is a doubling of the amount of target DNA after each cycle.

Real-time PCR is very similar but requires the addition of one extra component to the mix: a fluorescent reporter to monitor the amplification during the reaction. Basically two different types of reporter can be used: DNA-binding dyes or dye-labeled sequence specific oligonucleotide primers or probes. DNA-binding dyes such as SYBR Green I exhibit little fluorescence when free in solution but increase their fluorescence up to 1,000 fold on binding to double stranded DNA (Fig. 14). These dyes have the advantage of being easier to design and faster to set up, and are initially more cost-effective because of the high purchase cost of labeled probes. In addition, creation of a melt-curve plotting the vartiation in fluorescence against the temperature allows the evaluation of the specificity of the PCR reaction. On the other hand DNA-binding dyes lack the added specificity of probes and do not allow multiplexing of PCRs.

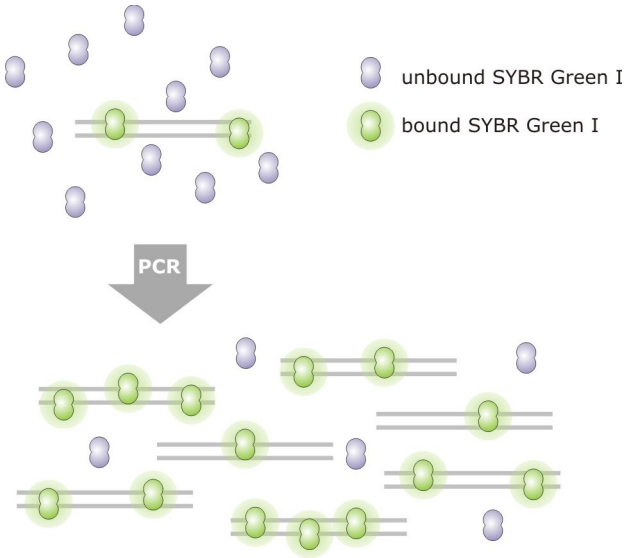

Figure 14: SYBR Green I detection principle

Many fluorescent primer- and probe-based chemistries have been devised and are available from different commercial vendors.

These chemistries are often based on the combined use of a reporter and a quencher. At the start of the PCR reaction the fluorescent signal is quenched by the close proximity of a quencher to the reporter. DNA amplification will subsequently result in the separation of quencher and reporter, and lead to increased fluorescent signaling (Fig. 15).

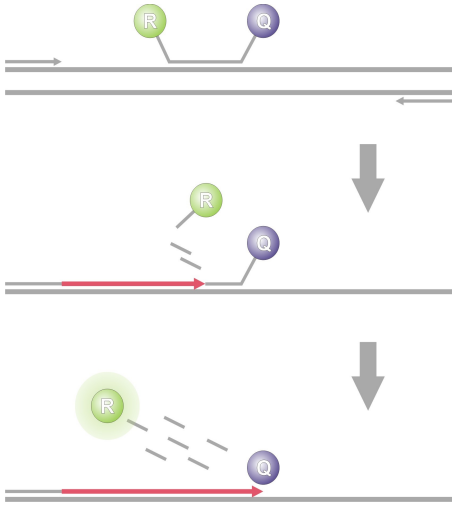

Figure 15: TaqMan probe detection principle (R=reporter, Q=quencher)

Specialized real-time PCR instruments allow the monitoring of the increase in fluorescence as more and more DNA is formed in each cycle. The intensity of fluorescence is then plotted against the cycle number (Fig. 16). Three different parts can be distinguished in this plot: in the beginning fluorescence does not exceed the background signal, then it increases exponentially, and finally it reaches the nonexponential phase. The cycle at which the fluorescence exceeds a given threshold is called the quantification cycle or Cq value. This general term was introduced in the RDML data format (real-time PCR data markup language, http://medgen.ugent.be/rdml/) to replace the various available descriptions (Ct for threshold cycle, TOP for take off point, Cp for crossing point). The Cq value is directly related to the amount of template at the start of the reaction: high template concentrations result in small Cq values whereas small amounts of template result in large Cq values. This linear relation between Cq value and logarithm of the initial amount of template is the basis for quantification with real-time PCR.

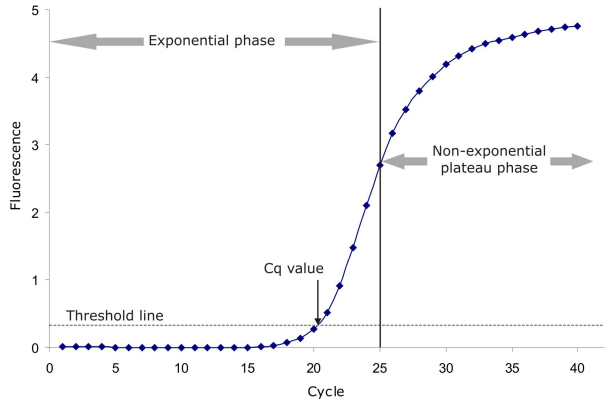

Figure 16: Amplification plot

2 qPCR based quantification

Quantification models

Two different types of quantification can be performed using real-time PCR: absolute and relative quantification.

Absolute quantification returns results for a single sample, independently of any other sample and should be used when interested in the intrinsic properties of a sample such as the number of viral particles per ml of blood. The absolute quantity of template in a sample is obtained by plotting the Cq values for a number of samples with known quantities and interpolating the quantity of the sample of interest (Fig. 17).

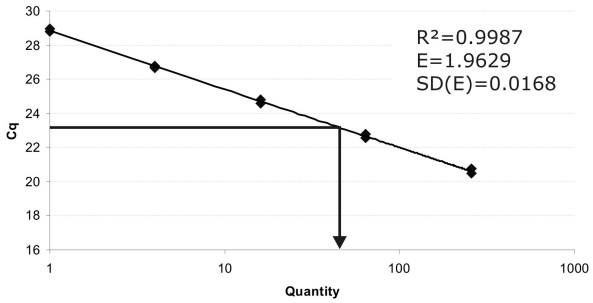

Figure 17: Absolute quantification based on a standard curve for samples with known quantity

Relative quantification, on the other hand, is based on the comparison of Cq values between a number of samples. It results in a ratio representing the relative amount (fold difference) of a target nucleic acid as compared to a reference sample. It could for example be used for the comparison of gene expression levels between patients and healthy individuals, between cancerous and normal tissue, or between treated and untreated cells.

Calculation of relative quantities

During the exponential phase of a PCR there is a linear relationship between the logarithm of the starting template copies and the number of amplification cycles required for the product to reach a threshold concentration. As a consequence the difference in Cq value between samples can be converted into the fold difference in their quantities. Assuming a doubling in the amount of target sequence each cycle, formula 1 describes the calculation of the relative quantity (RQ) of a given nucleic acid template for sample 1 as compared to sample 2.

$$RQ = \frac{Q_1}{Q_2} = 2^{Cq_2 - Cq_1} \qquad (1)$$

This approach is, however, usually not applicable for the analysis of copy numbers or expression levels of a given gene because the results also depend on the total amount of starting material. A ten fold higher expression of a gene could for example be masked if ten times less cDNA was used as the input of the real-time qPCR reaction. One can try to minimize the difference in total input RNA / DNA, but this is often not possible and can usually not be guaranteed. Therefore, data is commonly normalized to correct for differences in the amount of input nucleic acids. Very often reference genes, i.e. genes with the same expression level in all samples being compared, are used for this purpose. The ΔΔCt or Livak method (formula 2) improves formula 1 to take normalization against a reference gene (ref) into account and allows the calculation of normalized relative quantities for a gene of interest (goi) (*Livak 2001*).

$$NRQ = 2^{-\Delta\Delta Cq}$$
$$\Delta\Delta Ct = (Cq_{goi} - Cq_{ref})_2 - (Cq_{goi} - Cq_{ref})_1 \qquad (2)$$

The Livak method assumes 100% amplification efficiency, i.e. a doubling of DNA each cycle, for both the gene of interest and the reference gene. This assumption is, however, not always valid in real life experiments. Amplification efficiencies are not always 100% and can differ between the gene of interest and the reference gene. Therefore, Pfaffl et al. developed formula 3 that allows calculation of normalized relative quantities taking variable amplification efficiencies (E) into account (*Pfaffl 2001*).

$$NRQ = \frac{E_{goi}^{\Delta Cq_{goi}}}{E_{ref}^{\Delta Cq_{ref}}} \qquad (3)$$

In theory reference genes should be able to correct for differences in DNA quantity or quality, but they rely on the assumption that they are stably expressed in all samples. Perfect reference genes with equal expression levels in all samples are, however, hard to find, if they exist at all. Therefore, it was suggested to use the geometric mean of a set of reference genes for the normalization of the relative quantities. This geometric mean should better reflect the differences in starting DNA amounts, and should therefore better correct these differences (*Vandesompele 2002*). Formula 4 is an adaptation of the Pfaffl formula that allows normalization with a set of (n) reference genes.

$$NRQ = \frac{E_{goi}^{\Delta Cq_{goi}}}{\sqrt[n]{\prod E_{ref}^{\Delta Cq_{ref}}}} \qquad (4)$$

This formula is reduced to that of Pfaffl if only one reference gene is used. If, in addition, 100% amplification efficiency is used for both the gene of interest and the reference gene, it equals the formula published by Livak et al.

3 qBase

Nucleic acid quantification in general and gene expression analysis more specifically are becoming increasingly important in biological research and clinical decision making, with real-time quantitative PCR (qPCR) becoming the method of choice for expression profiling of selected genes. Advancements in instruments and detection chemistry, and improved assay design guidelines have made the practical performance of qPCR measurements feasible for most users. However, accurate and straightforward processing of the raw data as well as the management of large and growing data sets remain the major hurdles in this type of PCR based gene expression analysis.

Therefore we created the qBase software that automates the elaborate process of the correct calculation of relative quantities from qPCR data (paper 4). This program allows data to be imported from the numerous data formats currently being used. The qBase

Browser module allows data to be managed by organizing them into experiments and projects, and by providing a means for annotating data. A second part of qBase, the Analysis module, allows data from multiple runs to be analyzed as a whole without limitations on the number of samples, genes or replicates. An automated raw data quality control is included to prevent bad data being used in calculations. qBase employs an advanced and universally applicable quantification algorithm that allows gene specific amplification efficiencies and normalization with multiple reference genes to be used (formula 4). The obtained results can easily be exported in tabular format, or presented as a single-gene or multi-gene histogram.

In addition to the functions and automation provided by qBase, a number of new calculation methods were developed to improve on data analysis (paper 4). Firstly, the error on the estimated amplification efficiency is calculated and propagated throughout calculations. Secondly, algorithms for inter-run calibration were developed to allow the comparison between samples located on different plates.

No other software packages with comparable functionality are available for the moment. qBase has been recognized as a very useful and advanced tool for qPCR data analysis by the scientific community. This is reflected by the fact that the program has been downloaded by over 2000 users from more than 80 countries in 18 months.

Paper 6

Hellemans et al. Genome Biology 2007

Hellemans J, Mortier G, De Paepe A, Speleman F, Vandesompele J. qBase relative quantification framework and software for management and automated analysis of real-time quantitative PCR data. Genome Biol. 2007 Feb 9;8(2):R19

Method

Open Access

qBase relative quantification framework and software for management and automated analysis of real-time quantitative PCR data

Jan Hellemans, Geert Mortier, Anne De Paepe, Frank Speleman and Jo Vandesompele

Address: Center for Medical Genetics, Ghent University Hospital, De Pintelaan, B-9000 Ghent, Belgium.

Correspondence: Jo Vandesompele. Email: Joke.Vandesompele@UGent.be

Published: 9 February 2007

Genome ***Biology*** 2007, **8**:R19 (doi:10.1186/gb-2007-8-2-r19)

The electronic version of this article is the complete one and can be found online at http://genomebiology.com/2007/8/2/R19

Received: 31 August 2006
Revised: 7 December 2006
Accepted: 9 February 2007

Abstract

Although quantitative PCR (qPCR) is becoming the method of choice for expression profiling of selected genes, accurate and straightforward processing of the raw measurements remains a major hurdle. Here we outline advanced and universally applicable models for relative quantification and inter-run calibration with proper error propagation along the entire calculation track. These models and algorithms are implemented in qBase, a free program for the management and automated analysis of qPCR data.

Background

Since its introduction more than 10 years ago [1], quantitative PCR (qPCR) has become the standard method for quantification of nucleic acid sequences. The ease of use and high sensitivity, specificity and accuracy has resulted in a rapidly expanding number of applications with increasing throughput of samples to be analyzed. The software programs provided along with the various qPCR instruments allow for straightforward extraction of quantification cycle values from the recorded fluorescence measurements, and at best, interpolation of unknown quantities using a standard curve of serially diluted known quantities. However, these programs usually do not provide an adequate solution for the processing of these raw data (coming from one or multiple runs) into meaningful results, such as normalized and calibrated relative quantities. Furthermore, the currently available tools all have one or more of the following intrinsic limitations: dedicated for one instrument, cumbersome data import, a limited number of samples and genes can be processed, forced number of replicates, normalization using only one reference gene, lack of data quality controls (for example, replicate variability, negative controls, reference gene expression stability), inability to calibrate multiple runs, limited result visualization options, lack of experimental archive, and closed software architecture.

To address the shortcomings of the available software tools and quantification strategies, we modified the classic delta-delta-Ct method to take multiple reference genes and gene specific amplification efficiencies into account, as well as the errors on all measured parameters along the entire calculation track. On top of that, we developed an inter-run calibration algorithm to correct for (often underestimated) run-to-run differences.

Our advanced models and algorithms are implemented in qBase, a flexible and open source program for qPCR data management and analysis. Four basic principles were

followed during development of the program: the use of correct models and formulas for quantification and error propagation, inclusion of data quality control where required, automation of the workflow as much as possible while retaining flexibility, and user friendliness of operation. Our quantification framework and software fit exactly in current thinking that places emphasis on getting every step of a real-time PCR assay right (such as RNA quality assessment, appropriate reverse transcription, selection of a proper normalization strategy, and so on [2]), especially if small differences between samples need to be reliably demonstrated. In this entire workflow, data analysis is an important last step.

Results and discussion

Determination of the error on estimated amplification efficiencies

qBase employs a proven, advanced and universally applicable relative quantification model. An important underlying assumption is that PCR efficiency is assay dependent and sample independent. While this may not be true in every experimental situation, there is currently no consensus on how sample specific PCR efficiencies should be calculated and used for robust quantification. Most evaluation studies attribute a lack of precision to these sample specific efficiency estimation methods. Hence, the gold standard is still the use of a PCR efficiency estimated by a serial dilution series (preferably of pooled cDNA samples, to mimic as much as possible the actual samples to be measured), at least if one aims at accurate and precise quantification. Sample specific PCR efficiency estimation has its usefulness, but currently only for outlier detection [3-5].

Calculation of relative quantities from quantification cycle values requires knowledge of the amplification efficiency of the PCR. As stated above, amplicon specific amplification efficiencies are preferably determined using linear regression (formulas 1 and 5 in Materials and methods) of a serial dilution series with known quantities (either relative or absolute). However, the error on the estimated amplification efficiency is almost never determined, nor taken into account. This error can be calculated using linear regression as well (formulas 2 to 4 and 6), and should subsequently be propagated during conversion of the quantification cycle values to the relative quantities. The formula for the error on the slope provides the mathematical basis to learn how more accurate amplification efficiency estimates can be achieved, that is, by expanding the range of the dilution and including more measurement points.

Calculation of normalized relative quantities and error minimization

Methods for the conversion of quantification cycle values (Cq; see Materials and methods for terminology) into normalized relative quantities (NRQs) were first reported in 2001. The simplest model described by Livak and Schmittgen [6] assumes 100% PCR efficiency (reflected by a value of 2 for the base E of the exponential function) and uses a single reference gene for normalization:

$$NRQ = 2^{\Delta\Delta Ct}$$

Pfaffl [7] modified the above model by adjusting for differences in PCR efficiency between the gene of interest (goi) and a reference gene (ref):

$$NRQ = \frac{E_{goi}^{\Delta Ct,goi}}{E_{ref}^{\Delta Ct,ref}}$$

This model constituted an improvement over the classic delta-delta-Ct method, but cannot deal with multiple (f) reference genes, which is required for reliable measurements of subtle expression differences [8]. Therefore, we further extended this model to take into account multiple stably expressed reference genes for improved normalization. Although not yet published, this advanced and generalized model of relative quantification has been applied previously in our nucleic acid quantification studies [8-12].

$$NRQ = \frac{E_{goi}^{\Delta Ct,goi}}{\sqrt[f]{\prod_{o}^{f} E_{ref_o}^{\Delta Ct,ref_o}}}$$

The calculation of relative quantities, normalization and corresponding error propagation is detailed in formulas 7-16.

The basic principle of the delta-Cq quantification model is that a difference (delta) in quantification cycle value between two samples (often a true unknown and calibrator or reference sample) is transformed into relative quantities using the exponential function with the efficiency of the PCR reaction as its base. In principle, any sample can be selected as calibrator, either a real untreated control, or the sample with the highest or lowest expression. In addition, any arbitrary cycle value can be chosen as the calibrator quantification cycle value. The choice of calibrator sample or cycle value does not influence the relative quantification result; while numbers may be different, the actual fold differences between the samples remain identical, so results are fully equivalent and thus only rescaled. However, the choice of calibrator quantification cycle value does have a profound influence on the final error on the relative quantities if the error on the estimated amplification efficiency (see above) is taken into account in the error propagation procedure. To address this issue, we developed an error minimization approach that uses the arithmetic mean quantification cycle value across all samples for a gene within a single run as the calibrator quantification cycle value. As the increase in error is proportional to the difference in quantification cycle between the sample of interest and the calibrator (formula 12), the overall final error is

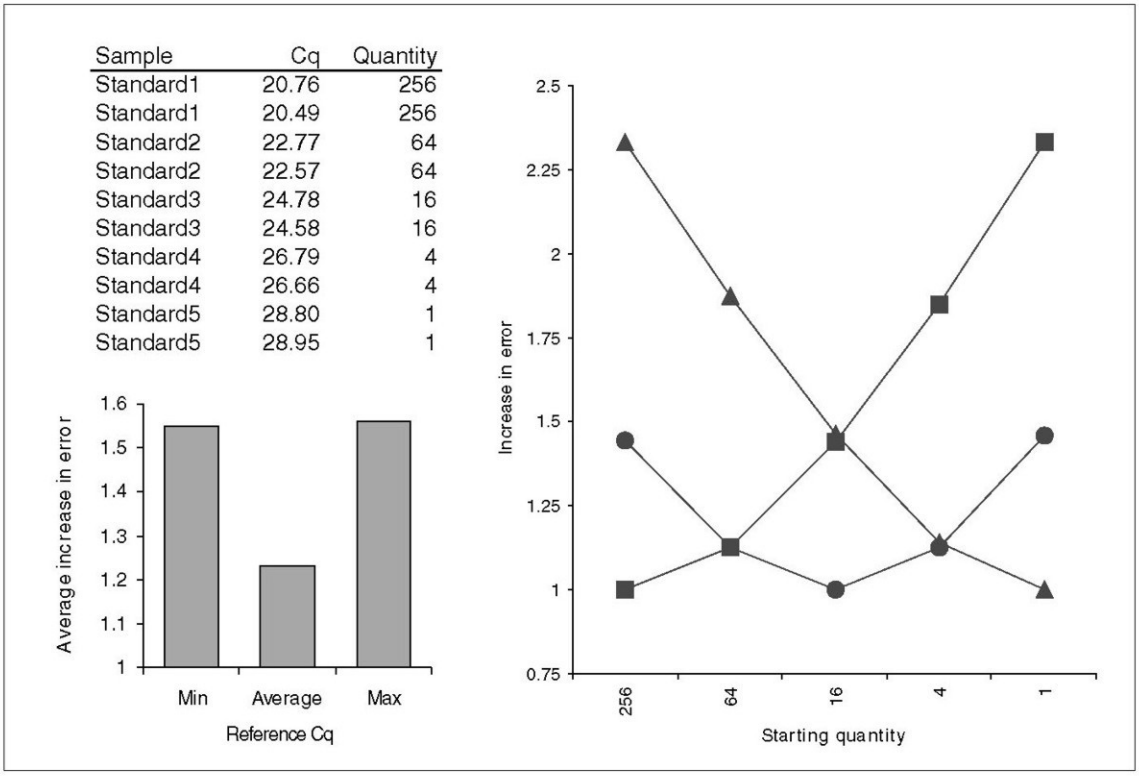

Figure 1
Effect of reference quantification cycle value on increase in error. Relative quantities were calculated for a simulated experiment with a five point four-fold dilution series using, respectively, the lowest Cq (squares), the average Cq (circles) or the highest Cq (triangles) as the reference quantification cycle value. Cq and quantity values are shown at the top left. The increase in the error on relative quantities for the different samples is shown at the top right, with the average increase depicted on the lower left graph.

minimized if the mean quantification cycle is used as the calibrator quantification cycle value (Figure 1).

Evaluation of normalization

The normalization of relative quantities with reference genes relies on the assumption that the reference genes are stably expressed across all tested samples. When using only one reference gene, its stability can not be evaluated. The use of multiple reference genes does not only produce more reliable data, but permits an evaluation of the stability of these genes as well. Previously, we developed a method for the identification of the most stably expressed reference genes in a set of samples [8,13]. The same stability parameter (formulas 21-25) can also be used to evaluate the measured reference genes in an actual quantification experiment. In addition, we calculate here another powerful indicator for expression stability in the actual experiment (formulas 17-20): the coefficient of variation of normalized reference gene relative quantities. Ideally, a reference gene should display the same expression level across all samples after normalization. Consequently, the coefficient of variation indicates how stably the gene is expressed.

To provide reference values for acceptable gene stability values (M) and coefficients of variation (CV), we calculated these normalization quality parameters for our previously established reference gene expression data matrix obtained for 85 samples belonging to 5 different human tissue groups [8]. Table 1 shows that mean CV and M values lower than 25% and 0.5, respectively, are typically observed for stably expressed reference genes in relatively homogeneous sample panels. For more heterogeneous panels, the mean CV and M values can increase to 50% and 1, respectively.

While the use of multiple stably expressed reference genes is currently considered to be the gold standard for normalization of mRNA expression, other strategies might be more appropriate for specific applications, such as: counting cell numbers and expressing mRNA expression levels as copy numbers per cell; using a biologically relevant, specific

Table 1

Reference gene expression stability evaluation

Tissue type	Gene	CV (%)	M	Mean CV (%)	Mean M
Neuroblastoma	*UBC*	31.84	0.740	30.89	0.703
	SDHA	27.40	0.660		
	HPRT1	37.11	0.736		
	GAPDH	27.21	0.675		
Fibroblast	*YHWAZ*	18.19	0.408	14.81	0.365
	HPRT1	8.84	0.308		
	GAPDH	17.40	0.378		
Leukocyte	*B2M*	15.76	0.400	15.81	0.394
	UBC	15.79	0.389		
	YWHAZ	15.89	0.393		
Bone marrow	*YWHAZ*	17.77	0.383	15.47	0.372
	UBC	13.60	0.356		
	RPL13A	15.03	0.376		
Normal pool	*TBP*	47.51	1.099	43.73	0.925
	HPRT1	46.99	0.988		
	HMBS	31.16	0.849		
	SDHA	49.50	0.869		
	GAPDH	43.50	0.819		

internal reference (sometimes referred to as *in situ* calibration); or normalizing against DNA (for overview of alternative strategies, see [14]). Clearly, no single strategy is applicable to every experimental situation and it remains up to individual researchers to identify and validate the method most appropriate for their experimental conditions. Important to note is that the presented qBase framework and software is compatible with most of the above mentioned normalization strategies.

Inter-run calibration

Two different experimental set-ups can be followed in a qPCR relative quantification experiment. According to the preferred sample maximization method, as many samples as possible are analyzed in the same run. This means that different genes (assays) should be analyzed in different runs if not enough free wells are available to analyze the different genes in the same run. In contrast, the gene maximization set-up analyzes multiple genes in the same run, and spreads samples across runs if required (Figure 2). The latter approach is often used in commercial kits or in prospective studies. It is important to realize that in a relative quantification study, the experimenter is usually interested in comparing the expression level of a particular gene between different samples. Therefore, the sample maximization method is highly recommended because it does not suffer from (often underestimated) technical (run-to-run) variation between the samples.

Whatever set-up is used, inter-run calibration is required to correct for possible run-to-run variation whenever all samples are not analyzed in the same run. For this purpose, the experimenter needs to analyze so-called inter-run calibrators (IRCs); these are identical samples that are tested in both runs. By measuring the difference in quantification cycle or NRQ between the IRCs in both runs, it is possible to calculate a correction or calibration factor to remove the run-to-run difference, and proceed as if all samples were analyzed in the same run.

Inter-run calibration is required because the relationship between quantification cycle value and relative quantity is run dependent due to instrument related variation (PCR block, lamp, filters, detectors, and so on), data analysis settings (baseline correction and threshold), reagents (polymerase, fluorophores, and so on) and optical properties of plastics. Important to note is that inter-run calibration should be performed on a gene per gene basis. It is not sufficient to determine the quantification cycle or relative quantity relation for one primer pair; the experimenter should do this for all assays.

To provide experimental proof of the advantage of sample maximization over gene maximization with respect to reduction in variation, we designed and performed an experiment consisting of five different runs (Figure 2). The results for one of the genes are shown in Figure 3. With gene maximization, 11 samples are spread over runs 1 and 2. Samples 1 to 3 occur in both runs and can thus be used as IRCs. Run 5 contains all 11 samples in a sample maximization set-up. When comparing the Cq values for the IRCs between runs 1 and 2, it is apparent that those in run 2 are systematically higher (0.77 cycles). After conversion of Cq values into NRQs (and thus

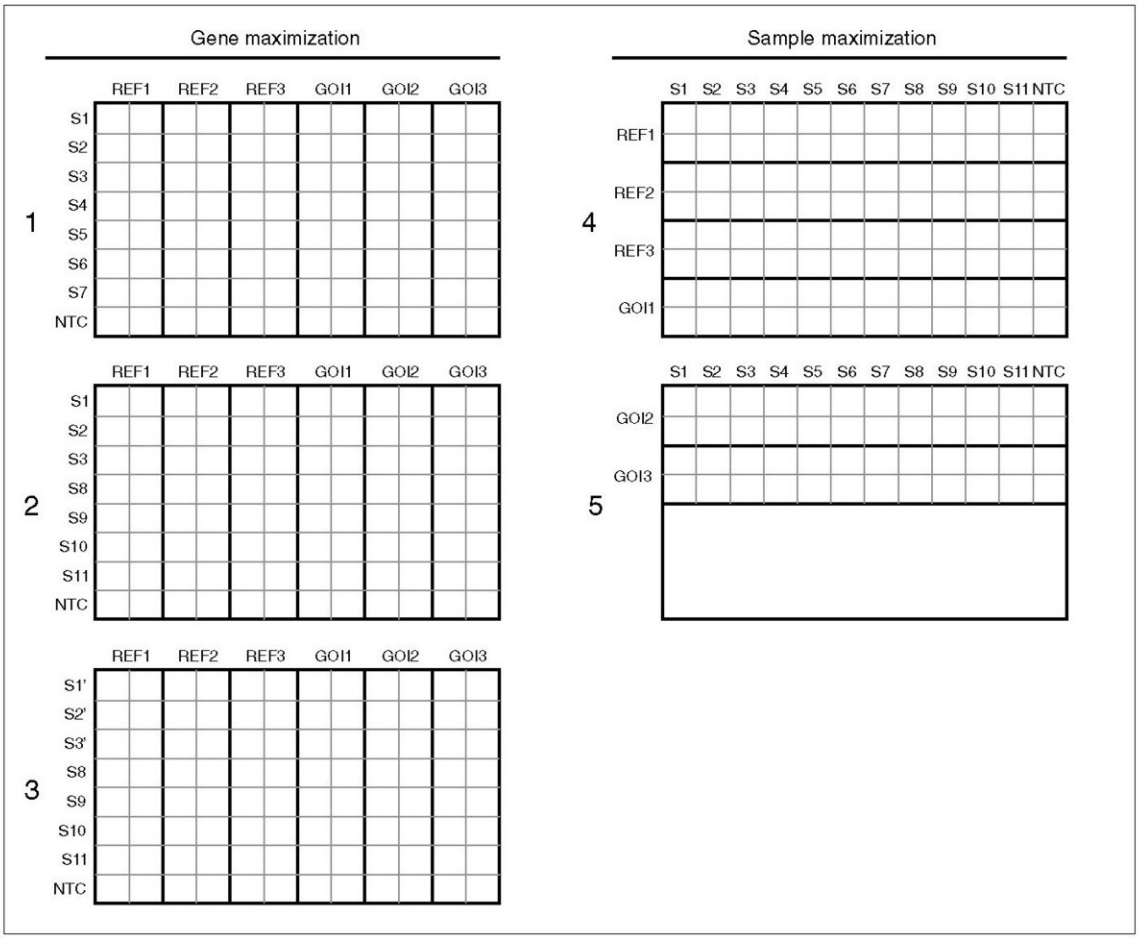

Figure 2
Experimental setup. Experimental setup used to evaluate the effects of inter-run calibration. On the right side, a sample maximization approach is used to analyze 6 genes for 11 samples in 1.5 run. With gene maximization (left side), IRCs (S1, S2, S3) are required to allow comparison of S5-S7 (run 1) to S8-S11 (run 2 or 3), thus requiring two full runs. The IRCs in run 2 are measured on the same cDNA dilution whereas the IRCs in run 3 are measured on newly prepared cDNA from the same RNA.

taking into account the Cq run-to-run differences for 3 reference genes as well), the NRQ values for samples 1 to 3 differ, on average, by 72% (Additional data file 1). It is important to realize that these values are merely examples. Although the differences can be minimized in a well designed and controlled experiment, they can be much bigger and are generally unpredictable. Anyway, by performing proper inter-run calibration, these run-dependent differences can be corrected and the resulting expression pattern (obtained by calibrating the gene maximization set-up) becomes highly similar to that from the sample maximization method (where there is no run-to-run variation).

To our knowledge, there is only one instrument software that can perform such a correction, but the algorithm is based on the Cq values of a single IRC. Although it can be valid to calibrate data based on Cq values, this method has the drawback that the same template dilution needs to be used in all the runs to be calibrated (for example, nucleic acids from a new cDNA synthesis or a new dilution cannot be reliably used). It is often much more straightforward and easier to calibrate the runs based on the NRQs of the IRCs (formulas 13-16). The quantity (and to some extent also the quality) of the calibrating input material is adjusted after normalization. This has the important advantage that independently prepared cDNA

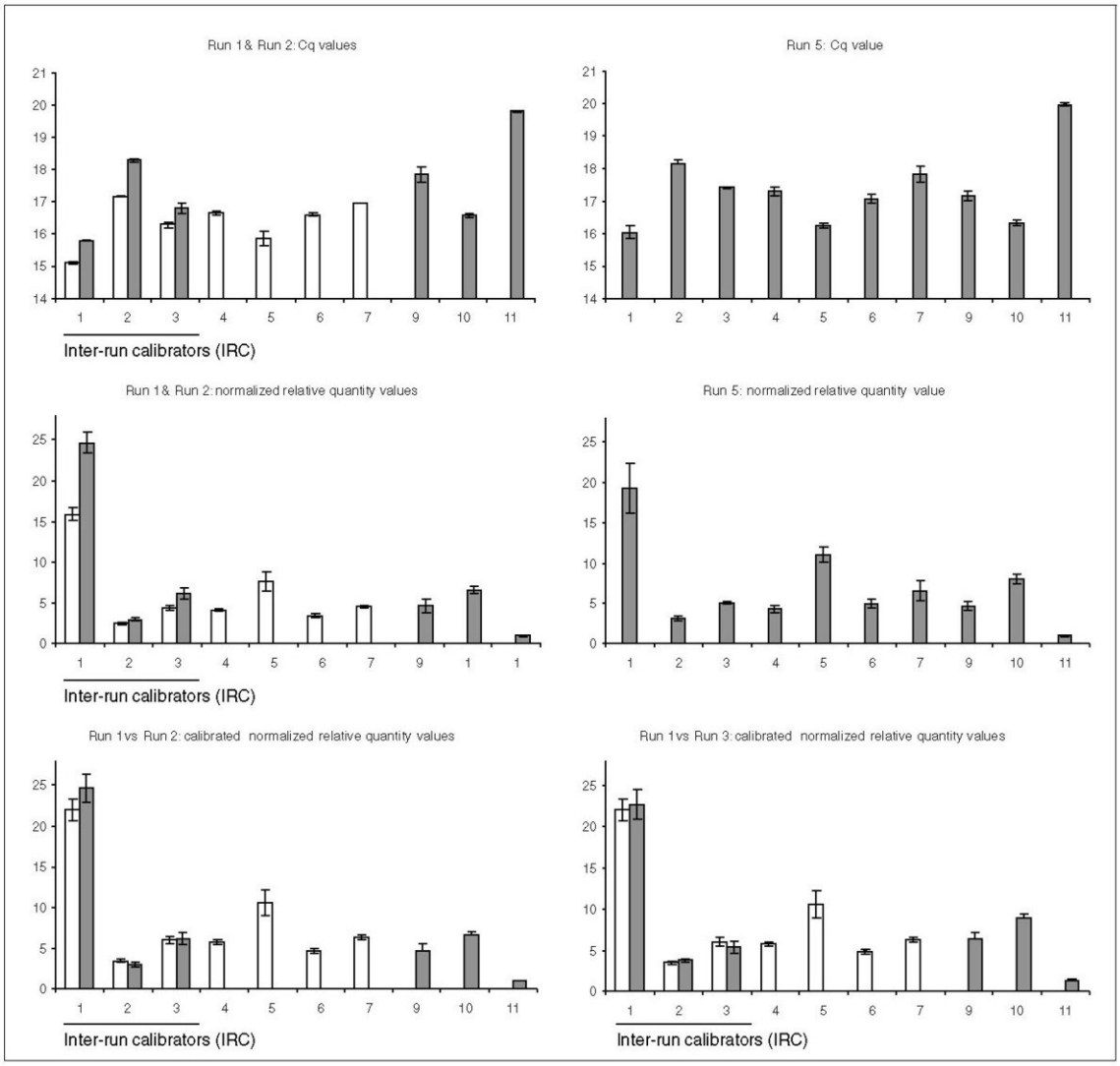

Figure 3
Experimental data comparing sample and gene maximization. The sample maximization approach (run 5) is compared to the gene maximization approach (runs 1 and 2 or 1 and 3). The difference between the IRCs is 0.77 for the Cq values, 72% for the NRQ values, and eliminated after inter-run calibration. Grey and white within the same display item indicates that data comes from different runs.

of the same RNA source can be used as a calibrator in the different runs (which allows addition of extra runs, even when the cDNA of the calibrator is run out). To some extent, even a biological replicate (for example, regrown cells) can be used for inter-run calibration when doing the calibration on the NRQs, provided that the experimenter realizes this introduces some level of biological replicate variation (but still adequately removes inter-run variation). The validity of using independently prepared cDNA as calibrator is demonstrated by the experiment described in Figure 2. Inter-run calibration between runs 1 and 3 based on IRCs from different cDNA preparations results in the same expression pattern as that obtained with sample maximization or inter-run calibration with the same cDNA (Figure 3). This is also clearly demonstrated by calculating the ratio of the calibrated NRQs (CNRQs) in runs 2 and 3 (mean ratio: 0.985, 95% CI: [0.945, 1.026]) (Additional data file 2).

It is also advisable to use multiple IRCs. A failed calibrator does not ruin an experiment if two or more are available. In

Table 2

Effects of the number and selection of IRCs on the increase in error and the fold difference between calibrated NRQs

	Increase in error		Fold difference between calibrated normalized quantities	
	Mean [95% CI]	Max	Mean [95% CI]	Max
1 IRC				
run1-run2	1.684 [1.579, 1.797]	10.98	1.048 [1.034, 1.061]	1.143
run1-run3	1.68 [1.576, 1.79]	10.98	1.053 [1.038, 1.067]	1.135
2 IRCs				
run1-run2	1.374 [1.289, 1.466]	7.73	1.024 [1.017, 1.03]	1.069
run1-run3	1.489 [1.415, 1.567]	7.73	1.026 [1.019, 1.033]	1.065
3 IRCs				
run1-run2	1.399 [1.292, 1.513]	5.28		
run1-run3	1.394 [1.288, 1.508]	5.28		

addition, calibration with multiple IRCs gives more precise results with a smaller error. Based on our real calibration experiment, inter-run calibration using a single IRC inherently increases the uncertainty on the relative quantity by about 70% whereas a set of 3 IRCs increases it by only 40% (Table 2). Although it is still advisable to choose the sample maximization setup, inter-run calibration based on the NRQs of multiple IRCs provides reliable results and flexibility in the source of the IRCs.

It is important to note that formulas 13'-16' can only be used for inter-run calibration if the same set of IRCs is used in all runs to be calibrated. For more complex experimental set-ups (whereby different combinations of IRCs are used in the various runs), advanced inter-run calibration algorithms are currently being developed in our laboratory (whereby the challenge is the proper propagation of the errors).

The process of inter-run calibration is very analogous to normalization. Normalization removes the sample specific non-biological variation, while inter-run calibration removes the technical run-to-run variation between samples analyzed in different runs. As such, the same formulas can be used to calculate the inter-run calibration factor (the geometric mean of the different IRCs' NRQs; formulas 13'-16'), and the same quality parameters can be applied to monitor the inter-run calibration process (provided multiple IRCs are used; formulas 21'-25'). Calculation of the IRC stability measure allows the evaluation of the quality of the calibration, which depends on the results of the IRCs. Our experiment shows that, with low M values (Additional data file 2: $M \cong 0.1$), virtually identical results are obtained for the different selections of IRCs (Table 2). If inconsistent or erroneous data were obtained for one of the IRCs, higher IRC-M values would be obtained and dissimilar results would be calculated for different sets of IRCs. Therefore, the IRC stability measure M is of great value to determine the quality of the IRCs (provided more than one IRC is used), and to verify whether the calibration procedure is trustworthy.

qBase

Calculation of NRQs for large data sets, followed by inter-run calibration, is a difficult, error prone and time consuming process when performed in a spreadsheet, especially if errors have to be propagated throughout all calculations. To automate these calculations, and to provide data quality control and result visualization, we developed the software program qBase (Figure 4a). This program is composed of two modules: the 'qBase Browser' for managing and archiving data and the 'qBase Analyzer' for processing raw data into biologically meaningful results.

qBase Browser

The Browser allows users to import and to organize hierarchically runs from most currently available qPCR instruments. In qBase, data are structured into three layers: raw data from the individual runs (plates) are stored in the run layer; the experiment layer groups data from different runs that need to be processed and visualized together; and the project layer combines a number of related experiments (for example, biological replicates of the same experiment). This hierarchical structure provides a clear framework to manage qPCR data in a straightforward and simple manner. The qBase Browser window is split into two parts: the bottom of the screen provides an explorer-like window to browse through the data; and the top of the screen contains a separate window displaying the annotation of the selected run, experiment or project. The qBase Browser allows the deletion and addition of projects, experiments and runs. The facility for exporting and importing projects and experiments is a convenient way to exchange data between different qBase users.

Data import

Each qPCR instrument has its own method of data collection and storage, accompanied by a large heterogeneity in export files with respect to file format, table layout and used terminology. During import into qBase, the different instrument export files are translated into a common internal format. This format contains information on the well name, sample

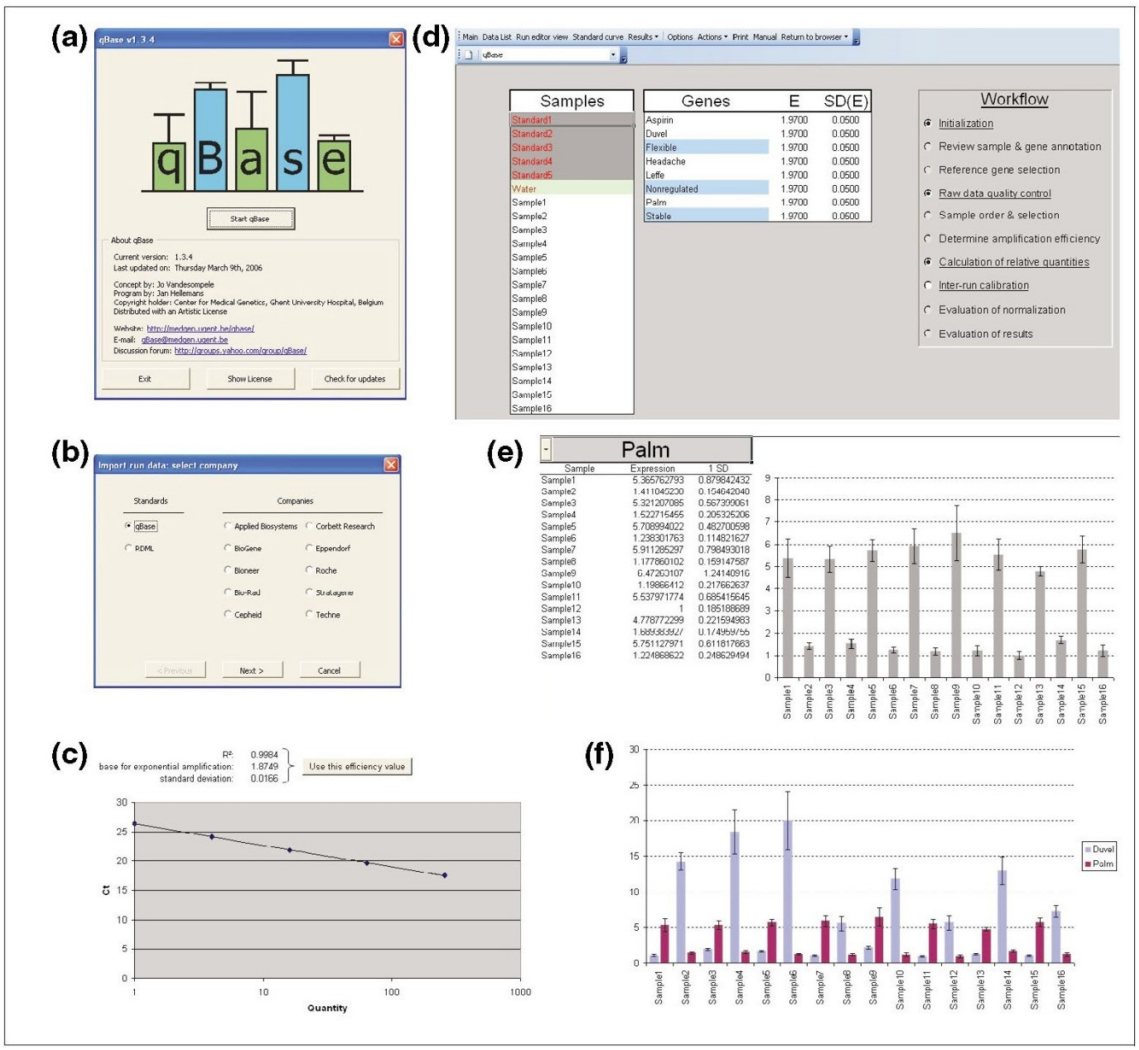

Figure 4
qBase. **(a)** qBase start up screen; **(b)** import wizard allowing selection of the format of the input file; **(c)** standard curve with a five point four-fold dilution series used to calculate the amplification efficiency; **(d)** qBase Analyzer main window with the workflow on the right and sample and gene list on the left - special sample types and reference genes are highlighted; **(e)** single gene histogram; **(f)** multi-gene histogram.

type, sample and gene name, quantification cycle value, starting quantity values (for standards), and the exclusion status. The last field indicates whether the measurement should be excluded from further calculations without actually discarding the measurement.

Data can be imported from a number of data formats. Two standards (qBase internal format and RDML (Real-time PCR Data Markup Language)) and a number of instrument specific formats are supported. The qBase standard consists of a Microsoft Excel table in which the columns correspond to the information that is used internally by qBase. RDML is a universal format under development for the exchange of qPCR data under the form of XML files [15].

The import wizard guides users through the process of data import (Figure 4b). To address the limitation that some instrument software packages provide only a single identifier

field for a well (while there are numerous variables, such as sample and gene name, sample type, and so on), qBase offers the possibility to extract multiple types of information from a single identifier. As such, the identifier 'UNKN|JohnSmith|Gremlin' could, for instance, be extracted to sample type 'UNKN' (unknown), sample name 'JohnSmith' and gene name 'Gremlin'.

qBase analyzer

The Analyzer is the data processing module for experiments. It performs relative quantification with proper error propagation along all quantifications, provides a number of quality controls and visualizes NRQs. This process involves several consecutive steps, some of them to be interactively performed by the user, others automatically executed by the program. Users are guided through the analysis by means of a simple workflow scheme in the main screen of the qBase Experiment Analyzer (Figure 4d).

Step 1: Initialization

The first step in the workflow is the (automatic) initialization of an experiment, during which raw data from all individual run files from the same experiment are combined into a single data table. The initialization procedure also generates a non-redundant list of all the samples and genes within the experiment. There are no limits on the number of replicates, genes or samples contained within an experiment, except for those imposed by Excel (no more than 65,535 wells can be stored into a single experiment). The absence of such limitations is a major improvement compared to the existing PCR data analysis tools, which are usually limited to processing data from a single plate or run with a fixed number of sample replicates. In qBase, data points with identical sample and gene names are automatically identified as technical replicates, except when the wells are located in different runs. In the latter case, they are interpreted as IRCs and renamed as such, that is, an appendix is added to indicate the run in which they are analyzed. Within the sample and gene lists on the main screen, a color code is used to label the reference genes and special sample types (standards, no template controls, no amplification controls, and IRCs; Figure 4d).

Step 2: Review sample and gene annotation

Sample and gene names can be easily modified in all runs belonging to the same experiment. This is very useful for achieving consistent naming of samples and genes across runs. To change names in only a selection of wells in a particular run, a run editor is available in qBase. This editor visualizes the plate (or rotor) layout with well annotation. It allows the modification of gene and sample names, as well as sample types and quantities in individually selected cells or in a range of neighboring cells. Together these tools allow users to review and correct the input annotation.

Step 3: Reference gene selection

Accurate relative quantification requires appropriate normalization to correct for non-specific experimental variation, such as differences in starting quantity and quality between the samples. The current consensus is that multiple stably expressed reference genes are required for accurate and robust normalization, especially for measuring subtle expression differences. While different tools are available to determine which candidate reference genes are stably expressed (for example, geNorm [8,13], BestKeeper [16], Normfinder [17]), almost no software is available to perform straightforward normalization using more than one reference gene (with the exception of the commercial Bio-Rad iQ5 and the REST 2005 software). qBase allows gene expression levels to be normalized using up to five reference genes that can easily be selected from the gene list.

Step 4: Raw data quality control

Several problems and mistakes can occur when preparing and performing qPCR reactions. The erroneous data produced by these problems need to be detected and excluded from further data analysis to prevent obscuring valuable information or generating false positive results. qBase provides several important quality control checks to evaluate whether: a no template control (NTC) is present for all genes (primer pairs); the quantification cycle values of NTCs are larger than a user defined threshold; the difference in quantification cycle value between samples of interest and NTCs is larger than a user defined threshold; the difference in quantification cycle value between replicated reactions is less than a user defined threshold; and genes are spread over multiple runs (meaning that not all samples tested for a particular gene are analyzed in the same run).

After data quality control, a message box reports all quality issue alerts and the involved data points are color-coded in the data list. This allows users to easily evaluate their data and to select data points for exclusion from analysis without actually removing the data themselves.

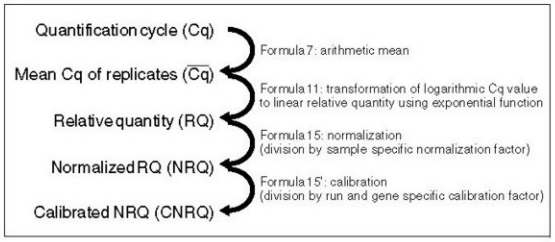

Figure 5
qBase calculation workflow.

Step 5: Sample order and selection

During initialization, samples are ordered alphanumerically, but the order of the samples can be adjusted in a user defined

way. Samples can be re-ordered in the list by using the up and down keyboard arrows or the sample context menu. Samples that do not need to show up in the results can be excluded by using the delete button on the keyboard or the sample context menu. Apart from changing the default sample order and display selection in the Analyzer main screen, this can also be modified in a temporary gene specific manner when reviewing the results (see below).

Step 6: Amplification efficiencies

All quantification models transform (logarithm) quantification cycle values into quantities using an exponential function with the efficiency of the PCR reaction as its base. Although these models and derivative formulas have been used for years, no model or software has taken into account the error (uncertainty) on the calculated efficiency. qBase is the first tool that takes the error on the amplification efficiency into account by means of proper error propagation.

Within qBase, gene specific amplification efficiencies can be specified in three ways. A default amplification efficiency (and error) can be set to all genes, or it can be provided for each gene individually. In the latter case, the efficiencies and corresponding errors can be simply typed (for example, when calculated in an independent experiment), or calculated from a standard dilution series. qBase provides an interface for the evaluation of standard curves whereby outlier reactions can be removed. Amplification efficiencies are calculated by means of linear regression and can be saved to the gene list, in order to be taken into account during further calculation steps (Figure 4c).

Step 7: Calculation of relative quantities

After raw qPCR data (quantification cycle values) quality control, reference gene(s) selection and amplification efficiency estimation, qBase can calculate the normalized and rescaled quantities. This process is fully automated and involves the following steps: calculation of the average and the standard deviation of the quantification cycle values for all technical replicates (data points with identical gene and sample names) - the program automatically detects the number of replicates for each sample-gene combination and can deal with a variable number of replicates (formulas 7-8); conversion of quantification cycle values into relative quantities based on the gene specific amplification efficiency (formulas 9-12); calculation of a sample specific normalization factor by taking the geometric mean of the relative quantities of the reference genes (formulas 13-14); normalization of quantities by division by the normalization factor (formulas 15-16); rescaling of the normalized quantities as requested by the user (either relative to the sample with the highest or lowest relative quantity, or relative to a user defined calibrator) (Figure 5). For each step in the calculation of normalized and rescaled relative quantities, qBase propagates the error.

Depending on the settings, qBase will use the classic delta-delta-Ct method (100% PCR efficiency and one reference gene) [6], the Pfaffl modification of delta-delta-Ct (gene specific PCR efficiency correction and one reference gene) [7] or our generalized qBase model (gene specific PCR efficiency correction and multiple reference gene normalization).

Evaluation of normalization

Normalization can be monitored by inspecting the normalization factors for all samples, or by calculating reference gene stability parameters. In an experiment with perfect reference genes, identical sample input amounts of equal quality, the normalization factor should be similar for all samples. Variations indicate unequal starting amounts, PCR problems or unstable reference genes. The qBase normalization factor histogram allows easy identification of these potential problems.

One of the unique features of qBase is the option to normalize the relative quantities with multiple reference genes, resulting in more accurate and reliable results. In addition, qBase evaluates the stability of the applied reference genes (and hence the reliability of the normalization) by calculating two quality measures: the coefficient of variation of the normalized reference gene expression levels; and the geNorm stability M-value. Both values are only meaningful, or can be calculated only if multiple reference genes are quantified. The lower these quality values, the more stably the reference genes are expressed in the tested samples. Based on our reported data on the expression of 10 candidate reference genes in 85 samples from 13 different human tissues [8], we have calculated the above mentioned quality parameters and propose acceptable values for M and CV in Table 1. Note that the limits of acceptance largely depend on the required accuracy and resolution of the relative quantification study.

Step 8: Inter-run calibration

qBase is especially useful and unique for analysis of experiments containing multiple runs. As users are usually interested in comparing the expression for a given gene between different samples, the sample maximization experimental set-up is the preferred set-up because it minimizes technical (run-to-run) variation between the samples. Nevertheless, the gene maximization set-up is also frequently used. To correct the inter-run variation introduced by this set-up as much as possible, qBase allows runs to be calibrated (on a gene specific basis) using one or multiple IRCs (Figure 5). If no sample(s) is (are) measured for the same gene in the different runs, qBase can not perform calibration and inter-run differences are assumed to be nil. Another unique and important aspect is that inter-run calibration is performed after normalization, which greatly enhances the flexibility in experimental design, as it is no longer obligatory that the same IRC template is used throughout all runs (as such, a new batch of cDNA can be synthesized, and variations will be canceled out during normalization).

Step 9: Evaluation of results

Normalized and rescaled relative quantities can be presented in three ways: a single-gene histogram, a multi-gene histogram, or a table. The default sample order and sample selection is defined in the main qBase window by editing the sample list. For the single-gene histogram (Figure 4e) the default order and selection can be changed to an alphanumerical, a user defined or a quantity based (that is, decreasing quantities) order. The option menu allows users to define the size of the error to be displayed (one or more standard error of the mean units). For both histogram views, the scale of the Y-axis can be switched from linear to logarithmic mode and vice versa. The multi-gene histogram (Figure 4f) is instrumental for comparing expression patterns (but not the actual expression levels) between different genes (because each gene is rescaled independently). The genes to be shown in the histogram can be selected from a gene list. Data from the table view (with or without error values) can be easily exported for further processing in other dedicated programs.

Distribution

qBase is freely available for non-commercial research and can be downloaded from the qBase website [18].

Manual and tutorial

For the training of new qBase users we have designed a demo experiment that is explained in detail in a step-by-step tutorial. Demo experiment 1 consists of 4 runs (96-well format) containing 16 samples, 5 standards, and a no template control to be analyzed for 5 genes of interest and 3 reference genes. Demo experiment 2 adds two runs to the initial experiment, expanding it with eight additional samples and three calibrators for inter-run calibration. After training, complete analysis of these six plates can be performed in less than an hour. This includes data import, correction of well annotation, quality control, determination of amplification efficiencies, inter-run calibration, calculations and results interpretation. To our knowledge, there are no other tools available that can perform all these functions. Conventional spreadsheet calculations would take considerably longer, are error prone and do not include quality control.

Conclusion

Although qPCR has been around for more than ten years, the employed calculation models are still amenable for improvement. Here we report our advanced, and proven, model for relative quantification that uses gene-specific amplification efficiencies and allows normalization with multiple reference genes. Errors are propagated throughout all calculation steps, and previously ignored errors, such as the uncertainty on the estimated amplification efficiency, are now taken into account. In addition, we developed an inter-run calibration method that allows samples analyzed in different runs to be compared against each other.

We implemented these improved and innovative methods in an easy to use, Microsoft Excel based tool for the management and the automated analysis of qPCR data, coined qBase. This freely available software package incorporates several data quality controls and uses an advanced relative quantification model with efficiency correction, multiple reference gene normalization, inter-run calibration and error propagation along each step of the calculations. A configurable graphical results output and the possibility to import and export experiments allow easy results interpretation and data exchange, respectively.

As a final comment, we would like to point out that, although our framework and program help management and interpretation of mRNA data, assessment of biological relevance or statistical significance requires the correlation of these mRNA data with protein levels or activity, and the measurement of biological replicates, respectively.

Materials and methods

Terminology

According to the Real-time PCR Data Markup Language (RDML) we used the proposed universal terms for the plethora of available descriptions (for example, quantification cycle value (Cq) instead of cycle threshold value (Ct), take off point (TOP) or crossing point (Cp)).

Error propagation

Error propagation is performed using the delta method, based on a truncated Taylor series expansion.

Symbols used in formulas

N, number of replicates i; g, number of genes j; c, number of IRCs m, m'; r, number of runs l, l'; s, number of samples k; f, number of reference genes p, p'; h, number of standard curve points q with known quantity Q; Cq, quantification cycle; CF, calibration factor; NF, normalization factor; RQ, relative quantity (relative to other samples within the same run for the same gene); NRQ, normalized relative quantity; SE, standard error; IRC, inter-run calibrator; CV, coefficient of variation; A, column matrix in which each element consists of the $\log_2$ transformed (normalized) relative quantity ratio; V, geNorm pairwise variation; M, geNorm stability parameter.

Determination of amplification efficiencies

A standard curve can be generated from the Cq and quantity values of a dilution series measured for the same amplicon within a single run. The slope and its standard error can be calculated for this curve by means of linear regression:

$$slope_{jl} = \frac{\sum_{q=1}^{h}\left(Q_{qjl} - \overline{Q_{jl}}\right)\left(Cq_{qjl} - \overline{Cq_{jl}}\right)}{\sum_{q=1}^{h}\left(Q_{qjl} - \overline{Q_{jl}}\right)^2} \qquad \text{(formula 1)}$$

$$s_{e,jl} = \sqrt{\frac{\sum_{q=1}^{h}\left(Cq_{qjl,measured} - Cq_{qjl,predicted}\right)^2}{h-2}} \quad \text{(formula 2)}$$

$$s_{x,jl} = \sqrt{\frac{1}{h-1}\sum_{q=1}^{h}\left(Q_{qjl} - \overline{Q_{jl}}\right)^2} \quad \text{(formula 3)}$$

$$SE\left(slope_{jl}\right) = \frac{s_{e,jl}}{s_{x,jl}(h-1)} \quad \text{(formula 4)}$$

The base for exponential amplification *E*, and its standard error *SE(E)* are calculated from these values:

$$E_{jl} = 10^{\left(\frac{1}{slope_{jl}}\right)} \quad \text{(formula 5)}$$

$$SE\left(E_{jl}\right) = \frac{E_{jl}\cdot\ln(10)\cdot SE\left(slope_{jl}\right)}{slope_j^2} \quad \text{(formula 6)}$$

Conversion of Cq values into relative quantities

Step 1

Calculation of the average Cq value for all replicates of the same gene/sample combination *jk* within a given run *l*:

$$\overline{Cq_{jkl}} = \frac{\sum_{i=1}^{n} Cq_{ijkl}}{n} \quad \text{(formula 7)}$$

$$SE\left(Cq_{jkl}\right) = \sqrt{\frac{1}{n(n-1)}\sum_{i=1}^{n}\left(Cq_{ijkl} - \overline{Cq_{jkl}}\right)^2} \quad \text{(formula 8)}$$

Step 2

Transformation of mean Cq value into RQ using the gene specific PCR efficiency E_{jl}, with minimization of the overall error:

$$Cq_{refernce,jl} = \overline{Cq_{jl}} = \frac{\sum_{k=1}^{s} Cq_{jkl}}{s} \quad \text{(formula 9)}$$

$$\Delta Cq_{jkl} = Cq_{reference,jl} - Cq_{jkl} \quad \text{(formula 10)}$$

$$RQ_{jkl} = E_{jl}^{\Delta Cq_{jkl}} \quad \text{(formula 11)}$$

$$SE\left(RQ_{jkl}\right) = \sqrt{RQ_{jkl}^2\left[\left(\frac{\Delta Cq_{jkl}\ SD\left(E_{jl}\right)}{E_{jl}}\right)^2 + \left(\ln\left(E_{jl}\right)\ SD(\overline{Cq_{jkl}})\right)^2\right]} \quad \text{(formula 12)}$$

Normalization: inter-run calibration

The procedures for normalization and inter-run calibration are highly analogous and are therefore described in parallel.

Step 1

Calculation of the normalization factor *NF* for sample *k* based on the RQs of the reference genes *p*.

Step 1'

Calculation of the calibration factor *CF* for gene *j* in run *l* based on the NRQs of the IRCs *m*:

$$NF_k = \sqrt[f]{\prod_{p=1}^{f} RQ_{pk}} \quad \text{(formula 13)}$$

$$CF_{jl} = \sqrt[c]{\prod_{m=1}^{c} NRQ_{jlm}} \quad \text{(formula 13'; for definition of } NRQ\text{, see formula 15)}$$

$$SE\left(NF_k\right) = NF_k\sqrt{\sum_{p=1}^{f}\left(\frac{SE\left(RQ_{pk}\right)}{f\cdot RQ_{pk}}\right)^2} \quad \text{(formula 14)}$$

$$SE\left(CF_{jl}\right) = CF_{jl}\sqrt{\sum_{m=1}^{c}\left(\frac{SE\left(NRQ_{jlm}\right)}{c\cdot NRQ_{jlm}}\right)^2} \quad \text{(formula 14')}$$

Step 2

Conversion of RQs into NRQs.

Step 2'

Conversion of NRQs into CNRQs:

$$NRQ_{jk} = \frac{RQ_{jk}}{NF_k} \quad \text{(formula 15)}$$

$$CNRQ_{jkl} = \frac{NRQ_{jkl}}{CF_{jl}} \quad \text{(formula 15')}$$

$$SE\left(NRQ_{jk}\right) = NRQ_{jk}\sqrt{\left(\frac{SE\left(NF_k\right)}{NF_k}\right)^2 + \left(\frac{SE\left(RQ_{jk}\right)}{RQ_{jk}}\right)^2} \quad \text{(formula 16)}$$

$$SE\left(CNRQ_{jkl}\right) = CNRQ_{jkl}\sqrt{\left(\frac{SE\left(CF_{jl}\right)}{CF_{jl}}\right)^2 + \left(\frac{SE\left(NRQ_{jkl}\right)}{NRQ_{jkl}}\right)^2} \quad \text{(formula 16')}$$

Coefficient of variation of NRQs of a reference gene

Step 1

Calculation of the mean NRQ for all samples *k* and a given reference gene *p*:

$$\overline{NRQ_p} = \frac{\sum_{k=1}^{s} NRQ_{pk}}{s} \quad \text{(formula 17)}$$

$$SE\left(NRQ_p\right)=\sqrt{\frac{1}{s-1}\sum_{k=1}^{s}\left(NRQ_{pk}-\overline{NRQ_p}\right)^2} \quad \text{(formula 18)}$$

Step 2

Calculation of the coefficient of variation CV of a given reference gene p across all samples k:

$$CV_p=\frac{SE\left(NRQ_p\right)}{\overline{NRQ_p}} \quad \text{(formula 19)}$$

Step 3

Calculation of the mean coefficient of variation for all reference genes:

$$\overline{CV}=\frac{\sum_{p=1}^{f}CV_p}{f} \quad \text{(formula 20)}$$

Reference gene and IRC stability parameter M

Since normalization and inter-run calibration are highly analogous, quality evaluation using the stability parameter M is similar as well. Therefore, both methods are explained in parallel.

Step 1

Calculation of the s × 1 matrix A^{gene} in which the kth element is the $\log_2$ transformed ratio between the relative quantities (not yet normalized) of two reference genes p and p' in sample k; matrix A^{sample} is calculated in an analogous manner.

Step 1'

Calculation of the g × 1 matrix A^{irc} in which the jth element is the $\log_2$ transformed ratio between the NRQs of two IRCs m and m' for the same gene j within a run l; matrix A^{run} is calculated in an analogous manner:

$$\left(\forall p,p'\in\left[1,f\right],p\neq p'\right):A^{gene}_{pp'k}=\log_2\left(\frac{RQ_{kp}}{RQ_{kp'}}\right) \quad \text{(formula 21)}$$

$$\left(\forall m,m'\in\left[1,c\right],m\neq m'\right):A^{irc}_{mm'jl}=\log_2\left(\frac{NRQ_{mjl}}{NRQ_{m'jl}}\right) \quad \text{(formula 21')}$$

Step 2

Calculation of the mean log transformed ratio and the standard deviation V^{gene} for all samples k and a given reference gene combination (p, p'). V^{gene} is the geNorm pairwise variation V for two reference genes.

Step 2'

Calculation of the mean log transformed ratio and the standard deviation V^{irc} for all runs l and a given IRC combination (m, m') and a given gene j. V^{sample} and V^{run} are calculated similarly from A^{sample} and A^{run}, respectively:

$$A^{gene}_{pp'}=\frac{\sum_{k=1}^{s}A^{gene}_{pp'k}}{s} \quad \text{(formula 22)}$$

$$A^{irc}_{mm'j}=\frac{\sum_{l=1}^{r}A^{irc}_{mm'jl}}{r} \quad \text{(formula 22')}$$

$$V^{gene}_{pp'}=SD\left(A^{gene}_{pp'}\right)=\sqrt{\frac{1}{s-1}\sum_{k=1}^{s}\left(A^{gene}_{pp'k}-\overline{A^{gene}_{pp'}}\right)^2} \quad \text{(formula 23)}$$

$$V^{irc}_{mm'j}=SD\left(A^{irc}_{mm'j}\right)=\sqrt{\frac{1}{r-1}\sum_{l=1}^{r}\left(A^{irc}_{mm'jl}-\overline{A^{irc}_{mm'j}}\right)^2} \quad \text{(formula 23')}$$

Step 3

Calculation of the arithmetic mean M^{gene} of all pairwise variations V^{gene} of a given reference gene p with all other tested reference genes p'. M^{gene} represents the geNorm gene stability measure M for a particular reference gene p.

Step 3'

Calculation of the arithmetic mean M^{irc} of all pair wise variations V^{irc} of a given IRC m with all the other IRCs m', for the same gene j. M^{sample} and M^{run} are calculated similarly from V^{sample} and V^{run}, respectively:

$$M^{gene}_{p}=\frac{\sum_{p'=1}^{f}V^{gene}_{pp'}}{f-1} \quad \text{(formula 24)}$$

$$M^{irc}_{mj}=\frac{\sum_{m'=1}^{c}V^{irc}_{mm'j}}{c-1} \quad \text{(formula 24')}$$

Step 4

Calculation of the mean stability measure for all reference genes.

Step 4'

Calculation of the mean stability measure for all IRCs:

$$\overline{M^{gene}}=\frac{\sum_{p=1}^{f}M^{gene}_{p}}{f} \quad \text{(formula 25)}$$

$$\overline{M^{irc}_{j}}=\frac{\sum_{m=1}^{f}M^{irc}_{mj}}{f} \quad \text{(formula 25')}$$

Calculations on the effect of inter-run calibration

The calculations for Figure 3 and Additional data file 1 have been performed as described in the formulas listed above. Difference in Cq is defined as the mean difference between the IRCs in run 1 and run 2. Fold change is defined as the ratio of the geometric mean of the (C)NRQs of the IRCs in run 1 and run 2.

For the calculation of the effects of inter-run calibration, NRQ values were retrieved from qBase for runs 1, 2 and 3 independently. Inter-run calibration was performed as described in formulas 13'-16', using one, two or three IRCs (Additional data file 2). The effect of inter-run calibration with two IRCs was calculated on the three sets of two IRCs (IRCs 1,2 versus IRCs 1,3 versus IRCs 2,3). Similarly, the effect of inter-run calibration with one IRC was calculated over all individual IRCs.

The increase in error is defined as the ratio of the relative error after and before calibration. The 95% confidence interval (CI) for this increase was calculated on log-transformed ratios. For the investigation of the effect of the selection of (sets of) IRCs from the three available calibrators, CNRQs for the different calibrated data sets were rescaled to allow them to be compared. The fold difference between the data sets was log transformed and a 95% CI was calculated. The effect of calibration with identical or independently prepared cDNA was studied similarly to the effect of the selection of IRCs. The IRC stability measure was calculated as described in formulas 21'-25'.

Additional data files

The following additional data are available with the online version of this paper. Additional data file 1 contains all the data and calculations leading to the results presented in Figure 3. Additional data file 2 contains all the data and calculations that were used for the evaluation of the effect of inter-run calibration on the final results. The conclusions of these calculations are represented, in part, in Table 2.

Acknowledgements

We would like to thank our colleagues at the Center for Medical Genetics for evaluating qBase and providing valuable feedback, and Kristel Van Steen for careful review of the formulas. Jo Vandesompele is a post-doctoral researcher from the Fund of Scientific Research Flanders (FWO). Jan Hellemans is funded by the Institute for the Promotion of Innovation by Science and Technology in Flanders (IWT).

References

1. Heid CA, Stevens J, Livak KJ, Williams PM: **Real time quantitative PCR.** *Genome Res* 1996, **6**:986-994.
2. Nolan T, Hands RE, Bustin SA: **Quantification of mRNA using real-time RT-PCR.** *Nat Protocols* 2006, **1**:1559-1582.
3. Bar T, Stahlberg A, Muszta A, Kubista M: **Kinetic Outlier Detection (KOD) in real-time PCR.** *Nucleic Acids Res* 2003, **31**:e105.
4. Goll R, Olsen T, Cui G, Florholmen J: **Evaluation of absolute quantitation by nonlinear regression in probe-based real-time PCR.** *BMC Bioinformatics* 2006, **7**:107.
5. Nordgard O, Kvaloy JT, Farmen RK, Heikkila R: **Error propagation in relative real-time reverse transcription polymerase chain reaction quantification models: the balance between accuracy and precision.** *Anal Biochem* 2006, **356**:182-193.
6. Livak KJ, Schmittgen TD: **Analysis of relative gene expression data using real-time quantitative PCR and the 2(-Delta Delta C(T)) method.** *Methods* 2001, **25**:402-408.
7. Pfaffl MW: **A new mathematical model for relative quantification in real-time RT-PCR.** *Nucleic Acids Res* 2001, **29**:e45.
8. Vandesompele J, De Preter K, Pattyn F, Poppe B, Van Roy N, De Paepe A, Speleman F: **Accurate normalization of real-time quantitative RT-PCR data by geometric averaging of multiple internal control genes.** *Genome Biol* 2002, **3**:RESEARCH0034.
9. Hellemans J, Preobrazhenska O, Willaert A, Debeer P, Verdonk PC, Costa T, Janssens K, Menten B, Van Roy N, Vermeulen SJ, *et al.*: **Loss-of-function mutations in LEMD3 result in osteopoikilosis, Buschke-Ollendorff syndrome and melorheostosis.** *Nat Genet* 2004, **36**:1213-1218.
10. Hoebeeck J, van der Luijt R, Poppe B, De Smet E, Yigit N, Claes K, Zewald R, de Jong GJ, De Paepe A, Speleman F, Vandesompele J: **Rapid detection of VHL exon deletions using real-time quantitative PCR.** *Lab Invest* 2005, **85**:24-33.
11. Loeys BL, Chen J, Neptune ER, Judge DP, Podowski M, Holm T, Meyers J, Leitch CC, Katsanis N, Sharifi N, *et al.*: **A syndrome of altered cardiovascular, craniofacial, neurocognitive and skeletal development caused by mutations in TGFBR1 or TGFBR2.** *Nat Genet* 2005, **37**:275-281.
12. Poppe B, Vandesompele J, Schoch C, Lindvall C, Mrozek K, Bloomfield CD, Beverloo HB, Michaux L, Dastugue N, Herens C, *et al.*: **Expression analyses identify MLL as a prominent target of 11q23 amplification and support an etiologic role for MLL gain of function in myeloid malignancies.** *Blood* 2004, **103**:229-235.
13. **geNorm** [http://medgen.ugent.be/genorm]
14. Vandesompele J, Kubista M, Pfaffl MW: **Reference gene validation software for improved normalization.** In *Real-time PCR: An Essential Guide* 2nd edition. Edited by: Edwards K, Logan J, Saunders N. Horizon Scientific Press; Norwich in press.
15. **RDML** [http://medgen.ugent.be/RDML]
16. Pfaffl MW, Tichopad A, Prgomet C, Neuvians TP: **Determination of stable housekeeping genes, differentially regulated target genes and sample integrity: BestKeeper - Excel-based tool using pair-wise correlations.** *Biotechnol Lett* 2004, **26**:509-515.
17. Andersen CL, Jensen JL, Orntoft TF: **Normalization of real-time quantitative reverse transcription-PCR data: a model-based variance estimation approach to identify genes suited for normalization, applied to bladder and colon cancer data sets.** *Cancer Res* 2004, **64**:5245-5250.
18. **qBase** [http://medgen.ugent.be/qbase]

Chapter 5

Discussion

General discussion and future perspectives

1 Background

The main goal of this thesis was the identification of the genetic and molecular defects responsible for a selection of skeletal dysplasias. To achieve this aim, a close collaboration between molecular biologists, bioinformaticists and clinicians was often necessary.

Clinical background

As the understanding of bone disorders assumes knowledge about the normal state of the skeleton, the study of skeletal dysplasias is rooted in the description of human anatomy. One of the most influential books on human anatomy "De humani corporis fabrica" (On the workings of the human body) was published in 1543 and written by Andreas Vesalius, a Flemish anatomist who is often referred to as the founder of modern human anatomy (*Vesalius 1543*). It took until the end of the nineteenth century before the first skeletal dysplasias were described. The twentieth century witnessed a considerable increase in the number of recognizable skeletal disorders, resulting in the creation of the first 'International Nomenclature of Constitutional Diseases of Bone' in 1970 (*McKusick 1971*). This nomenclature has been revised several times, but the continued identification of new disorders and their defects will require future updates of this nomenclature.

There is not only an evolution in the clinical, radiographic and pathologic description of these disorders, but, even more so, in the identification of their underlying molecular defects. The main driving forces behind the progress in the determination of causal genetic defects are the advances made in linkage mapping and DNA sequencing technologies.

Linkage mapping

The concept of mapping genes against a map of genetic markers was invented, in 1980, by Botstein et al. (*Botstein 1980*). It allows the localization of genes responsible for inherited disorders in sufficiently large, affected families. The recognition in 1989 of polymorphic microsatellites as an abundant class of genetic markers (*Weber 1989*) allowed easier and faster genotyping as compared to the RFLP markers that were proposed by Botstein et al. The next major improvement was the construction of large genetic maps by institutes such as Généthon and Marshfield (*Weissenbach 1992, Dib 1996, Broman 1998*). These maps allowed the creation of easy to use commercial sets of genetic markers such as Applied Biosystems' LMS v2.0 which was used in this thesis.

My first genome-wide linkage analysis (mapping of the gene for acrocapitofemoral dysplasia) took about a year. Since this initial effort, the speed by which a genome-wide mapping can be performed in the Center for Medical Genetics Ghent has increased considerably. Due to the availability of better (i.e. faster and more sensitive) and automated capillary sequencers, better software and more processing power, this kind of analysis can currently be performed in just a few weeks time.

DNA sequencing

The second technology required for the identification of the molecular defects responsible for genetic disorders is DNA sequencing. Also this technique underwent a considerable progress since the publication of the Sanger method which has currently become the most widely applied sequencing technology (*Sanger 1975*). At the beginning of my thesis in 2001, the Center for Medical Genetics Ghent had a sequencing capacity of about 38,000 bp / day using a ABI377 slab gel sequencer. By the end of 2005 this capacity had increased to about 1,300,000 bp / day using two capillary sequencers (ABI3130xl and ABI3730xl). In fact, when plotted against the initial capacity of 600 bp / day in 1990 we have witnessed a doubling of sequencing capacity every 18 months. This progress is very similar to Moore's Law that predicted a doubling of the number of transistors on integrated circuits (a rough

measure of computer processing power) every 18 months (*Moore 1965*).
To cope with the increase in sequencing capacity, analysis and interpretation of its results is now facilitated by automated sequence analysis software packages such as SeqScape. Our latest step in the progress of sequencing technology is the creation of a facility that centralizes data management and automates all post-PCR pipetting steps required for the preparation of sequences.

In this stimulating environment of increasing possibilities, I had the honor to conduct my research on the genetic and molecular basis of skeletal dysplasias. This thesis represents the most relevant and successful results obtained during my period as a PhD student. They include the identification of the gene responsible for respectively acrocapitofemoral dysplasia (*IHH*) and osteopoikilosis (*LEMD3*), and the creation of a framework and software for improved and automated qPCR data analysis (qBase). However, not all of the projects I was engaged in were as successful or relevant as these three.
A genome-wide linkage analysis was performed on a family with the RHYNS syndrome (acronym for: retinitis pigmentosa – hypopituitarism – nephronophtisis – skeletal dysplasia) which resulted in the localization of a candidate region on chromosome 3. Our candidate gene approach did, however, not reveal the causal mutation for this syndrome. Subsequent collaboration with the research group of Hildebrandt resulted in the identification of mutations in the NPHP5 gene, the fifth gene found to be responsible for nephronophtisis (*Otto 2005*). Genetic analysis on an extended family with X-linked mental retardation revealed a candidate region that, due to the large size of the linkage interval, did not allow pinpointing the affected gene. There is also an ongoing effort to identify the gene responsible for the prenatal form of Caffey disease. By means of homozygosity mapping, a candidate region with suggestive linkage has been found on chromosome 16. DNA from paraffin embedded tissue of a deceased fetus with Caffey is currently used to reduce the candidate region in the hope to identify the causal gene.

2 The indian hedgehog gene

Acrocapitofemoral dysplasia, abbreviated as ACFD, seems to be a very rare, autosomal recessively inherited skeletal dysplasia. It was recently described by Mortier et al. as a disorder characterized clinically by a disproportionate short stature with brachydactyly, and radiographically by cone-shaped epiphyses in hands and hips (*Mortier 2003*). Since the delineation of this dysplasia, no more than five patients have been identified. All patients live in either Belgium or the Netherlands, and all were involved in our search for the causal gene responsible for this disorder.

Results

A genome-wide homozygosity mapping performed on the gDNA of three ACFD patients revealed linkage of this disease to chromosome 2. With the genetic information of all patients and a number of relatives, a linkage interval of 5 cM on 2q35-q36 could be delineated. Calculation of a 8.02 LOD-score demonstrated that linkage of this region to the causal mutation was highly significant. Subsequently, based on their known function and involvement in related disorders, a selection of 4 candidate genes was made out of the 75 genes within the linkage interval. Sequencing of the indian hedgehog (IHH) gene ultimately revealed the presence of homozygous missense mutations in all patients (c.137C>T for the Belgian family and c.569T>C for the Dutch family) (Paper 1: *Hellemans 2003*). It is quite remarkable that the clinical description and the identification of the genetic cause of this disease were both published within the same year. In addition, ACFD is probably one of the few mendelian disorders for which a mutation has been found in all known patients.

Remaining questions and discussion

Although the identification of missense mutations in the IHH gene has elucidated the genetic basis of acrocapitofemoral dysplasia, a number of additional questions remain to be resolved. Firstly, we have not yet been able to fully explain the differences between ACFD and brachydactyly type A1 (BDA1) when considering the nature and position of the *IHH* mutations. Both disorders are caused by missense mutations in the N-terminal signaling domain of *IHH* (*Paper 1:*

Hellemans 2003, Gao 2001). BDA1 is an autosomal dominant disorder characterized mainly by brachydactyly, whereas ACFD is recessively inherited and, in addition to brachydactyly, characterized by a disproportionate short stature. ACFD is not merely the homozygous presentation of BDA1 since the heterozygous carriers of a ACFD mutation do not show brachydactyly type A1. Therefore, ACFD and BDA1 mutations are supposed to affect IHH signaling differently. Mapping of the different mutations on the tertiary structure of sonic hedgehog, a close homologue of indian hedgehog, suggested differentially affected domains. The limited number of identified mutations (2 and 6 for respectively ACFD and BDA1) did, however, not allow drawing any reliable conclusions. Identification of additional mutations would allow the more precise delineation of the affected domains, and permit more directed assays to investigate the differential effects of the recessive and dominant mutations on IHH signaling. The second unexplained feature of these IHH missense mutations is the fact that they do not affect all growth plates equally. This enigma does not only relate to ACFD and BDA1, but is encountered in a large number of skeletal dysplasias.

Micromass culture data and future perspectives

Micromass-cultures (MM-C) mimic in-vitro the first steps of endochondral ossification. This is achieved by culturing limb bud mesenchymal cells in high density, resulting in the spontaneous differentiation into chondrocytes followed by further maturation. MM-Cs allow the study of the effect of virally induced transgenes or added molecules on endochondral ossification (*Mello 1999*). We decided to use this system for the investigation of the effects of the ACFD and BDA1 mutations on IHH signaling. I had the pleasure to receive an excellent training in the creation and analysis of MM-Cs in the research lab of Prof Stephan Mundlos (Max Planck Institute for Molecular Genetics, Berlin). Avian viruses responsible for the transgene expression of wild-type or mutant (c.137C>T, c.298G>A, c.383G>A and c.569T>C) chicken IHH were produced. Subsequently, a series of micromass-cultures were created in parallel and either left untreated or infected with one of these viruses. Some interesting observations were made when comparing normal control cultures with cultures overexpressing indian hedgehog:

- In contrast to wild-type cultures, the borders of the IHH cultures did not attach well to the plate, resulting in the detachment from their support. The meaning or implications of this finding have not yet been clarified.
- IHH cultures grew less in height than their wild-type counterparts. Although this seems contradictory to the proliferation inducing effect of IHH, it might be explained by reduced chondrocyte hypertrophy resulting from IHH overexpression.
- Nodule formation was significantly inhibited in IHH cultures and the typical alcian blue staining of these nodules was reduced. This suggests the presence of less sulfated proteoglycans in the cartilaginous matrix which indicates reduced chondrocyte maturation.
- Alcian blue staining also revealed the presence of a previously undescribed structure resembling a comet. It consists of a small intensely colored nodule (core) surrounded by a flat region with lower than average staining (tail). Beyond this flat region the culture is again averagely stained and slightly more elevated.
- Alkaline phosphatase (ALP) activity was 30-40 fold reduced in IHH cultures, confirming the less matured phenotype of IHH overexpressing MM-Cs.

These findings largely correspond to the known functions of IHH in the growth plate. The effects of IHH on cell-plate attachment, and the appearance of special structures in MM-Cs overexpressing IHH were unexpected and require further investigation. In situ hybridization with stage specific chondrocyte markers such as COL10 could clarify the composition of the IHH induced comet-like structures in MM-Cs and might provide important new insights into the effects of IHH on chondrocyte differentiation and on osteoblasts.

Comparison of the cultures infected with wild-type IHH, ACFD-IHH or BDA1-IHH did not reveal any differences. These data indicate that ACFD and BDA1 missense mutations do not result in complete loss of function of IHH. This finding is in agreement with the observation that a complete loss of Ihh in mice results in a much more severe

phenotype (*St-Jacques 1999*). The consequence of the amino acid substitutions may be explained by a) altered receptor binding capacities resulting in small quantitative effects, b) effects on hedgehog modifications or multimerization which could affect the signaling range and activity of IHH, or by c) changes in epitopes which are involved in the interaction with other proteins such as hedgehog interacting protein (HHIP) or matrix elements like heparan sulfate proteoglycans. Since micromass-cultures now appear unlikely to pinpoint the specific effect of BDA1 and ACFD mutations on IHH signaling, alternative approaches will be required.

Surface plasmon resonance measurements could be used to quantify the effects of the amino acid substitutions on the affinity of IHH for PTCH (hedgehog receptor) or HHIP (inhibitor of hedgehog signaling). Although it might provide valuable information it does require the purification of multiple different proteins which constitutes a big obstacle for a genetic lab. The investigation of the effect of the ACFD or BDA1 missense mutations on the processing of IHH is more straightforward. It can be achieved by overexpressing the different forms (mutant and wild-type) of IHH, followed by Western-blot analysis. These blots will allow to verify whether IHH is still cleaved to release the N-terminal signaling domain, whether palmitoyl and cholesterol modifications are added and whether free diffusable multimers are formed.

It can be anticipated that in vitro models for studying the effect of the identified mutations on IHH signaling will not be able to solve all remaining questions given the fact that ACFD and BDA1 only affect a limited set of bones and our data indicating that these mutations do not result in a complete loss of function. The delineation of the mutational spectrum of acrocapitofemoral dysplasia and brachydactyly type A1, and the more precise description of the IHH interaction domains are expected to facilitate the study of the effects of the involved missense mutations in the near future.

3 The LEM domain containing 3 gene

Osteopoikilosis, the Buschke-Ollendorff syndrome (BOS) and melorheostosis are rare skeletal dysplasias characterized by increased bone density. In osteopoikilosis and BOS multiple, small sclerotic lesions are distributed over the skeleton, whereas only a single or a small number of lesions are present in melorheostosis. Osteopoikilosis and BOS are usually asymptomatic conditions. They show autosomal dominant inheritance and can co-occur within the same family. Melorheostosis, on the other hand, is a more severe disorder which often results in contractures and chronic pain. It usually occurs as a sporadic anomaly but has repeatedly been reported in families with osteopoikilosis or BOS.

Results

Because these conditions can be observed within the same family, we and others assumed that osteopoikilosis, BOS and melorheostosis represent allelic conditions. A genome-wide linkage analysis performed on a Belgian family with 7 osteopoikilosis / BOS patients revealed linkage of this condition with chromosome 12. Inclusion of the haplotype data obtained in two additional osteopoikilosis / BOS families (one with the co-occurrence of melorheostosis) confirmed this linkage (LOD= 6.69) and defined the boundaries of a 23.55 cM linkage interval. This interval was quite large and did not reveal any obvious candidate genes. The identification of a microdeletion, partially overlapping with the linkage interval, in a patient with the unusual association of osteopoikilosis with short stature and mental retardation was the breakthrough in this project. Together, the microdeletion and the linkage interval defined a smaller region containing only 23 genes, of which *LEMD3* was selected as the prime suspect gene. The identification of loss-of-function mutations in this gene, subsequently demonstrated the causality of *LEMD3* in the etiology of osteopoikilosis and its related disorders (*Paper 2: Hellemans 2004*).

For the investigation of the spectrum of *LEMD3* mutations, a larger series of patients was investigated. A total of 46 patients were studied, including 2 patients with osteopoikilosis, short stature and mental retardation (group A), 17 probands with osteopoikilosis or BOS (group B), 4 families with the co-occurrence of melorheostosis and BOS (group C), and 23 unrelated patients with isolated melorheostosis (group D). Both patients of group A had a microdeletion on

12q14 (*Menten 2007*). The identification of 14 loss-of-function mutations in the patients of group B confirmed that haploinsufficiency for LEMD3 can result in osteopoikilosis or Buschke-Ollendorff syndrome. Although *LEMD3* mutations were found in all 4 melorheostosis patients of group C, only 1 out of 23 patients with sporadic melorheostosis (group D) had a *LEMD3* mutation. Based on these data we concluded that the genetic defect in the majority of sporadic and isolated melorheostosis cases remains unknown (Paper 3: *Hellemans 2006*).

LEMD3 encodes a protein of the inner nuclear membrane whose function in humans was largely unknown at the beginning of our study. The *Xenopus* homologue (Xman1, SANE) was shown to interact with BMP specific Smads leading to reduced BMP signaling. We performed a yeast two hybrid screening to investigate similar interactions for human LEMD3. In addition to its *Xenopus* homologue, human LEMD3 was found to interact with both BMP and TGFβ specific Smads. The effect of LEMD3 overexpression on BMP and TGFβ signaling was investigated in two different experiments measuring, respectively, the expression of target genes by qPCR and the induction of a TGFβ responsive luciferase. Both experiments demonstrated an antagonistic effect of LEMD3 on BMP and TGFβ signaling (Paper 2: *Hellemans 2004*). Loss of function mutations in *LEMD3* consequently result in an increased signaling. Since BMP and TGFβ signaling have been found to have a stimulatory effect on bone formation, the sclerosing bone phenotype in osteopoikilosis patients probably results from increased signaling of these growth factors.

Remaining questions and discussion

At least two questions remain unanswered for the moment. Firstly, what is the genetic defect in the majority of sporadic and isolated melorheostosis patients? Secondly, why is the sclerosis not generalized in osteopoikilosis but restricted to numerous small foci?

Since melorheostosis usually occurs as a sporadic condition, linkage analysis can not be used for the identification of the major genetic defect in this group of patients. The co-occurrence of melorheostosis with osteopoikilosis or BOS in the same family, and the observation of two cases of melorheostosis in the same family (unpublished data) suggest that LEMD3 and its pathways are involved in the pathogenesis of melorheostosis and *LEMD3*. Analysis of these pathways may thus provide valuable insights in the etiology of melorheostosis.

We have tried to explain the scattered appearance of sclerotic lesions by proposing a second hit in the affected spots. Sequence analysis of the LEMD3 gene on skin and/or bone lesions in a BOS patient and 2 patients with melorheostosis could, however, not reveal such additional mutations. These results can be interpreted in three ways. Firstly, somatic *LEMD3* mutations may be present but go undetected because they reside in only a subset of cells and culturing selects against these cells. A similar situation is encountered in neurofibromatosis type I where special culturing conditions are required to prevent counterselection of cells with a second, somatic mutation (*Serra 2000*). Secondly, the somatic mutation may be located outside *LEMD3*, perhaps in a gene within the same signaling pathway. Finally, somatic mutations may not be involved at all but normal fluctuations in gene expression cause the locally reduced LEMD3 levels to be insufficient for the maintenance of normal bone homeostasis.

Future perspectives

Two approaches are currently being prepared for the further molecular analysis of the effect of *LEMD3* haploinsufficiency. These are Lemd3 knock-out mice, and an in-vitro RNAi system. Lemd3 knock-out mice were obtained from BayGenomics (http://baygenomics.ucsf.edu/) and are currently being bred in the VIB mouse facility. Homozygous Lemd3 knock-out mice are reported to die during embryonic development around stage E11 due to defects in vascular remodeling (*Ishimura 2006*). Lemd3$^{+/-}$ mice, on the other hand, are normal in terms of growth, fertility and lifespan. In contrast to what we expected for *Lemd3* haploinsufficiency, skin histology appeared normal and no signs of bone abnormalities were found by magnetic resonance imaging. Since these data are not shown, and no X-ray or CT scans have been performed we are still interested to further investigate the bone phenotype of Lemd3$^{+/-}$ mice. In case typical disseminated sclerotic lesions are found by means of X-ray or bone histology, genetic and molecular analysis will

be used to compare normal and affected bone. This should, hopefully, provide new insights into the development of the bone sclerosis found in osteopoikilosis and BOS patients.
The second approach involves an in-vitro system in which RNA interference is used to reduce the expression of *LEMD3* in human osteoblasts, and thus mimic the effects of an osteopoikilosis mutation. A set of oligos encoding *LEMD3* hairpin RNAs were created and transferred into eukaryotic expression vectors which are now ready to be used in knock-down experiments. 6 different osteoblast cultures will be prepared for pairwise analysis: control cells versus cells with *LEMD3* knock-down, both in basal conditions and after BMP or TGFβ stimulation. Expression profiles for these cultures will be obtained via gene expression microarrays and confirmed by means qPCR.
The search for the genetic defect in patients with isolated melorheostosis is another important aspect of the planned research. Since linkage analysis can not be used in this group of patients, a candidate gene approach is considered. Affected tissue, suitable for the detection of both germline and somatic mutations, will be obtained via our collaboration with the melorheostosis association (http://www.melorheostosis.com). The genetic service unit of the Center for Medical Genetics Ghent will allow us to perform the large amounts of sequencing and qPCR analyses in a fast and cost efficient manner. The selection of candidate genes will initially focus on the genes within the LEMD3 regulated BMP and TGFβ signaling pathways. This selection will later on be updated with the data from the experiments on the effect of *LEMD3* haploinsufficiency, thus integrating both aspects of the planned research. Important insights in the defects of melorheostosis patients may also be obtained from a thorough histological and expression analysis of the bone lesions of these patients.

4 qBase

Since its introduction in 1993 (*Higuchi 1993*) and the creation of the first commercial instrument more than 10 years ago (*Heid 1996*), qPCR has successfully become the standard method for quantification of nucleic acid sequences. The improvements in detection chemistry, protocols and equipment have made qPCR attainable for most research groups. Accurate quantification with qPCR does not only require reliable measurement of Cq (Ct, Cp or TOP) values, but also the correct processing of these raw values. The latter is the major remaining hurdle in qPCR based nucleic acid quantification. The problem is twofold: on the one hand better algorithms are required for reliable quantification (qBase framework), and, on the other hand, automation is desired to improve on the error prone and time consuming spreadsheet based calculations (qBase program).

qBase framework

The basic principle of relative quantification is the conversion of Cq values into relative quantities (RQ). The ΔΔCq method adjusted this basic principle to allow normalization of relative quantities based on the results for a reference gene (*Livak 2001*). Accurate quantification does however require a more complex set of formulas. With the qBase framework we aimed to provide these formulas, as well as a description of important concepts and ways to perform quality control.
We improved on the quantification formula of Pfaffl (*Paffl 2001*) in order to allow normalization with multiple reference genes and taking into account the error on the amplification efficiency (Paper 4). In the previously developed quantification models, the reference Cq value could be chosen arbitrarily. This choice does however influence the error on the relative quantities as calculated by our new model. Selection of the average Cq value as the reference quantification cycle does result in a minimization of the overall error and is therefore the preferred approach. We also developed an inter-run calibration procedure that works on normalized data. This approach is compatible with inter-run calibrators (IRC) using the same cDNA, or even IRCs derived from the same RNA (Paper 4). Together these formulas allow more accurate results to be obtained. In addition, proper error propagation provides a better estimate of the uncertainty on the calculated relative quantities.
Another important aspect in qPCR analysis is the experimental setup. As soon as the number of measurements exceeds the number of available positions in a single run, PCR mixes need to be spread over multiple

runs. This can be achieved in several ways, but no formal preference for either of these possibilities had been published. We argued that the sample maximization approach, putting as much samples as possible in a single run and spreading genes across runs as required, is preferable because it minimizes the nonspecific sample to sample variation. When using gene maximization, an approach proposed in a number of commercial kits, or in general when the samples for a given gene are spread over multiple runs, the variation caused by run-to-run differences needs to be corrected for by means of inter-run calibration.

The third important element of the qBase framework is the development of quality controls. These include a control on the raw Cq values (ΔCq between technical replicates and Cq value for no template controls) as well as measures for the reliability of normalization and inter-run calibration. In the geNorm paper, Vandesompele et al. described a method to select the most stable reference genes out of a set of candidate reference genes (Vandesompele 2002). This stability measure can also be used to evaluate the quality of normalization in subsequent experiments, provided that multiple reference genes have been used. We also realized that inter-run calibration and normalization are in fact analogues procedures: an IRC is for inter-run calibration what a reference gene is for normalization. Therefore, the stability measure developed to asses reference genes quality during normalization can be used for the evaluation of IRCs during inter-run calibration. These quality controls allow easy detection of bad data points, low quality reference genes and unreliable IRCs, thus avoiding skewing of qPCR results.

qBase program

All these new methods require significantly more calculations to obtain results, thus increasing the need for automation even more. We developed qBase to facilitate qPCR data processing (*qBase Analyzer*) and to manage the ever increasing amounts of qPCR data (*qBase Browser*) (*Paper 4: Hellemans 2007*). This freely available tool (http://medgen.ugent.be/qBase) allows reliable results (normalized and calibrated relative quantities) to be calculated rather quickly and permits them to be presented both graphically and in table format. It can, within the limits posed by Excel, process an unlimited number of samples and genes spread across different runs and with variable numbers of technical replicates. The calculations can deal with gene specific amplification efficiencies, multiple reference genes and inter-run calibration, and perform proper error propagation in each of these steps including the error on the amplification efficiency. In addition, qBase contains a number of quality controls analyzing the raw Cq data, verifying the stability of the reference genes, and testing the reliability of inter-run calibration.

Future perspectives

The current qBase framework addresses many shortcomings in the existing calculation methods, but it is as of yet not complete. Firstly, it lacks a description of how to perform absolute quantification and how this can be combined with normalization. Secondly, it can only deal with gene specific amplification efficiencies. The possibility to use a single amplification efficiency per gene might sometimes be too restricted. If, for example, the expression of a gene was measured in two plates using a different master mix, the amplification efficiency might differ between the plates and a run-gene specific amplification efficiency might be more appropriate. Also, recently a large interest has grown in the measurement and usage of sample specific amplification efficiencies (e.g. *Rutledge 2003*). This concept is not compatible with the current qBase framework. Thirdly, the current inter-run procedures based on normalized relative quantities are not compatible with all possible experimental setups, or with experiments with missing data points. To solve this issue we are currently working on complex inter-run calibration procedures that allow calibration of any kind of setup. The major problem faced in these algorithms is the proper error propagation. We are currently collaborating with Kristel Van Steen and Peter Konings to provide an adequate solution. Finally, calculation of quantities is not the last step in quantification experiments. These quantities need to be processed statistically to allow funded interpretation of the results. The required statistical methods are usually available, but they need to brought closer to the researcher to be more easily, and correctly, applied.

Much work can still be done from a methodological point of view, but these methods need to be incorporated in software to make them readily available, and easily applicable as well. In the past qBase has been written as a free Excel application. This approach does however not allow it to be developed much further. With the aid of UGent and funding from the IOF (Industrieel Onderzoeksfonds) we will develop qBasePlus as a commercial package. This software should be more user friendly, and work platform independent (i.e. not only on Microsoft but also on Macintosh). Upcoming improvements or additions to the qBase framework will only be implemented in this commercial package. A well developed framework and software package for qPCR data analysis will address the major remaining problem in qPCR based quantification experiments and allow this technology to be applied more easily.

References

Abad V, Uyeda JA, Temple HT, De Luca F, Baron J. 1999. Determinants of spatial polarity in the growth plate. Endocrinology 140(2):958-62.

Akiyama H, Chaboissier MC, Martin JF, Schedl A, de Crombrugghe B. 2002. The transcription factor Sox9 has essential roles in successive steps of the chondrocyte differentiation pathway and is required for expression of Sox5 and Sox6. Genes & development 16(21):2813-28.

Andersen PE, Jr. 1989. Prevalence of lethal osteochondrodysplasias in Denmark. American journal of medical genetics 32(4):484-9.

Ash P, Loutit JF, Townsend KM. 1980. Osteoclasts derived from haematopoietic stem cells. Nature 283(5748):669-70.

Benli IT, Akalin S, Boysan E, Mumcu EF, Kis M, Turkoglu D. 1992. Epidemiological, clinical and radiological aspects of osteopoikilosis. J Bone Joint Surg Br 74(4):504-6.

Bi W, Deng JM, Zhang Z, Behringer RR, de Crombrugghe B. 1999. Sox9 is required for cartilage formation. Nature genetics 22(1):85-9.

Botstein D, White RL, Skolnick M, Davis RW. 1980. Construction of a genetic linkage map in man using restriction fragment length polymorphisms. Am J Hum Genet 32(3):314-31.

Broman KW, Murray JC, Sheffield VC, White RL, Weber JL. 1998. Comprehensive human genetic maps: individual and sex-specific variation in recombination. American journal of human genetics 63(3):861-9.

Brunet LJ, McMahon JA, McMahon AP, Harland RM. 1998. Noggin, cartilage morphogenesis, and joint formation in the mammalian skeleton. Science 280(5368):1455-7.

Buschke A, Ollendorff H. 1928. Dermatofibrosis lenticularis disseminata und osteopathia condensans disseminata. Derm Wschr 86:257-262.

Camera G, Mastroiacovo P. 1982. Birth prevalence of skeletal dysplasias in the Italian Multicentric Monitoring System for Birth Defects. Progress in clinical and biological research 104:441-9.

Chen H, Johnson RL. 1999. Dorsoventral patterning of the vertebrate limb: a process governed by multiple events. Cell and tissue research 296(1):67-73.

Connor JM, Connor RA, Sweet EM, Gibson AA, Patrick WJ, McNay MB, Redford DH. 1985. Lethal neonatal chondrodysplasias in the West of Scotland 1970-1983 with a description of a thanatophoric, dysplasialike, autosomal recessive disorder, Glasgow variant. American journal of medical genetics 22(2):243-53.

Debeer P, Pykels E, Lammens J, Devriendt K, Fryns JP. 2003. Melorheostosis in a family with autosomal dominant osteopoikilosis: Report of a third family. Am J Med Genet 119A(2):188-93.

Dib C, Faure S, Fizames C, Samson D, Drouot N, Vignal A, Millasseau P, Marc S, Hazan J, Seboun E et al. 1996. A comprehensive genetic map of the human genome based on 5,264 microsatellites. Nature 380(6570):152-4.

Dreyer SD, Zhou G, Baldini A, Winterpacht A, Zabel B, Cole W, Johnson RL, Lee B. 1998. Mutations in LMX1B cause abnormal skeletal patterning and renal dysplasia in nail patella syndrome. Nature genetics 19(1):47-50.

Ducy P, Zhang R, Geoffroy V, Ridall AL, Karsenty G. 1997. Osf2/Cbfa1: a transcriptional activator of osteoblast differentiation. Cell 89(5):747-54.

Dudley AT, Ros MA, Tabin CJ. 2002 A re-examination of proximodistal patterning during vertebrate limb development. Nature 418(6897):539-44.

Eisman JA. 1999. Genetics of osteoporosis. Endocrine reviews 20(6):788-804.

Felix R, Cecchini MG, Fleisch H. 1990a. Macrophage colony stimulating factor restores in vivo bone resorption in the op/op osteopetrotic mouse. Endocrinology 127(5):2592-4.

Felix R, Cecchini MG, Hofstetter W, Elford PR, Stutzer A, Fleisch H. 1990b. Impairment of macrophage colony-stimulating factor production and lack of resident bone marrow macrophages in the osteopetrotic op/op mouse. Journal of bone and mineral research 5(7):781-9.

Fernandez-Tresguerres-Hernandez-Gil I, Alobera-Gracia MA, del-Canto-Pingarron M, Blanco-Jerez L. 2006. Physiological bases of bone regeneration II. The remodeling process. Medicina oral, patologia oral y cirugia bucal 11(2):E151-7.

Foster JW, Dominguez-Steglich MA, Guioli S, Kowk G, Weller PA, Stevanovic M, Weissenbach J, Mansour S, Young ID, Goodfellow PN et al. 1994. Campomelic dysplasia and autosomal sex reversal caused by mutations in an SRY-related gene. Nature 372(6506):525-30.

Gao B, Guo J, She C, Shu A, Yang M, Tan Z, Yang X, Guo S, Feng G, He L. 2001. Mutations in IHH, encoding Indian hedgehog, cause brachydactyly type A- 1. Nat Genet 28(4):386-8.

Gao YH, Shinki T, Yuasa T, Kataoka-Enomoto H, Komori T, Suda T, Yamaguchi A. 1998. Potential role of cbfa1, an essential transcriptional factor for osteoblast differentiation, in osteoclastogenesis: regulation of mRNA expression of osteoclast differentiation factor (ODF). Biochemical and biophysical research communications 252(3):697-702.

Gori F, Hofbauer LC, Dunstan CR, Spelsberg TC, Khosla S, Riggs BL. 2000. The expression of osteoprotegerin and RANK ligand and the support of osteoclast formation by stromal-osteoblast lineage cells is developmentally regulated. Endocrinology 141(12):4768-76.

Green AE, Jr., Ellswood WH, Collins JR. 1962. Melorheostosis and osteopoikilosis, with a review of the literature. Am J Roentgenol Radium Ther Nucl Med 87:1096-111.

Gustavson KH, Jorulf H. 1975. Different types of osteochondrodysplasia in a consecutive series of newborns. Helvetica paediatrica acta 30(3):307-14.

Hall CM. 2002. International nosology and classification of constitutional disorders of bone (2001). Am J Med Genet 113(1):65-77.

Hartmann C, Tabin CJ. 2001 Wnt-14 plays a pivotal role in inducing synovial joint formation in the developing appendicular skeleton. Cell 104(3):341-51.

Heaney RP, Abrams S, Dawson-Hughes B, Looker A, Marcus R, Matkovic V, Weaver C. 2000. Peak bone mass. Osteoporos Int. 11(12):985-1009.

Heid CA, Stevens J, Livak KJ, Williams PM. 1996. Real time quantitative PCR. Genome Res 6(10):986-94.

Hellemans J, Coucke PJ, Giedion A, Paepe AD, Kramer P, Beemer F, Mortier GR. 2003. Homozygous Mutations in IHH Cause Acrocapitofemoral Dysplasia, an Autosomal Recessive Disorder with Cone-Shaped Epiphyses in Hands and Hips. Am J Hum Genet 72(4):1040-6.

Hellemans J, Debeer P, Wright M, Janecke A, Kjaer KW, Verdonk PCM, Savarirayan R, Basel L, Moss C, Roth J, David A, De Paepe A, Coucke P, Mortier GR. 2006. Germline LEMD3 mutations are rare in sporadic patients with isolated melorheostosis. Hum Mutat. 27(3):290

Hellemans J, Preobrazhenska O, Willaert A, Debeer P, Verdonk PC, Costa T, Janssens K, Menten B, Van Roy N, Vermeulen SJ, Savarirayan R, Van Hul W, Vanhoenacker F, Huylebroeck D, De Paepe A, Naeyaert JM, Vandesompele J, Speleman F, Verschueren K, Coucke PJ, Mortier GR. 2004. Loss-of-function mutations in LEMD3 result in osteopoikilosis, Buschke-Ollendorff syndrome and melorheostosis. Nat Genet 36(11):1213-8.

Hellemans J, Mortier G, De Paepe A, Speleman F, Vandesompele J. 2007. qBase relative quantification framework and software for management and automated analysis of real-time quantitative PCR data. Genome Biol. 8(2):R19

Higuchi R, Fockler C, Dollinger G, Watson R. 1993. Kinetic PCR analysis: real-time monitoring of DNA amplification reactions.

Bio/technology (Nature Publishing Company) 11(9):1026-30.

Hunziker EB. 1994. Mechanism of longitudinal bone growth and its regulation by growth plate chondrocytes. Microscopy research and technique 28(6):505-19.

Ishimura A, Ng JK, Taira M, Young SG, Osada S. 2006. Man1, an inner nuclear membrane protein, regulates vascular remodeling by modulating transforming growth factor beta signaling. Development (Cambridge, England) 133(19):3919-28.

Janssens K, Vanhoenacker F, Bonduelle M, Verbruggen L, Van Maldergem L, Ralston S, Guanabens N, Migone N, Wientroub S, Divizia MT et al. 2006. Camurati-Engelmann disease: review of the clinical, radiological, and molecular data of 24 families and implications for diagnosis and treatment. J Med Genet 43(1):1-11.

Jobert AS, Zhang P, Couvineau A, Bonaventure J, Roume J, Le Merrer M, Silve C. 1998. Absence of functional receptors for parathyroid hormone and parathyroid hormone-related peptide in Blomstrand chondrodysplasia. The Journal of clinical investigation 102(1):34-40.

Kallen B, Knudsen LB, Mutchinick O, Mastroiacovo P, Lancaster P, Castilla E, Robert E. 1993. Monitoring dominant germ cell mutations using skeletal dysplasias registered in malformation registries: an international feasibility study. International journal of epidemiology 22(1):107-15.

Kang S, Graham JM, Jr., Olney AH, Biesecker LG. 1997. GLI3 frameshift mutations cause autosomal dominant Pallister-Hall syndrome. Nature genetics 15(3):266-8.

Karp SJ, Schipani E, St-Jacques B, Hunzelman J, Kronenberg H, McMahon APBR. 2000. Indian hedgehog coordinates endochondral bone growth and morphogenesis via parathyroid hormone related-protein-dependent and -independent pathways. Development 127(3):543-8.

Komori T, Yagi H, Nomura S, Yamaguchi A, Sasaki K, Deguchi K, Shimizu Y, Bronson RT, Gao YH, Inada M et al. 1997. Targeted disruption of Cbfa1 results in a complete lack of bone formation owing to maturational arrest of osteoblasts. Cell 89(5):755-64.

Kornak U, Mundlos S. 2003. Genetic disorders of the skeleton: a developmental approach. Am J Hum Genet 73(3):447-74.

Krane SM. 2005. Identifying genes that regulate bone remodeling as potential therapeutic targets. The Journal of experimental medicine 201(6):841-3.

Lathrop GM, Lalouel JM. 1984. Easy calculations of lod scores and genetic risks on small computers. American journal of human genetics 36(2):460-5.

Lefebvre V, Li P, de Crombrugghe B. 1998. A new long form of Sox5 (L-Sox5), Sox6 and Sox9 are coexpressed in chondrogenesis and cooperatively activate the type II collagen gene. The EMBO journal 17(19):5718-33.

Léri A, Joanny J. 1922. Une affection non décrite des os. Hyperostose "en coulée" sur toute la longueur d'un membre ou "mélorhéostose". Bull et Mém Soc Méd Hôp paris 46:1141-1145.

Li J, Sarosi I, Yan XQ, Morony S, Capparelli C, Tan HL, McCabe S, Elliott R, Scully S, Van G et al. 2000. RANK is the intrinsic hematopoietic cell surface receptor that controls osteoclastogenesis and regulation of bone mass and calcium metabolism. Proceedings of the National Academy of Sciences of the United States of America 97(4):1566-71.

Livak KJ, Schmittgen TD. 2001. Analysis of relative gene expression data using real-time quantitative PCR and the 2(-Delta Delta C(T)) Method. Methods 25(4):402-8.

MacCabe JA, Errick J, Saunders JW, Jr. 1974. Ectodermal control of the dorsoventral axis in the leg bud of the chick embryo. Developmental biology 39(1):69-82.

Marieb E, Hoehn K. 2006. Human Anatomy & Physiology: Benjamin Cummings.

McKusick VA, Scott CI. 1971. A nomenclature for constitutional disorders of bone. J Bone Joint Surg Am 53(5):978-86.

Mello MA, Tuan RS. 1999. High density micromass cultures of embryonic limb bud mesenchymal cells: an in vitro model of

endochondral skeletal development. In Vitro Cell Dev Biol Anim 35(5):262-9.

Menten B, Buysse K, Zahir F, Hellemans J, Hamilton SJ, Costa T, Fagerstrom C, Anadiotis G, Kingsbury D, McGillivray BC, Marra MA, Friedman JM, Speleman F, Mortier GR. 2007. Osteopoikilosis, short stature and mental retardation as key features of a new microdeletion syndrome on 12q14. J Med Genet. [Epub ahead of print].

Minina E, Kreschel C, Naski MC, Ornitz DM, Vortkamp A. 2002. Interaction of FGF, Ihh/Pthlh, and BMP signaling integrates chondrocyte proliferation and hypertrophic differentiation. Dev Cell 3(3):439-49.

Moore G. 1965. Cramming more components onto integrated circuits. Electronics 38(8):114-117.

Morinobu M, Nakamoto T, Hino K, Tsuji K, Shen ZJ, Nakashima K, Nifuji A, Yamamoto H, Hirai H, Noda M. 2005. The nucleocytoplasmic shuttling protein CIZ reduces adult bone mass by inhibiting bone morphogenetic protein-induced bone formation. The Journal of experimental medicine 201(6):961-70.

Mortier GR. 2001. The diagnosis of skeletal dysplasias: a multidisciplinary approach. European journal of radiology 40(3):161-7.

Mortier GR, Kramer PP, Giedion A, Beemer FA. 2003. Acrocapitofemoral dysplasia: an autosomal recessive skeletal dysplasia with cone shaped epiphyses in the hands and hips. J Med Genet 40(3):201-7.

Mundlos S, Otto F, Mundlos C, Mulliken JB, Aylsworth AS, Albright S, Lindhout D, Cole WG, Henn W, Knoll JH et al. 1997. Mutations involving the transcription factor CBFA1 cause cleidocranial dysplasia. Cell 89(5):773-9.

Nakashima K, Zhou X, Kunkel G, Zhang Z, Deng JM, Behringer RR, de Crombrugghe B. 2002. The novel zinc finger-containing transcription factor osterix is required for osteoblast differentiation and bone formation. Cell 108(1):17-29.

Nilsson O, Marino R, De Luca F, Phillip M, Baron J. 2005. Endocrine regulation of the growth plate. Hormone research 64(4):157-65.

Nishio Y, Dong Y, Paris M, O'Keefe RJ, Schwarz EM, Drissi H. 2006 Runx2-mediated regulation of the zinc finger Osterix/Sp7 gene. Gene. 10;372:62-70.

Niswander L. 2002. Interplay between the molecular signals that control vertebrate limb development. The International journal of developmental biology 46(7):877-81.

Niswander L. 2003. Pattern formation: old models out on a limb. Nature reviews 4(2):133-43.

O'Rahilly R, Gardner E. 1975. The timing and sequence of events in the development of the limbs in the human embryo. Anatomy and embryology 148(1):1-23.

Offiah AC, Hall CM. 2003. Radiological diagnosis of the constitutional disorders of bone. As easy as A, B, C? Pediatr Radiol 33(3):153-61.

Orioli IM, Castilla EE, Barbosa-Neto JG. 1986. The birth prevalence rates for the skeletal dysplasias. Journal of medical genetics 23(4):328-32.

Otto EA, Loeys B, Khanna H, Hellemans J, Sudbrak R, Fan S, Muerb U, O'Toole JF, Helou J, Attanasio M et al. 2005. Nephrocystin-5, a ciliary IQ domain protein, is mutated in Senior-Loken syndrome and interacts with RPGR and calmodulin. Nature genetics 37(3):282-8.

Otto F, Thornell AP, Crompton T, Denzel A, Gilmour KC, Rosewell IR, Stamp GW, Beddington RS, Mundlos S, Olsen BR et al. 1997. Cbfa1, a candidate gene for cleidocranial dysplasia syndrome, is essential for osteoblast differentiation and bone development. Cell 89(5):765-71.

Parrot J. 1886. Sur la malformation achondroplasique et le dieu Phtah. In: Parrot J, editor. La syphilis héréditaire et le rachitis. p 280-284.

Pfaffl MW. 2001. A new mathematical model for relative quantification in real-time RT-PCR. Nucleic Acids Res 29(9):e45.

Quinn JM, Elliott J, Gillespie MT, Martin TJ. 1998. A combination of osteoclast differentiation factor and macrophage-colony stimulating factor is sufficient for both human and mouse osteoclast formation in vitro. Endocrinology 139(10):4424-7.

Rasmussen SA, Bieber FR, Benacerraf BR, Lachman RS, Rimoin DL, Holmes LB. 1996. Epidemiology of osteochondrodysplasias: changing trends due to advances in prenatal diagnosis. Am J Med Genet 61(1):49-58.

Riddle RD, Johnson RL, Laufer E, Tabin C. 1993. Sonic hedgehog mediates the polarizing activity of the ZPA. Cell 75(7):1401-16.

Rockwood C, Wilkins K, King R. Fractures in Children: Lippincott.

Rutledge RG, Cote C. 2003. Mathematics of quantitative kinetic PCR and the application of standard curves. Nucleic acids research 31(16):e93.

Saiki RK, Gelfand DH, Stoffel S, Scharf SJ, Higuchi R, Horn GT, Mullis KB, Erlich HA. 1988. Primer-directed enzymatic amplification of DNA with a thermostable DNA polymerase. Science 239(4839):487-91.

Saiki RK, Scharf S, Faloona F, Mullis KB, Horn GT, Erlich HA, Arnheim N. 1985. Enzymatic amplification of beta-globin genomic sequences and restriction site analysis for diagnosis of sickle cell anemia. Science 230(4732):1350-4.

Sanger F, Coulson AR. 1975. A rapid method for determining sequences in DNA by primed synthesis with DNA polymerase. Journal of molecular biology 94(3):441-8.

Schipani E, Lanske B, Hunzelman J, Luz A, Kovacs CS, Lee K, Pirro A, Kronenberg HM, Juppner H. 1997. Targeted expression of constitutively active receptors for parathyroid hormone and parathyroid hormone-related peptide delays endochondral bone formation and rescues mice that lack parathyroid hormone-related peptide. Proc Natl Acad Sci U S A 94(25):13689-94.

Seeley R, Stephens T, Tate P. 2006. Anatomy and Physiology: McGraw-Hill.

Serra E, Rosenbaum T, Winner U, Aledo R, Ars E, Estivill X, Lenard HG, Lazaro C. 2000. Schwann cells harbor the somatic NF1 mutation in neurofibromas: evidence of two different Schwann cell subpopulations. Hum Mol Genet 9(20):3055-64.

Shiang R, Thompson LM, Zhu YZ, Church DM, Fielder TJ, Bocian M, Winokur ST, Wasmuth JJ. 1994. Mutations in the transmembrane domain of FGFR3 cause the most common genetic form of dwarfism, achondroplasia. Cell 78(2):335-42.

Shier D, Butler JN, Lewis R. 1996. Hole's Human Anatomy and Physiology: McGraw-Hill.

Simonet WS, Lacey DL, Dunstan CR, Kelley M, Chang MS, Luthy R, Nguyen HQ, Wooden S, Bennett L, Boone T et al. 1997. Osteoprotegerin: a novel secreted protein involved in the regulation of bone density. Cell 89(2):309-19.

Spranger J, Brill P, Poznanski A. 2002. Bone Dysplasia - An Atlas of Genetic Disorders of Skeletal Development: Oxford University Press.

Stieda A. 1905. Über umschriebene Knochenverdichtungen im Bereich der Substantia spongiosa in Roentgenbilde. Beitr Klin Chir 45:700-703.

St-Jacques B, Hammerschmidt M, McMahon AP. 1999. Indian hedgehog signaling regulates proliferation and differentiation of chondrocytes and is essential for bone formation. Genes Dev 13(16):2072-86.

Stoll C, Dott B, Roth MP, Alembik Y. 1989. Birth prevalence rates of skeletal dysplasias. Clinical genetics 35(2):88-92.

Storm EE, Kingsley DM. 1999. GDF5 coordinates bone and joint formation during digit development. Developmental biology 209(1):11-27.

Summerbell D. 1974. Interaction between the proximo-distal and antero-posterior co-ordinates of positional value during the specification of positional information in the early development of the chick limb-bud. Journal of embryology and experimental morphology 32(1):227-37.

Sun X, Mariani FV, Martin GR. 2002. Functions of FGF signalling from the apical ectodermal ridge in limb development. Nature 418(6897):501-8.

Superti-Furga A, Bonafe L, Rimoin DL. 2001. Molecular-pathogenetic classification of genetic disorders of the skeleton. Am J Med Genet 106(4):282-93.

Superti-Furga A, Unger S. 2007 Nosology and classification of genetic skeletal disorders: 2006 revision. Am J Med Genet A. 143(1):1-18.

Takahashi N, Akatsu T, Udagawa N, Sasaki T, Yamaguchi A, Moseley JM, Martin TJ, Suda T. 1988. Osteoblastic cells are involved in osteoclast formation. Endocrinology 123(5):2600-2.

Teitelbaum SL, Ross FP. 2003. Genetic regulation of osteoclast development and function. Nature reviews 4(8):638-49.

Tickle C. 1981. The number of polarizing region cells required to specify additional digits in the developing chick wing. Nature 289(5795):295-8.

Trivier E, De Cesare D, Jacquot S, Pannetier S, Zackai E, Young I, Mandel JL, Sassone-Corsi P, Hanauer A. 1996. Mutations in the kinase Rsk-2 associated with Coffin-Lowry syndrome. Nature 384(6609):567-70.

Urist M. 1980. Fundamental and Clinical Bone Physiology: Lippincott.

Vandesompele J, De Preter K, Pattyn F, Poppe B, Van Roy N, De Paepe A, Speleman F. 2002. Accurate normalization of real-time quantitative RT-PCR data by geometric averaging of multiple internal control genes. Genome Biol 3(7):RESEARCH0034.

Vesalius A. 1543. De Humani corporis fabrica.

Vortkamp A, Gessler M, Grzeschik KH. 1991. GLI3 zinc-finger gene interrupted by translocations in Greig syndrome families. Nature 352(6335):539-40.

Vortkamp A, Lee K, Lanske B, Segre GV, Kronenberg HM, Tabin CJBR. 1996. Regulation of rate of cartilage differentiation by Indian hedgehog and PTH-related protein. Science 273(5275):613-22.

Wagner T, Wirth J, Meyer J, Zabel B, Held M, Zimmer J, Pasantes J, Bricarelli FD, Keutel J, Hustert E et al. 1994. Autosomal sex reversal and campomelic dysplasia are caused by mutations in and around the SRY-related gene SOX9. Cell 79(6):1111-20.

Weber JL, May PE. 1989. Abundant class of human DNA polymorphisms which can be typed using the polymerase chain reaction. Am J Hum Genet 44(3):388-96.

Weissenbach J, Gyapay G, Dib C, Vignal A, Morissette J, Millasseau P, Vaysseix G, Lathrop M. 1992. A second-generation linkage map of the human genome. Nature 359(6398):794-801.

Yang X, Matsuda K, Bialek P, Jacquot S, Masuoka HC, Schinke T, Li L, Brancorsini S, Sassone-Corsi P, Townes TM et al. 2004. ATF4 is a substrate of RSK2 and an essential regulator of osteoblast biology; implication for Coffin-Lowry Syndrome. Cell 117(3):387-98.

Yasuda H, Shima N, Nakagawa N, Mochizuki SI, Yano K, Fujise N, Sato Y, Goto M, Yamaguchi K, Kuriyama M et al. 1998a. Identity of osteoclastogenesis inhibitory factor (OCIF) and osteoprotegerin (OPG): a mechanism by which OPG/OCIF inhibits osteoclastogenesis in vitro. Endocrinology 139(3):1329-37.

Yasuda H, Shima N, Nakagawa N, Yamaguchi K, Kinosaki M, Mochizuki S, Tomoyasu A, Yano K, Goto M, Murakami A et al. 1998b. Osteoclast differentiation factor is a ligand for osteoprotegerin/osteoclastogenesis-inhibitory factor and is identical to TRANCE/RANKL. Proc Natl Acad Sci U S A 95(7):3597-602.

Yoshida H, Hayashi S, Kunisada T, Ogawa M, Nishikawa S, Okamura H, Sudo T, Shultz LD, Nishikawa S. 1990. The murine mutation osteopetrosis is in the coding region of the macrophage colony stimulating factor gene. Nature 345(6274):442-4.

Zhao M, Harris SE, Horn D, Geng Z, Nishimura R, Mundy GR, Chen D. 2002. Bone morphogenetic protein receptor signaling is necessary for normal murine postnatal bone formation. J Cell Biol 157(6):1049-60.

Summary

Genetic abnormalities in the development, growth, and maintenance of cartilage and bone can result in the many and varied forms of skeletal dysplasias (osteochondrodysplasias). Common clinical manifestations include short stature, early-onset osteoartritis, fractures due to osteoporosis, joint pain and even extraskeletal malformations. The phenotypic severity of this heterogeneous group of disorders ranges from asymptomatic to death in the neonatal period. Although single entities had been described in the nineteenth century, considerable heterogeneity was recognized by the middle of last century leading to the current description of about 300 skeletal dysplasias. They are individually rare, but collectively quite common with an estimated prevalence of 2 to 5 per 10,000 newborns.
The most important aim of my PhD thesis was to identify the genes responsible for a selection of skeletal dysplasias. In this thesis, the results for acrocapitofemoral dysplasia, osteopoikilosis and melorheostosis are presented.

Acrocapitofemoral dysplasia (ACFD) is a recently described skeletal dysplasia with autosomal recessive inheritance, characterized clinically by a short stature with short limbs, and radiographically by cone-shaped epiphyses, mainly in hands and feet. These cone-shaped epiphyses reflect an early stage in the premature fusion of the growth plate that will ultimately result in shortening of the involved skeletal elements.
ACFD has so far been identified in two consanguineous families, both of which were included in a homozygosity mapping strategy to identify the causal gene. Using 400 microsatellite markers from a commercial kit for genome wide linkage analysis, the causal mutation could be mapped to an interval of 5 cM on chromosome 2q35-q36. Based on their known function and involvement in related disorders, *IGFBP2*, *IGFBP5*, *IHH* and *STK36* were selected as candidate genes (candidate gene approach). Subsequently, sequencing of *IHH* revealed the presence of homozygous missense mutations in all affected individuals: c.137C>T for both patients of a Belgian family and c.569T>C for the three patients of a Dutch family. Both mutations were considered causal for the phenotype because they segregate along with the phenotype and affect completely conserved amino acids. These mutations disturb the normal function of IHH in the growth plate and probably cause an increased rate of chondrocyte differentiation leading to a premature epimetaphyseal fusion of the involved growth plate.

Osteopoikilosis, Buschke-Ollendorff syndrome (BOS) and melorheostosis are rare sclerosing dysplasias. Osteopoikilosis is a benign, usually asymptomatic condition with autosomal dominant inheritance that is characterized by a symmetric but unequal distribution of multiple hyperostotic areas in different parts of the skeleton. Osteopoikilosis often co-occurs with disseminated connective tissue nevi and is then known as the Buschke-Ollendorff syndrome. Melorheostosis, on the other hand, is a more severe disorder that is radiographically characterized by an asymmetric flowing hyperostosis of the cortex of tubular bones that is often accompanied by abnormalities of adjacent soft tissue. Melorheostosis usually causes joint contractures, stiffness and chronic pain.
The occurrence of one or more of these conditions in the same individual or family suggested that they may represent allelic disorders. A genome wide linkage analysis was performed on three families in which affected individuals had osteopoikilosis with or without manifestations of BOS or melorheostosis. This resulted in a linkage interval of 24 cM on chromosome 12q12-q14.3. Subsequently, a microdeletion, partially overlapping this interval, was identified in an unrelated patient with the unusual association of osteopoikilosis, short stature and learning disabilities. This finding reduced the candidate region to a 3 Mb interval containing 23 genes. Using a candidate gene approach, *LEMD3* was selected for sequencing which subsequently lead to the identification of heterozygous

loss-of-function mutations in all patients from these 3 families. Mutation analysis in a larger set of patients confirmed that almost all individuals with osteopoikilosis or BOS have an inactivating *LEMD3* mutation, whereas most sporadic patients with isolated melorheostosis have normal results after *LEMD3* analysis.
By means of a yeast-two-hybrid screening, LEMD3 was shown to interact with the MH2 domain of both BMP and TGFβ specific SMADs. Two functional experiments demonstrated an inhibitory effect of LEMD3 on SMAD mediated BMP and TGFβ signaling. Increasing amounts of LEMD3 reduced the expression of SMAD target genes after BMP stimulation, and similarly LEMD3 overexpression resulted in reduced luciferase activity in cells with constitutively active TGFβ signaling.

Whereas the first part of this thesis aimed to identify the genetic defects for a selection of skeletal dysplasias, the focus in the second part was partially shifted to the development of improved methods and a program for automated qPCR analysis.
Nucleic acid quantification in general and gene expression analysis more specifically are becoming increasingly important in biological research and clinical decision making, with real-time quantitative PCR (qPCR) becoming the method of choice for expression profiling of selected genes. Advancements in instruments and detection chemistry, and improved assay design guidelines have made the practical performance of qPCR measurements feasible for most users. However, accurate and straightforward processing of the raw data as well as the management of large and growing data sets remain the major hurdles in this type of PCR based gene expression analysis.
My dissatisfaction with the available qPCR tools led me to write a program for qPCR data management and analysis: qBase.
This program allows data to be imported in any of the numerous data formats being used. These data can be managed by organizing them into runs, experiments and projects, and by annotating them in the qBase *Browser* module. The *Analysis* module subsequently allows data from multiple runs to be analyzed as a whole without limitations on the number of samples, genes or replicates. An automated raw data quality control is included to prevent inprecise data being used in calculations. qBase employs an advanced quantification algorithm that allows gene specific amplification efficiencies and normalization with multiple reference genes to be used. The obtained results can easily be exported in tabular format, or visualized as a gene-specific or multi-gene histogram.
In addition to the functionalities of the qBase program a number of new calculation methods were developed to improve data analysis. Firstly, the error on the estimated amplification efficiency is calculated and propagated throughout calculations. Secondly, algorithms for inter-run calibration were developed to correct for the often underestimated run-to-run variation, and to allow comparing results from samples located on different plates. Together, the improved calculation methods and the qBase program allow for faster and more reliable qPCR analysis.
No other packages with comparable functionality are available for the moment. qBase has been recognized as a very useful and advanced tool for qPCR data analysis by the scientific community. This is reflected by the fact that the program has been downloaded (http://medgen.ugent.be/qBase) by over 2000 users from more than 80 countries.

Samenvatting

Genetische afwijkingen in de ontwikkeling, groei en homeostase van kraakbeen en bot kunnen resulteren in een van de vele vormen van skeletdysplasieën (osteochondrodysplasias). Klinisch worden deze aandoeningen veelal gekenmerkt door kleine gestalte, osteoartritis op jonge leeftijd, botbreuken ten gevolge van osteoporose, gewrichtspijn en zelfs extraskeletale afwijkingen. De ernst van deze heterogene groep aandoeningen varieert van asymptomatisch tot vroegtijdig overlijden in de neonatale periode. De eerste types werden reeds in de negentiende eeuw gedefinieerd, maar de herkenning van aanzienlijke heterogeniteit halverwege vorige eeuw leidde tot de beschrijving van 300 skeletdysplasieën op dit moment. Individueel zijn deze aandoeningen zeldzaam, maar gezamelijk zijn ze redelijk frequent met een geschatte prevalentie van 2 tot 5 per 10.000 geboortes.
De hoofddoelstelling van mijn doctoraatsthesis was de identificatie van de genen verantwoordelijk voor een selectie van skeletdysplasieën. In deze thesis worden de resultaten voor acrocapitofemorale dysplasie, osteopoikilosis en melorheostosis voorgesteld.

Acrocapitofemorale dysplasie (ACFD) is een recent beschreven skeletdysplasie met autosomaal recessieve overerving die klinisch gekarakteriseerd wordt door kleine gestalte met korte ledematen, en radiologisch door kegelvormige epiphysen, voornamelijk in handen en voeten. Deze kegelvormige epiphysen typeren een vroeg stadium van de premature sluiting van de groeischijf die uiteindelijk resulteert in een verkorting van de getroffen botten.
ACFD werd tot op heden geïdentificeerd in twee consanguine families die beiden geïncludeerd werden in een homozygoziteitsmapping voor de identificatie van het causale gen. Met behulp van de 400 microsatelliet merkers uit een commerciële kit voor genoomwijd koppelingsonderzoek kon de causale mutatie gelokaliseerd worden binnen een interval van 5 cM op chromosoom 2q35-q36. Op basis van hun gekende functie en betrokkendheid in verwante aandoeningen werden *IGFBP2*, *IGFBP5*, *IHH* en *STK36* geselecteerd als kandidaat genen. Vervolgens kon door middel van sequeneren een homozygote *IHH* mutatie aangetoond worden in alle aangetaste individuen: c.137C>T in de patiënten van de Belgische familie en c.569T>C in de drie patiënten van de Nederlandse familie. Aangezien beide mutaties samen met het phenotype segregeren en volledig geconserveerde aminozuren aantasten werden ze als causaal beschouwd. De premature epimetaphysaire sluiting in ACFD patiënten wordt waarschijnlijk veroorzaakt door een verhoogde differentiatiesnelheid van kraakbeencellen ten gevolge van een verstoorde werking van IHH in de groeischijf.

Osteopoikilosis, Buschke-Ollendorff syndrome (BOS) en melorheostosis zijn zeldzame scleroserende dysplasieën. Osteopoikilosis is een goedaardige, meestal asymptomatische aandoening met autosomaal dominante overerving. Ze wordt getypeerd door het ongelijkmatig maar symmetrisch voorkomen van kleine hyperostotische letsels in verschillende delen van het skelet. Osteopoikilosis komt vaak voor in combinatie met bindweefseelletsels en staat dan gekend als het Buschke-Ollendorff syndroom. Melorheostosis is daarentegen een ernstigere aandoening die radiologisch gekenmerkt wordt door een asymmetrisch vloeiende hyperostose van de cortex van de lange beenderen. Het zacht weefsel rond deze skeletale letselts is ook vaak aangetast. Melorheostosis patiënten lijden meestal aan gewrichtscontracturen, stijfheid van de aangetaste ledematen en chronische pijn.
Het voorkomen van osteopoikilosis, BOS en melorheostosis in dezelfde patiënt of familie suggereerde dat ze allelische aandoeningen zijn. Een genoomwijd koppelingsonderzoek werd uitgevoerd op 3 families waarin osteopoikilosis, al dan niet in combinatie met BOS of melorheostosis, voorkomt. Hiermee werd een gekoppelde regio van 24 cM op chromosoom 12q12-q14.3 geïdentificeerd. Vervolgens werd in een patiënt met de ongewone combinatie van osteopoikilosis met

kleine gestalte en leerproblemen een microdeletie gevonden die de gekoppelde regio gedeeltelijk overlapte. Op basis hiervan kon de kandidaatregio gereduceerd worden tot een interval van 3 Mb dat slechts 23 genen bevatte. Met behulp van een kandidaat-gen benadering werd *LEMD3* geselecteerd voor sequentie analyse. Dit resulteerde uiteindelijk in de identificatie van heterozygote loss-of-function mutaties in alle patiënten van de drie onderzochte families. Mutatie analyse in een grotere set patiënten bevestigde vervolgens dat bijna alle individuen met osteopoikilosis of BOS een inactiverende *LEMD3* mutatie draagden, terwijl de meeste sporadische patiënten met geïsoleerde melorheostosis normale resultaten hadden voor *LEMD3*.
Door middel van een yeast-two-hybrid screening kon aangetoond worden dat LEMD3 interageert met het MH2 domein van BMP en TGFβ specifieke SMAD's. In twee functionele experimenten kon een inhibitorisch effect van LEMD3 op SMAD gemedieerde BMP en TGFβ signalisatie aangetoond worden. Toenemende hoeveelheden LEMD3 reduceerden de expressie van SMAD gereguleerde genen na BMP stimulatie, en LEMD3 overexpressie resulteerde in een verlaagde luciferase activiteit in cellen met een consitutief actieve TGFβ signalisatie.

In het eerste deel van deze thesis werd getracht de genetische defecten verantwoordelijk voor een selectie van skeletdysplasieën te identificeren. In een tweede deel verschoof de focus gedeeltelijk naar de ontwikkeling van verbeterde methodes en een programma voor geautomatiseerde qPCR analyse.
De quantificatie van nucleïnezuren, en in het bijzonder genexpressieanalyse, worden steeds belangrijker in zowel biologisch onderzoek als in de klinische diagnostiek. Real-time quantitative PCR (qPCR) is momenteel de geprefereerde methode geworden voor het bepalen van de expressieprofielen voor een selectie van genen. Verbeterde instrumenten en detectiemethoden, alsook geoptimaliseerde richtlijnen voor het opstellen van experimenten hebben de praktische uitvoering van qPCR experimenten haalbaar gemaakt voor de meeste gebruikers. Nochtans blijven de accurate en eenvoudige verwerking van de ruwe data, alsook het beheer van steeds groter wordende data sets grote hindernissen voor dit type van PCR gebaseerde gen expressie analyse.
De ontevredenheid over de beschikbare qPCR tools zette me ertoe aan om een programma te schrijven (qBase) waarmee de qPCR data zowel beheerd als geanalyseerd kunnen worden.
De Browser module van dit programma laat toe om data te importeren vanuit de verschillende formaten die momenteel in omloop zijn. Deze data kunnen dan vervolgens beheerd worden door ze te annoteren en te organiseren in runs, experimenten en projecten. In de Analyse module kunnen de data van een verzameling runs geanalyzeerd worden zonder beperkingen op het aantal stalen, genen of technische herhalingen. Een automatische controle op de ruwe data kan voorkomen dat data van lage qualiteit gebruikt worden bij de berekeningen. qBase past een geavanceerd quantificatie algoritme toe waarmee rekening gehouden kan worden met genspecifieke amplificatie efficienties en normalisatie op basis van meerdere referetiegenen uitgevoerd kan worden. De berekende resultaten kunnen eenvoudig in tabelvorm geëxporteerd worden, of gevisualiseerd worden in grafiekvorm voor een enkel of voor meerdere genen.
Naast de functionaliteit die door het qBase programma wordt geboden, werden ook een aantal nieuwe berekeningsmethoden ontwikkeld voor verbeterde data analyse. Ten eerste werd de fout op de geschatte amplificatie efficientie berekend en gepropageerd doorheen alle berekeningen. Ten tweede werd een algoritme ontwikkeld om te corrigeren voor de vaak onderschatte variatie tussen runs zodat de resultaten van stalen op verschillende platen met elkaar vergeleken kunnen worden. De verbeterde berekeningsmethoden en het qBase programma laten gezamelijk een snellere en betere analyse van qPCR experimenten toe.
Op dit moment zijn geen paketten beschikbaar met een functionaliteit die vergelijkbaar is aan die van qBase. Het feit dat qBase reeds door meer dan 2000 gebruikers uit 80 landen werd gedownload (http://medgen.ugent.be/qBase) toont aan dat dit programma erkend wordt als een zeer bruikbare tool voor geavanceerde qPCR analyzes.

Résumé

Des anomalies génétiques dans le développement, la croissance et le maintien du cartilage et des os peuvent mener à des formes de dysplasies osseuses (ostéochondrodysplasies) nombreuses et variées. Parmi les manifestations cliniques habituelles l'on observe: petite stature, ostéoarthrite précoce, fractures dues à l'ostéoporose, arthralgie et même des malformations extrasquelettiques. La sévérité phénotypique de ce groupe hétérogène d'affections varie d'asymptomatique à la mort en période néonatale. Bien que des cas particuliers aient été décrits dans le courant du dix-neuvième siècle, c'est l'hétérogénéité importante, identifiée vers le milieu du siècle dernier, qui a mené à la description actuelle d'environ 300 dysplasies osseuses. Ils sont rares pris individuellement, mais collectivement ils sont assez commun avec une prévalence estimée de 2 à 5 par 10.000 nouveaux-nés.
Le principal objectif de ma thèse PhD était d'identifier les gènes responsables d'une sélection de dysplasies osseuses. Dans cette thèse sont présentés les résultats pour la dysplasie acrocapitofémorale, l'ostéopoécilie et la mélorhéostose.

La dysplasie acrocapitofémorale (ACFD) est une dysplasie osseuse récemment décrite d'hérédité autosomique récessive, caractérisée cliniquement par une petite stature avec des membres courts, et radiographiquement par des épiphyses coniques, principalement aux mains et aux pieds. Ces épiphyses coniques révèlent un stade précoce dans la fusion prématurée du cartilage épiphysaire qui aboutira finalement à un raccourcissement des éléments squelettiques concernés.
ACFD a jusqu'à présent été identifiée en deux familles consanguines, qui toutes deux ont été inclues dans une stratégie de cartographie par homozygotie pour identifier le gène causal. A l'aide de 400 marqueurs microsatellites d'un kit commercial pour l'analyse de liaison du génome entier, la mutation causale a été localisée à un intervalle de 5 cM dans le chromosome 2q35-q36. Basé sur leur fonction connue et implication dans des affections apparentées, *IGFBP2*, *IGFBP5*, *IHH* et *SKT36* ont été sélectionnés comme gènes candidats (l'approche du gène candidat).
Ensuite, la détermination de la séquence d'*IHH* a révélé la présence de mutations faux-sens homozygote dans tous les individus atteints: c.137C>T pour les deux patients d'une famille belge et c.569T>C pour les trois patients d'une famille néerlandaise. Les deux mutations ont été considérées causales pour le phénotype et atteignent des aminoacides entièrement conservées. Ces mutations perturbent le fonctionnement normal d'IHH dans le cartilage épiphysaire et provoquent vraisemblablement un plus haut degré de différentiation chondrocyte causant une fusion épimetaphyseale prématurée du cartilage épiphysaire impliqué.

L'ostéopoécilie, le syndrome de Buschke-Ollendorff (BOS) et la mélorhéostose sont des dysplasies sclérosantes rares. L'ostéopoécilie est une maladie bénigne, généralement asymptomatique d'hérédité autosomique dominante, qui se caractérise par une distribution symétrique mais inégale de multiples zones hyperostotiques sur différentes parties du squelette. On entend par le syndrome de Buschke-Ollendorff une maladie associant l'ostéopoécilie et des naevi conjonctifs disséminés. La mélorhéostose, par contre, est une affection plus grave, radiographiquement caractérisée par une hyperostose en coulée asymétrique du cortex des os tubulaires qui est souvent accompagnée d'anormalités des tissus mous adjacentes. La mélorhéostose cause souvent des contractures des articulations, des raideurs et des maux chroniques.
Lorsqu'une ou plusieurs de ces maladies se produisent au sein d'un même individu ou famille cela laisse présumer qu'il s'agit d'affections alléliques. Une analyse de liaison du génome entier a été effectuée chez trois familles ou des individus atteints avaient ostéopoécilie avec ou sans expressions de BOS ou de mélorhéostose. Ceci a mené à un intervalle de 24 cM dans le chromosome 12q12-q14.3. Ensuite une microdeletion,

recouvrant partiellement cet intervalle, a été identifié dans un patient sans liens de parenté avec les trois familles précitées, mais avec une association inhabituelle d'ostéopoécilie, petite stature et troubles d'apprentissage. Cette découverte a réduit la région candidate à un intervalle de 3 Mb contenant 23 gènes. En utilisant une approche du gène candidat, *LEMD3* a été sélectionné pour la détermination de la séquence qui a ensuite mené à l'identification des mutations hétérozygotes "perte de fonction" dans tous les patients de ces 3 familles. Une analyse de mutations dans un groupe plus important de patients a confirmé que presque tous les individus avec l'ostéopoécilie ou le BOS ont une mutation inactivant *LEMD3*, alors que la plupart des patients ayant la mélorhéostose montrent des résultats normaux après analyse *LEMD3*.
Le système du double hybride en levure a révélé une interaction entre LEMD3 d'une part et le domaine MH2 de deux types de SMADs d'autre part (les uns réagissant spécifiquement sur BMP, les autres sur TGFβ). Deux études fonctionnelles ont démontré un effet inhibiteur de LEMD3 sur la signalisation de BMP et TGFβ qui est mediée pat les SMADs. Des niveaux croissants de LEMD3 ont réduit l'expression des gènes cibles SMAD après stimulation par BMP, et, de façon similaire, une surexpression de LEMD3 a conduit à une baisse de l'activité luciférase dans les cellules ayant une signalisation TGFβ constitutivement active.

La première partie de cette thèse visait à identifier les défauts génétiques pour une sélection de dysplasies osseuses. Dans la seconde partie par contre, l'accent a été déplacé partiellement vers le développement de méthodes améliorées et d'un programme pour des analyses qPCR automatiques.
La quantification des acides nucléiques en général et plus spécifiquement l'analyse de l'expression des gènes jouent un rôle toujours plus important dans la recherche biologique et la prise de décision clinique, avec la PCR quantitative en temps réel (qPCR) devenant la méthode de choix pour le profilage d'expression de gènes sélectionnés. Des progrès dans les instruments et les réactifs, et de meilleures directives pour la conception de l'analyse ont rendu les performances pratiques des dénombrements qPCR faisables pour la plupart des utilisateurs. Bien que le traitement fiable et sérieux des données brutes, ainsi que la gestion du grand –et toujours croissant– volume de données restent les principaux obstacles à surmonter dans ce type d'analyse de l'expression des gènes basé sur PCR.
Mon insatisfaction face aux outils qPCR disponibles m'a incité à écrire un programme pour la gestion et l'analyse des données qPCR: qBase.
Ce programme permet d'importer des données de n'importe lequel des nombreux formats en usage. Les données peuvent être gérées, en les organisant en runs, études et projets et en les annotant dans le module qBase Browser (Navigateur qBase). Le module Analysis (Analyse) permet par la suite d'analyser des données de plusieurs runs en tant qu'un ensemble, sans limitations quant au nombre d'échantillons, de gènes ou de répétitions. Un contrôle automatique de qualité des données brutes est inclus pour éviter que des données imprécises soient utilisées dans les calculs. qBase fait usage d'un algorithme de quantification avancée permettant des efficacités de l'amplification spécifique du gène et une normalisation avec utilisation de multiples gènes de référence. Les résultats obtenus peuvent facilement être exportés en format tabulaire, ou visualisés par un histogramme spécifique du gène ou multigénique.
En plus des fonctionnalités du programme qBase un nombre de nouvelles méthodes de calcul a été développé afin d'améliorer l'analyse des données. En premier lieu, l'erreur sur l'efficacité de l'amplification estimée est calculée et propagée dans les calculs. En second lieu, des algorithmes pour l'étalonnage de différents runs ont été développés afin de corriger pour la variation entre les runs, souvent sous-estimée, et de permettre la comparaison des résultats pour des échantillons localisés sur différents cartilages. Les méthodes de calcul améliorées combinées au programme qBase permettent une analyse qPCR plus rapide et plus fiable.
Pour le moment il n'y a pas d'autres progiciels disponibles avec une fonctionnalité comparable. qBase a été reconnue par la communauté scientifique comme un outil très utile et avancé pour l'analyse de données qPCR. Le fait que plus de 2000 utilisateurs dans plus de 80 pays ont téléchargé (http://medgen.ugent.be/qBase) le programme en est la preuve.

Curriculum Vitae

Personalia

Jan Hellemans
Ghent University Hospital
Center for Medical Genetics Ghent, MRB
De Pintelaan 185, B-9000 Ghent
+32 9 240 55 35 (phone), +32 9 240 65 49 (fax)
Jan.Hellemans@UGent.be

Education

1990-1996	Math-Sciences (8h), Sint-Jan Bergmanscollege, Merksem
1996-1998	Chemistry, Ghent University, Ghent
1998-2000	Biotechnology, Ghent University, Ghent Thesis: "Analyse van selectiemerkerrecyclage in de filamenteuze fungi *Aspergillus niger* en *Trichoderma reesei"*

Attended courses and trainings

Linkage analysis course, HGMP-RC Training Course, MRC Rosalind Franklin Centre for Genomics Research (RFCGR). September 25th-27th 2002. London, UK

Training for construction and analysis of chicken micromass cultures, Max Planck Institute for Molecular Genetics, Research Group Mundlos: Development and Disease. January – March 2004. Berlin, Germany.

Professional activities

2001-2002	Scientific coworker at the Center for Medical Genetics Ghent
2002-2006	Ph.D. candidate at the Center for Medical Genetics Ghent
2007	Scientific coworker at the Center for Medical Genetics Ghent

Articles included in the Science Citation Index

Hellemans J, Coucke PJ, Giedion A, De Paepe A, Kramer P, Beemer F, Mortier GR. Homozygous mutations in IHH cause acrocapitofemoral dysplasia, an autosomal recessive disorder with cone-shaped epiphyses in hands and hips. Am J Hum Genet. 2003 Apr; 72(4):1040-6.

Hellemans J, Preobrazhenska O, Willaert A, Debeer P, Verdonk PC, Costa T, Janssens K, Menten B, Van Roy N, Vermeulen SJ, Savarirayan R, Van Hul W, Vanhoenacker F, Huylebroeck D, De Paepe A, Naeyaert JM, Vandesompele J, Speleman F, Verschueren K, Coucke PJ, Mortier GR. Loss-of-function mutations in LEMD3 result in osteopoikilosis, Buschke-Ollendorff syndrome and melorheostosis. Nat Genet. 2004 Nov;36(11):1213-8.

Otto EA, Loeys B, Khanna H, Hellemans J, Sudbrak R, Fan S, Muerb U, O'Toole JF, Helou J, Attanasio M, Utsch B, Sayer JA, Lillo C, Jimeno D, Coucke P, De Paepe A, Reinhardt R, Klages S, Tsuda M, Kawakami I, Kusakabe T, Omran H, Imm A, Tippens M, Raymond PA, Hill J, Beales P, He S, Kispert A, Margolis B, Williams DS, Swaroop A, Hildebrandt F. Nephrocystin-5, a ciliary IQ domain protein, is mutated in Senior-Loken syndrome and interacts with RPGR and calmodulin. Nat Genet. 2005 Mar;37(3):282-8.

Loeys BL, Chen J, Neptune ER, Judge DP, Podowski M, Holm T, Meyers J, Leitch CC, Katsanis N, Sharifi N, Xu FL, Myers LA, Spevak PJ, Cameron DE, De Backer J, Hellemans J, Chen Y, Davis EC, Webb CL, Kress W, Coucke P, Rifkin DB, De Paepe AM, Dietz HC. A syndrome of altered cardiovascular, craniofacial, neurocognitive and skeletal

development caused by mutations in TGFBR1 or TGFBR2. Nat Genet. 2005 Mar;37(3):275-81.

Hellemans J, Debeer P, Wright M, Janecke A, Kjaer KW, Verdonk PCM, Savarirayan R, Basel L, Moss C, Roth J, David A, De Paepe A, Coucke P, Mortier GR. Germline LEMD3 mutations are rare in sporadic patients with isolated melorheostosis. Hum Mutat. 2006 Mar;27(3):290

Menten B, Buysse K, Zahir F, Hellemans J, Hamilton SJ, Costa T, Fagerstrom C, Anadiotis G, Kingsbury D, McGillivray BC, Marra MA, Friedman JM, Speleman F, Mortier GR. Osteopoikilosis, short stature and mental retardation as key features of a new microdeletion syndrome on 12q14. J Med Genet. 2007 Jan 12; [Epub ahead of print].

Hellemans J, Mortier G, De Paepe A, Speleman F, Vandesompele J. qBase relative quantification framework and software for management and automated analysis of real-time quantitative PCR data. Genome Biol. 2007 Feb 9;8(2):R19

Gass J, Hellemans J, Mortier G, Griffiths M, Burrows N. Buschke-Ollendorff Syndrome: a manifestation of LEMD3 mutation. Submitted to J Am Acad Dermatol.

Coppieters F, Leroy BP, Beysen D, Hellemans J, De Bosscher K, Haegeman G, Robberecht K, De Jaegere S, Wuyts W, Coucke PJ, De Baere E. Recurrent mutation in the first zinc finger of the orphan nuclear receptor NR2E3 causes autosomal dominant retinitis pigmentosa. Submitted to Am J Hum Genet.

Book chapters

Hellemans J, Mortier G. LEMD3 and Osteopoikilosis, the Buschke-Ollendorff Syndrome and Melorheostosis. In: Epstein C, Erickson R, Wynshaw-Boris A (eds) Inborn Errors of Development, 2nd edition. Oxford University Press, New York

Hellemans J, Mortier G. IHH and Acrocapitofemoral Dysplasia and Brachydactyly A1. In: Epstein C, Erickson R, Wynshaw-Boris A (eds) Inborn Errors of Development, 2nd edition. Oxford University Press, New York

Contributions to encyclopedias

Hellemans J, Mortier GR. Melorheostosis. In: Lang F (Ed.) Encyclopedia of Molecular Mechanisms of Diseases. Springer, New York

Attended congresses, workshops and meetings

Genetic analysis workshop organized by Applied Biosystems, April 4th 2001, Brussels, Belgium

ESDN meeting, June 2002, Ghent, Belgium

ESDN meeting, December 2003, Paris, France

2nd meeting of the Belgian Society for Human Genetics 2002, February 22nd 2002, Brussels, Belgium

3rd meeting of the Belgian Society for Human Genetics 2003, January 7th 2003, Leuven, Belgium

European Society for Human Genetics 2003, May 3-6 2003, Birmingham, UK

Symposium on 'Genetics of multifactorial diseases', December 17th 2003, Antwerp, Belgium

Annual meeting of the American Society for Human Genetics 2004, October 26-30 2004, Toronto, Canada

Seminar in VUB, December 2004, Brussels, Belgium

5th meeting of the Belgian Society for Human Genetics 2005, January 28th 2005, Liege, Belgium

Benelux Bioinformatics Conference 2005, April 14-15, Ghent, Belgium

European Human Genetics conference 2005, May 7-10 2005, Prague, Czech

7th meeting of the International Skeletal Dysplasia Society, August 25-28 2005, Martigny, Swiss

2nd International qPCR Symposium, September 5-7 2005, Freising-Weihenstephan, Germany

6th meeting of the Belgian Society for Human Genetics, February 17th 2006, Antwerp, Belgium

3rd International qPCR Symposium, March 26-30 2007, Freising-Weihenstephan, Germany

Oral presentations

Mapping of the gene for ACFD to chromosome 2. ESDN meeting, June 2002, Ghent, Belgium

Acrocapitofemoral dysplasia (ACFD): from patient to gene. European Society for Human Genetics 2003, May 3-6 2003, Birmingham, UK

Loss of function mutations in MAN1 result in osteopoikilosis, Buschke-Ollendorff syndrome and melorheostosis. Annual meeting of the American Society for Human Genetics 2004, October 26-30 2004, Toronto, Canada

Loss of function mutations in LEMD3 result in osteopoikilosis, Buschke-Ollendorff syndrome and melorheostosis. Seminar in VUB, December 2004, Brussels, Belgium

Loss of function mutations in MAN1 result in osteopoikilosis, Buschke-Ollendorff syndrome and melorheostosis. 5th meeting of the Belgian Society for Human Genetics 2005, January 28th 2005, Liege, Belgium

Mutation analysis of LEMD3 in osteopoikilosis, Buschke-Ollendorff syndrome and melorheostosis patients. 7th meeting of the International Skeletal Dysplasia Society, August 25-28 2005, Martigny, Swiss

qBase: relative quantification software for management and automated analysis. Inivted speaker at the 2nd International qPCR Symposium, 5-7 september 2005, Freising-Weihenstephan, Germany (*Inivted speaker*)

Advanced and universally applicable models for relative quantification with flexible inter-run calibration and proper error propagation. 3rd International qPCR Symposium, March 26-30 2007, Freising-Weihenstephan, Germany (*Inivted speaker*)

RDML: real-time PCR data markup language. 3rd International qPCR Symposium, March 26-30 2007, Freising-Weihenstephan, Germany (*Inivted speaker*)

Posters

Hellemans J, Kramer PPG, Giedion A, Beemer FA, De Paepe A, Coucke P, Mortier GR. Homozygosity mapping in a new metaphyseal chondrodysplasia. 2nd meeting of the Belgian Society for Human Genetics 2002, February 22nd 2002, Brussels, Belgium

Hellemans J, Kramer PPG, Giedion A, Beemer FA, De Paepe A, Coucke P, Mortier GR. Homozygous mutations in IHH cause acrocapitofemoral dysplasia. 3rd meeting of the Belgian Society for Human Genetics 2003, January 7th 2003, Leuven, Belgium

Hellemans J, Mortier GR, De Paepe A, Speleman F, Vandesompele J. qBASE: an Excel application for the management and automatic analysis of real-time quantitative PCR data. Benelux Bioinformatics Conference 2005, April 14-15, Ghent, Belgium

Hellemans J, Debeer P, Verdonk P, Van Hul W, Wright M, De Paepe A, Coucke P, Mortier GR. Mutation analysis of LEMD3 in osteopoikilosis, Buschke-Ollendorff syndrome and melorheostosis patients European Human Genetics conference 2005, May 7-10 2005, Prague, Czech

Leroy BP, Robberecht K, Coppieters F, Beysen D, Hellemans J, Coucke PJ, De Baere E. Autosomal dominant retinitis pigmentosa in a large Belgian family: linkage-based exclusion mapping of 13 known loci. Annual meeting of the American Society for Human Genetics 2005, October 25-29 2005, Salt Lake City, USA

Hellemans J, Mortier GR, De Paepe A, Speleman F, Vandesompele J. qBase: relative quantification software for management and automated analysis of real-time quantitative PCR data. 6th meeting of the Belgian Society for Human Genetics, February 17th 2006, Antwerp, Belgium

Hellemans J, Debeer P, Wright M, Janecke A, Kjaer KW, Verdonk PCM, Savarirayan R, Basel L, Moss C, Roth J, David A, De Paepe A, Coucke P, Mortier GR. Germline LEMD3 mutations are responsible for osteopoikilosis and Buschke-Ollendorff syndrome, but are rare in sporadic patients with isolated melorheostosis. 6th meeting of the Belgian Society for Human Genetics, February 17th 2006, Antwerp, Belgium

Jennes I, Menten B, Buysse K, Hellemans J, De Paepe A, Speleman F, Mortier GR. Report of two cases with an interstitial deletion on 12q14: a new microdeletion syndrome? 6th meeting of the Belgian Society for Human Genetics, February 17th 2006, Antwerp, Belgium

Leroy BP, Coppieters F, Robberecht K, Beysen D, Hellemans J, Coucke PJ, De Baere E. Autosomal dominant retinitis pigmentosa in a large Belgian family: linkage-based exclusion mapping of 13 known loci. 6th meeting of the Belgian Society for Human Genetics, February 17th 2006, Antwerp, Belgium

Leroy BP, Coppieters F, Robberecht K, Beysen D, Hellemans J, Coucke PJ, De Baere E. Autosomal dominant retinitis pigmentosa in a large Belgian family: linkage-based exclusion mapping of 17 known loci. ARVO 2006 annual meeting, April 30th May 4th 2006, Fort Lauderdale, USA

Hellemans J, Mortier GR, De Paepe A, Speleman F, Vandesompele J. qBase: relative quantification software for management and automated analysis of real-time quantitative PCR data. European Human Genetics conference 2006, May 6-9 2006, Amsterdam, Netherlands

Gass J, Griffiths M, Hellemans J, Mortier G, Burrows N. Buschke-Ollendorff syndrome: a manifestation of *LEMD3* mutation, 86th Annual Meeting of the British Association of Dermatologists, July 4-7 2006, Manchester, UK

Preston P, Hellemans J, Mortier G, Moss C. An asymmetrical connective tissue naevus in the Buschke-Ollendorff syndrome demonstrating no loss of heterozygosity of *LEMD3*, 86th Annual Meeting of the British Association of Dermatologists, July 4-7 2006, Manchester, UK

Courses and trainings

Application of normalization and calculation software: geNorm & qBASE. qPCR Matrix Workshop, September 7-9 2005, Freising-Weihenstephan, Germany

qBASE: Management and automated analysis of real-time qPCR. Quantitative PCR techniques Course, October 12-14 2005, Avans Hogeschool Breda, Netherlands

TATAA Biocenter Open Courses in QPCR - Biostatistics module, March 17th 2006, Ghent, Belgium

EMBO Practical Course on Quantification of Gene Expression by qPCR, June 17-22 2006, EMBL Heidelberg, Germany

qBase: framework and program. 2nd workshop of the Marie Curie Conferences and Training Courses on arrayCGH and Molecular Cytogenetics, October 16-20 2006, Ghent, Belgium

qBase: framework and program. Quantitative PCR techniques Course, October 25-27 2006, Avans Hogeschool Breda, Netherlands

TATAA Biocenter Open Courses in QPCR - Biostatistics module, June 18-21 2007, Ghent, Belgium

EMBO Practical Course on Quantification of Target Sequences by qPCR, June 23-28 2007, EMBL Heidelberg, Germany